ISBN 978-82-471-5983-5 (printed ver.)
ISBN 978-82-471-5997-2 (electronic ver.)
ISSN 1503-8181

Zhen Gao
Doctoral Thesis

Theses at NTNU, 2008:11

Zhen Gao

Stochastic Response Analysis of Mooring Systems with Emphasis on Frequency-domain Analysis of Fatigue due to Wide-band Response Processes

Theses at NTNU, 2008:11

NTNU
Norwegian University of
Science and Technology
Thesis for the degree of
doctor philosophiae
Faculty of Engineering Science and Technology
Department of Marine Technology

NTNU
Norwegian University of
Science and Technology

NTNU
Norwegian University of
Science and Technology

Zhen Gao

Stochastic Response Analysis of Mooring Systems with Emphasis on Frequency-domain Analysis of Fatigue due to Wide-band Response Processes

Thesis for the degree of doctor philosophiae

Trondheim, February 2008

Norwegian University of
Science and Technology
Faculty of Engineering Science and Technology
Department of Marine Technology

NTNU
Norwegian University of
Science and Technology

Acknowledgements

I first would like to thank my supervisor, Prof. Torgeir Moan. During the past four years, Prof. Moan helped me gradually to know what is and how to do research work, which, I believe, is the most valuable thing I gained in this period. His teaching, supervision, advices and encouragement have always been useful for my Ph.D. study from the beginning to the end. Through many, many times of discussions on research methodology, theoretical background of e.g. mooring analysis and fatigue analysis, simulations and calculations, paper writings, etc., I personally learned a lot from Prof. Moan in many aspects of doing research work: working hard, reading extensively and carefully, being clear about basic concepts and fundamental theories, being sensitive to new information and novel ideas, being patient to listen to and answer questions, having a broad professional knowledge, having a good memory, and so on. It is my great pleasure to be one of his students.

Many other people helped and supported me in many ways during the study and I want to thank all of them. Dr. Haibo Chen at Scandpower gave me many useful advices for Ph.D. study and in my view he is always a good example to me. I also learned a lot about risk analysis when Haibo was working on the project of DP Drilling Safety in 2005. Halvor Lie at Marintek explained the simplified dynamic model of cable lines, provided the vessel data for mooring analysis and helped me to use MIMOSA. I am very glad to cooperate with Efren Ayala-Uraga in structural response analysis. Thanks also go to Dr. Sverre Haver at Statoil for discussing the modeling of sea environment and for providing the wave data and Dr. Svein E. Heggelund at Marintek for helping in building the finite element models of chain links and in using ABAQUS. The discussions with Prof. Arvid Næss and Dr. Oleg Gaidai at CeSOS, NTNU, on the slowly varying forces of moored structures and some theoretical aspects of stochastic analysis are highly appreciated.

Certainly, it is my pleasure to do my Ph.D. study under the unique research environment at CeSOS, which is quite international, competitive and productive. I would like to thank all professors and all colleagues at CeSOS and at the Department of Marine Technology for their kind helps in the past several years, including Prof. Odd M. Faltinsen, Prof. Carl M. Larsen, Prof. Bernt J. Leira, Sigrid B. Wold, Dr. Tristan Perez, Dr. Wenbo Huang, Dr. Xiangyuan

Zheng, Dr. Trong Dong Nguyen, Dr. Hui Sun, Renato Skejic, Prashant Kumar Soni, Muk Chen Ong, Jie Wu, Lin Hong, Zhi Shu, Bin Zhang and many others.

I also wish to acknowledge the financial support from the Research Council of Norway through CeSOS, NTNU.

Finally, I want to give my special thanks to my family in China and my wife, Jingzhe Jin. Their love has been the main support for me to study and live abroad during these years.

Zhen Gao

November 14, 2007
Trondheim, Norway

Abstract

Mooring systems are widely used in the offshore industry to limit the horizontal excursions of a floating structure from desired position in order for the structure to fulfill the required tasks. Safety of mooring systems is therefore crucial for successful marine operations.

Under the environmental actions of waves, wind and current, large dynamic tension in mooring lines can be excited at both wave frequency (WF) and low frequency (LF). Due to the nonlinearities of environmental loads and mooring systems, both WF and LF tension are non-Gaussian random processes. In this thesis, stochastic nonlinear mooring line tension has been modeled in an efficient way, by which, motion-induced WF tension is approximated by a simplified dynamic model, while LF tension is evaluated based on a quasi-static analysis. Especially, non-Gaussian fatigue of each frequency component has been explicitly estimated in the frequency domain, and fatigue induced by the combined tension, so-called bimodal fatigue problem, has been dealt with. The frequency-domain method for fatigue analysis has been exemplified by mooring analysis of a semi-submersible and validated by time-domain simulations and rainflow cycle counting method.

The degrading mechanism of e.g. corrosion has an influence on mooring system reliability, since mooring lines are normally submerged in sea water for a long period of interest. A time-variant reliability problem is formulated herein using a probabilistic analysis of corrosion. The problem is solved by a piece-wise constant model of line strength and the effect of corrosion on mooring safety has been analyzed in terms of annual failure probability increasing with time.

Another problem discussed in this thesis is mooring system response in a partially damaged condition. Extensive mooring analyses have been carried out using varying long-term environmental conditions and considerable increases of tension loads in the neighboring mooring lines have been obtained due to failure of one line. Significant variations in the yearly and even seasonal wave conditions and the induced extreme and fatigue responses of mooring systems together with other marine vessels, like an FPSO and a semi-submersible, have been analyzed. These variations could have a notable effect on the safety assessment of these structures.

In addition, an efficient method for estimating the damping of LF vessel motions caused by mooring systems has been proposed based on the simplified dynamic model of mooring lines. The accuracy of the calculated damping coefficients in surge and sway including the cross terms has been verified by time-domain simulations using a finite element method.

As an interesting extension of bimodal fatigue analysis, a novel frequency-domain method for estimating trimodal fatigue damage has been developed considering the interaction between the high, intermediate and low frequency components. Such a process might occur for combined responses of moored structures involving vortex induced vibrations. The proposed method has been verified to be accurate and practically acceptable by rainflow counting algorithm based on time-domain simulations of a series of ideal trimodal Gaussian processes.

Furthermore, this method has been generalized and applied to Gaussian processes with general wide-band spectra. In this way, three equivalent processes have been first defined based on the division of the response spectrum into three parts with the same variances. The wide-band fatigue damage is then estimated using the same procedure as for ideal trimodal processes. Extensive time series have been simulated for different kinds of wide-band processes, including typical marine structural responses induced by waves and wind. It is noted that the narrow-band approximation can be applied to estimate the wide-band fatigue damage if the Vanmarcke's bandwidth parameter is less than 0.5. The proposed method has been validated with the simulation results and compared with other empirical methods. Although the idea of the proposed method is simple, it seems to be applicable for a wide range of spectral types.

Moreover, previous research work on frequency-domain fatigue analysis has mainly focused on single-slope SN curves. In this thesis, fatigue analysis considering two-slope SN curves has been carried out and especially the methods of bimodal fatigue analysis have been generalized and the accuracy has been verified by time-domain simulations.

List of Appended Papers

This thesis consists of an introductory part, seven papers (two published journal papers, four published conference papers and one accepted journal paper) and an additional work related to the papers.

The following seven papers are reported in Appendix A:

Paper 1:
Fatigue damage induced by nonGaussian bimodal wave loading in mooring lines
Zhen Gao and Torgeir Moan
Published in Applied Ocean Research 2007; Vol. 29, pp. 45-54

Paper 2:
Frequency-domain fatigue analysis of wide-band stationary Gaussian processes using a trimodal spectral formulation
Zhen Gao and Torgeir Moan
Accepted for publication in International Journal of Fatigue

Paper 3:
Uncertainty of wave-induced response of marine structures due to long-term variation of extratropical wave conditions
Torgeir Moan, Zhen Gao and Efren Ayala-Uraga
Published in Marine Structures 2005; Vol. 18, No. 4, pp. 359-382

Paper 4:
Time variant reliability of mooring system considering corrosion deterioration
Zhen Gao, Torgeir Moan and Svein E. Heggelund
Published in Proceedings of the 24th International Conference of Offshore Mechanics and Arctic Engineering (OMAE2005), June 12-16, 2005, Halkidiki, Greece

Paper 5:
Sensitivity study of extreme value and fatigue damage of line tension in mooring system with one line failure under varying annual environmental conditions
Zhen Gao and Torgeir Moan
Published in Proceedings of the 17th International Offshore and Polar Engineering Conference (ISOPE2007), July 1-6, 2007, Lisbon, Portugal

Paper 6:
Fatigue damage under combined high and low frequency Gaussian load processes considering a two-slope SN curve
Zhen Gao and Torgeir Moan
Published in Proceedings of the 10th International Conference on Applications of Statistics and Probability in Civil Engineering (ICASP10), July 31-August 3, 2007, Tokyo, Japan

Paper 7:
Mooring line damping estimation by a simplified dynamic model
Halvor Lie, Zhen Gao and Torgeir Moan
Published in Proceedings of the 26th International Conference on Offshore Mechanics and Arctic Engineering (OMAE2007), June 10-15, 2007, San Diego, California, USA

Additional work as an extension of *Paper 3* and *Paper 5* is reported in Appendix B:

Extension 1:
Variability of structural responses of marine structures due to seasonal and yearly wave data
Zhen Gao and Torgeir Moan

Regarding the authorship of these seven papers and my contributions, I have been the first author of *Papers 1, 2, 4, 5* and *6* as well as the additional work and I was responsible for establishing the models, performing the calculations, providing the results and writing the papers under the supervision of Prof. Torgeir Moan. He was the second author of these papers and made helpful corrections and comments. Svein E. Heggelund (the third author of *Paper 4*) helped me to set up the finite element model of chain links and made corrections on the text. As the second author of *Papers 3* and *7*, I was also involved in running the analyses, providing most of the figures and writing some parts of these two papers. Prof. Torgeir Moan (the first author) initiated the study related to *Paper 3* and Efren Ayala-Uraga (the third author) provided the contour-line plots and wrote the introduction. Halvor Lie (the first author) proposed the model of mooring line damping in *Paper 7* and Prof. Torgeir Moan (the third author) made comments on that paper.

In addition, the following two papers worked out during the study are not included in this thesis:

Other paper 1:
Corrosion of working chains continuously immersed in seawater
Robert E. Melchers, Torgeir Moan and Zhen Gao
Published in Journal of Marine Science and Technology 2007; Vol. 12, No. 2, pp. 102-110
(Not considered as a part of the study because of scope)

Other paper 2:
Wave-induced fatigue damage of mooring chain under combined non-Gaussian low and wave frequency loads
Zhen Gao and Torgeir Moan
Published in Proceedings of the 25th International Conference on Offshore Mechanics and Arctic Engineering (OMAE2006), June 4-9, 2006, Hamburg, Germany
(Not included because of some overlaps with *Paper 1*)

Table of Contents

Chapter 1

Introduction

1.1 Background

Floating structures are frequently used by the oil and gas industry for drilling, well intervention, production and storage at sea. They are often used in other offshore activities as well, like the aquaculture industry and the exploitation of renewable energy from wind, waves and ocean current.

Under environmental actions of waves, wind and current, a freely floating structure exhibits offsets different from the desired point for normal operations. It is crucial to keep the structure within limits of excursions and orientation for safety of personnel, protection of the environment and stability and serviceability of it. Therefore, a station-keeping system is used and attached to the floating structure. The function of a station-keeping system (ISO 2005) is to restrict the horizontal excursions of the floating structure within prescribed limits, as well as to provide means of active or passive directional control when the structure's orientation is important for safety or operational considerations. Different from a fixed platform whose global motions are negligible and only due to the structural deformation, it is not desirable to keep a moored floating structure motionless and in general the floating structure is allowed to have restricted dynamic motions (e.g. the wave frequency motions) in normal operations. In such conditions, the station-keeping system provides forces to balance the mean constant environmental actions, while the first-order wave forces are not counteracted and as a result the wave frequency motions of the structure are not influenced by the station-keeping system. However, the natural period of the moored structure is close to that of the excitation of e.g. the second-order wave forces and this causes the slowly varying resonant vessel motions.

Depending upon the principle for providing restoring forces, a station-keeping system can be passive (e.g. a mooring system), active (e.g. a dynamic positioning (DP) system) or combined active-passive (e.g. a thruster-assisted mooring system).

Mooring systems are used for anchoring a floating structure to the sea floor with e.g. catenary, taut or semi-taut lines. Mooring lines consisting of steel chain links and sometimes steel wire ropes have a catenary shape with heavy weight, while synthetic fibre ropes are normally straightened in a taut mooring system and used especially for deep water. These components are often combined in one mooring line to sustain abrasion at the fairlead and friction on sea bottom with chain links and to decrease the weight of the whole line using ropes in between.

Dynamic positioning (ISO 2005) is a station-keeping technique consisting of on-board thrusters (and sometimes rudders) that are automatically controlled to maintain a floating structure's position and/or heading. Propulsive forces produced by the thrusters/rudders normally counteract only the mean and slowly varying actions due to wind, waves and current so as to maintain the structure within pre-set tolerances at a desired point above the sea floor and on a pre-defined heading. However, in harsh sea states, the WF forces might be compensated as well by a DP system to obtain a relatively stable working condition. A DP system has an obvious advantage in deep water, compared to conventional mooring systems which get a payload penalty due to the heavy weight of e.g. chains.

A thruster-assisted mooring system can also be applied for instance to control the heading of a ship e.g. in a single point mooring or to assist in resisting environmental loads in extreme conditions, while dynamic environmental forces in normal conditions are mainly compensated by the mooring system. Mooring line tension in extreme sea states can be reduced with thruster assistance. However, in order to assess the safety of the whole system, design check should be carried out for loss of one mooring line as well as for loss of thruster assistance.

Due to its simplicity and passivity, mooring systems are frequently used in the offshore oil and gas industry. Various types of mooring arrangements are envisaged, e.g. single point mooring and spread mooring. Single point mooring is often used for ship-shaped floating structures such as floating production, storage and offloading structures (FPSOs) and allows the connected vessel to vary its heading (weathervane). One example is the turret mooring system as shown in Figure 1.1, where a number of mooring lines are attached to a cylinder and the ship is allowed to rotate around this cylinder. A spread mooring system consists of multiple lines terminated at different locations of the structure and provides an almost constant heading of it. An example of the spread mooring system of an FPSO is shown in Figure 1.2.

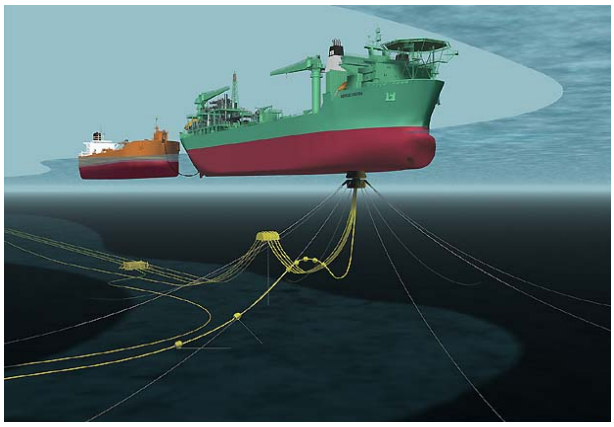

Figure 1.1 Turret mooring system of an FPSO (Courtesy of APL)

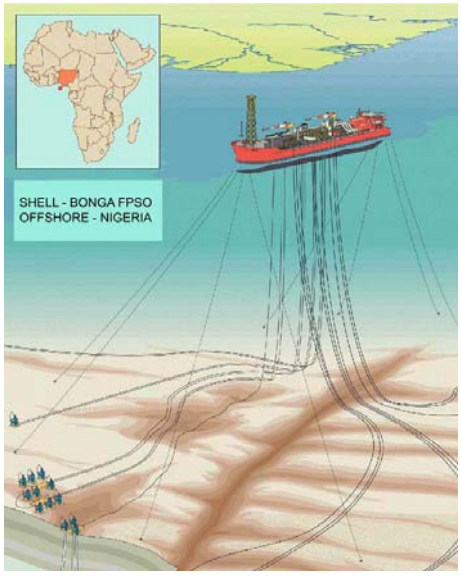

Figure 1.2 Spread mooring system of an FPSO (Courtesy of SHELL)

Moreover, mooring systems might be economically suitable for anchoring fish farms, wind turbine devices and wave energy converters (WECs). Different from mooring systems for large floating structures like ships, semi-submersibles or spars, mooring systems for fish farms should be analyzed in a coupled manner to take account of flexibility of the nets and considerable forces resulting from the mooring lines. For a motion-based WEC, the station-keeping performance should not only be the design consideration of the mooring system and the effect of mooring system on the efficiency of wave energy absorption should be evaluated as well (Johanning et al. 2006).

This thesis focuses on mooring systems used by the offshore oil and gas industry for which design codes are well established by international organizations, including classification societies, e.g. ISO 19901-7 (ISO 2005), API RP 2SK (API 2005) and DNV OS-E301 (DNV 2004). Various limit states are considered in design, i.e. ultimate limit state (ULS), fatigue limit state (FLS), accidental limit state (ALS) and serviceability limit state (SLS). Normally,

ULS is considered for both permanent moorings when the floating structures are deployed for long-term operations, e.g. for the whole service life of 20 years, and temporary moorings with short operational periods. FLS might be required only for permanent moorings when the accumulated fatigue damage in mooring lines is considerable. However, since fatigue is a cumulative phenomenon, it is important to consider the total damage for a given mooring line if it has been used in many services. ALS design checks considering line failure due to abnormal causes might be a relevant criterion as well. Moreover, SLS criteria are usually determined based on the requirements for the structures to fulfil their intended mission. ULS and FLS are to ensure that the individual mooring lines have adequate strength to withstand the load effects imposed by extreme environmental conditions and cyclic loading, respectively. Both ULS and FLS are considered for an intact mooring system, while ALS is to ensure that the system has adequate capacity to withstand the failure of one mooring line.

Mooring system design is usually carried out by a semi-probabilistic load resistance factor design (LRFD) method. In order to take into account the uncertainties involved in the analyses of load effects and strength resistance, appropriate safety factors are normally applied and calibrated by reliability analysis. Depending on the methods of quasi-static or dynamic analysis of mooring response, safety factors vary for different consequences of system failure. As defined by the offshore standard DNV OS-E301 (DNV 2004), two consequence classes are introduced in the ULS and ALS, i.e. the Class 1 where mooring system failure is unlikely to lead to unacceptable consequences such as loss of life, collision with an adjacent platform, uncontrolled outflow of oil or gas, capsize or sinking, and the Class 2 where failure may well lead to these consequences. Although the semi-probabilistic method is applied to mooring system design, the consideration of ALS and consequence classes reflects a thinking of risk analysis.

As we know, compared with the semi-probabilistic method, reliability and risk analyses are more advanced methods for safety assessment. They will be briefly touched upon in *Chapter 4*.

Dynamic mooring response consists of two frequency components, i.e. wave frequency (WF) component mainly induced by the first order wave forces and low frequency (LF) component caused by the slowly varying environmental forces. For design purposes, mooring analysis needs to be carried out to estimate extreme value and fatigue damage of the combined mooring line tension. Usually, the following rule for load combination is applied to predict the extreme line tension in a short-term period, by which the extreme value is estimated as the maximum of two sums, i.e. sums of the expected extreme WF (or LF) tension plus the significant value of LF (or WF) tension. Fatigue under combined WF and LF tension is recognized as a so-called bimodal fatigue problem which will be discussed later in this thesis.

Mooring analysis for design purposes is usually based on the Gaussian assumption for the mooring line tension of both the WF and LF components. For instance, the formula developed by Jiao and Moan (1990) is widely used in design codes like ISO 19901-7 (2005), API RP 2SK (API 2005) and DNV OS-E301 (DNV 2004) for estimating the mooring line fatigue. In fact, due to the nonlinear effects of the second order wave forces and the wind force acting on the floating structure, the resulting LF mooring line tension is typically non-Gaussian, see e.g. Næss (1986), Faltinsen (1990) and Stansberg (1991). The WF line tension mainly induced by the WF motions of the structure is non-Gaussian as well due to the drag forces acting on the line. Furthermore, the static excursion-tension relationship of one mooring line is typically nonlinear. Sea bottom friction and contact could also increase the nonlinearity of mooring systems. Influence of these nonlinearities on the prediction of extreme value and fatigue damage of mooring line tension needs to be investigated.

A structure under cyclic loading will experience fatigue damage in the components, where crack starts to grow and propagate from an initial stage to a situation when it turns to be large enough to make the components or even the entire structure fail to carry the external loads. While the structural response for ULS criteria refer to extreme conditions, fatigue analysis needs to consider the damage effect of each load cycle and to determine whether structural failure occurs or not due to the cumulative damage over a period of interest.

Fatigue analysis can be carried out by a fracture mechanics or a SN approach. The former method allows detailed modelling of the crack propagation, while the SN approach is based on an SN curve established by use of laboratory tests under constant amplitude loads. Both methods commonly predict linear cumulative damage when dealing with variable amplitude loading. This thesis focuses on the SN approach.

The SN approach needs the following information to calculate the fatigue damage, i.e. distribution of the effective stress ranges, SN curve and damage accumulation law. The Miner-Palmgren linear damage rule (Miner 1945) is usually applied to estimate the total fatigue damage as a sum of damage due to each effective load cycle.

An SN curve is defined as a relationship between the stress range S and the number to failure N of a specimen under a constant-amplitude test with this stress range.

$$N = KS^{-m} \tag{1.1}$$

where K and m are the material parameters.

SN curves for various materials and specimens under different environmental conditions have been well established by constant-amplitude tests. Examples of SN curves for stud and studless chain links are shown in Figure 1.3. These are single-slope SN curves in air and in

sea water, respectively. In addition, many fatigue tests show that specimens can experience more load cycles for low stress ranges than those predicted by single-slope SN curves and this effect can be well modelled by two-slope or even multi-slope SN curves. An example of two-slope SN curve is shown in *Paper 6*.

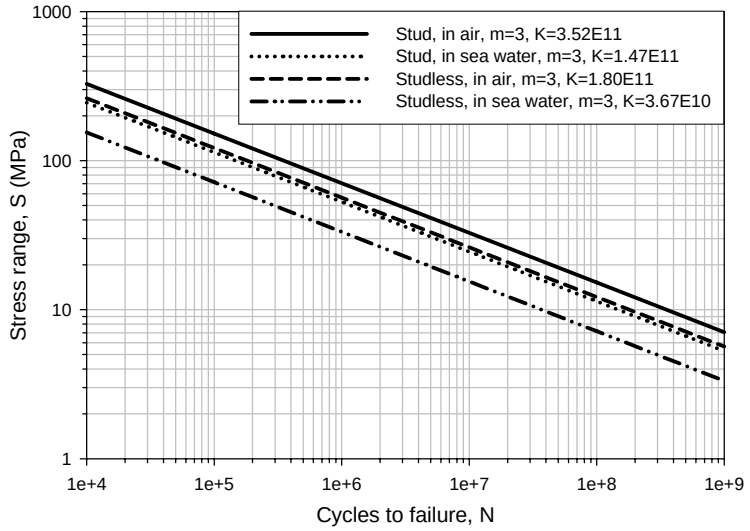

Figure 1.3 Examples of SN curves for stud and studless chain links in air and in sea water (Mathisen, 1999a)

Prediction of effective stress ranges is much more complicated. For deterministic time series of loading, fatigue damage estimation is straightforward based on the time-domain cycle counting methods such as the peak counting, the range counting, the level-crossing counting and the rainflow counting, see e.g. ASTM (1985). The rainflow cycle counting algorithm originally proposed by Matsuishi and Endo (1968) is believed to be the best method for fatigue damage estimation (Dowling 1972 and Watson and Dabell 1975). However, offshore structures are often subjected to stochastic loads induced by waves, wind and current which are random in nature. In order to account for the randomness, it is mandatory but time-consuming to generate many time series of responses required to cover the relevant sea states in the scatter diagram and limit the statistical uncertainty. In such situations, fatigue damage can be calculated based on the stress range distribution predicted by the frequency-domain methods, by which only spectral density functions of the load effects (stress range) are used. However, there is no simple and explicit relationship between the effective stress range distribution and the general response spectrum.

As we know, the shape of spectral density function of a certain response has a significant effect on the prediction of the induced fatigue damage. The Vanmarcke's bandwidth parameter is often used to characterize a random process and is defined as (Vanmarcke 1972),

$$\delta = \sqrt{1 - m_1^2 / (m_0 m_2)} \tag{1.2}$$

where m_i is the *i*th order spectral moment. The value of bandwidth parameter is between 0 and 1. A process is narrow-banded if this parameter is close to 0. Otherwise, it is wide-banded. Other bandwidth parameters defined based on higher spectral moments might also be used.

For a narrow-band Gaussian process, the effective stress range is twice the positive amplitude of the response and follows a Rayleigh distribution. Fatigue damage due to this process can be analytically estimated based on the Palmgren-Miner rule as

$$D_{NB} = \frac{\nu_0 T}{K}(2\sqrt{2}\sigma)^m \Gamma(1+\frac{m}{2}) \tag{1.3}$$

where σ is the standard deviation of the stress process, ν_0 is the mean zero up-crossing rate, T is the duration, $\Gamma()$ represents the Gamma function, K and m are the material parameters for a single-slope SN curve.

Often the load effects are not ideally narrow-banded and their spectra cover a wider range of frequencies. Fatigue damage of wide-band processes is hard to obtain in the frequency domain. Nevertheless, it is clear that damage estimates based on the narrow-band assumption are always conservative. Also, the actual wide-band fatigue damage is often expressed as the narrow-band result multiplied with a correction factor. Various methods have been proposed to estimate this factor in terms of the spectral moments.

The bimodal process is a special wide-band process that occurs often. Frequency-domain methods have been proposed to determine the fatigue damage for such processes, by e.g. Jiao and Moan (1990), Sakai and Okamura (1995), Fu and Cebon (2000), and Benasciutti and Tovo (2007), using different principles for combining the damage associated with the two frequency components. For practical use, bimodal fatigue damage could also be expressed in terms of individual damage as proposed by for instance Lotsberg (2005) and Huang and Moan (2006).

One practical extension of bimodal fatigue problem is the trimodal fatigue damage estimation, which could a problem encountered for instance for a riser system. A riser system attached to a moored vessel could experience vortex induced vibrations (VIV) with high frequencies in addition to the forces induced by the WF and LF vessel motions. According to the current procedure for fatigue analysis of risers, the WF and LF fatigue damage is first estimated and then the VIV contribution is separately added to obtain the total fatigue damage (Chakrabarti 2005). In this way, no interaction between the VIV response and the WF and LF response has been considered. In principle, the fatigue damage will then be underestimated because of the nonlinear relationship between the fatigue damage and the stress range. Fatigue damage for

stress spectra consisting of three frequency components is therefore interesting to study in a way that all interactions can be considered simultaneously.

Furthermore, bimodal and trimodal processes are special wide-band processes. Frequency-domain methods for general wide-band fatigue damage estimation are certainly of great interest and importance. Although the rainflow cycle counting method is the best method for fatigue analysis, it is only applicable in the time domain and it has no closed-form solution in the frequency domain. Most of the frequency-domain methods for wide-band fatigue damage estimation are therefore based on the empirical correction on the narrow-band estimate. Bouyssy et al. (1993) and Benasciutti and Tovo (2006) compared different methods considering various wide-band spectral shapes. Among them, the formulae of Dirlik (1985) and Benasciutti and Tovo (2005) give the most accurate estimates of fatigue damage in comparison with the results of the time-domain simulations.

Moreover, the responses of marine structures are not always Gaussian. Nonlinear loads and nonlinearities in structural systems make the load effects non-Gaussian. Time-domain cycle counting methods can be applied to non-Gaussian processes in the same manner as to Gaussian processes. However, frequency-domain methods may not be able to consider the complete effects of non-Gaussianity on fatigue damage estimation. It seems that the best way to deal with non-Gaussian processes is to approximate them by a monotonic transformation of Gaussian processes and estimate the fatigue damage by making use of higher order statistical moments, notably skewness and kurtosis. The effect of non-Gaussian features of the loading on the fatigue damage was studied by e.g. Winterstein (1988) and Wang and Sun (2005), by accounting for the effect of the skewness and kurtosis of the whole process.

1.2 Objectives and scope of the thesis

This thesis is written as a summary of the published or accepted papers, including 3 journal papers and 4 conference papers as listed in Appendix A. One extension of the papers is included in Appendix B. The scope of the thesis is shown in Figure 1.4 where the main topics and the interconnection between these papers are illustrated.

Safety of mooring systems is one of the main topics dealt with in this thesis. Several key issues are investigated in detail, like bimodal fatigue damage induced by non-Gaussian mooring line tension (*Paper 1*), mooring system reliability considering strength deterioration (*Paper 4*), mooring response analysis in damaged conditions (*Paper 5* and *Extension 1*) and mooring line damping (*Paper 7*).

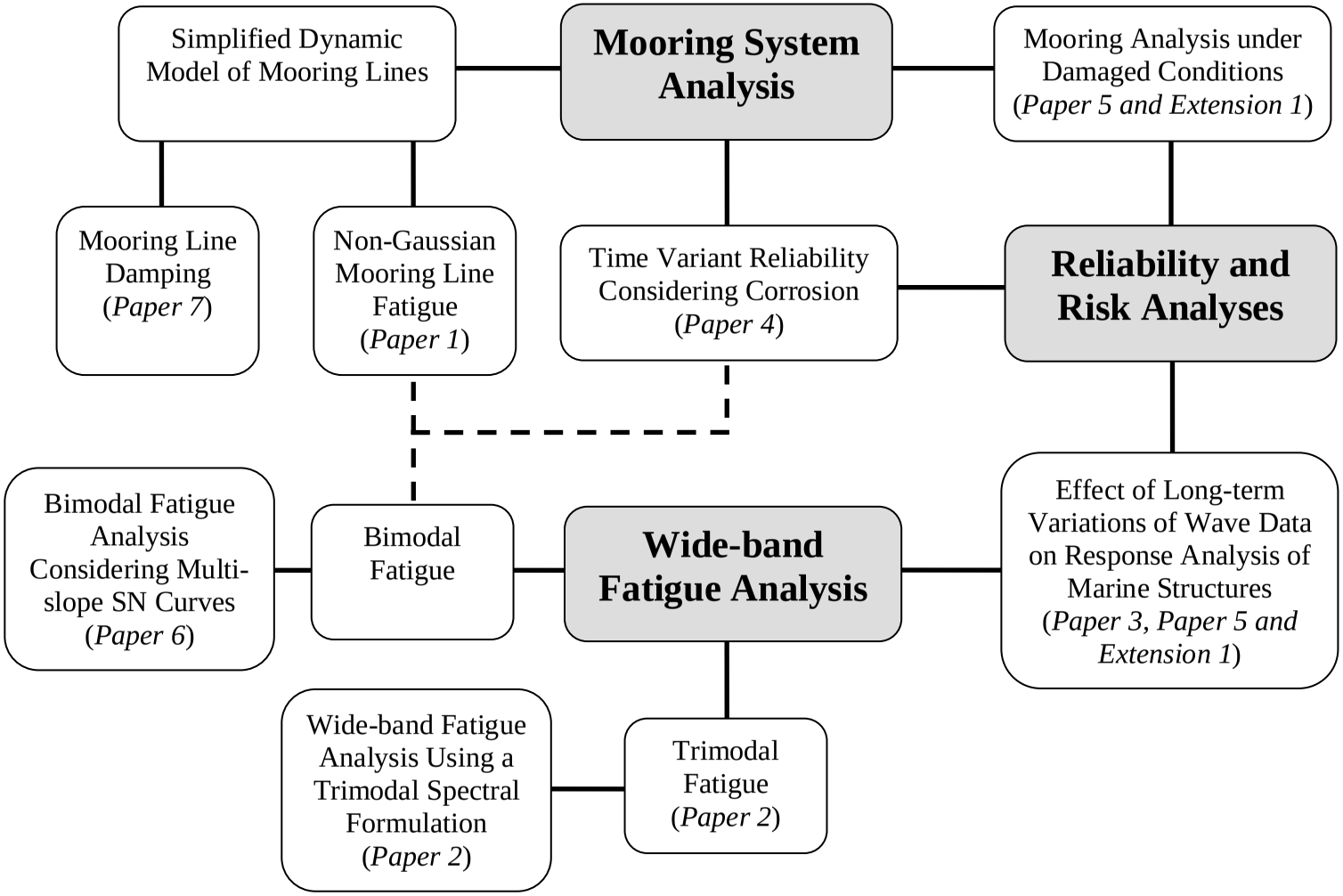

Figure 1.4 Scope of the thesis and interconnection between the appended papers

As indicated above, both WF and LF mooring line tension are nonlinear and the combined tension certainly has a non-Gaussian statistical property. One of the purposes of this thesis is therefore to explicitly investigate the non-Gaussianity of mooring system response and to study the corresponding effect especially on the induced fatigue damage, which is reported in *Paper 1* at length.

Mooring system performance under deteriorated and even damaged conditions is very important to the overall safety. One objective herein is to study the mooring response in such situations and the influence on system reliability assessment, see *Paper 4*, *Paper 5* and *Extension 1*.

Another main topic of this thesis is the frequency-domain methods of fatigue analysis. Fatigue analyses of multi-modal and generally wide-band processes have been studied and discussed.

As we know, most of the frequency-domain methods consider only single-slope SN curves. The purpose of *Paper 6* is to verify the accuracy of such methods for two-slope or even multi-slope SN curves as well as for non-Gaussian processes by time-domain simulations and rainflow cycle counting.

Fatigue damage of general wide-band processes is hard to obtain in the frequency domain. However, it is believed that it could be beneficial to start with some special cases of wide-band processes first, such as bimodal or trimodal processes, study the properties of these processes in detail and then generalize the common principles of fatigue calculation to more general wide-band processes. Therefore, as reported in *Paper 2*, one objective of this thesis is to generalize the fatigue analysis method from bimodal process to trimodal process and then apply the method to estimate general wide-band fatigue damage.

Furthermore, it is noted that long-term variations (e.g. due to seasons or from year to year) of environmental conditions at sea can be quite significant. These variations cause significant variations of the structural responses as well and influence the safety assessment, especially for structures which are temporarily in a damaged condition. These issues are touched upon in *Paper 3*, *Paper 5* and *Extension 1*.

Chapter 2

Mooring System Analysis

2.1 Overview of mooring analysis

Mooring analysis includes both the vessel motion analysis and the analysis of mooring line tension. Vessel motion responses are caused by steady wave, wind and current forces, wave frequency (WF) and low frequency (LF) wave loads as well as LF wind forces. While the LF wave forces are relatively small compared with the WF forces, the effect on the vessel motions can be significant due to the resonance of the entire moored structure. Moreover, mooring line tension is mainly induced by the motions at the fairlead and the contribution of wave forces directly acting on the lines is relatively small (Larsen and Fylling 1982). As a result, the tension response consists of the mean, WF and LF components similar to the motion response.

Coupled analysis where both the vessel motion and mooring line tension responses are simultaneously obtained is normally applicable in the time domain, while the frequency-domain analysis is usually carried out in an uncoupled way.

Reaction forces of mooring systems to the first-order wave forces are negligible and therefore, the WF vessel motions can be predicted without consideration of the mooring systems and the LF motions. However, on the other hand, the LF vessel motions are due to the resonant phenomena and certainly dependent on the mooring systems, especially the damping contribution from mooring lines. Furthermore, mooring line damping is mainly caused by the drag forces induced by the WF vessel motions. In addition, another source of the damping of the LF motions is the wave drift damping which is also affected by the WF motions. In this sense, the LF motions of the vessel present the dependency on the WF motions.

Regarding the dynamic mooring line tension, a quasi-static analysis might be applied where the tension response, e.g. the short-term extreme value, is estimated at the total extreme

vessel motions based on the displacement-tension characteristics of the mooring lines. However, the WF mooring line tension is a direct result of the WF fairlead motions and normally needs to be calculated by a dynamic model. In this way, it is dependent on the vessel position where the mooring system might be linearized and this position is determined considering the mean and LF vessel motions. For example, the linearization can be made at the position of the total extreme motions minus the WF extreme motions (MARINTEK 2003).

Mooring system analysis, including fatigue analysis, is the main focus of this thesis. Case studies are mainly carried out on the mooring system of a large semi-submersible with a weight of 52500ton and a draught of 21m. The mooring system has 16 identical chain-wire-chain mooring lines with 4 lines grouped at each corner of the semi-submersible.

2.2 Vessel motion analysis

Floating structures and their mooring systems experience interaction under environmental forces. The dynamic mooring line tension is normally predicted based on the vessel motions which are first determined.

Floating structures considered herein are ships, semi-submersibles, spars, etc., and they are usually modelled as rigid bodies in motion analysis. Vessel motion response in a stationary and short-term sea state can be split into three components:

- mean displacement due to mean environmental loads,
- LF motions with natural periods of the moored vessel in surge, sway and yaw directions due to LF wind loads and second order wave loads,
- motions at the frequency of incoming waves due to first order wave loads.

Mean offset of the floating vessel is determined at an equilibrium position under the combined mean forces of waves (mean wave drift), wind and current by considering the nonlinear restoring forces of the mooring system. Dynamic motions are established at the equilibrium position of the vessel.

Dynamic analysis of vessel motions includes both steady-state response in the intact or damaged conditions of the mooring system and transient response induced by mooring line failure or thruster failure if a thruster-assisted mooring is used. The steady-state response can be solved both in the frequency domain and in the time domain. The frequency-domain analysis is commonly used with linear models and the choice between these models depends

on how good a linearization will be. The transient response is usually obtained by a time-domain analysis.

The equation of motions for the vessel in regular waves may be written as

$$M\ddot{x} + C\dot{x} + D_1\dot{x} + D_2 f(\dot{x}) + K(x)x = q(t, x, \dot{x}) \tag{2.1}$$

$$\begin{aligned} M &= m + A \\ A &= A(\omega) = A(\infty) + a(\omega) \\ C &= C(\omega) = C(\infty) + c(\omega) = c(\omega) \end{aligned} \tag{2.2}$$

where

t	time variable
ω	frequency of incident waves
$x, \dot{x}, \ddot{x}$	vectors of displacement, velocity and acceleration
m	body mass matrix
$A(\omega)$	frequency-dependent added mass matrix
$C(\omega)$	frequency-dependent potential damping matrix
D_1	linear damping matrix
D_2	quadratic damping matrix
$K(x)$	position-dependent stiffness matrix
$f(\dot{x})$	vector function where each element is given by $\dot{x}_i \lvert \dot{x}_i \rvert$
$q(t, x, \dot{x})$	excitation force vector

The excitation force on the right-hand side of Equation (2.1) includes the following components,

$$q(t, x, \dot{x}) = q_{WI} + q_{WA}^{(1)} + q_{WA}^{(2)} + q_{CU} + q_{oth} \tag{2.3}$$

where

q_{WI}	wind drag force
$q_{WA}^{(1)}$	first order wave excitation force
$q_{WA}^{(2)}$	second order wave excitation force
q_{CU}	current drag force
q_{oth}	other forces including forces from the mooring system

The whole differential equation of vessel motions can be solved in the time domain by use of convolution integral of the retardation function, and alternatively the motions can be separated into a WF part and an LF part,

$$x = x_{WF} + x_{LF} \tag{2.4}$$

where x_{WF} and x_{LF} refer to the WF and LF vessel motions, respectively.

The WF motions can be obtained by a linear analysis where the quadratic damping is linearized and set to be zero and the stiffness matrix is assumed to be position-independent. The equation of WF vessel motions is reduced to

$$(m + A(\omega))\ddot{x}_{WF} + (C(\omega) + D_1)\dot{x}_{WF} + Kx_{WF} = q_{WA}^{(1)} \tag{2.5}$$

Only the first order wave forces need to be considered in the WF motion analysis and the linearized system can be easily solved in the frequency domain. The WF vessel response is Gaussian because it results from a linear system subjected to Gaussian loading.

However, in order to solve the LF vessel motions, forces from the mooring system need to be considered together with the slowly-varying forces of waves, wind and current. The LF motion equation is shown as follows and it is normally solved by a time-domain method,

$$(m + A(\omega = 0))\ddot{x}_{LF} + D_1\dot{x}_{LF} + D_2 f(\dot{x}_{LF}) + Kx_{LF} = q_{WI} + q_{WA}^{(2)} + q_{CU} + q_{oth} \tag{2.6}$$

where the potential damping is zero for small frequencies ($C(\omega = 0) = 0$). Due to the second order wave forces and the nonlinear wind and current forces, the LF vessel motions exhibit non-Gaussian properties.

Mooring systems provide not only time-varying restoring forces but also damping forces. Both forces must be taken into account in the LF response analysis and the effects might be obtained by a linearization centered on the mean position of the vessel.

The effects of a single riser are usually negligible in comparison with the effects of the mooring lines, but the effects of multiple risers may need to be included as well. Similarly, risers may cause restoring, damping and excitation forces.

2.3 Low frequency damping

The LF motion response is typically narrow-banded since it is dominated by the resonant response at the natural frequency of the moored structure. The motion amplitude is highly dependent on the stiffness of the mooring system and the damping.

Damping of the LF motions is a critical parameter, which may be difficult to quantify. If model tests are available, they can provide a basis for quantifying the damping. It is dependent on water depth, the number of mooring lines and risers in addition to the actual sea

state and current profile. There is a substantial degree of uncertainty in the estimation of LF damping of which there are four main sources:

- viscous damping of the structure,
- wave drift damping,
- mooring and riser system damping,
- thrusters damping if applicable.

Some examples of damping coefficients can be found in e.g. DNV OS-E301 (DNV 2004):
For a ship in 150m water depth, with 12 mooring lines and no risers:

- the surge damping coefficient is 5% to 10% of critical damping,
- the sway damping coefficient is 15% to 20% of critical damping;

For a twin-pontoon drilling semi-submersible in 450m water depth, with 8 mooring lines and no risers:

- the surge damping is 10% of critical damping,
- the sway damping is 15% of critical damping.

Relative importance of these damping sources has been discussed by e.g. Wichers and Huijsmans (1990), Molin (1993) and Triantafyllou et al. (1994).

Oscillation of a structure in a viscid fluid could induce periodic vortex shedding and provide damping forces to the structure. Viscous effects on the LF motions of ships are significant in sway and yaw motion modes (Graham 1980) and could be calculated by strip theory and the cross-flow principle (Faltinsen 1990). For structures with cylindrical components like semi-submersibles or spars, the viscous damping could be estimated based on the Morison equation as illustrated by e.g. Chakrabarti (1984), Larsen and Huse (1993), Downie et al. (1995) and Lie (2006).

It is well known that structures advancing in waves could experience an added resistance and this explains the wave drift damping phenomenon by interpreting the LF vessel motion as a forward and backward speed (Faltinsen 1990). Wave drift damping has been studied or discussed by Zhao et al. (1988), Zhao and Faltinsen (1988), Sclavounos (1989), Hermans (1991) and Newman (1993).

Mooring systems also contribute damping of the LF vessel motions (Molin 1993 and Webster 1995). The damping effect increases with the presence of WF motions. Based on the quasi-static model of mooring lines, damping from the mooring system has been proposed by Huse (1991), Liu and Bergdahl (1998) and Bauduin and Naciri (2000).

In *Paper 7*, we propose an estimate of mooring line damping in the frequency domain based on a simplified dynamic model, originally developed by Larsen and Sandvik (1990). This method predicts the total damping of the mooring system to be about 20% smaller than that obtained by the time-domain simulations and yields conservative estimates of LF motions.

2.4 Mooring line response analysis

Studies of mooring line dynamics has been carried out by many researchers, like Larsen and Fylling (1982), Lindahl and Sjoberg (1983), Triantafyllou (1991), Liu and Bergdahl (1997) and Aranha and Pinto (2001). The Finite Element (FE) method has also been applied to model mooring lines. Comparative studies of frequency-domain and time-domain methods were performed by e.g. Kwan and Bruen (1991) and Brown and Mavrakos (1999).

Hydrodynamic excitation forces directly acting on mooring line components are normally negligible and mooring line response is mainly induced by the vessel motions at the fairlead and therefore consists of the mean, WF and LF components. Except locally in chain links (e.g. at the fairlead), the bending of mooring lines is normally negligible and only the tension needs to be calculated. Quasi-static analysis of the mooring system is usually appropriate to determine the mooring line tension due to mean and LF vessel displacements, while dynamic analysis is normally necessary for mooring line tension due to WF displacements of the vessel.

In design codes for mooring systems, the LF vessel motions are normally assumed to be Gaussian and the extreme value of the LF line tension is calculated by considering the nonlinear line characteristics. This is a good approximation only for small damping of LF motions. In fact, the quasi-static mooring line tension includes not only the nonlinearities due to the reaction and friction forces from the seabed and the offset-tension relationship, but also the non-Gaussian property of the LF vessel motions e.g. induced by second order wave forces. The non-Gaussianity of the LF line tension strongly relies on the damping of LF vessel motion and would normally imply a higher extreme value than the Gaussian one. The effect has been studied by e.g. Næss (1986), Stansberg (1991) and Stansberg (2000).

Although the WF vessel motions are Gaussian, the resulting dynamic line tension is non-Gaussian due to the nonlinear drag forces acting on the line as well as the nonlinear displacement-load characteristics of the line.

When the dynamic WF and LF line tension are determined separately, they should be combined to obtain the total extreme value and the induced total fatigue damage. The Gaussian assumption is widely adopted for design purposes.

So far the load effects in a single sea state have been considered. In reality, the long-term extreme value and fatigue damage need to be calculated for mooring systems with a long service life and the probabilities of occurrence of different environmental conditions should be taken into account.

Long-term extreme value of mooring line tension could be predicted by a full long-term analysis (Nordenstrøm 1971) by which all the relevant short-term sea states of interest were considered and it is normally quite time-consuming. Battjes (1977) also considered the correction term on the variation of the mean zero up-crossing rate of each short-term sea state when predicting the long-term response.

Alternatively the contour line method could be applied. By this method only some important sea states along the environmental contour line (or surface) with a certain return period of e.g. 20 years or 100 years, are considered. The contour line method only uses the information of extreme sea states and approximates the long-term extreme response by the short-term extreme value under these conditions. However, the environmental contour line is pre-determined and does not depend on the response type. Although the long-term extreme response is strongly correlated to the extreme sea states, other sea states could also contribute to the long-term response distribution. Moreover, the short-term extreme response also presents the variability which is different in different sea states. It would normally be under-estimating if the short-term variability is not included. In order to consider these effects, a high quantile than the median should be used when applying the contour line method. This quantile is response-dependent and needs to be determined or calibrated by the full long-term analysis.

Meling et al. (2000) used the contour line method to predict the extreme response of quasi-static mooring line tension. In *Paper 5* and *Extension 1*, we apply the contour line method by considering the dynamic analysis of line tension and verify the method with full long-term analyses.

The accuracy of the contour line method is exemplified in Figure 2.1 for predicting annual extreme line tension, where the relative error is defined as the difference of the results obtained by the contour line method and the full long-term analysis divided by the full long-term result. Seasonal and yearly environmental conditions are considered and a quantile of 70% of the distribution of the short-term extreme tension has been used when applying the

contour line method. The obtained relative errors are very small, within +/- 3%, except those based on the Summer data, where a maximum absolute value of the relative error of about 6.5% are obtained.

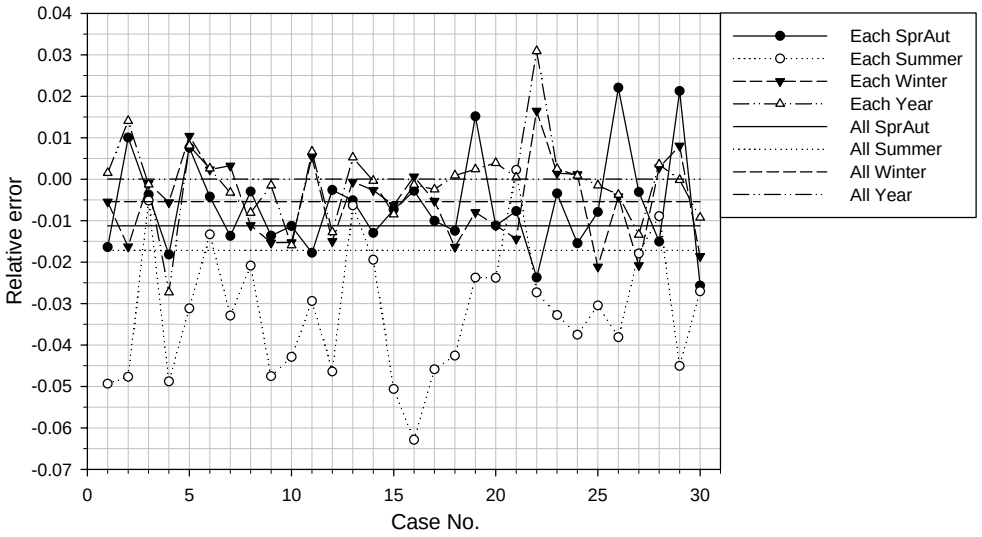

Figure 2.1 Relative error of the contour line method compared with the full long-term analysis for predicting the annual extreme mooring line tension based on the seasonal and yearly sea data of thirty years (In the figure, "Each" represents the results based on the data of individual years, while "All" represents the results when all of the data of thirty years are applied.)

Separate analyses of WF and LF mooring line tension result in the fatigue damage due to each frequency component. However, in order to assess the performance of mooring systems under fatigue loading, the total fatigue damage needs to be evaluated. Combination of WF and LF fatigue damage is not trivial even for a stationary short-term sea state. The process of mooring line tension consists of wave and low frequencies and it is called a bimodal process. Jiao and Moan (1990) proposed a very accurate method to predict bimodal fatigue damage under the assumption of Gaussianity. Other combination rules have also been suggested and some of them are introduced in *Chapter 3*.

In *Paper 1*, the Jiao and Moan's method is modified by considering the non-Gaussian properties of both WF and LF mooring line tension induced by wave loads in an explicit way and the total fatigue damage is estimated by numerical integration since no analytical formula is envisaged. The effect of non-Gaussianity has been included for the LF fatigue damage estimation by consideration of the skewness and kurtosis of LF line tension. The WF fatigue damage is predicted by the closed-form solution of Morison-type forces where a simplified dynamic model (Larsen and Sandvik 1990) of the mooring lines has been applied.

The mooring analysis mentioned above is a decoupled analysis by which vessel motion responses are uncoupled with mooring system responses and the mean, WF and LF responses are also uncoupled. The coupling effect might be important especially for deep water systems

and coupled mooring analysis has been studied by Ormberg et al. (1997), Ormberg and Larsen (1997), Sødahl et al. (1996), Sagrilo et al. (2002), etc. Ormberg et al. (1998) discussed the accuracy and the efficiency of analysis methods with different levels of coupling effect.

2.5 A simplified model to determine dynamic mooring line tension

Mooring lines are slender structures and the line tension induced by WF vessel motions should be estimated by dynamic analysis considering drag and inertia forces acting on the line. Quasi-static analysis based on the catenary configuration of mooring line might not properly describe the WF response. Usually the FE method is applied in the time-domain analysis and mooring components are modelled as truss elements under only tensile loads. Time-domain methods of mooring line dynamics can include all of the nonlinear effects and can be carried out for coupled analysis. However, it is quite time-consuming especially for analysis under random wave loads where many simulations with long duration have to be performed to obtain the appropriate statistics of line tension.

A simplified model of dynamic tension induced by the WF vessel motions at the fairlead has been proposed by Larsen and Sandvik (1990) for one mooring line. This model captures the main features of drag and inertia forces induced by the WF motions of the line and expresses them in terms of a spring/damper system. The dynamic line tension is obtained by a single degree-of-freedom system and appears as a Morison-type force. Lie and Sødahl (1993) applied this model to estimate the extreme WF dynamic line tension and showed that the simplified model agrees reasonably well with the results obtained by time-domain simulations with an FE method. A brief description of the method is given in *Paper 7*. Although this simplified model was originally proposed to estimate extreme mooring line tension, it has been successfully applied to predict the LF damping from the mooring system.

As mentioned above, the method used to determine the fatigue damage of mooring lines under bimodal non-Gaussian loading in *Paper 1* is also directly established on the basis of this simplified dynamic model for the WF loading.

Chapter 3

Wide-band Fatigue Analysis

3.1 General

As mentioned above, fatigue damage induced by a random process of structural response is strongly dependent on the bandwidth parameter of its spectrum. However, it is impossible to theoretically obtain an exact relationship between the fatigue damage and the bandwidth parameter by a frequency-domain method for a general wide-band Gaussian process. Many researchers contributed to fatigue analysis of special wide-band processes like bimodal processes (Jiao and Moan 1990, etc.) or empirical modelling of wide-band fatigue damage (Dirlik 1985, Benasciutti and Tovo 2005, etc.).

On the other hand, fatigue analysis can also be carried out in the time domain by various cycle counting methods. Although it is very time-consuming, the rainflow cycle counting method normally gives the most accurate estimates among all of these methods.

In this chapter, several typical counting methods will be introduced first based on the time-domain description of the response. Then frequency-domain fatigue analysis will be addressed.

3.2 Time-domain fatigue analysis

Time-domain fatigue analysis is based on time series of stress and is only applicable when the time-varying response is available. As already mentioned, cycle counting methods can then be applied to all types of response time series, independent of the fundamental properties of the response. The counting algorithm is identical for narrow-band or wide-band, stationary or non-stationary, and Gaussian or non-Gaussian processes.

In fact, time-domain methods use only the information provided by the series of peaks (local maxima) and valleys (local minima). According to different principles for constructing the effective stress ranges from these identified peaks and valleys, various cycle counting methods are envisaged and their procedures are defined by e.g. ASTM (1985), including the peak counting, the range counting, the level-crossing counting and the rainflow counting.

The peak counting method identifies all peaks in the stress history and uses the peaks above a defined reference level to estimate the fatigue damage. The reference level corresponding to the mean stress is usually applied. If the effect of the mean stress is not considered, each stress range is then assumed to be twice the difference of each peak value minus the mean value. This method basically assumes a symmetric property centred at the mean value. However, not all of the peaks are positive for a general wide-band process and this fatigue damage estimate is based on the total number of all peaks, therefore, a quite conservative estimate is usually obtained by the peak counting method. Moreover, actual valleys should also be used in the cycle counting especially for asymmetric responses.

The range counting method considers a peak and the following valley as half a cycle of stress range as well as a valley and the following peak. The total fatigue damage is obtained as the sum of the damage from all of the half cycles by which a single half cycle is assumed to induce half value of the fatigue damage due to a complete load cycle with the same stress range. This method is established on the local load cycles and ignores the effect of global large load cycles. Therefore, it always underestimates the true wide-band fatigue damage.

Instead of using the values of peaks and valleys directly, the level-crossing counting method forms cycles of stress range based on the counting of up-crossings above and down-crossings below the mean value at fixed load levels usually defined with constant increments and centred at the mean value. All identified level-crossings are used to form the largest possible cycle first, followed by the second largest, and so on. This method takes the interaction between cycles into account and gives priority to large load cycles. It is actually equivalent to the narrow-band assumption which is demonstrated by Rychlik (1993) to be the upper bound of the expected fatigue damage.

The rainflow method was first proposed by Matsuishi and Endo (1968) and it is also known as the pagoda-roof method with its original version. This method has proved to be the most accurate method for estimating fatigue damage under random processes by e.g. Dowling (1972) and Watson and Dabell (1975). The rainflow counting algorithm is briefly described in the following.

We consider a stress time series of peaks and valleys with the time axis vertically downward as shown in Figure 3.1 and in this way the lines connecting peaks and valleys form a series of pagoda roofs. The rainflow method applies the following general rules to produce stress cycles.

- Each rainflow begins at the beginning of the time series and successively at the inside of every peak and valley.
- Rainflow initiating at a peak (or a valley) drops down until it reaches opposite a peak more positive (or a valley more negative) than the peak (or the valley) it started from.
- Rainflow also stops when it meets the rainflow from a roof above.
- Rainflow must terminate at the end of the time series.
- The horizontal length of each rainflow is counted as a half cycle with that stress range.

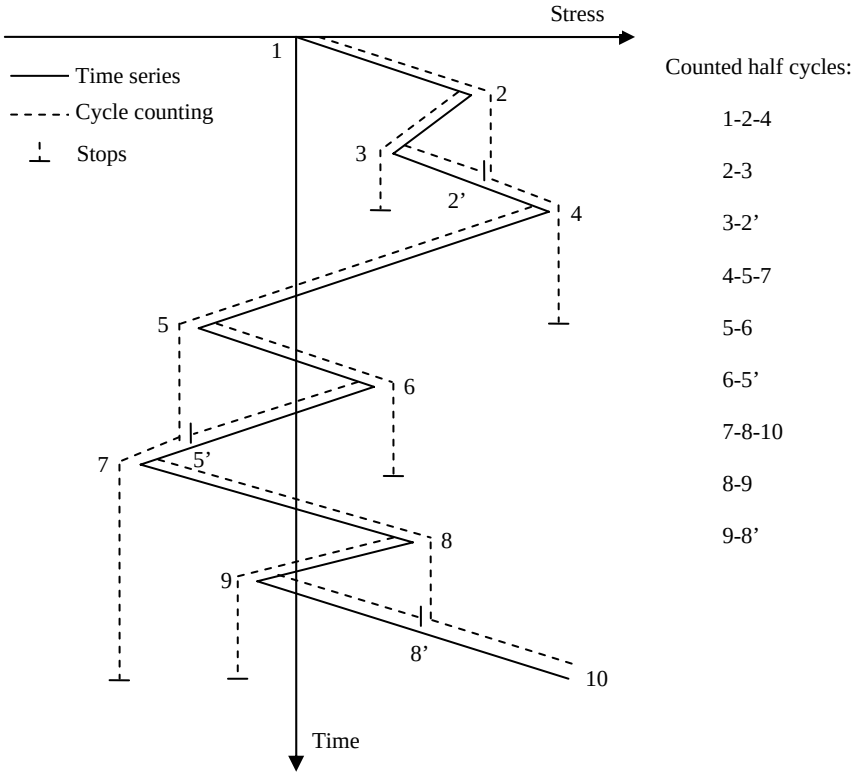

Figure 3.1 Illustration of the rainflow cycle counting method

As shown in Figure 3.1, the first rainflow starts from the beginning at 1 as a valley, the second one from the peak 2, the third one from the valley 3, and so on. The end at 10 is considered as a peak herein. There are totally 9 half cycles can be extracted from this time series.

The rainflow initiating at the valley 1 drops down at 2 and ends at 4 because the following valley 5 has smaller value than the initial point 1. Therefore, a half cycle of 1-2-4 has been identified. The same rule can be applied to determine the half cycle of 5-6.

The second rainflow starts from 2 and stops at 3, which leads to a half cycle of 2-3, because the following peak 4 has larger value than 2. Similarly, the half cycles of 4-5-7 and 8-9 can be extracted based on the same rule due to the largest peak at 10.

The half cycles of 3-2', 6-5' and 9-8' are determined because the rainflows started at 3, 6 and 9, respectively, meet the rainflows from roofs above.

The half cycle of 7-8-10 is formed because the time series ends at 10.

When all of the 9 half cycles have been identified, the horizontal length of each cycle is used as an effective stress range to calculate the fatigue damage based on e.g. the linear damage accumulation law.

This is the original proposal of the rainflow cycle counting algorithm (Matsuishi and Endo 1968). Other versions of the method can be found such as the 3-point algorithm (ASTM 1985), the 4-point algorithm (Amzallag et al. 1994) and the non-recursive definition proposed by Rychlik (1987). All these algorithms lead to the same results of fatigue damage. Therefore, no details of other versions are given herein.

Moreover, the time-domain rainflow results obtained in this thesis are based on Rychlik's definition by using the Matlab Toolbox – WAFO (The WAFO Group 2000).

In general, fatigue damage obtained by the counting methods described above have the following relationship (e.g. Tovo 2002),

$$D_{RC} \le D_{RFC} \le D_{LCC} (= D_{NB}) \le D_{PC} \tag{3.1}$$

where D_{RC}, D_{RFC}, D_{LCC} and D_{PC} represent the fatigue damage estimated by the range counting, the rainflow counting, the level-crossing counting and the peak counting methods, respectively, and D_{NB} denotes the narrow-band approximation.

3.3 Frequency-domain methods for multi-modal Gaussian processes

As mentioned above, time-domain analysis with cycle counting methods are extremely time-consuming especially for random fatigue analysis where a great number of time series of responses must be generated and analyzed. Frequency-domain methods are more computationally efficient. However, the most accurate method, the rainflow cycle counting

method, does not have a closed-form solution in the frequency domain for a general wide-band Gaussian process. In order to propose an accurate frequency-domain method, one must focus on the spectral type and start with particular random processes. Herein, multi-modal Gaussian processes are introduced first and methods for estimating the corresponding fatigue damage are discussed.

The multi-modal Gaussian process is a Gaussian process where the energy of the process concentrates at several well-separated frequencies and therefore the spectral density function shows multiple peaks. Bimodal processes are special cases of multi-modal processes where only two central frequencies can be identified. This kind of process occurs frequently in the responses of marine structures, e.g. mooring system response as discussed in *Chapter 2*, wave-induced and springing responses of tension leg platform (TLP) and large ships, etc. These responses mainly have one frequency component corresponding to the wave input and the other due to the resonance of flexible oscillations of the whole structure itself. Trimodal process could also be relevant for structural responses involving VIV as mentioned in *Chapter 1*. Examples of a bimodal and a trimodal Gaussian process are shown in Figures 3.2 and 3.3 with the Vanmarcke's bandwidth parameters of 0.62 and 0.73, respectively.

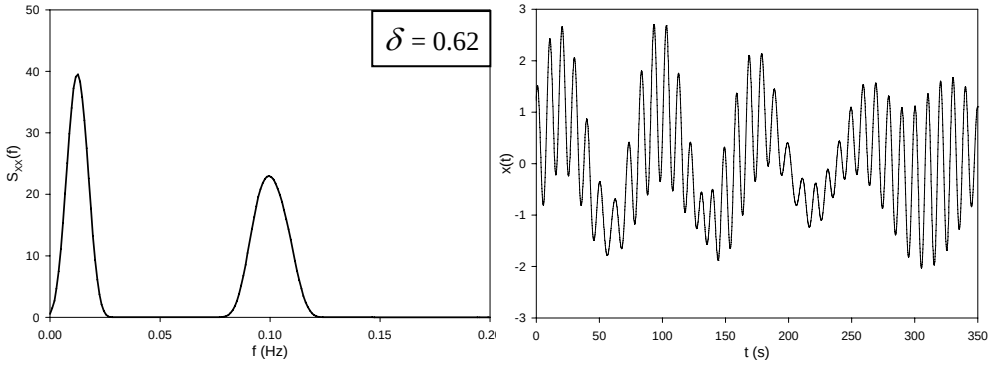

Figure 3.2 Example of a bimodal Gaussian process (Left: spectral density function; Right: time series.)

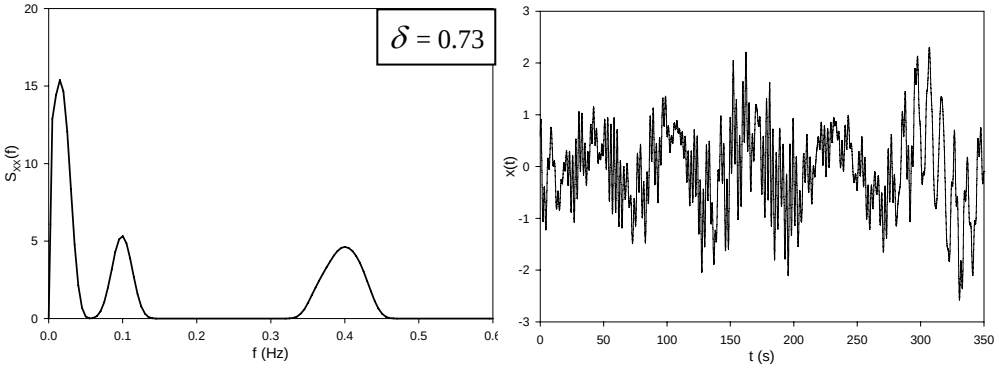

Figure 3.3 Example of a trimodal Gaussian process (Left: spectral density function; Right: time series.)

Often wide-band fatigue damage is expressed as a correction on the narrow-band approximation. However, for a bimodal process with a high frequency (HF) and a low frequency (LF), the rainflow algorithm extracts two types of load cycles: one is the large

cycles considering the interaction between the HF and LF components and the other is the small HF cycles only. Various methods for bimodal fatigue damage estimation under the Gaussian assumption have been proposed by many researchers, e.g. Jiao and Moan (1990), Sakai and Okamura (1995), Fu and Cebon (2000) and Benasciutti and Tovo (2007).

Jiao and Moan (1990) expressed the bimodal fatigue damage as the sum of the HF damage plus the damage induced by an equivalent process of the HF envelope plus the LF process. The number of small cycles is determined by the mean zero up-crossing rate of the HF component, while the number of large cycles is given by that of the equivalent process. They also showed that a closed-form solution could be approximately obtained when assuming that the LF component dominates. This method is very accurate especially for large LF contributions. A brief description of the theory is provided in *Paper 1*. Moreover, this method has already been adopted in offshore standards, such as ISO 19901-7 (ISO 2005), API RP 2SK (API 2005) and DNV OS-E301 (DNV 2004), to estimate the fatigue damage in mooring lines.

Sakai and Okamura (1995) estimated the bimodal fatigue damage as the sum of each narrow-band component. In this way the fatigue damage is usually underestimated since no interaction between two components is considered.

Fu and Cebon (2000) assumed that the number of large cycles is directly associated with the LF cycles, while that of small cycles is equal to the difference of the HF number and the LF number by keeping the total number of counted cycles as the same as that of the HF cycles. Meanwhile, the same stress range distributions of short and long period cycles are applied to estimate the fatigue damage as in Jiao and Moan's formula. This method normally overestimates the fatigue damage since the number of long period cycles is usually less than that of the LF cycles due to the presence of the HF envelope process.

Benasciutti and Tovo (2007) made an improvement on Fu and Cebon's method by using the mean zero up-crossing rate of the equivalent process to determine the number of long period cycles in the same manner as Jiao and Moan did, while keeping the number of small cycles unchanged. They also compared these methods as well as general methods for wide-band fatigue damage calculation with time-domain simulations. It is found that the single moment method originally proposed by Larsen and Lutes (1991), Benasciutti and Tovo's formula (Benasciutti and Tovo 2005), the modified Fu and Cebon's method as well as Jiao and Moan's method provide quite accurate estimates. But Jiao and Moan's method gives a damage correction factor which is larger than 1, when the process is close to a narrow-band one. However, in such a case, the narrow-band approximation is good enough and no correction factor needs to be applied on the estimation of fatigue damage.

Alternatively, explicit formulae, such as Lotsberg (2005), Huang and Moan (2006), etc., can be applied to estimate the bimodal fatigue damage by using individual damage. They are more practical and desirable for design purposes where the fatigue damage of individual components might be available. Some of these formulae have been introduced and assessed in *Paper 6*.

In addition, most of the frequency-domain methods were obtained for a single-slope SN curve (for instance with the slope parameter equal to 3, 5 and so on) and the accuracy was well documented. However, two-slope SN curves are frequently used for offshore structures and the corresponding accuracy of these methods needs to be checked as well. *Paper 6* deals with this problem. Methods of Jiao and Moan, Lotsberg, and Huang and Moan, have been extended by using a two-slope SN curve and new formulae have been derived for the corresponding bimodal fatigue damage estimation. The accuracy is also examined based on time-domain simulations.

The trimodal process is a generalization of the bimodal process. So far, no specific method has been proposed to estimate the resulting fatigue damage for such a process. Although it can be evaluated by general methods (see e.g. Dirlik 1985, Benasciutti and Tovo 2005, etc.) considering the trimodal process as a general wide-band process, it is of intrinsic value to start with the analysis of the trimodal process and the interaction between the three frequency components. Therefore, a novel method is proposed in *Paper 2* for estimating the trimodal fatigue damage under the Gaussian assumption. This method is actually an extension of Jiao and Moan's method originally derived for bimodal processes. The basic principle of the proposed method is illustrated in Table 3.1 for multi-modal Gaussian processes.

Table 3.1 Illustration of fatigue damage due to multi-modal Gaussian processes (In the table, $X_i(t)$, $R_i(t)$ and $P_i(t)$ represent the component processes, the Rayleigh amplitude processes and the equivalent component processes, respectively, 1...i denote the component number with decreasing frequencies and D denotes the fatigue damage.)

Gaussian process	Compo-nent	Total process	Equivalent component process for fatigue analysis	Fatigue damage
Narrow-band	$X_1(t)$	$X(t) = X_1(t)$	$P_1(t) = X_1(t)$	$D = D_{P1}$
Bimodal	$X_1(t)$ $X_2(t)$	$X(t) =$ $X_1(t) + X_2(t)$	$P_1(t) = X_1(t)$ $P_2(t) = R_1(t) + X_2(t)$	$D =$ $D_{P1} + D_{P2}$
Trimodal	$X_1(t)$ $X_2(t)$ $X_3(t)$	$X(t) =$ $X_1(t) + X_2(t) + X_3(t)$	$P_1(t) = X_1(t)$ $P_2(t) = R_1(t) + X_2(t)$ $P_3(t) = R_1(t) + R_2(t) + X_3(t)$	$D =$ $D_{P1} + D_{P2} + D_{P3}$
Multi-modal	$X_1(t)$ … $X_i(t)$	$X(t) =$ $X_1(t) + ... + X_i(t)$	$P_1(t) = X_1(t)$ … $P_i(t) = R_1(t) + ... + R_{i-1}(t) + X_i(t)$	$D =$ $D_{P1} + ... + D_{Pi}$

As shown in the table, the trimodal fatigue damage is estimated by defining three equivalent processes to model the load cycles with long, moderate and short periods, respectively. The damage is determined for each of the equivalent process and summed up. It is seen that the effect of the process with a short period load cycle (high frequencies) on the process with low frequencies has been taken into account. The stress range distributions of the equivalent processes are obtained by using the Rayleigh envelopes of narrow-band Gaussian processes. Meanwhile, the mean zero up-crossing rates are directly calculated by using the Rice formula (Rice 1944) since the explicit expressions of the three equivalent processes are available.

The procedure defined for trimodal fatigue damage estimation is quite general and is very easy to apply considering more general multi-modal processes as shown in Table 3.1.

3.4 Frequency-domain methods for general wide-band Gaussian processes

A general wide-band Gaussian process contains all frequency components and the process itself does not display any particular feature as shown by two examples in Figure 3.4 with the Vanmarcke's bandwidth parameters of 0.5 and 0.61, respectively. The corresponding power spectrum normally has a continuous density function and covers a wide range of frequencies.

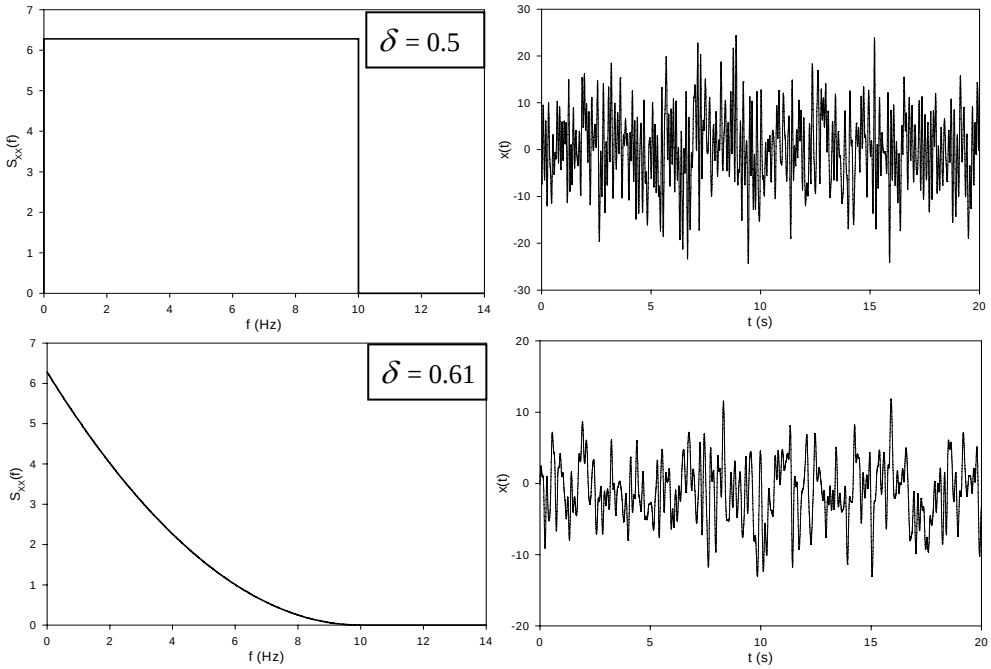

Figure 3.4 Two examples of general wide-band Gaussian processes (Left: spectral density functions; Right: time series.)

Before performing any fatigue analysis of a wide-band process, it is very important to calculate the bandwidth parameter first. As shown in *Paper 2* of this thesis, the narrow-band approximation is quite acceptable for a process whose bandwidth parameter is less than 0.5. For such cases, the narrow-band assumption will overestimate the fatigue damage by up to 20%. When the bandwidth parameter is less than 0.3, the error is 10% at most.

Frequency-domain methods for general wide-band fatigue analysis have been proposed by many researchers since the 1980s. They include Wirsching and Light (1980), Dirlik (1985), Gall and Hancock (1985), Larsen and Lutes (1991), Naboishikov (1991), Zhao and Baker (1992) and Benasciutti and Tovo (2005). Wide-band fatigue damage is normally expressed by an empirical correction term on the narrow-band result. Dirlik's empirical formula (DK, Dirlik 1985) and Benasciutti and Tovo's empirical formula (BT, Benasciutti and Tovo 2005) have been verified to be the best among empirical approximations of the rainflow counting method. Therefore, only the DK and BT formulae are introduced herein.

Dirlik (1985) proposed an approximate closed-form solution for the probability density function of effective rainflow stress ranges by using a combination of an exponential and two Rayleigh distributions. A large set of numerical simulations with various spectral shapes have been generated and a best fit has been performed to establish the empirical distribution. Fatigue damage can be obtained by the following closed-form expression,

$$D_{DK} = \frac{\nu_P T}{K}(2\sigma)^m (D_1 Q^m \Gamma(1+m) + (\sqrt{2})^m (D_2 R^m + D_3)\Gamma(1+\frac{m}{2})) \tag{3.2}$$

where σ is the standard deviation of the random process, ν_P is the mean rate of peaks, $\nu_P = \frac{1}{2\pi}\sqrt{\frac{m_4}{m_2}}$, T is the duration of interest, K and m are the material parameters of the SN curve, and $\Gamma()$ denotes the Gamma function. The parameters of D_1, D_2, D_3, Q and R are given as follows,

$$\begin{aligned} &\alpha_2 = \frac{m_2}{\sqrt{m_0 m_4}};\ X_m = \frac{m_1}{m_0}(\frac{m_2}{m_4})^{\frac{1}{2}};\ D_1 = \frac{2(X_m - \alpha_2^2)}{1+\alpha_2^2};\ R = \frac{\alpha_2 - X_m - D_1^2}{1-\alpha_2 - D_1 + D_1^2};\\ &D_2 = \frac{1-\alpha_2 - D_1 + D_1^2}{1-R};\ D_3 = 1 - D_1 - D_2;\ Q = \frac{1.25(\alpha_2 - D_3 - D_2 R)}{D_1} \end{aligned} \tag{3.3}$$

Recently, another empirical formula was proposed by Benasciutti and Tovo (2005). As shown by Inequality (3.1), the rainflow fatigue damage is bounded by the narrow-band approximation and the range counting method. Starting from this point, they proposed a formula of wide-band fatigue damage by using a linear combination of the narrow-band and range counting results which are easy to obtain by closed-form expressions in the frequency domain. The formula is given as the following equation,

$$D_{BT} = bD_{NB} + (1-b)D_{RC} = (b + (1-b)\alpha_2^{m-1})D_{NB} \tag{3.4}$$

where the coefficient b is empirically obtained based on extensive numerical simulations,

$$b = \frac{(\alpha_1 - \alpha_2)(1.112(1 + \alpha_1\alpha_2 - (\alpha_1 + \alpha_2))\exp(2.11\alpha_2) + (\alpha_1 - \alpha_2))}{(\alpha_2 - 1)^2} \tag{3.5}$$

where

$$\alpha_1 = m_1 / \sqrt{m_0 m_2}\,;\ \alpha_2 = m_2 / \sqrt{m_0 m_4} \tag{3.6}$$

Benasciutti and Tovo (2006) also compared the DK and BT formulae with other methods and they concluded that these two formulae predict the most accurate fatigue damage in comparison with the time-domain rainflow method. Although these two formulae were empirically derived based on different spectra, they gave quite similar results. Moreover, the BT method was found to be slightly more accurate than the DK method.

A great number of numerical simulations of various wave and wind induced responses of marine structures have also been generated in *Paper 2*. Accurate, but slightly underestimated fatigue damage is obtained by these two formulae when compared with the rainflow results.

The wide-band fatigue methods mentioned above are mainly based on empirism. It is also interesting to study the wide-band process itself and to investigate how the rainflow load cycles are obtained in the time domain.

As shown by the analysis procedure for an ideal trimodal process in *Paper 2*, three equivalent processes are successfully defined and used to approximate the rainflow fatigue damage. In this case, the theory of Jiao and Moan has been extended from bimodal Gaussian processes to trimodal processes and verified to give accurate results. It implies that this procedure could be further generalized for random processes with more modes. This multi-modal procedure could then be used to approximate the damage for a general wide-band process if these modes could be defined or identified for general processes. Therefore, in the same *Paper 2*, a novel method is proposed to estimate the fatigue damage of a general wide-band Gaussian process using a trimodal or even a multi-modal spectral formulation. The method requires an equal division of the wide-band spectrum into three segments with the same variances as illustrated in Figure 3.5.

An equivalent trimodal process is therefore defined by assuming each segment to be narrow-banded. The general wide-band fatigue damage can then be estimated in the same way as for an ideal trimodal process.

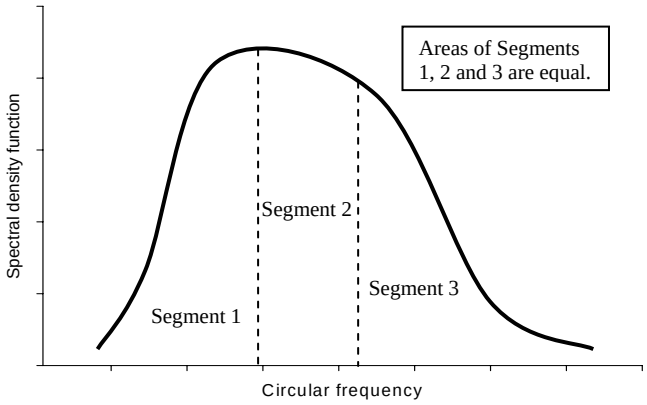

Figure 3.5 Division of a general wide-band spectral density function into three equal-variance segments

The proposed method has been applied to various spectral types of responses of marine structures as well as artificially defined wide-band spectra. The accuracy of the method has also been examined in *Paper 2*.

Herein, the accuracy of the proposed method as well as other frequency-domain methods are shown in Figures 3.6-3.8 considering ideal bimodal and trimodal spectra, general wide-band spectra defined by Dirlik (1985) and Benasciutti and Tovo (2005) and typical spectra of wave- and wind-induced linear structural responses, respectively. The results are represented as the ratios of fatigue damage obtained by the frequency-domain methods and by the time-domain rainflow cycle counting method. In addition, they are all expressed as a function of the Vanmarcke's bandwidth parameter defined in Equation (1.2).

The proposed method generally works well for ideal multi-modal Gaussian processes with large bandwidth parameters as shown in Figure 3.6, while it might overestimate the fatigue damage for bandwidth parameters less than 0.5 where the narrow-band approximation provides acceptable estimates. For general wide-band processes in Figure 3.7, the proposed method gives accurate estimates of fatigue damage with the bandwidth of 0.5-0.85 and over-predicts them with large bandwidth. However, the overestimation can be alleviated by dividing the wide-band spectrum into more segments, see *Paper 2*. In addition, as shown in Figure 3.8, typical spectra of linear wave- and wind-induced responses might have limited bandwidth and in this sense, the proposed method has practical usefulness with acceptable accuracy.

Empirical formulae of Dirlik and Benasciutti and Tovo predict the fatigue damage quite close to the rainflow results and in general, the accuracy are not dependent on the value of bandwidth, although they both slightly underestimate the fatigue damage for general wide-band processes and overestimate those of ideal multi-modal processes in some cases with extremely large bandwidth parameters.

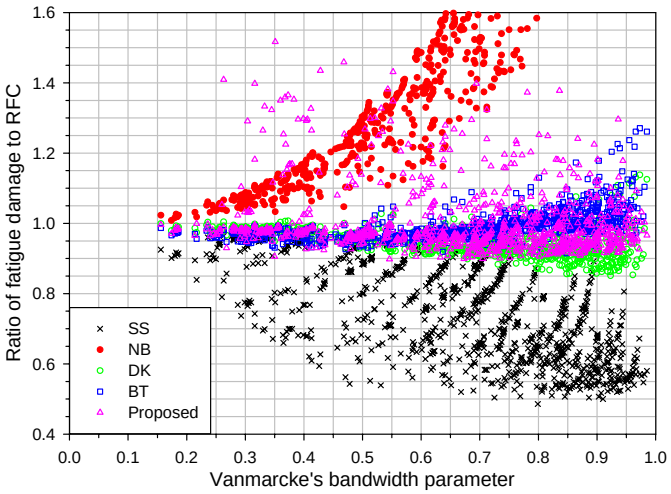

Figure 3.6 Ratio of fatigue damage of ideal bimodal and trimodal spectra to RFC as a function of bandwidth parameter ("RFC" – the rainflow cycle counting method, "SS" – the simple sum of the components, "NB" – the narrow-band approximation, "DK" – the Dirlik's formula, "BT" – the Benasciutti and Tovo's formula, "Proposed" – the proposed method. The NB ratios greater than 1.6 are not shown in the figure.)

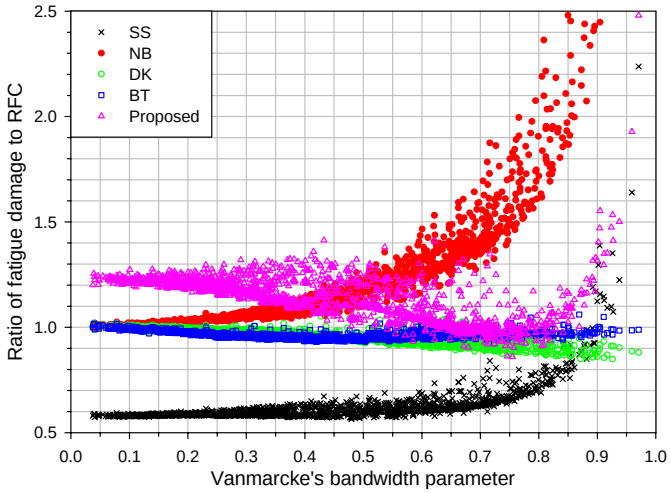

Figure 3.7 Ratio of fatigue damage of Dirlik's and Benasciutti and Tovo's spectra to RFC as a function of bandwidth parameter (The NB ratios greater than 2.5 are not shown in the figure.)

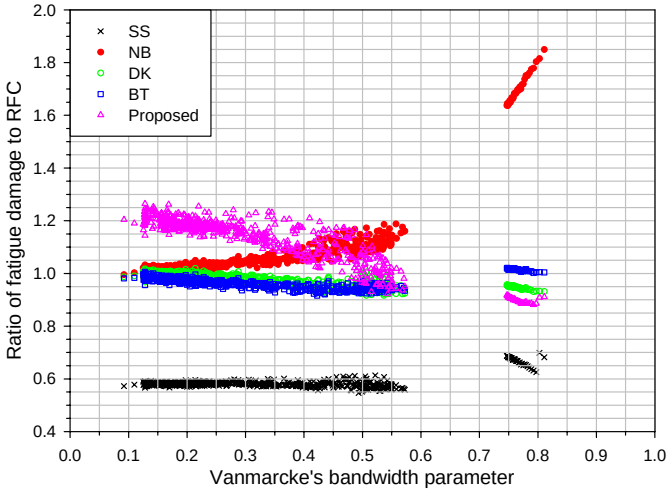

Figure 3.8 Ratio of fatigue damage of typical spectra of wave-induced (bandwidth of 0-0.6) and wind-induced (bandwidth of 0.7-0.9) responses to RFC as a function of bandwidth parameter

3.5 Effect of non-Gaussianity on fatigue

The wave-induced response of marine structures is often non-Gaussian due to the nonlinear environmental forces and/or the nonlinear properties of the structural system itself.

Although fatigue damage under non-Gaussain load can be estimated by the time-domain counting methods in the same straightforward manner as for Gaussian processes, they are difficult to obtain in the frequency domain, especially for wide-band processes.

Depending on the structural nonlinearity, non-Gaussianity may cause an increase in the fatigue damage estimates as compared with that based on the Gaussian assumption. For instance, the fatigue damage induced by the drag force can be 2.5 times the one under the Gaussian assumption, see Madsen et al. (1986). However, for slightly nonlinear responses like the HF springing response of a TLP, the non-Gaussian fatigue damage is only a few percent higher than the Gaussian one as indicated by e.g. Næss et al. (1994). Gao and Moan (2006) showed that the non-Gaussian fatigue damage due to the merely LF mooring response is about 1.3 times the Gaussian estimate for the sea state which contributes the most fatigue damage in a long-term period. Moreover, under particular conditions, the nonlinear fatigue damage is even smaller than that based on the Gaussian assumption of the Morison force, see Madsen et al. (1986) and Winterstein (1988).

Usually, a non-Gaussian process is often dealt with by considering it as a monotonic transformation of a Gaussian process. Parametric formulae are often used to define this kind of transformation. For example, a Hermite model has been adopted by Winterstein (1985 and 1988). Ochi and Ahn (1994) applied a monotonic exponential function, while Sarknai et al. (1994) used a power-law model. Non-parametric definition of the transformation has also been applied by e.g. Rychlik et al. (1997).

Higher order moments of the non-Gaussian random process like skewness and kurtosis are normally involved in the transformation and the fatigue damage is therefore estimated based on the evaluation of the effect of skewness and kurtosis, see Winterstein (1988) and Wang and Sun (2005). Most studies in this area were based on the assumption that the non-Gaussian process is narrow-banded.

As an example, Winterstein's model has been applied in *Paper 1*. The ratio of the non-Gaussian and Gaussian fatigue damage as a function of the kurtosis is given.

If the response nonlinearity can be explicitly expressed and the amplitude distribution can be obtained e.g. by a numerical integration, the non-Gaussian fatigue damage might be directly

calculated as shown in *Paper 1* where the LF mooring line tension is obtained based on Næss' approximation (Næss 1986) and the WF tension is expressed as a Morison-type force by using the simplified dynamic model (Larsen and Sandvik 1990), and finally the theory of Jiao and Moan has been extended to estimate the total fatigue damage when both the WF and LF line tension are non-Gaussian processes.

Chapter 4

Reliability and Risk Analyses

4.1 General

The safety of marine structures is normally assessed on the basis of a comparison of load effects due to environmental actions and structural resistance. Traditionally, the comparison was only made using the characteristic values of load effects and strength. However, a variety of uncertainties affect the estimate of random environmental loads on marine structures. In addition, structural strength is also subjected to uncertainties due to e.g. the variation of material and geometrical imperfection. Therefore, probability-based methods are more suited to evaluate the structural safety. The LRFD method frequently adopted in design of marine structures is a semi-probabilistic method by which the uncertainties are reflected in the recommended partial safety factors. Furthermore, detailed probabilistic modelling of loads and strength need to be established in order to perform a complete structural reliability analysis. In this way, a reliability problem should be formulated and the failure probability can be calculated to represent the corresponding safety level in a certain period.

In reliability analyses, only the failure probability of the considered structure due to normal uncertainties within a reference period of interest is calculated and the safety assessment is based on this quantity and no failure consequence is explicitly considered. However, most failures are initiated by human errors and developed into catastrophes if no correct actions are performed. For this reason, a broader approach of risk analysis should be applied to estimate the probability of undesirable events as well as their consequences. In particular, the risk analysis should include all causes of failure to the risk. However, it remains a challenge to estimate the probability of human errors that, say, cause mooring line failure when performing a risk analysis of mooring systems.

4.2 Structural reliability analysis

A reliability analysis starts with estimating uncertainties involved in the predictions of applied loads and structural strength. These uncertainties include physical uncertainty, e.g. the variation of environmental actions, statistical uncertainty, modelling uncertainty, etc. Among them, it is very important to assess the modelling uncertainty before any reliability calculation since any prediction of loads and even strength is based on a certain model which is just an approximation of the reality. The reliability estimate is strongly dependent on the accuracy and the quality of the adopted model.

For a time-invariant reliability problem, the load effects are assumed to be time-independent, and the uncertainty model of structural strength is given by the as-welded structure and also does not change during the period due to deterioration. In reality, both change with time. However, if only the load effects are considered to be varying with time and they can be represented by e.g. the extreme response in a period of interest rather than the dynamic response itself, the reliability problem can be solved in the same manner.

This analysis involves an estimation of failure probability defined as

$$P_f = P(R - S < 0) \tag{4.1}$$

where $P(A)$ expresses the probability of event A, and R and S are the resistance and load effect variables, respectively, $R - S$ is the failure function and $R - S < 0$ represents the event of structural failure.

In general, the load effects and resistance are expressed by a more detailed model by which all relevant random variables are collected in a vector $\mathbf{X}$. Therefore, Equation (4.1) could be written in a more general way as a multiple integral of the joint probability density function of random variables over the failure domain,

$$P_f = P(g(\mathbf{X}) < 0) = \int_{g(\mathbf{x})<0} f_{\mathbf{X}}(\mathbf{x}) d\mathbf{x} \tag{4.2}$$

where $g(\mathbf{X})$ is the failure function, $g(\mathbf{X}) < 0$ represents the failure domain and $f_{\mathbf{X}}(\mathbf{x})$ is the joint probability density function of $\mathbf{X}$.

The time-invariant reliability problem described above, can be solved by analytical methods such as the first and second order reliability methods (FORM and SORM) or simulation methods such as crude Monte Carlo simulation, simulations with variance-reduction techniques like Latin Hypercube simulation, importance sampling, etc., see, for example, Thoft-Christensen and Baker (1982), Madsen et al. (1986), Melchers (1987).

Time-variant reliability analysis deals with the problem when the structural resistance varies with time as well. Marine structures are exposed to sea environment conditions and subjected to deteriorations due to e.g. corrosion. The structural strength obviously decreases when it is corroded. Time-variant reliability analysis of marine structures has been studied by e.g. Hagen and Tvedt (1991), Marley and Moan (1992), and Ayala-Uraga and Moan (2007).

4.3 Reliability analysis of mooring systems

Mooring reliability has been thoroughly studied in the DEEPMOOR project considering the ULS, FLS and ALS (Mathisen et al. 1998, Mathisen et al. 1999a and Mathisen et al. 1999b). Analyses were carried out for two types of offshore structures i.e. FPSOs and semi-submersibles, for two sets of environmental conditions i.e. on the Norwegian continental shelf and in the Gulf of Mexico, for various water depths from 70m to 2000m, and for different mooring components such as chain links and steel wire ropes. Partial safety factors in semi-probabilistic design equations of mooring lines have been recommended and calibrated by the reliability analyses. These safety factors are now adopted in the offshore standard DNV OS-E301 (DNV 2004).

As considered in the DEEPMOOR project, overload and fatigue reliability analyses are normally carried out for mooring components. Meanwhile, a mooring system usually consists of multiple mooring lines and a systems reliability approach needs to be applied. Moreover, long-term reliability of mooring systems is established on the assumption of piece-wise stationary short-term sea states and is solved by a nested reliability analysis (Wen and Chen 1987) where the long-term mooring line tension is modelled by e.g. the response surface method as a function of environmental variables such as significant wave height, spectral peak period, mean wind and current velocities, which characterize short-term conditions. While the strength model is normally considered to be time-invariant and the failure probability corresponding to a long-term period is calculated based on the formulation of a series system of sea states and conditional on the strength values.

Reliability analysis of mooring systems has been also studied by other researchers, e.g. Luo and Ahilan (1991), Larsen and Mathisen (1996) and Snell et al. (1999). In most of mooring reliability analyses, mooring line strength is modelled by considering the whole line as a series system and it is assumed to be time-invariant through the entire period of interest. In reality, mooring lines are subjected to various degrading mechanisms such as sea water corrosion for partially and fully submerged components, wear at the fairlead and friction at sea bottom. As a result, the strength decreases with respect to time. It is important to take this

effect into account by a time-variant reliability formulation especially for permanent moorings. Moreover, degrading mechanisms are normally subjected to large uncertainties. For example, many long-term tests on sea water corrosion show a significant variation of corrosion rate. Recently, the chain corrosion in the condition of continuous immersion has been discussed by Melchers et al. (2007). This uncertainty also needs to be considered in the strength estimation of degrading mooring lines.

Paper 4 of this thesis deals with the time-variant reliability analysis of the mooring system due to corrosion deterioration. A probabilistic corrosion model proposed by Melchers (1995) is applied to represent the material loss of chain links and the strength distribution is obtained based on the corroded mooring line. Time-variant overload reliability has been calculated by a piece-wise constant formulation from year to year. The high corrosion rate for chain links in the splash zone has a significant effect on the increase of failure probability with time.

4.4 Aspects of risk analysis

Compared with the structural reliability analysis, a risk analysis is a more thorough way to assess the safety to persons, environment and assets. The basic idea of a risk analysis is to combine the probability of accidental events with the consequences of them (Vinnem 1999),

$$Risk = \sum P_i * C_i \tag{4.3}$$

where P_i and C_i express the probability and the consequence of accident No. i, respectively.

Risk assessment analyzes all causes of failure as well as all possible consequences. The causes of failure include accidental loads such as ship impacts or abnormal resistance such as fabrication defects and corrosion fatigue. These causes are mainly due to human errors which could be very difficult to analyze and quantify theoretically. Quantitative measures can only be achieved by collected data. The consequences are ultimately related to personnel, environmental damage and loss of assets. Normally, qualitative or quantitative methods are used for both cause and consequence analyses.

For a mooring system, the failure consequences are those directly induced by loss of position of the floating structure due to mooring line failure, and include for instance oil leakage from broken risers, drilling blowouts and collision with other structures in the vicinity. Mooring risk analysis has been touched upon by e.g. Stiff et al. (2003), Mathisen and Larsen (2004) and Petruska et al. (2007). Moreover, after Hurricane Ivan, Katrina and Rita moved through

the Gulf of Mexico in 2004 and 2005, API issued an interim document (API RP 95F (API 2007)) to provide some guidelines for the safety assessment of mobile offshore drilling unit (MODU) mooring systems, including the simplified risk assessment.

As indicated above, the residual strength of a mooring system with one or more lines failed is very important to the safety of the floating structure. The most recent design codes require ALS checks of the residual strength after failure of one line. This is a practical system requirement for overall risk assessment with respect to free floating of the structure and possible riser failure. In service, it might take some time to have the failed line identified, repaired or replaced and meanwhile, the floating structure needs to be kept functioning in this damaged condition. *Paper 5* of this thesis deals with analyses of steady-state responses of the mooring system of a semi-submersible when one mooring line is failed. The effect of mooring line failure on the predictions of extreme value and fatigue damage has been illustrated. Although the paper does not perform a complete risk analysis, the obtained information is useful for judging the safety of the whole system.

Moreover, the safety of marine structures is very sensitive to the environmental condition they are exposed to, especially in partially damaged conditions. The variation of environmental conditions is significant e.g. from season to season and even from year to year, as reported in *Paper 3* and *Extension 1*. Annual wave data of 29 years at a site in the Northern North Sea provided by Statoil ASA are applied in analyses of the linear responses of typical marine structures like FPSO and semi-submersible in *Paper 3*. Groups of 2-year and 4-year scatter diagrams have also been used to evaluate the effect of statistical uncertainty on the prediction of structural responses. Seasonal wave data are used for structural analysis of the mooring system as well as the FPSO and semi-submersible in *Extension 1* and the sensitivity of the response to these environmental data has been analyzed.

Chapter 5

Conclusions and Recommendations for Future Work

5.1 Conclusions

Many issues related to mooring analysis have been studied in this thesis, including fatigue damage induced by non-Gaussian mooring line tension, time-variant reliability analysis of corroded mooring lines, mooring analysis in damaged conditions and mooring line damping.

Fatigue damage estimation of mooring lines due to bimodal non-Gaussian tension has been dealt with in *Paper 1*. Based on the Jiao and Moan's theory, an efficient frequency-domain method has been proposed and verified by time-domain analysis of a simplified, but accurate mechanical model.

A total of 16 sea states have been analyzed both in the frequency and time domains. The WF mooring line tension is found to be slightly non-Gaussian and have a skewness of zero for moderate sea states, while the LF tension typically has a positive skewness and a kurtosis of more than three. The statistical properties of both the WF and LF mooring line tension are numerically obtained by the frequency-domain method and agree very well with the time-domain results. The estimated frequency-domain fatigue damage of the WF, LF and combined line tension has been compared with the rainflow counting results. The maximum relative error is about 11-13% in fatigue damage estimates. This implies that the accuracy of the proposed method is acceptable for estimating the bimodal non-Gaussian fatigue damage in practice. Moreover, the mooring line tension is mainly dominated by the WF component in the case studies. Although the non-Gaussian property of the short-term fatigue damage becomes more significant for more severe sea states, the long-term fatigue estimate is quite close to the Gaussian result because the moderate sea states contribute most to the total fatigue damage, see *Paper 1*.

Paper 4 deals with time-variant reliability analysis of mooring systems considering the ULS for degrading chain links by applying a probabilistic corrosion model.

It is found that although the number of chain links in the splash zone is small, the corrosion rate in this area is quite high. This degradation is found to have a significant influence on the strength of the whole mooring line. Time-variant reliability analyses have been performed by approximating the mooring line strength as a constant for each year. The predicted annual failure probability increases significantly due to corrosion over years. In the worst case, the predicted safe service life, corresponding to an annual acceptable failure probability of 10^{-4}, is about 12.5 years considering the ULS, while the original design life is about 20 years without the corrosion effect.

As already mentioned, from a risk analysis perspective, it is interesting to know the performance of a mooring system after failure of one line. Extensive long-term mooring analyses of extreme values and fatigue damage with annual and seasonal scatter diagrams of thirty years of the Northern North Sea have been carried out and reported in *Paper 5* and *Extension 1* considering different mooring configurations. Response estimates are obtained for the intact and damaged conditions.

Based on the 30-year data, the annual extreme line tension is found to increase by 80% and by 115% in the worst cases after failure of one line for the 16-line and 12-line systems, respectively, while the annual fatigue damage can increase by 225% and 350%. On the average, increases of 25% and 70% in the annual extreme tension and in the total fatigue damage due to failure of one line are obtained and the fatigue damage is found more sensitive to failure.

Moreover, for the prediction of long-term extreme mooring tension, simplified analyses based on the contour line method have been compared with the full long-term analyses and a quantile of 70% of the short-term extreme value of dynamic tension is found to yield accurate the long-term (annual) extreme estimates.

In *Paper 7*, a practical simple approach to estimate the damping of LF vessel motions from the mooring system has been proposed. The simplified dynamic model has been successfully applied to predict the line damping coefficients, including possible coupling between surge and sway. As compared with the coefficients obtained by the time-domain simulations, this frequency-domain method predicts a damping coefficient which is 30% smaller for each mooring line and about 20% smaller for the whole mooring system. These results imply a slightly conservative estimate of the LF vessel motions.

Case studies of mooring analysis in this thesis are carried out based on a limited set of catenary systems for a semi-submersible. The results obtained herein in terms of numbers might not be directly applicable to other mooring systems, like taut-line systems or other offshore structures, like FPSOs. It is certainly desirable to do more work in this connection.

The effect of the variation of annual and seasonal sea conditions on other structural responses of e.g. an FPSO and a semi-submersible has also been illustrated in *Paper 3* and *Extension 1*.

The annual extreme value of the significant wave height is found to vary by a factor of 1.6. This factor is defined as the maximum value divided by the minimum value of the annual extremes based on the sea data of 30 individual years. The predicted 20-year extreme value varies by a factor of 1.7 for the mid-ship bending moment of the FPSO and 1.5 for the stresses on a brace-column joint of the semi-submersible, while the obtained annual fatigue damage varies by a factor of 4.3 and 1.9 for the FPSO and the semi-submersible, respectively. The corresponding factor for the mooring line tension is found to be 1.9 and 2.0 for the annual extreme mooring line tension of the 16-line and 12-line systems, respectively, while the factor for the annual fatigue damage is 4.4 and 4.5, respectively. The variation in annual loading has a correspondingly significant influence on the safety of marine structures.

As shown in *Extension 1*, the winter data contribute most to the annual extreme value of significant wave height as well as to both the predictions of extreme structural responses and corresponding fatigue damage.

Various aspects of frequency-domain methods for prediction of wide-band fatigue damage have been investigated, considering both single- and two-slope SN curves.

Since fatigue analysis of wide-band load processes with frequency-domain methods previously have only considered single-slope SN curves, it is necessary to validate such methods for two-slope SN curves. In *Paper 6*, therefore, several methods for determining the bimodal Gaussian fatigue damage have been generalized to the calculation with two-slope SN curves. New formulae of fatigue damage have been derived and the accuracy has been examined by the rainflow counting method.

In general, the frequency-domain methods predict conservative fatigue estimates in most cases. Among them, the fatigue damage obtained by Jiao and Moan's method and by Huang and Moan's formula with the bandwidth correction factor proposed by Benasciutti and Tovo, agree very well with the rainflow results. Huang and Moan's formula with the regularity correction factor predicts conservative fatigue damage for ideal bimodal processes, while the

DNV formula always overestimates the damage and might only be suitable for processes with well-separated high and low frequencies.

A novel method for trimodal Gaussian fatigue damage estimation has been proposed in *Paper 2*. This method is developed based on the theory of Jiao and Moan for bimodal processes by use of the envelopes of the narrow-band frequency components. The generalization of the method for multi-modal processes has also been illustrated. Furthermore, the method has been developed to estimate fatigue damage for more general wide-band processes by using a trimodal (or even a multi-modal) spectral formulation.

The accuracy of the proposed method and other general frequency-domain methods has been checked by comparison with the rainflow results. As long as the trimodal process is not dominated by the LF component and the three frequency components are well separated, the proposed method predicts the fatigue damage quite close to the rainflow results. Both the empirical formulae proposed by Dirlik and by Benasciutti and Tovo are also found to give accurate estimates of the trimodal fatigue damage.

More general wide-band processes have been simulated by considering spectra relevant for typical responses in offshore structures induced by waves and wind and generally defined spectra. It is found that the bandwidth parameter gives quite important information for fatigue analysis. If the Vanmarcke's bandwidth parameter is less than 0.5, the narrow-band assumption can very well be used to estimate the wide-band fatigue damage, since a maximum 30% overestimation is expected. If the bandwidth parameter is in the range of 0.5-0.85, the proposed method predicts accurate fatigue damage compared with the rainflow results on average. For bandwidth parameters greater than 0.85, it might significantly overestimate the fatigue damage. However, such cases are not very relevant in practice. Moreover, it has been shown that more accurate estimates can be obtained by using a spectral formulation with more modes to cover the broad-band processes. The empirical formulae of Dirlik as well as Benasciutti and Tovo give quite accurate fatigue damage estimates for all of the spectral shapes and bandwidth parameters considered herein.

5.2 Recommendations for future work

Mooring analysis performed in this thesis is mainly based on separate analyses of WF and LF vessel motions and the assumption of independence has to be made for estimating the combined mooring line tension. In reality, both high values of the WF and LF tension are expected to occur not simultaneously but closely in time due to the same large wave groups.

Although the two fundamental WF and LF processes are not likely to be highly correlated because of the periodical effect, the amplitudes of both processes might be so. Further work is needed to determine such correlation coefficient. Alternatively, it is better to perform a coupled analysis normally applied in the time domain. However, considering the computational effort, an efficient coupled analysis applicable in the frequency domain is more desirable. More work needs to be done on such methods.

The damping of LF vessel motions is crucial for the assessment of the safety of mooring systems. Mooring line damping has been discussed herein. Accurate and efficient methods for estimating the damping from other sources, like the viscous force acting on the vessel, is required, since the current procedure is still based on empirical estimates or model tests.

Mooring chains are not only subjected to sea water corrosion, but also other types of deterioration like wear at the fairlead, friction on sea bottom and crack growth. Since the mooring line is formulated as a series system, it is important to study and consider all of the mechanisms of degradation to determine the line strength. Moreover, corrosion is a very complicated phenomenon itself and involves a number of uncertainties. More data of in situ measurements and tests are needed to estimate corrosion rates and to validate corrosion models.

In order to make a thorough safety assessment of mooring systems, a full risk analysis should be aimed at where failures of mooring lines (or the whole system) due to abnormal loads or resistance should be carefully examined and possible consequences should be identified accordingly. Mooring risk analysis certainly needs more research. The information gained from the mooring analyses in the damaged conditions as obtained in this work can be combined with the uncertainties about failure of one or more lines due to abnormal causes towards the aim of obtaining an estimate of the risk.

The mooring system of a semi-submersible is analyzed in this thesis. Mooring systems of other marine structures such as WECs, wind turbine platforms and fish farms, might be quite different from those of floating vessels used in the offshore oil and gas industries. Research work remains to be done regarding analysis and design of mooring for these structures. For instance, for an energy absorption device, the effect of the mooring system on the efficiency of energy capture should be assessed as well, while for a flexible floating structure, a fully coupled analysis would be more appropriate to apply in order to obtain the proper behavior of the whole system including mooring lines.

Other station-keeping systems have been used as well in industry, e.g. DP systems and thruster-assisted mooring systems, and the corresponding safety issues need to be studied. For

mooring system with thrusters, a high level of uncertainty might be involved in the performance of thrusters in waves and it is of great significance to study these effects on the overall performance and safety of such system.

A method based on the trimodal spectral formulation has been proposed to estimate wide-band fatigue in this work with a main focus on Gaussian processes. It is expected that the proposed method can also be applicable to non-Gaussian processes, but the accuracy of the method needs to be investigated.

References

Amzallag, C., Gerey, J.P., Robert, J.L. & Bahuaud, J. (1994) Standardization of the rainflow counting method for fatigue analysis. International Journal of Fatigue; Vol. 16, pp. 287-293.

API (2005) Recommended practice for design and analysis of stationkeeping systems for floating structures. API RP 2SK.

API (2007) Gulf of Mexico MODU Mooring Practices for the 2007 Hurricane Season - Interim Recommendations. API RP 95F.

Aranha, J.A.P. & Pinto, M.O. (2001) Dynamic tension in risers and mooring lines: an algebraic approximation for harmonic excitation. Applied Ocean Research; Vol. 23, pp. 63-81.

ASTM (1985) Standard practices for cycle counting in fatigue analysis. Designation E 1049-85.

Ayala-Uraga, E. & Moan, T. (2007) Time-variant reliability assessment of FPSO hull girder with long cracks. Journal of Offshore Mechanics and Arctic Engineering; Vol. 129, pp. 81-89.

Battjes, J.A. (1977) Probabilistic aspects of ocean waves. Proceedings of Safety of Structures under Dynamic Loading. Trondheim, Norway.

Bauduin, C. & Naciri, M. (2000) A contribution on quasi-static mooring line damping. Journal of Offshore Mechanics and Arctic Engineering; Vol. 122, pp. 125-133.

Benasciutti, D. & Tovo, R. (2005) Spectral methods for lifetime prediction under wide-band stationary random processes. International Journal of Fatigue; Vol. 27, pp. 867-877.

Benasciutti, D. & Tovo, R. (2006) Comparison of spectral methods for fatigue analysis of broad-band Gaussian random processes. Probabilistic Engineering Mechanics; Vol. 21, pp. 287-299.

Benasciutti, D. & Tovo, R. (2007) On fatigue damage assessment in bimodal random processes. International Journal of Fatigue; Vol. 29, pp. 232-244.

Bouyssy, V., Naboishikov, S.M. & Rackwitz, R. (1993) Comparison of analytical counting methods for Gaussian processes. Structural Safety; Vol. 12, pp. 35-57.

Brown, D.T. & Mavrakos, S. (1999) Comparative study on mooring line dynamic loading. Marine Structures; Vol. 12, pp. 131-151.

Chakrabarti, S.K. (1984) Steady drift force on vertical cylinder – viscous vs. potential. Applied Ocean Research; Vol. 6, No. 2, pp. 73-82.

Chakrabarti, S.K. (2005) Handbook of offshore engineering. Elsevier Publishers, UK.

Chen, H., Moan, T. & Verhoeven, H. (2006a) Critical barriers to prevent loss of position. Proceedings of the European Safety and Reliability Conference, Lisbon, Portugal.

Chen, H., Moan, T. & Verhoeven, H. (2006b) Critical DGPS failure on the Norwegian Continental Shelf. Proceedings of the European Safety and Reliability Conference, Lisbon, Portugal.

Chen, H., Moan, T. & Verhoeven, H. (2007) Safety of dynamic positioning operations on mobile offshore drilling rigs. Submitted to Journal of Reliability Engineering and Systems Safety.

Dirlik, T. (1985) Application of computers in fatigue. Ph.D. Thesis, University of Warwick.

DNV (2004) Offshore Standard - Position Mooring. DNV OS-E301.

Dowling, N.E. (1972) Fatigue-failure predictions for complicated stress-strain histories. American Society for Testing and Materials, Journal of Materials; Vol. 7, No. 1, pp. 71-87.

Downie, M.J., Graham, J.M.R., Zhao, Y.D. & Zhou, C.Y. (1995) The viscous damping of a submerged pontoon undergoing forced combined motions in the presence of a weak current. International Journal of Offshore and Polar Engineering; Vol. 5, No.4, pp. 236-241.

Faltinsen, O.M. (1990) Sea loads on ships and offshore structures. Cambridge Ocean Technology Series. Cambridge University Press, UK.

Fu, T.T. & Cebon, D. (2000) Predicting fatigue lives for bi-modal stress spectral densities. International Journal of Fatigue; Vol. 22, pp. 11-21.

Gall, D.S. & Hancock, J.W. (1985) Fatigue crack growth under narrow and broad band stationary loading. Marine Technology Centre, Glasgow University.

Gao, Z. & Moan, T. (2006) Wave-induced fatigue damage of mooring chain under combined non-Gaussian low and wave frequency loads. Proceedings of the 25th International Conference on Offshore Mechanics and Arctic Engineering, Hamburg, Germany; Paper No. OMAE2006-92389.

Graham, J.M.R. (1980) The forces on sharp-edged cylinder in oscillatory flow at low Keulegan-Carpenter numbers. Journal of Fluid Mechanics; Vol. 97, pp. 331-346.

Hagen, O. & Tvedt, L. (1991) Vector process out-crossing as a parallel system sensitivity measure. American Society of Civil Engineers, Journal of Engineering Mechanics; Vol. 117, No. 10, pp. 2201-2220.

Hermans, A.J. (1991) Second order wave forces and wave drift damping. Ship Technology Research; Vol. 38, pp. 163-172.

Huang, W. & Moan, T. (2006) Fatigue under combined high and low frequency loads. Proceedings of the 25th International Conference on Offshore Mechanics and Arctic Engineering, Hamburg, Germany; Paper No. OMAE2006-92247.

Huse, E. (1991) New development in prediction of mooring system damping. Proceedings of the Offshore Technology Conference, Houston; Paper No. 6593.

ISO (2005) Petroleum and natural gas industries - Specific requirements for offshore structures - Part 7: Stationkeeping systems for floating offshore structures and mobile offshore units. ISO 19901-7.

Jiao, G. & Moan, T. (1990) Probabilistic analysis of fatigue due to Gaussian load processes. Probabilistic Engineering Mechanics; Vol. 5, No. 2, pp. 76-83.

Johanning, L., Smith, G.H. & Wolfram, J. (2006) Mooring design approach for wave energy converters. Proceedings of the Institution of Mechanical Engineers – Part M – Journal of Engineering for the Maritime Environment; Vol. 220, No. 4, pp. 159-174.

Kwan, C.T. & Bruen, F.J. (1991) Mooring line dynamics – comparison of time domain, frequency domain, and quasi-static analyses. Proceedings of the Offshore Technology Conference, Houston; Paper No. 6657.

Larsen, C.M. & Fylling, I.J. (1982) Dynamic behaviour of anchor lines. Norwegian Maritime Research; Vol. 10, No. 3, pp. 18-32.

Larsen, K. & Huse, E. (1993) Practical procedures for estimation of viscous scale effects in model testing of floating structures. Proceedings of the 3rd International Offshore and Polar Engineering Conference, Singapore.

Larsen, C.E. & Lutes, L.D. (1991) Predicting the fatigue life of offshore structures by the single-moment spectral method. Probabilistic Engineering Mechanics; Vol. 6, No. 2, pp. 96-108.

Larsen, K. & Mathisen, J. (1996) Reliability-based mooring design for a drilling semisubmersible. Proceedings of the 6th International Offshore and Polar Engineering Conference, Los Angeles, California; Vol. IV, pp. 457-466.

Larsen, K. & Sandvik, P.C. (1990) Efficient methods for the calculation of dynamic mooring line tension. Proceedings of the 1st European Offshore Mechanics Symposium, Trondheim.

Lie, H. (2006) Improved mooring analysis for mobile offshore units. Presented at the Conference on Dynamic Positioning and Anchoring of Floating Installations, Bergen, Norway.

Lie, H. & Sødahl, N. (1993) Simplified dynamic model for estimation of extreme anchorline tension. Offshore Australia.

Lindahl, J. & Sjoberg, A. (1983) Dynamic analysis of mooring cables. Report Series A: 9, Deparment of Hydraulics, Chalmers University of Technology.

Liu, Y.G. & Bergdahl, L. (1998) Improvements on Huse's model for estimating mooring cable induced damping. Proceedings of the 17th International Conference on Offshore Mechanics and Arctic Engineering, Lisbon, Portugal; Paper No. OMAE98-0353.

Liu, Y.G. & Bergdahl, L. (1997) Frequency-domain dynamic analysis of cables. Engineering Structures; Vol. 19, No. 6, pp. 499-506.

Lotsberg, I. (2005) Background for revision of DNV-RP-C203 fatigue analysis of offshore steel structure. Proceedings of the 24th International Conference on Offshore Mechanics and Arctic Engineering, Halkidiki, Greece; Paper No. OMAE2005-67549.

Luo, W. & Ahilan, R.V. (1991) Mooring safety assessment using reliability techniques. Proceedings of the Offshore Technology Conference, Houston; Paper No. 6783.

Madsen, H.O., Krenk, S. & Lind, N.C. (1986) Methods for Structural Safety. Prentice-Hall, New Jersey.

MARINTEK (2003) User's Documentation Mimosa, Version 5.7. Report No. 516413.00.01.

Marley, M.J. & Moan, T. (1992) Time variant formulation for fatigue reliability. Proceedings of the 11th International Conference on Offshore Mechanics and Arctic Engineering, Alberta, Canada; Paper No. OMAE92-1203.

Mathisen, J., Hørte, T., Larsen, K. & Sogstad, B. (1998) DEEPMOOR - Design Methods for Deep Water Mooring Systems, Calibration of an Ultimate Limit State. DNV Report No. 97-3583.

Mathisen, J., Hørte, T., Lie, H. & Sogstad, B. (1999a) DEEPMOOR - Design Methods for Deep Water Mooring Systems, Calibration of a Progressive Collapse Limit State. DNV Report No. 97-3581.

Mathisen, J., Hørte, T., Moe, V. & Lian, W. (1999b) DEEPMOOR - Design Methods for Deep Water Mooring Systems, Calibration of a Fatigue Limit State. DNV Report No. 98-3110.

Mathisen, J. & Larsen, K. (2004) Risk-based inspection planning for mooring chain. Journal of Offshore Mechanics and Arctic Engineering; Vol. 126, pp. 250-257.

Matsuishi, M. & Endo, T. (1968) Fatigue of metals subjected to varying stress. Presented to the Japan Society of Mechanical Engineers, Fukuoka, Japan.

Melchers, R.E. (1987) Structural Reliability: Analysis and Prediction. Ellis Horwood, UK.

Melchers, R.E. (1995) Probabilistic modeling of seawater corrosion of steel structures. Proceedings of the 7th International Conference on Applications of Statistics and Probability in Civil Engineering, Paris; Vol. 1, pp. 265-270.

Melchers, R.E., Moan, T. & Gao, Z. (2007) Corrosion of working chains continuously immersed in seawater. Journal of Marine Science and Technology; Vol. 12, No. 2, pp. 102-110.

Meling, T.S., Johannessen, K., Haver, S. & Larsen, K. (2000) Mooring analysis of a semi-submersible by use of IFORM and contour surfaces. Proceedings of the 19th Conference on Offshore Mechanics and Arctic Engineering, New Orleans; OMAE 2000/OSU OFT-4141.

Miner, M.A. (1945) Cumulative damage in fatigue. Journal of Applied Mechanics; Vol. 12, pp. 159-164.

Molin, B. (1993) Second-order hydrodynamics applied to moored structures. Nineteenth WEGEMT School, Numerical simulation of hydrodynamics: ships and offshore structures.

Naboishikov, S. (1991) On the distribution of local extremes, ranges and means of Gaussian processes. Proceedings of the 4th IFIP WG 7.5 Conference, Munich; pp. 305-312.

Newman, J.N. (1993) Wave-drift damping of floating bodies. Journal of Fluid Mechanics; Vol. 249, pp. 241-259.

Nordenstrøm, N. (1971) Methods for predicting long term distributions of wave loads and probability of failure for ships, Part 1, Environmental conditions and short term response. DNV Report No. 71-2-S.

Næss, A. (1986) The statistical distribution of second-order slowly-varying forces and motions. Applied Ocean Research; Vol. 8, No. 2, pp. 110-118.

Næss, A., Berstad, A.J. & Moen, L.A. (1994) Stochastic fatigue analysis of the tethers of a tension leg platform. Proceedings of the 2nd International Conference on Computational Stochastic Mechanics, Athens, Greece.

Ochi, M.K. & Ahn, K. (1994) Probability distribution applicable to non-Gaussian random processes. Probabilistic Engineering Mechanics; Vol. 9, pp. 255-264.

Ormberg, H., Fylling, I.J., Larsen, K. & Sødahl, N. (1997) Coupled analysis of vessel motions and mooring and riser system dynamics. Proceedings of the 16th International Conference on Offshore Mechanics and Arctic Engineering, Yokohama, Japan.

Ormberg, H. & Larsen, K. (1997) Coupled analysis of floater motion and mooring dynamics for a turret moored tanker. Proceedings of the 8th International Conference on the Behaviour of Offshore Structures, Delft, the Netherlands.

Ormberg, H., Sødahl, N. & Steinkjer, O. (1998) Efficient analysis of mooring systems using de-coupled and coupled analysis. Proceedings of the 17th International Conference on Offshore Mechanics and Arctic Engineering, Lisbon, Portugal; Paper No. OMAE98-0351.

Petruska, D., Stone, B., Kwan, T., Zimmerman, E., Devlin, P., Wishahy, M. & O'Connor, P. (2007) Improved moored MODU design codes for hurricane season. Proceedings of the Offshore Technology Conference, Houston; Paper No. 18900.

Rice, S.O. (1944) Mathematical analysis of random noise. Bell System Technical Journal; Vol. 23, pp. 283-332 and Vol. 24, pp. 46-156.

Rychlik, I. (1987) A new definition of the rain-flow cycle counting method. International Journal of Fatigue; Vol. 9, No. 2, pp. 119-121.

Rychlik, I. (1993) On the 'narrow-band' approximation for expected fatigue damage. Probabilistic Engineering Mechanics; Vol. 8, pp. 1-4.

Rychlik, I., Johannesson, P. & Leadbetter, M.R. (1997) Modelling and statistical analysis of ocean-wave data using transformed Gaussian processes. Marine Structures; Vol. 10, pp. 13-47.

Sagrilo, L.V.S., Siqueira, M.Q., Ellwanger, G.B., Lima, E.C.P., Ferreira, M.D.A.S. & Mourelle, M.M. (2002) A coupled approach for dynamic analysis of CALM systems. Applied Ocean Research; Vol. 24, pp. 47-58.

Sakai, S. & Okamura, H. (1995) On the distribution of rainflow range for Gaussian random processes with bimodal PSD. The Japan Society of Mechanical Engineers, International Journal Series A; Vol. 38, No. 4, pp. 440-445.

Sarkani, S., Kihl, D.P. & Beach, J.E. (1994) Fatigue of welded joints under narrow-band non-Gaussian loadings. Probabilistic Engineering Mechanics; Vol. 9, pp. 179-190.

Sclavounos, P.D. (1989) The wave-drift damping of a floating bodies. Fourth International Workshop on Water Waves and Floating Bodies.

Snell, R., Ahilan, R.V. & Versavel, T. (1999) Reliability of mooring systems: Applications to polyester moorings. Proceedings of the Offshore Technology Conference, Houston; Paper No. 10777.

Stansberg, C.T. (1991) A simple method for estimation of extreme values of non-Gaussian slow-drift responses. Proceedings of the 1st International Offshore and Polar Engineering Conference, Edinburgh, UK; Vol. III, pp. 442-451.

Stansberg, C.T. (2000) Prediction of extreme slow-drift amplitudes. Proceedings of the 19th Conference on Offshore Mechanics and Arctic Engineering, New Orleans; Paper No. OMAE00-6135.

Stiff, J., Ferrari, J., Ku, A. & Spong, R. (2003) Comparative risk analysis of two FPSO mooring configuration. Proceedings of the Offshore Technology Conference, Houston; Paper No. 15377.

Sødahl, N., Hagen, Ø. & Løken, A. (1996) Efficient analysis methods for design of risers and mooring systems. Mooring and Riser Systems: New Material and Design Solutions. IIR Symposium, Aberdeen.

Thoft-Christensen, P. & Baker, M.J. (1982) Structural Reliability Theory and its Applications. Springer Verlag, Berlin, Germany.

Tovo, R. (2002) Cycle distribution and fatigue damage under broad-band random loading. International Journal of Fatigue; Vol. 24, pp. 1137-1147.

Triantafyllou, M.S. (1991) Dynamics of cables, towing cables and mooring systems. The Shock and Vibration Digest; Vol. 23, No. 7, pp. 3-8.

Triantafyllou, M.S., Yue, D.K.P. & Tein, D.Y.S. (1994) Damping of moored floating structures. Proceedings of the Offshore Technology Conference, Houston; Paper No. 7489.

Vanmarcke, E.H. (1972) Properties of spectral moments with applications to random vibration. American Society of Civil Engineers, Journal of Engineering Mechanics; Vol. 98, pp. 425-446.

Vinnem, J.E. (1999) Offshore Risk Assessment: Principles, Modelling and Applications of QRA Studies. Kluwer Academic Publishers, the Netherlands.

The WAFO Group (2000) WAFO - A Matlab toolbox for analysis of random waves and loads. Version 2.0.02.

Watson, P. & Dabell, B.J. (1975) Cycle counting and fatigue damage. Symposium on statistical aspects of fatigue testing, Warwick University.

Wang, X. & Sun, J.Q. (2005) Effect of skewness on fatigue life with mean stress correction. Journal of Sound and Vibration; Vol. 282, pp. 1231-1237.

Webster, W.C. (1995) Mooring-induced damping. Ocean Engineering; Vol. 22, No. 6, pp. 571-591.

Wen, Y.K. & Chen, H.C. (1987) On fast integration for time variant structural reliability. Probabilistic Engineering Mechanics; Vol. 2, No. 3, pp. 156-162.

Wichers, J.E.W. & Huijsmans, R.H.M. (1990) The contribution of hydrodynamic damping induced by mooring chains on low frequency vessel motions. Proceedings of the Offshore Technology Conference, Houston; Paper No. 6218.

Winterstein, S.R. (1985) Non-normal responses and fatigue damage. American Society of Civil Engineers, Journal of Engineering Mechanics; Vol. 111, No. 10, pp. 1291-1295.

Winterstein S.R. (1988) Nonlinear vibration models for extremes and fatigue. American Society of Civil Engineers, Journal of Engineering Mechanics; Vol. 114, No. 10, pp. 1772-1790.

Wirsching, P.H. & Light, M.C. (1980) Fatigue under wide band random stresses. Proceedings of the American Society of Civil Engineers, Journal of the Structural Division; Vol. 106, No. ST7, pp. 1593-1607.

Zhao, R. & Faltinsen, O.M. (1988) A comparative study of theoretical models for slowdrift sway motions of a marine structure. Proceedings of the 7th International Conference on Offshore Mechanics and Arctic Engineering, New York; Vol.2, pp. 153-158.

Zhao, R., Faltinsen, O.M. Krokstad, J.R. & Aanesland, V. (1988) Wave-current interaction effects on large-volume structures. Proceedings of the 5th International Conference on the Behaviour of Offshore Structures, Trondheim, Norway; Vol. 2, pp. 623-638.

Zhao. W. & Baker, M.J. (1992) On the probability density function of rainflow stress range for stationary Gaussian processes. International Journal of Fatigue; Vol. 14, No. 2, pp. 121-135.

Appendix A

Appended Papers

Paper 1

Fatigue damage induced by nonGaussian bimodal wave loading in mooring lines

Published in
Applied Ocean Research 2007; Vol. 29, pp. 45-54

Available online at www.sciencedirect.com
ScienceDirect
Applied Ocean Research 29 (2007) 45–54
Applied Ocean Research
www.elsevier.com/locate/apor

Fatigue damage induced by nonGaussian bimodal wave loading in mooring lines

Zhen Gao*, Torgeir Moan

Centre for Ships and Ocean Structures, Norwegian University of Science and Technology, Otto Nielsens v 10, N-7491, Trondheim, Norway

Received 20 October 2006; received in revised form 14 May 2007; accepted 1 June 2007
Available online 23 July 2007

Abstract

Catenary mooring lines are typically subjected to bimodal loads, comprising of a wave frequency (WF) component due to the first-order wave forces and a low frequency (LF) component induced by the second-order wave forces. For moored vessels, the LF forces due to current and wind also play a role. Only dynamic wave loads are considered herein, while current and wind loads are modeled as constant forces. Because of the nonlinearities of the mooring line characteristics, the dynamic line tension and the second-order responses, both the WF and LF line tensions are in principle nonGaussian. These facts make it difficult to estimate the combined fatigue damage of mooring lines in the frequency domain. A fatigue combination rule based on the Jiao and Moan's theory has been extended to cover the nonGaussian case. The purpose of this paper is to improve and validate the frequency-domain method by time-domain analysis based on a simplified, but accurate mechanical model of the dynamic line tension. Improvements on the LF and combined fatigue damage estimation have been made by considering the nonsymmetrical property of the LF line tension distribution. Both the WF and LF mooring line tensions due to wave loading have been simulated in the time domain for different sea states and the combined fatigue damage has been estimated by using the rainflow cycle counting algorithm. The accuracy of the frequency-domain method for estimating the bimodal nonGaussian fatigue damage of mooring lines has been verified by the time-domain simulations and is considered to be acceptable.

Keywords: Fatigue damage; NonGaussian loading; Bimodal process; Frequency domain; Time domain; Rainflow cycle counting

1. Introduction

Catenary mooring lines are pre-tensioned and subjected to dynamic loads caused by the wave frequency (WF) vessel motions and the low frequency (LF) motions normally occurring in the horizontal plane. The WF vessel motions in all six degrees of freedom are Gaussian and can be very well predicted by using linear transfer functions without accounting for the effect of mooring system. However, the LF vessel motions induced by waves are typically nonGaussian due to the nonlinear second-order slowly-varying wave forces (as well as the interactions with LF varying wind and current) and are coupled with the mooring line dynamics.

Dynamic mooring line tension depends on the vessel motions and the line characteristics. Usually, as the same as the tension due to the mean forces of waves (mean wave drift), wind and current, the LF line tension can be quasistatically estimated because of the relative large oscillation periods. Due to the narrow-band property of the LF motion response, the LF line tension is also narrow-banded. In order to accurately calculate the tension induced by the WF vessel motion, a dynamic model of mooring line must be applied, e.g. the simplified model proposed by Larsen and Sandvik [1]. Due to the drag force acting on the line and the geometrical nonlinearity, the WF line tension is in principle nonGaussian as well. Moreover, the WF line tension typically has a dominating central frequency equal to that of the WF vessel motion. Therefore, the WF line tension could also be assumed to be narrow-banded. As a consequence, the combined WF and LF tension is a nonGaussian wide-band process, although the individual components can both well be assumed to be narrow-banded.

An appropriate estimation of the effective stress range distribution of the total process is crucial for fatigue analysis under wide-band loads. For bimodal Gaussian processes, several frequency-domain combination rules are available and Benasciutti and Tovo [2] discussed and compared these

* Corresponding author. Tel.: +47 73595736; fax: +47 73595528.
E-mail addresses: zhen.gao@marin.ntnu.no (Z. Gao), torgeir.moan@marin.ntnu.no (T. Moan).

0141-1187/$ - see front matter © 2007 Elsevier Ltd. All rights reserved.
doi:10.1016/j.apor.2007.06.001

methods. Furthermore, fatigue damage due to the nonGaussian process is usually obtained by approximating the process with a nonlinear transformation of a standard Gaussian process, e.g. the Hermite moment model proposed by Winterstein [3]. However, for mooring system, nonlinearities of the WF and LF line tensions can be explicitly expressed by using the simplified model. Therefore, based on the theory of Jiao and Moan [4], Gao and Moan [5] extended the combination principle to estimate the mooring chain fatigue damage due to the nonGaussian bimodal wave loading.

In the time domain, fatigue damage can be accurately estimated from the total WF and LF time series of mooring line tensions in a straightforward manner based on the rainflow cycle counting method [6–8]. To obtain the tension time series, various simulation methods can be applied. A commonly used simulation method with deterministic amplitudes and random phases assumes that a random Gaussian process can be obtained by the addition of a finite number of only sine or cosine components with phases randomly generated and amplitudes fixed by the spectral values at the specified frequencies. However, Tucker et al. [9] pointed out that this method results in constrained simulations and does not simulate a random Gaussian process correctly. Langley [10] also found that this method does not give correct statistical properties, especially higher moments, e.g. the skewness and the kurtosis. It is even worse for nonGaussian processes. Therefore, in order to generate the slowly-varying force and responses in a correct way, one must use the simulations with random amplitudes of both sine and cosine components.

The purpose of this paper is first to improve the frequency-domain method for estimating the fatigue damage of nonGaussian bimodal processes by considering the effect of non-zero skewness, and then to validate the method by time-domain analysis based on a simplified model of the mooring line tension. The LF fatigue damage estimated by the previous frequency-domain method [5] might be too conservative in some cases because of the assumption of the symmetry of the maxima and minima made in the tension range distribution. Therefore, improvements on the LF and combined fatigue damage calculations have been made by using the average value of the probability density functions (PDFs) of the positive and negative amplitudes instead of the positive one only. Time-domain simulations of the WF and LF mooring line tensions at the fairlead have been carried out and the resulting fatigue damage has been estimated by the rainflow cycle counting algorithm. Fatigue damage obtained by the frequency-domain method has been compared with the simulation result. The comparison shows that the accuracy of the frequency-domain method is good and practically acceptable for fatigue damage estimation.

2. Simplified model of mooring line tension

In general, the total mooring line tension at the fairlead in a stationary and ergodic sea state can be expressed by the following expression:

$$T(t) = T_P + T_M + T_{\mathrm{WF}}(t) + T_{\mathrm{LF}}(t) \tag{1}$$

where the time-invariant variables T_P and T_M are the pre-tension and the mean line tension due to the mean forces of waves, wind and current acting on the vessel in a given short-term period, the random processes $T_{\mathrm{WF}}(t)$ and $T_{\mathrm{LF}}(t)$ are the tensions due to the WF and LF vessel motions, respectively, and t is the time variable.

2.1. Pre-tension and mean line tension

Mooring line pre-tension is determined by the static line configuration without considering any environmental force and can be changed by adjusting the line length or the vessel draft according to the operation requirements for the vessel.

Mean line tension results from the mean forces of waves (mean wave drift), wind and current which are directly acting on the vessel. In a realistic sea state of e.g. the North Sea environment, the mean wave and wind forces are the main contributions to the total mean line tension for a semi-submersible, while the current force is typically small. However in some other locations, like the Amazon mouth or the Angola river mouth, very high current loads have been observed. For an FPSO, the current force in sway direction could be very large due to the large acting area. In this paper, only the wave forces are dynamically considered and wind and current loads are modeled as constant forces together with the mean wave drift force.

2.2. Dynamic wave frequency line tension

Since the dynamic mooring line tension is mainly induced by the motions at the fairlead, the vessel motions must be estimated first. The WF vessel motions can be easily calculated from the wave spectrum and the linear rigid-body motion transfer functions in surge, sway, heave, roll, pitch and yaw directions. Similarly, the LF vessel motions can be obtained by the wave spectrum and the quadratic transfer functions only in the horizontal plane, i.e. in surge, sway and yaw directions. If low frequency wind and current spectra are defined (e.g. API, NPD), the resulting LF motions can be calculated as well.

Typically, the effect of mooring system on the WF vessel motion is quite small and is normally neglected. Moreover, as Larsen and Fylling [11] stated, compared with the wave forces directly acting on the line, the tension induced by the vessel motion dominates. Therefore, the dynamic WF line tension considered herein is just the tension induced by the WF vessel motion. But this tension must be analysed dynamically, especially when the WF vessel motion is relatively large.

A simplified model [1,12] which captures the main features of the dynamic tension from the drag and inertia forces of the mooring line can be applied. The WF tension at the fairlead of a single mooring line is described as,

$$T_{\mathrm{WF}}(t) = c^* \,|\dot{u}(t)|\, \dot{u}(t) + k_G u(t) + \omega^2 m^* x_{\mathrm{WF}}^{\mathrm{TUE}}(t) \tag{2}$$

where $u(t)$ and $\dot{u}(t)$ are the generalized motion and velocity of the assumed shape of mooring line deformation due to the upper end motion of the line. This assumed shape is determined by a quasistatic analysis when the upper end is displaced two times the standard deviation of the dynamic vessel motion from

the equilibrium position. Statistically this corresponds to the significant motion. $x_{\mathrm{WF}}^{\mathrm{TUE}}(t)$ is the WF tangential motion of the line upper end, ω is the wave frequency, c^* and m^* are the generalized damping and mass coefficients, respectively. These coefficients are obtained from the quasistatic line shape at the equilibrium position. The drag and inertia forces are integrated along the mooring line. The resulting system is a single degree-of-freedom system. k_G is the geometric stiffness coefficient, which is taken as the secant stiffness when the line upper end is moved from the equilibrium position to the position of the significant motion. Eq. (2) expresses the dynamic WF line tension with a specific wave frequency ω, while in irregular sea states, one must combine Eq. (2) with the wave spectrum to get the resulting WF line tension. Moreover, the WF vessel motion is narrow-banded and therefore the WF line tension can also be assumed to be narrow-banded.

The accuracy of the simplified model of WF line tension has been verified by Larsen and Sandvik [1]. They compared the mooring line tension obtained by the simplified model with the time-domain simulations based on a finite element method of the line, using the program RIFLEX [13]. The simplified model results in very good estimates of the dynamic line tension. The results are slightly conservative with respect to both the standard deviation and the extreme value of the tension. The extreme dynamic line tension is found to be 10% higher than the estimate obtained by RIFLEX.

Basically, Eq. (2) is a Morison force expression with a drag term and an equivalent inertia term. $x_{\mathrm{WF}}^{\mathrm{TUE}}(t)$ is Gaussian. By linearizing the drag term, $u(t)$ and $\dot{u}(t)$ could be solved and they could both be assumed to be Gaussian as well. According to Borgman [14], the PDF of the individual maximum of the WF line tension is therefore composed of a Rayleigh distribution for low cumulative probabilities and an exponential distribution for high cumulative probabilities,

$$f_{T_{\mathrm{WF\,max}}}(y) = \begin{cases} (3k^2+1)y\exp\left(-(3k^2+1)\dfrac{y^2}{2}\right) & 0 \le y \le y_0 \\ \dfrac{\sqrt{3k^2+1}}{2k}\exp\left(-\dfrac{\sqrt{3k^2+1}}{2k}\left(y-\dfrac{y_0}{2}\right)\right) & y > y_0 \end{cases} \tag{3}$$

where $y_0 = 1/(2k\sqrt{3k^2+1})$ and k is a measure of the relative importance of the drag and inertia terms [12].

If only the drag term is considered, the distribution turns into an exponential distribution. If on the other hand the inertia term dominates, the distribution is close to a Rayleigh distribution. Therefore, the drag/inertia ratio parameter determines the shape of the distribution. The PDFs corresponding to $k = 0.2$, 0.5, 1 and 2 are plotted in Fig. 1. An increasing value of k implies increasing importance of the drag term and a thicker upper tail of the PDF. The WF mooring line tension is dominated by the equivalent inertia contribution of the mass and added-mass forces of the mooring line and the geometrical restoring force which is varying due to the oscillating motion of the line upper end at the fairlead. According to Madsen [15], the resulting fatigue damage due to the WF line tension will be slightly smaller than that based on the Gaussian assumption,

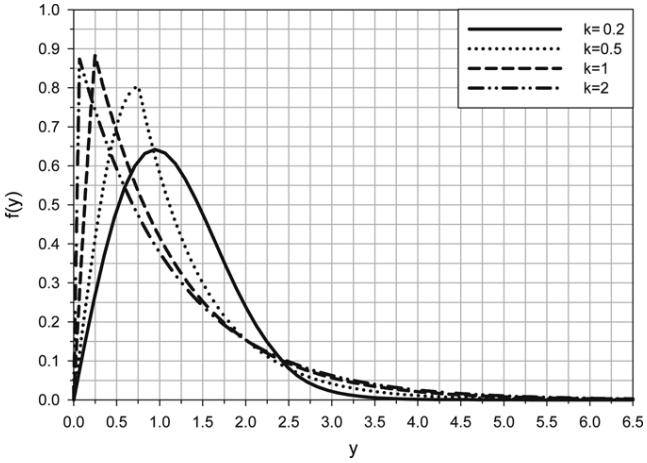

Fig. 1. Combined Rayleigh and exponential PDFs with different values of k.

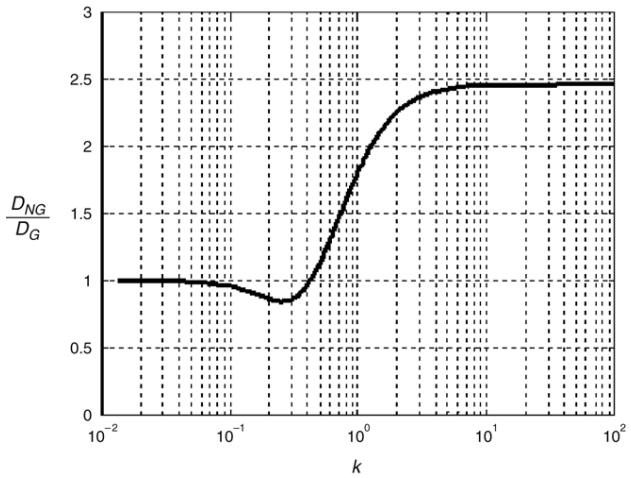

Fig. 2. Ratio of the nonGaussian fatigue damage to the Gaussian one as a function of k.

see Fig. 2. For instance, if $k = 0.3$, the ratio of the nonGaussian fatigue damage to the Gaussian one is about 0.85.

2.3. Quasistatic low frequency line tension

Because of the nonlinearity of the second-order wave forces, the resulting LF vessel motion response is typically nonGaussian [16,17]. According to Stansberg [16], the distribution of the maximum slow-drift response is between Rayleigh and exponential distributions.

Based on the quadratic transfer function, Næss [17] expressed the slowly-varying force as a second-order Volterra series. The PDF of the force is expressed by a summation of a series of exponential distributions as follows:

$$f_Z(z) = \begin{cases} \displaystyle\sum_{j=1}^{M}\frac{l_j}{2\mu_j}\exp\left(-\frac{z}{2\mu_j}\right) & z \ge 0 \\ \displaystyle\sum_{j=M+1}^{N}\frac{l_j}{2|\mu_j|}\exp\left(\frac{z}{2|\mu_j|}\right) & z < 0 \end{cases} \tag{4}$$

where $l_j = \prod_{\substack{k=1 \\ k\neq j}}^{N} (1 - \frac{\mu_k}{\mu_j})^{-1}$, in the expression μ_j ($j = 1, \ldots, M$) represents the positive eigenvalues and μ_j ($j = M+1, \ldots, N$) represents the negative eigenvalues of a reduced integral equation defined by the quadratic transfer function and the wave spectrum, see Næss [17] for details. Therefore the PDF of the LF vessel motion response can also be obtained by consideration of a linear system.

In general, the second-order LF force and response vary in time with relative long periods, e.g. one or several minutes, especially in deep water. The resulting LF mooring line tension at the fairlead can be quasistatically determined by the mooring line characteristics given by the catenary line equation and it is typically a nonlinear function between the in-plane horizontal motion and the tension at the upper end of the mooring line, which can be expressed as

$$T_{\mathrm{LF}}(t) = g(x_{\mathrm{LF}}^{\mathrm{UE}}(t)) \tag{5}$$

where $x_{\mathrm{LF}}^{\mathrm{UE}}(t)$ represents the horizontal LF motion of the upper end of the mooring line due to the LF vessel motion. Usually a cubic polynomial function represents the line characteristics very well and when the LF vessel motion is relatively small, even a linear function with the tangential stiffness gives a good approximation.

Finally, the LF line tension distribution can be determined from the obtained distribution of the motion response. By transformation, the distribution of the time-derivative of $T_{\mathrm{LF}}(t)$, i.e. $\dot{T}_{\mathrm{LF}}(t)$, can be obtained as well. Therefore, based on the narrow-band assumption, the PDF of the maximum LF mooring line tension can be obtained by the derivative of the mean up-crossing rate of the LF tension process [18],

$$f_{T_{\mathrm{LF\,max}}}(y) = -\frac{1}{\nu^{+}_{T_{\mathrm{LF}}}(0)} \frac{\mathrm{d}\nu^{+}_{T_{\mathrm{LF}}}(y)}{\mathrm{d}y} \tag{6}$$

where $\nu^{+}_{T_{\mathrm{LF}}}(y)$ is the mean up-crossing rate of LF line tension with level y, which can be determined by the Rice formula [19] as follows:

$$\nu^{+}_{T_{\mathrm{LF}}}(y) = \int_0^{+\infty} \dot{y}\, f_{T_{\mathrm{LF}},\dot{T}_{\mathrm{LF}}}(y, \dot{y})\mathrm{d}\dot{y} \tag{7}$$

where $f_{T_{\mathrm{LF}},\dot{T}_{\mathrm{LF}}}(y, \dot{y}) = f_{T_{\mathrm{LF}}}(y) f_{\dot{T}_{\mathrm{LF}}}(\dot{y})$ is the joint probability density of the LF line tension $T_{\mathrm{LF}}(t)$ and the corresponding time-derivative $\dot{T}_{\mathrm{LF}}(t)$ under the assumption of independence. For general nonGaussian processes, the PDF given by Eq. (6) and the mean up-crossing rate given by Eq. (7) can only be estimated numerically.

3. Frequency-domain fatigue damage

Based on a single-slope SN curve ($N = KS^{-m}$) and the effective stress range distribution, the accumulated fatigue damage can be estimated from all individual stress cycles by adopting the Miner–Palmgren rule [20],

$$D = \sum \frac{n_i}{N_i} = \frac{N_0}{K} E[S^m] \tag{8}$$

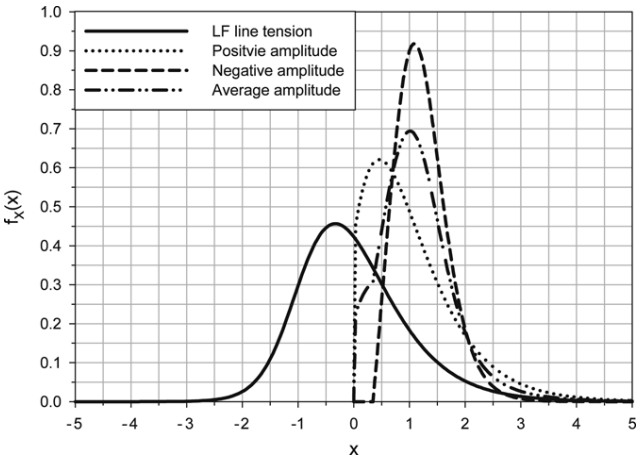

Fig. 3. Normalized PDFs of the LF line tension and amplitude at the fairlead as obtained for a sea state of $Hs = 4.75$ m and $Tp = 11.5$ s.

where N_0 is the total number of cycles, S denotes the effective stress range, $E[S^m]$ means the expectation of S^m, K and m are the material parameters. Typical value of m is 3 for the catenary mooring chain [21–23].

By modifying Eq. (8), the short-term narrow-band fatigue damage due to the WF or LF line tension can be written with respect to the distribution of stress amplitudes and the mean zero up-crossing rate as follows:

$$D = \frac{2^m T}{K} \nu_0 \int_0^{+\infty} y^m f_{\max}(y)\mathrm{d}y \tag{9}$$

where T is the duration of the sea state, ν_0 is the mean zero up-crossing rate and $f_{\max}(y)$ is the PDF of the line tension amplitude.

As done by Gao and Moan [5], only the positive amplitudes are used for estimating the fatigue damage due to the WF or LF components. As a consequence, the WF frequency-domain fatigue damage is close to the correct result due to the symmetry of the WF line tension, while the obtained LF fatigue damage for this reason will always be larger than the true value because of the positive skewness of the LF line tension. This effect will then be present for the combined fatigue damage and especially relevant if the LF component dominates. Therefore, in this paper, improvements have been made in the effective stress range distribution by using the average value of the PDFs of the positive and negative amplitudes for the same tension level instead of the positive one only, by which the effect of skewness on the fatigue damage has been considered. An example of the normalized PDFs of the LF line tension and amplitude at the fairlead as obtained for a sea state of $Hs = 4.75$ m and $Tp = 11.5$ s is shown in Fig. 3. Compared with the average amplitude PDF, the positive one predicts larger probability density values for high responses and it could lead to a significant overestimation of fatigue damage.

Fatigue damage due to the combined WF and LF line tension is not just the sum of the WF and LF fatigue damage components. When both the WF and LF processes are Gaussian, Jiao and Moan [4] approximated the combined fatigue damage as a sum of the WF fatigue damage and

the damage due to a process which is the sum of the LF process and the envelope of WF process. Compared with the rainflow counting results in the time domain, this frequency-domain method gives very accurate estimates of the total fatigue damage. Gao and Moan [5] extended this theory to combine the fatigue damage due to the nonGaussian WF and LF line tensions, which is briefly described as follows:

Assume that $P(t)$ is the sum process of the envelope of WF process and the LF process of mooring line tensions

$$P(t) = R_{\mathrm{WF}}(t) + T_{\mathrm{LF}}(t) \tag{10}$$

where $R_{\mathrm{WF}}(t)$ is the envelope of the WF line tension process $T_{\mathrm{WF}}(t)$ as described by Eq. (2).

Because the WF and LF line tension processes are assumed to be independent, the envelope of $P(t)$ can be expressed as

$$Q(t) = R_{\mathrm{WF}}(t) + R_{\mathrm{LF}}(t) \tag{11}$$

where $R_{\mathrm{LF}}(t)$ is the envelope of the LF line tension process $T_{\mathrm{LF}}(t)$ as described by Eq. (5).

Therefore, the distribution of individual maxima of $P(t)$ is the distribution of $Q(t)$, which can be estimated by the convolution integral of the distributions of $R_{\mathrm{LF}}(t)$ and $R_{\mathrm{WF}}(t)$. Similarly, the distribution of $P(t)$ can also be estimated by the convolution integral. This actually involves conservativeness, but the effect on the total fatigue damage is not significant since the number of cycles due to $P(t)$ is relatively low.

The time-derivative of $P(t)$ is,

$$\dot{P}(t) = \dot{R}_{\mathrm{WF}}(t) + \dot{T}_{\mathrm{LF}}(t). \tag{12}$$

Considering the nonGaussian WF mooring line tension, the process $R_{\mathrm{WF}}(t)$ is in principle not Rayleighian, $\dot{R}_{\mathrm{WF}}(t)$ is not Gaussian [4,24] and the distribution of $\dot{P}(t)$ is difficult to obtain. However, based on the narrow-band assumption, the mean zero up-crossing rate of $P(t)$ is close to that of the corresponding process when the Gaussian assumption is made and can be estimated by the Rice formula [19], see Eq. (7).

When the distribution of individual maxima and the mean zero up-crossing rate of $P(t)$ are available, fatigue damage due to $P(t)$ can be obtained by Eq. (9). According to Jiao and Moan [4], the total fatigue damage of the combined WF and LF tension is equal to the sum of the fatigue damages of $P(t)$ and $T_{\mathrm{WF}}(t)$.

In this paper, the frequency-domain fatigue damage calculation is carried out based on the above procedure for the nonGaussian bimodal mooring line tension. NonGaussian distribution functions of both the WF and LF line tensions and their maxima are calculated numerically. However, the Gaussian assumption is made for estimating the mean zero up-crossing rates and it is reasonable because of the narrow-band property of both the WF and LF components.

4. Time-domain simulation and fatigue damage

In order to obtain the WF and LF time series of the mooring line tensions based on the simplified model described above, the linear and the slowly-varying wave forces and the resulting vessel motions have to be simulated.

Because the WF vessel motions are Gaussian and one can simulate these time series very easily when the motion spectra are available by using the following expression:

$$\eta(t) = \mathrm{Re}\sum_{n=1}^{N} \hat{a}_n \exp(\mathrm{i}\omega_n t); \quad \hat{a}_n = a_n - \mathrm{i}b_n \tag{13}$$

where $\eta(t)$ represents the WF vessel motion at any point in any degree of freedom, ω_n is the nth frequency component, a_n and b_n are independent Gaussian random variables in the ensemble sense with zero mean and $E[a_n^2] = E[b_n^2] = S_{\eta\eta}(\omega_n)\mathrm{d}\omega$, in which $S_{\eta\eta}(\omega)$ is the onesided motion spectrum and $E[]$ denotes the ensemble average, Re denotes the real part of a complex number. According to the simplified dynamic model as shown by Eq. (2), the WF mooring line tension series can be obtained by combining the time series of the drag and inertia terms by generating them independently using Eq. (13).

The LF second-order wave forces can be expressed as [10]

$$F(t) = \mathrm{Re}\sum_{n=1}^{N}\sum_{m=1}^{M} \hat{a}_n \hat{a}_m^* H_{nm} \exp(\mathrm{i}(\omega_n - \omega_m)t) \tag{14}$$

where H_{nm} is the complex quadratic transfer function of wave forces, $\hat{a}_m^*$ is the complex conjugate of $\hat{a}_m$. Sum frequency components are neglected and only difference frequency components, which are interesting for mooring analysis, remain in Eq. (14). A double summation appears in Eq. (14) and it usually takes extremely long time to generate even a single sample because a large number of frequency components must be included in order to represent the correct statistical properties of the process. However, by using the Fast Fourier Transform (FFT), the simulation time can be significantly reduced. The LF vessel motion can also be generated by using Eq. (14) if the quadratic transfer function of motion is available and the resulting line tension can therefore be obtained based on a quasistatic analysis.

Simulation with Eq. (13) or Eq. (14) uses the Gaussian random variables multiplying the sine and cosine components and as Tucker et al. [9] and Langley [10] pointed out, it gives accurate statistical moments of the simulated process. In order to reproduce the spectrum correctly, one must take the average value over many simulations, about 20–30 simulations [10].

Finally, the total line tension series are obtained just by summing up the WF and LF tension series independently.

Estimating the fatigue damage from the time series is straightforward and the rainflow algorithm [6–8] for counting the effective tension range cycles is applied in this paper.

5. Validation of the frequency-domain method by time-domain analysis

The purpose of this paper is to validate the improved frequency-domain method for bimodal nonGaussian fatigue damage estimation of mooring line tension by extensive time-domain simulations based on the simplified dynamic model.

Since the accuracy of the simplified model has already been verified [1], no simulation of mooring line tension is directly carried out based on the finite element analysis. The mechanical

Table 1
Main particulars of the semisubmersible

Displacement (ton)	52 500
Length O.A. (m)	124
Breadth (m)	95
Draught (m)	21
Operational water depth (m)	340

models for the WF and LF mooring line tensions applied in the frequency-domain analysis are identical to those in the time-domain simulations, which are expressed by Eqs. (2) and (5), respectively. It implies that the nonlinear properties are also considered in the frequency-domain analysis, including the drag force acting on the line and the nonlinear line characteristics. The WF vessel motion is obtained by a linear analysis, while the induced WF line tension at the fairlead is nonlinear due to the effect of the drag force on the mooring line. Moreover, the WF and LF vessel motions are generated in the time domain by using the linear and quadratic motion transfer functions, respectively, and these transfer functions are also applied in the frequency-domain analysis. As a consequence, the differences in the statistical properties of the WF and LF tensions obtained by the frequency- and time-domain analyses are mainly due to the precision of the numerical integration in the frequency-domain approach and the spectrum discretization involved in the simulations.

For fatigue analysis, the rainflow cycle counting algorithm is applied in the time domain for all of the time series of the WF, LF and combined line tensions. However, in the frequency domain, the improved Jiao and Moan's method for nonGaussian processes is applied.

6. Case study

The same semisubmersible and mooring system as described in [5] have been used for case study. The main dimensions of the semisubmersible are listed in Table 1. A total of 16 identical catenary mooring lines with chain-wire-chain configurations have been applied. The pre-tension at the upper end of each mooring line is about 1320 kN and the diameter of studless chain links is 125 mm. The tension of the most-loaded mooring line at the fairlead due to the WF and LF surge motions of the vessel has been calculated and the induced fatigue damage has been estimated.

6.1. Simulation results and accuracy

The Pierson–Moskowitz (P–M) wave spectrum is applied. In order to get the correct statistical properties of the mooring line tension, especially those of the LF process, the spectrum is discretized with 5000 frequency components. It takes about 10 min to complete a single six-hour simulation on a PC with 1 GHz CPU. Sixteen different sea states have been simulated with significant wave height $Hs = 3.25$ m, 4.75 m, 6.25 m and 7.75 m and spectral peak period $Tp = 7.5$ s, 9.5 s, 11.5 s and 13.5 s. According to Gao and Moan [5], these sea states represent the most important area in a scatter diagram for fatigue damage estimation.

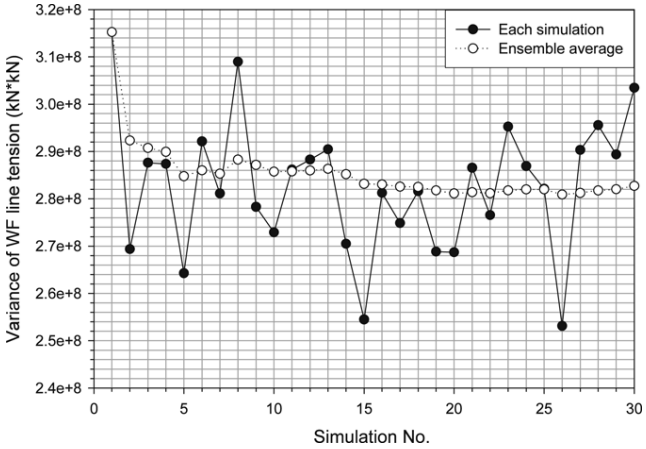

Fig. 4. Variance of the WF line tension in each simulation and on ensemble average as obtained for a sea state of $Hs = 4.75$ m and $Tp = 11.5$ s. (In Figs. 4–8, "Each simulation" corresponds to the result from Simulation No. i with a duration of 6 hours; "Ensemble average" means the average over Simulation No. 1 up to Simulation No. i.)

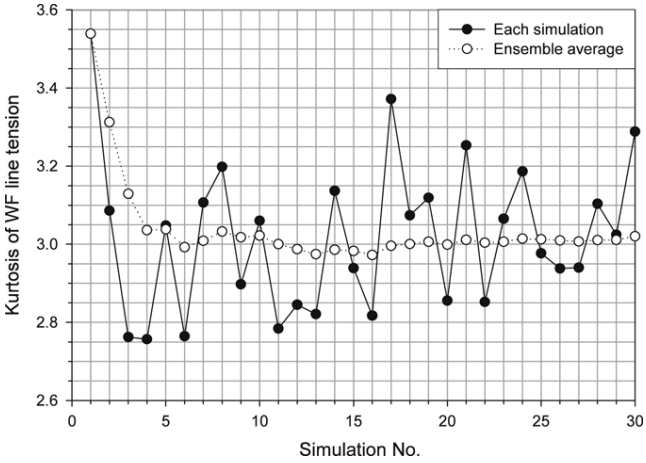

Fig. 5. Kurtosis of the WF line tension in each simulation and on ensemble average as obtained for a sea state of $Hs = 4.75$ m and $Tp = 11.5$ s.

Due to the randomness of a_n and b_n in Eqs. (13) and (14), the statistical properties of the simulated WF and LF mooring line tensions at the fairlead show a significant variance for different samples of a_n and b_n. One must average over many simulations to get stable values of the statistical moments. The statistical properties of the WF and LF mooring line tensions as obtained for a sea state with $Hs = 4.75$ m and $Tp = 11.5$ s are shown in Figs. 4–8. Thirty simulations, each with duration of 6 hours, were carried out. The statistical properties of each simulation together with the ensemble average over these simulations are plotted. It is observed that a stable statistics is obtained by running at least 15–20 simulations for the WF line tension process and 20–30 simulations for the LF one. This fact implied that 90–120 simulation hours are needed for the WF process and 120–180 hours for the LF one.

The skewness of the WF line tension is quite close to zero and is not presented herein. The kurtosis of the WF line tension is found to be close to three and it indicates that the equivalent inertia term dominates Eq. (2) and hence, implies a WF tension

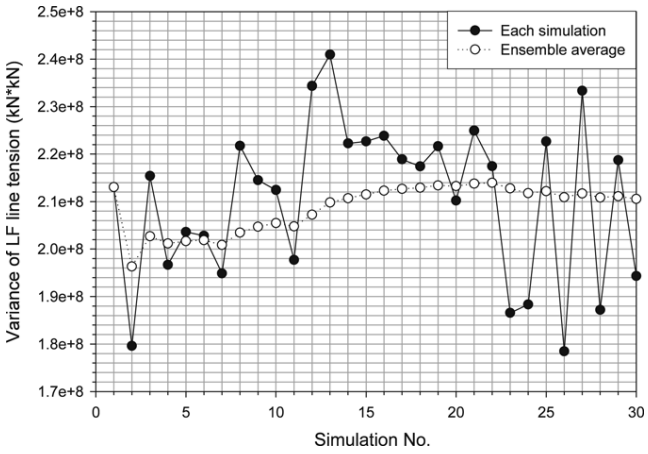

Fig. 6. Variance of the LF line tension in each simulation and on ensemble average as obtained for a sea state of $Hs = 4.75$ m and $Tp = 11.5$ s.

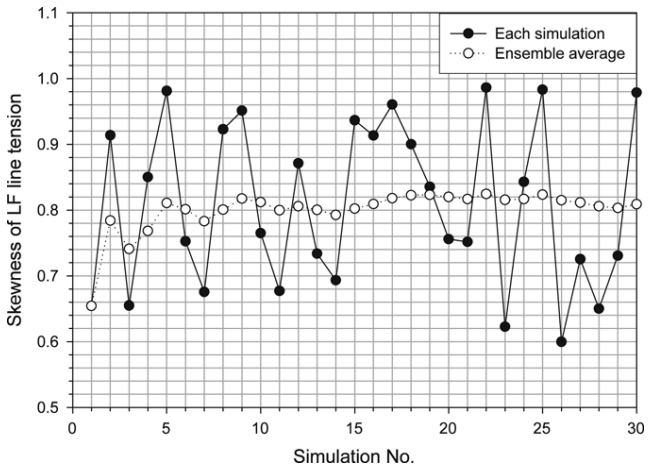

Fig. 7. Skewness of the LF line tension in each simulation and on ensemble average as obtained for a sea state of $Hs = 4.75$ m and $Tp = 11.5$ s.

which is approximately Gaussian. However the skewness of the LF process is about 0.8 and the kurtosis is close to 4.5. The positive skewness indicates that the process has a thicker upper tail in the PDF and a larger maximum compared with the Gaussian one. The kurtosis is larger than three, which indicates higher values both in the upper and lower tails of the PDF.

The effect of kurtosis on the fatigue damage has been demonstrated by Winterstein [3]. He approximated the ratio between the nonGaussian fatigue damage with a kurtosis of α_4 and the Gaussian fatigue damage by the following expression:

$$\frac{D_{NG}}{D_G} = 1 + m(m-1)(\alpha_4 - 3)/24 \tag{15}$$

where m is the slope parameter of SN curve. If we take $m = 3$ and $\alpha_4 = 4.5$ for the LF line tension process, the calculated nonGaussian fatigue damage is about 40% higher than that of the Gaussian process. This indicates that the fatigue damage can be significantly increased with a relatively large kurtosis.

However, in the present case, the variance of the WF line tension is larger than the LF variance, see Figs. 4 and 6. Considering the fact that the WF process implies more cycles,

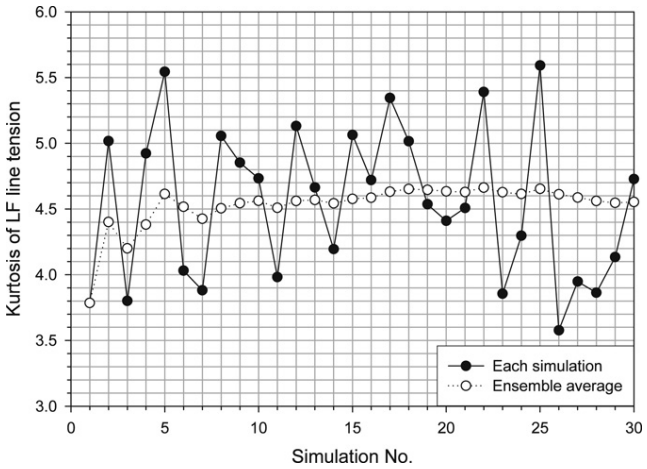

Fig. 8. Kurtosis of the LF line tension in each simulation and on ensemble average as obtained for a sea state of $Hs = 4.75$ m and $Tp = 11.5$ s.

the WF fatigue damage dominates the total fatigue damage. As a result, the total fatigue damage would be close to the fatigue damage under the Gaussian assumption.

6.2. Comparison of statistical properties of mooring line tension

As mentioned above, a total of 16 sea states were simulated. All of the statistical properties have been obtained from the simulations and have been compared with those calculated by the frequency-domain method, see Figs. 9–13. In all figures, the relative difference is presented, which is defined as the difference between the frequency- and time-domain results divided by the time-domain result.

For the WF line tension, the differences in the obtained variance and kurtosis are very small in all sea states, within $+/-2.5\%$ for the variance and $+/-1.5\%$ for the kurtosis. However for the LF line tension, the relative difference is slightly larger but still small, within $+/-3\%$ for the variance, $+/-6.5\%$ for the skewness and $+/-7\%$ for the kurtosis. Compared with the WF line tension, the LF line tension has fewer cycles for the same duration due to the larger oscillation period. This might be one reason why the relative differences between the frequency and time-domain analyses are larger for the LF line tension.

In general, the frequency-domain method accurately captures the relevant statistical properties of both the WF and LF line tensions. The discrepancies in the statistical properties are practically acceptable. This is a basic requirement for checking the accuracy of the frequency-domain method for fatigue damage estimation.

6.3. Comparison of short-term fatigue damage

Fatigue damages estimated by the frequency-domain and time-domain analyses are compared in Figs. 14–16 for the WF and LF components as well as for the total line tension.

Although the frequency-domain fatigue damage is slightly underestimated, the relative difference of the WF fatigue

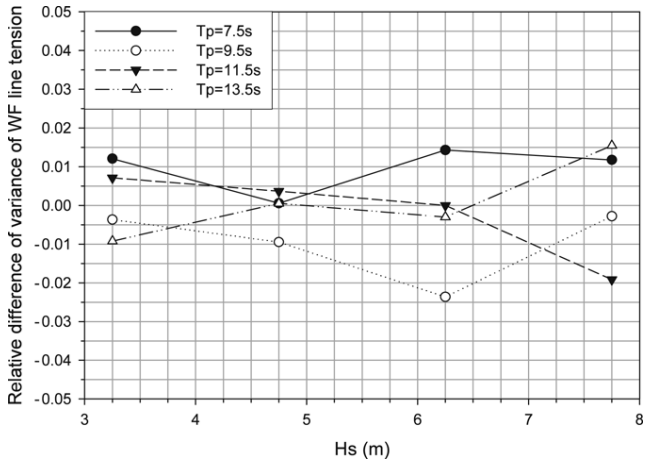

Fig. 9. Relative difference of variance of the WF line tension in different sea states between the frequency-domain result and the ensemble average over 30 six-hour time-domain simulations. ("Relative difference" in Figs. 9–16 is defined as the difference between the frequency- and time-domain results divided by the time-domain result.)

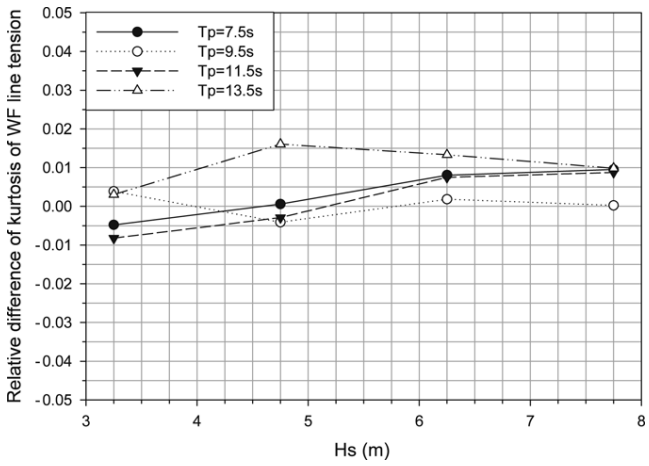

Fig. 10. Relative difference of kurtosis of the WF line tension in different sea states between the frequency-domain result and the ensemble average over 30 six-hour time-domain simulations.

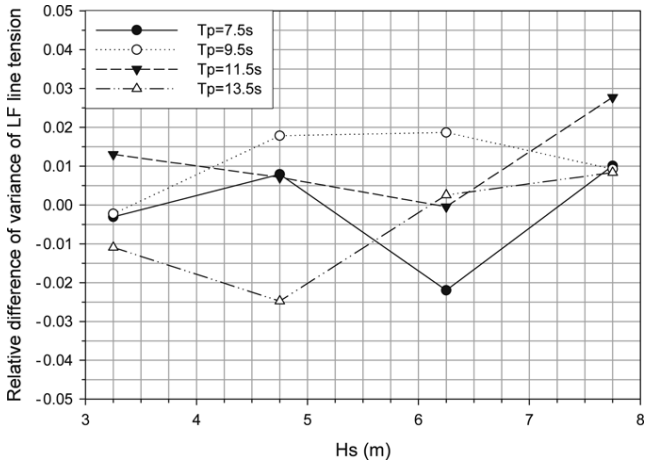

Fig. 11. Relative difference of variance of the LF line tension in different sea states between the frequency-domain result and the ensemble average over 30 six-hour time-domain simulations.

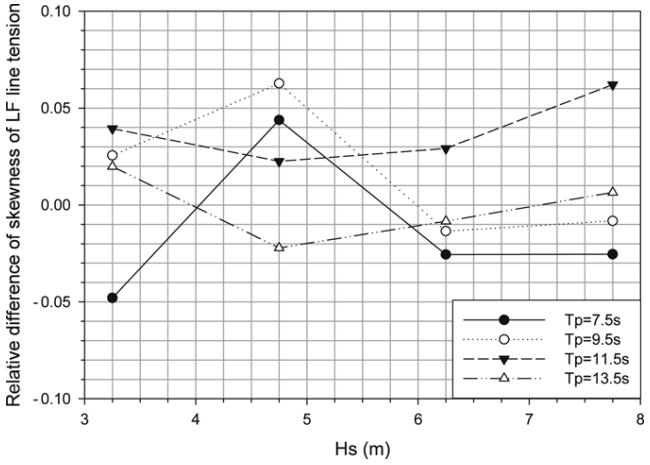

Fig. 12. Relative difference of skewness of the LF line tension in different sea states between the frequency-domain result and the ensemble average over 30 six-hour time-domain simulations.

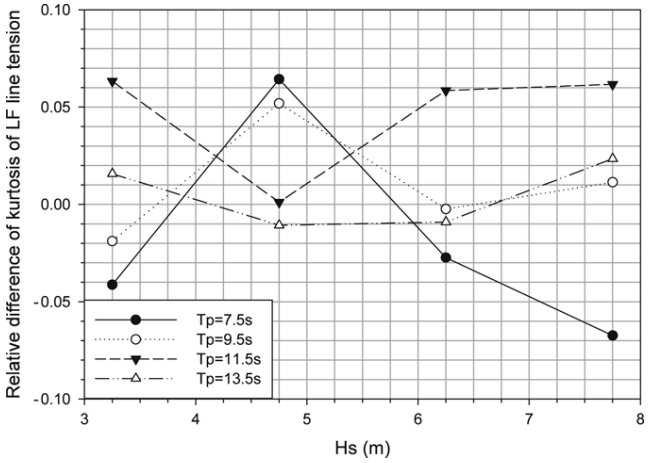

Fig. 13. Relative difference of kurtosis of the LF line tension in different sea states between the frequency-domain result and the ensemble average over 30 six-hour time-domain simulations.

damage is small, within +/−13%. Frequency-domain fatigue damage due to the LF motions, obtained based on the improved Jiao and Moan method with the average positive and negative amplitude distribution, seems always larger than that estimated by the rainflow counting method in the time domain. The maximum relative difference of the LF fatigue damage is about 12.5% and the accuracy is on the same level as for the WF fatigue damage. As already pointed out, the most important contribution to the combined fatigue damage in the present example comes from the WF component. Therefore, the total fatigue damage obtained by the simulations and the frequency-domain method is still close, within +/−11%, see Fig. 16.

In view of the significant uncertainties in the fatigue load effects and resistance, the accuracy of the frequency-domain method for estimating the WF, LF and combined fatigue damage is therefore considered to be acceptable. It also indicates that the frequency-domain combination rule is still applicable for this nonGaussian case.

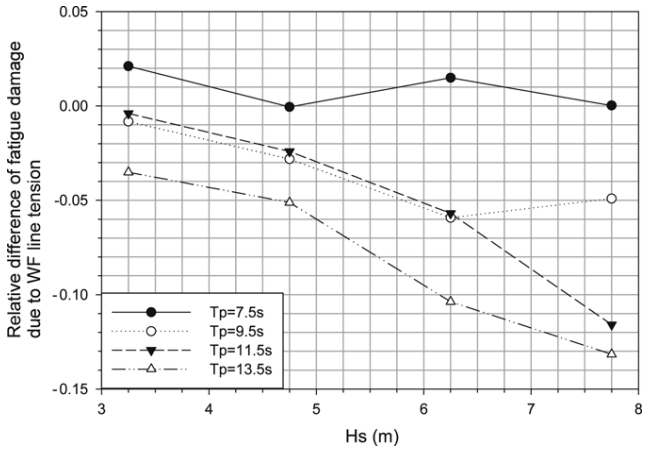

Fig. 14. Relative difference of fatigue damage due to the WF line tension in different sea states between the frequency-domain result and the ensemble average over 30 six-hour time-domain simulations.

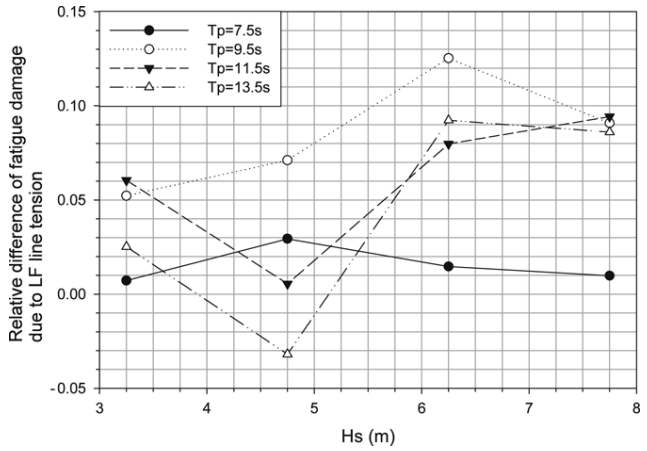

Fig. 15. Relative difference of fatigue damage due to the LF line tension in different sea states between the frequency-domain result and the ensemble average over 30 six-hour time-domain simulations.

6.4. Frequency-domain long-term fatigue damage

Long-term fatigue damage can be calculated by summing up the short-term fatigue damage multiplied with the occurrence probability of each sea state during the long-term period of interest. It is very time-consuming to compute the long-term fatigue damage in the time domain based on hundreds or thousands of short-term simulations.

The relative contributions of the fatigue damage from different sea states considering the Northern North Sea wave conditions as obtained by the present frequency-domain method are plotted in Fig. 17. For convenience, the total long-term fatigue damage in Fig. 17 is normalized to be 1. In the figure, we can clearly identify the sea states which contribute most to the long-term fatigue damage, i.e. the sea states with Hs from 3 to 8 m and Tp from 7 to 13 s. This information is quite useful because one can refine or check the long-term fatigue damage obtained by the frequency-domain method by just running the time-domain simulations for the identified important sea states. It saves significant computational time compared with a full long-term analysis in the time domain. The comparisons of

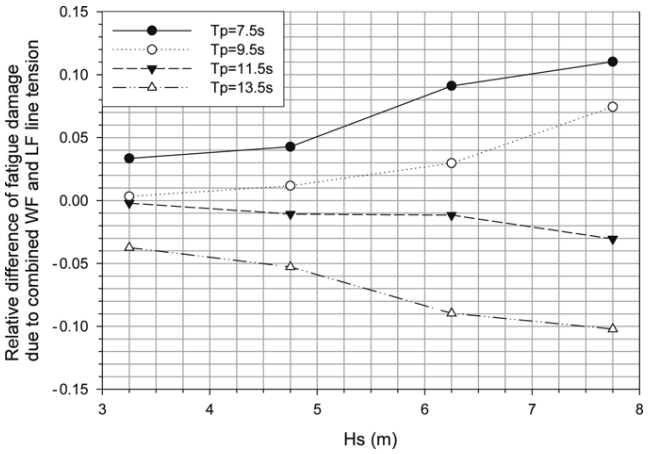

Fig. 16. Relative difference of fatigue damage due to the combined WF and LF line tension in different sea states between the frequency-domain result and the ensemble average over 30 six-hour time-domain simulations.

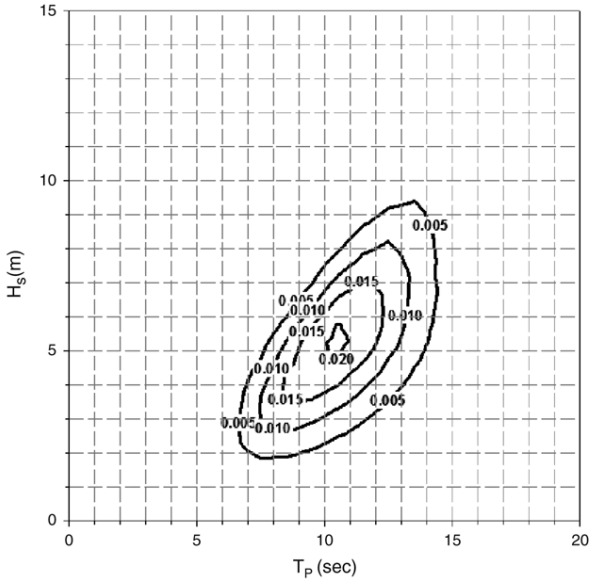

Fig. 17. Relative contributions of fatigue damage from different sea states due to the combined nonGaussian WF and LF mooring line tension considering the Northern North Sea wave conditions.

frequency- and time-domain short-term fatigue damage in the previous section are only made for these important sea states.

7. Conclusions

The purpose of this paper is to improve and validate the frequency-domain method for bimodal nonGaussian fatigue damage estimation of mooring line tension by time-domain analysis based on a simplified, but accurate mechanical model.

The frequency-domain method, originally proposed by Jiao and Moan for Gaussian processes, for the combined fatigue damage estimation has been improved by considering the skewness effect on the effective stress range distribution.

Simulation with Gaussian random variables of sine and cosine components has been applied to generate the WF and LF mooring line tension time series at the fairlead based on the simplified model. A total of 16 sea states have been considered

with 30 six-hour simulations for each. The statistical properties of both the WF and LF tensions are estimated and the fatigue damages of the WF, LF and combined tensions are obtained by the rainflow cycle counting method.

Because the WF mooring line tension is slightly different from Gaussian, the statistical properties of the time-domain simulations agreed very well with those of the frequency-domain estimates. The difference between the simulations and the frequency-domain analyses for the LF tension statistics is slightly larger, but the discrepancy is within +/−7% for all of the cases considered.

The obtained frequency-domain fatigue damage of the WF line tension agrees also well with those of the simulations. The resulting LF fatigue estimation seems always conservative and the accuracy level is similar as that for the WF line tension. The total fatigue damage is obtained based on the same theory of Jiao and Moan by which the nonGaussian amplitude distributions of the WF and LF line tensions are applied and the Gaussian assumption is made only for calculating the mean zero up-crossing rates of narrow-band components. The comparison of short-term fatigue damage with the time-domain result shows a reasonable agreement with the maximum relative error of 13%, 12.5% and 11% for the WF, LF and combined fatigue damage estimates, respectively. Although in the simulated sea states, the combined fatigue damage is dominated by the WF line tension, the accuracy of the method is expected to be acceptable as well for cases with the LF line tension dominating.

Acknowledgements

The authors wish to acknowledge the support from the Research Council of Norway through the Centre for Ships and Ocean Structures at the Norwegian University of Science and Technology in Trondheim, Norway.

References

[1] Larsen K, Sandvik PC. Efficient methods for the calculation of dynamic mooring line tension. In: 1st European offshore mechanics symposium. 1990. p. 482–9.

[2] Benasciutti D, Tovo R. Comparison of spectral methods for fatigue damage assessment in bimodal random processes. In: 9th international conference on structural safety and reliability. 2005. p. 3181–88.

[3] Winterstein SR. Nonlinear vibration models for extremes and fatigue. Journal of Engineering Mechanics 1988;114(10):1772–90.

[4] Jiao G, Moan T. Probabilistic analysis of fatigue due to Gaussian load processes. Probabilistic Engineering Mechanics 1990;5(2):76–83.

[5] Gao Z, Moan T. Wave-induced fatigue damage of mooring chain under combined non-Gaussian low and wave frequency loads. In: 25th international conference on offshore mechanics and arctic engineering. 2006. Paper no. OMAE2006-92389.

[6] Matsuishi M, Endo T. Fatigue of metals subjected to varying stress. Fukuoka (Japan): Japan Society of Mechanical Engineers; 1968.

[7] Rychlik I. A new definition of the rainflow cycle counting method. International Journal of Fatigue 1987;9(2):119–21.

[8] ASTM E 1049-85. Standard practices for cycle counting in fatigue analysis. ASTM International 2005.

[9] Tucker MJ, Challenor PG, Carter DJT. Numerical simulation of a random sea: A common error and its effect upon wave group statistics. Applied Ocean Research 1984;6(2):118–22.

[10] Langley RS. On the time-domain simulation of second-order wave forces and induced responses. Applied Ocean Research 1986;8(3):134–43.

[11] Larsen CM, Fylling IJ. Dynamic behaviour of anchor lines. Norwegian Maritime Research 1982;10(3):18–32.

[12] Lie H, Sødahl N. Simplified dynamic model for estimation of extreme anchorline tension. Offshore Australia. 1993.

[13] User's Manual RIFLEX, Version 3.2.3. MARINTEK report no. 519619. 2003.

[14] Borgman LE. Wave forces on piling for narrow-band spectra. Journal of the Waterways and Harbors Division, ASCE 1965;65–90.

[15] Madsen HO, Krenk S, Lind NC. Methods of structural safety. Prentice-Hall; 1986. p. 316–25.

[16] Stansberg CT. A simple method for estimation of extreme values of non-Gaussian slow-drift responses. In: 1st international offshore and polar engineering conference, vol. III. 1991. p. 442–51.

[17] Næss A. The statistical distribution of second-order slowly-varying forces and motions. Applied Ocean Research 1986;8(2):110–8.

[18] Næss A, Berstad AJ, Moen LA. Stochastic fatigue analysis of the tethers of a tension leg platform. In: 2nd international conference on computational stochastic mechanics. 1994.

[19] Rice SO. Mathematical analysis of random noise. Bell System Technical Journal 1944;vol. 23:283–332 and vol. 24, p. 46–156.

[20] Miner MA. Cumulative damage in fatigue. Journal of Applied Mechanics 1945;12:159–64.

[21] ISO. Petroleum and natural gas industries – specific requirements for offshore structures – Part 7: Stationkeeping systems for floating offshore structures and mobile offshore units. ISO 19901-7; 2005.

[22] DNV. Offshore standard — position mooring. DNV-OS-E301; 2001.

[23] API. Recommended practice for design and analysis of stationkeeping systems for floating structures. API RP 2SK; 1997.

[24] Toro GR. Probabilistic analysis of combined dynamic responses. Ph.D. thesis. Department of Civil Engineering, Stanford University; 1984.

Paper 2

Frequency-domain fatigue analysis of wide-band stationary Gaussian processes using a trimodal spectral formulation

Accepted for publication in
International Journal of Fatigue

Frequency-domain fatigue analysis of wide-band stationary Gaussian processes using a trimodal spectral formulation

Zhen Gao, Torgeir Moan

Centre for Ships and Ocean Structures and Department of Marine Technology,
Norwegian University of Science and Technology
Otto Nielsens vei 10, NO-7491, Trondheim, Norway

Abstract

In this paper, a procedure for fatigue analysis of a general wide-band stationary Gaussian process is developed in the frequency domain using a trimodal spectral formulation, based on a generalization of the principle proposed by Jiao and Moan for predicting bimodal fatigue damage. The novel method approximates the rainflow cycles with large amplitudes as the sum of the envelopes of the process components. First, the method is derived and the corresponding accuracy is demonstrated for ideal trimodal Gaussian processes whose spectra exhibit peaks at three well separated modes, each assumed to be narrow-banded. Hermite numerical integration method is applied to evaluate the fatigue damage due to a Rayleigh sum distribution since there is no closed-form solution for a random variable which is the sum of more than two Rayleigh random variables. Then, the method is further developed and applied to general wide-band Gaussian processes by dividing the spectrum into three segments with the same variances and calculating the fatigue damage in the same way as for the ideal trimodal processes. Based on extensive time series simulated with spectra of wave- and wind-induced linear structural responses and with generally defined wide-band spectra, the rainflow cycle counting method has been applied to estimate the fatigue damage in the time domain in order to check the accuracy of the proposed method and other frequency-domain methods. It is found that the narrow-band assumption can be very well made for a process with a Vanmarcke's bandwidth parameter which is less than 0.5. For most of the simulated processes with bandwidth parameters between 0.5 and 0.85, the proposed method slightly overestimates the fatigue damage on average. If the bandwidth is greater than 0.85, the fatigue damage obtained by the trimodal formulation may be significantly overestimated in some cases, however spectra with very high bandwidth parameters might be unrealistic. Anyway, it has been shown that the overestimation can be alleviated by using a formulation with more modes for these cases. Moreover, two empirical formulae for wide-band fatigue damage estimation, one derived by Dirlik and the other proposed by Benasciutti and Tovo, have also been verified to be very accurate but slightly underestimate the fatigue damage for a wide range of the bandwidth parameters considered in this paper.

Keywords: fatigue damage, wide-band Gaussian process, Vanmarcke's bandwidth parameter, multi-modal spectrum, Rayleigh sum distribution, Hermite numerical integration

1. Introduction

Prediction of fatigue life for structures subjected to wide-band stationary Gaussian processes has been widely studied by many researchers since the 1980s. Fatigue damage estimation generally involves two issues, i.e. cycle counting of equivalent stress ranges and accumulation of fatigue damage from each cycle. In fact, many studies contribute to the first one, i.e. estimating an equivalent stress range distribution either in the time domain or in the frequency domain. After the stress range distribution has been obtained, fatigue damage is usually evaluated by using, for example, the linear Palmgren-Miner rule [1].

In the time domain, it is straightforward to count the effective cycles based on the time series which can be obtained experimentally or numerically. Alternative cycle counting methods are envisaged, like peak counting, range counting, level-crossing counting, rainflow counting, etc. The rainflow cycle counting method was originally proposed by Matsuishi and Endo [2]. A new equivalent definition was given by Rychlik [3] and is more convenient for statistical analysis. The rainflow cycle counting algorithm is found to be the best method for fatigue damage estimation [4, 5] and is commonly applied as a reference to check the accuracy of frequency-domain methods. However, in order to reduce the statistical uncertainty and obtain stable fatigue damage estimates, a large number of time series with durations long enough have to be provided. This task could be extremely time-consuming. Alternatively, many frequency-domain methods have been proposed for estimating wide-band Gaussian fatigue damage on the basis of spectral analysis, and they are computationally efficient.

In the frequency domain, fatigue damage caused by general wide-band processes is usually obtained by a narrow-band approximation multiplied by a bandwidth correction factor, which could be empirically determined. Fatigue damage due to general wide-band stationary Gaussian processes can be evaluated by the methods proposed by Krenk [6], Wirsching and Light [7], Dirlik [8], Gall and Hancock [9], Zhao and Baker [10], Larsen and Lutes [11], Naboishikov [12], etc. Bouyssy et al. [13] compared various frequency-domain methods with the rainflow cycle counting algorithm using extensive simulations. It was concluded that the empirical formula proposed by Dirlik [8] is the best method for almost all of the assumed spectra. Recently, Benasciutti and Tovo [14] also proposed an empirical formula based on the extensive time-domain numerical simulations of five defined spectral types. When compared with the rainflow results, quite good fatigue damage approximations were obtained both by their formula and by Dirlik's formula.

Multi-modal processes are special wide-band processes whose spectra show multiple peaks at certain well separated modes. An ideal narrow-band process is the process which has only one peak in the power spectral density function. In marine technology and offshore engineering, linear structural responses due to waves can usually be assumed to be Gaussian

and narrow-banded with a spectral peak commonly corresponding to the peak frequency of wave input. Moreover, many other responses might show bimodal spectral properties, e.g. mooring system response, thruster response in waves, combined wave-induced and springing motions of TLP and large ships. In principle, methods for fatigue damage estimation of a general wide-band process can also be applied for a bimodal process. In addition, specific methods have been proposed by several researchers, such as Jiao and Moan [15], Sakai and Okamura [16] and Fu and Cebon [17], where different combination principles of the two frequency components have been applied. Benasciutti and Tovo [18] compared these methods and showed that quite accurate results were provided by Jiao and Moan's method as well as by the general methods such as the single-moment technique [11] and Benasciutti and Tovo's formula [14]. Moreover, bimodal fatigue damage could also be explicitly expressed by the individual fatigue damage components, such as DNV's formula [19] and Huang and Moan's formula [20].

Trimodal processes might also be involved in offshore engineering. For example, a riser system could be excited at both the wave frequency and low frequency under wave and wind loads when attached to a moored vessel. On the other hand, the riser system itself could experience vortex induced vibrations (VIV) with high frequencies under current action. As a result, the power spectrum of, for example, the riser bending moment could show at least three peaks. Traditionally, the fatigue damage due to VIV was separately calculated and was simply added to the wave and low frequency components to obtain the total fatigue damage. In principle, this results in an underestimation of the total fatigue damage. Therefore, a thorough procedure which simultaneously considers the interaction of all frequency components is certainly of interest.

In this paper, a procedure for estimating trimodal fatigue damage is proposed by generalizing the theory of Jiao and Moan [15]. Jiao and Moan's method accurately predicts the bimodal fatigue damage and has been widely used in many offshore codes, such as DNV-OS-E301 [21], API RP 2SK [22] and ISO 19901-7 [23]. Based on a fundamental study on the rainflow cycle counting of the time series, it seems that global load cycles with long periods could be enlarged by local cycles with short periods. The novel method actually uses this information and estimates the total fatigue damage as the sum of the fatigue damage due to the following three processes, i.e. the high frequency (HF) process, the intermediate frequency (MF) process plus the HF envelope process and the low frequency (LF) process plus both the HF and MF envelope processes. The accuracy of the proposed method has been examined by the rainflow counting for a variety of trimodal processes with different combinations of the variances and central frequencies of the HF, MF and LF components.

Furthermore, the method has also been generalized to general wide-band processes where the spectrum is equally divided into three segments with the same variances and the fatigue damage is calculated as done for the ideal trimodal processes. The proposed method together with several other frequency-domain methods are compared with the rainflow counting results considering a variety of time series of wave- and wind-induced structural

responses and the responses defined by general wide-band spectra.

In addition, two empirical formulae for wide-band fatigue damage estimation, one derived by Dirlik [8] and the other proposed by Benasciutti and Tovo [14], have also been verified to be very accurate but slightly underestimate the fatigue damage whatever the value of the bandwidth parameter is.

2. The proposed method for trimodal fatigue analysis

First, let us consider an ideal trimodal process, which is defined as the sum of three narrow-band random processes with well separated central frequencies, namely by:

$$Y(t) = X_H(t) + X_M(t) + X_L(t) \tag{1}$$

where $X_H(t)$, $X_M(t)$ and $X_L(t)$ represent the components with high, intermediate and low frequencies (ν_{0H}, ν_{0M} and ν_{0L}) and variances (σ_H^2, σ_M^2 and σ_L^2), respectively. These three components are assumed to be stationary, Gaussian and mutually independent.

Based on the narrow-band assumption, fatigue damage of each frequency component can be estimated by the Palmgren-Miner rule [1] as follows, if a single-slope SN curve ($N = KS^{-m}$) is adopted.

$$D = T / K * \nu_0 * \overline{S^m} \tag{2}$$

where ν_0 is the mean zero up-crossing rate, $\overline{S^m}$ denotes the expected value of the stress range S powered by m and equals to $(2\sqrt{2}\sigma)^m \Gamma(1+m/2)$ for a Gaussian process, where σ is the standard deviation of the process and $\Gamma()$ denotes the Gamma function, T is the total duration and K and m are the material parameters of the SN curve.

Fatigue damage of $Y(t)$ is not just the sum of the fatigue damage of the three frequency components because of the mutual interaction. Jiao and Moan [15] estimated bimodal fatigue damage as the sum of the fatigue damage due to two processes, one is the HF process and the other is the LF process plus the HF envelope process. In this paper, based on the same principle, trimodal fatigue damage can be estimated from three equivalent processes, as shown in Eq. (3).

$$D_Y = D_H + D_P + D_Q \tag{3}$$

where D_H is the fatigue damage due to the HF process, D_P is the fatigue damage due to the process $P(t) = R_H(t) + X_M(t)$ which is the MF process plus the HF envelope process $R_H(t)$, while D_Q is the fatigue damage due to the process $Q(t) = R_H(t) + R_M(t) + X_L(t)$ which is the LF process plus the HF envelope process $R_H(t)$ and the MF envelope process $R_M(t)$. It is implicitly assumed that the HF envelope process $R_H(t)$ has a similar oscillation period to $X_M(t)$. When $R_H(t)$ and $R_M(t)$ are used in conjunction with $X_L(t)$, they are also assumed to have similar oscillation periods. Both $P(t)$ and $Q(t)$ are narrow-banded under this assumption.

Moreover, the amplitude processes of $P(t)$ and $Q(t)$ can be simply written as

$R_P(t) = R_H(t) + R_M(t)$ and $R_Q(t) = R_H(t) + R_M(t) + R_L(t)$, respectively. Under the narrow-band Gaussian assumption for each component, $R_H(t)$, $R_M(t)$ and $R_L(t)$ are all Rayleigh processes and $R_P(t)$ and $R_Q(t)$ are Rayleigh sum processes with two and three components, respectively. All of these processes are listed in Table 1. As shown by the table, the procedure of fatigue analysis for bimodal and trimodal processes can be readily generalized to multi-modal processes.

Table 1 Defined random processes for fatigue analysis

Process component	Equivalent process for fatigue analysis	Amplitude of equivalent process (Rayleigh sum)
$X_H(t)$	$X_H(t)$	$R_H(t)$
$X_M(t)$	$P(t) = R_H(t) + X_M(t)$	$R_P(t) = R_H(t) + R_M(t)$
$X_L(t)$	$Q(t) = R_H(t) + R_M(t) + X_L(t)$	$R_Q(t) = R_H(t) + R_M(t) + R_L(t)$
...	...	...

In order to calculate the fatigue damage, the mean zero up-crossing rate and the equivalent stress range, which is obtained by the integral over the amplitude distribution of the process, should be calculated first. Analytical formulation of the fatigue damage due to $P(t)$ has been well established by Jiao and Moan [15]. Especially, the mean zero up-crossing rate of $P(t)$ was obtained using the Rice formula [24] as shown in Eq. (4),

$$\nu_{0P} = \int_0^\infty \dot{p} f_{P\dot{P}}(0, \dot{p}) d\dot{p} = \frac{1}{\sqrt{2\pi}} f_P(0) \sigma_{\dot{P}} = \sqrt{\lambda_{2H}\delta_H^2 + \lambda_{2M}} * \frac{\sigma_M}{2\pi(\sigma_H^2 + \sigma_M^2)} \tag{4}$$

where $\lambda_{iH} \approx (2\pi\nu_{0H})^i \sigma_H^2$ and $\lambda_{iM} \approx (2\pi\nu_{0M})^i \sigma_M^2$ are the *i*th spectral moments of the HF and MF components, respectively. $\delta_H = \sqrt{1 - \lambda_{1H}^2 / \lambda_{0H} / \lambda_{2H}}$ denotes the Vanmarcke's bandwidth parameter of the HF process.

The fatigue damage of $Q(t)$ is derived as follows.

Although there does not exist an analytical expression for the distribution of $Q(t)$ which is evaluated by a double convolution integral, the mean zero up-crossing rate can still be analytically obtained by the Rice formula.

$$\begin{aligned} \nu_{0Q} &= \int_0^\infty \dot{q} f_{Q\dot{Q}}(0, \dot{q}) d\dot{q} = \frac{1}{\sqrt{2\pi}} f_Q(0) \sigma_{\dot{Q}} = \sqrt{\lambda_{2H}\delta_H^2 + \lambda_{2M}\delta_M^2 + \lambda_{2L}} \\ &* \frac{(2\sigma_L\sqrt{\sigma_H^2 + \sigma_M^2 + \sigma_L^2} - \pi\sigma_H\sigma_M + 2\sigma_H\sigma_M \arctan(\sigma_H\sigma_M / \sigma_L / \sqrt{\sigma_H^2 + \sigma_M^2 + \sigma_L^2}))}{4\pi(\sqrt{\sigma_H^2 + \sigma_M^2 + \sigma_L^2})^3} \end{aligned} \tag{5}$$

where $\lambda_{iL} \approx (2\pi\nu_{0L})^i \sigma_L^2$ is the *i*th spectral moments of the LF component. $\delta_M = \sqrt{1 - \lambda_{1M}^2 / \lambda_{0M} / \lambda_{2M}}$ denotes the Vanmarcke's bandwidth parameter of the MF process. If the number of frequency components is greater than three, the mean zero up-crossing rate can not be obtained by an analytical formula and numerical estimation of a multiple convolution integral must be carried out.

It should be noted that the Vanmarcke's bandwidth parameters of the HF and MF

processes are used in Eqs. (4) and (5). They must be sufficiently small so that each process can be assumed to be narrow-banded. Asymptotically, they can be replaced by zeros. If the method is applied when the HF and MF processes are wide-banded, the result could be quite conservative. It is therefore recommended to use zeros for these bandwidth parameters as done in this paper.

The distribution of $R_Q(t)$ represents a weighted Rayleigh sum distribution where the values of the variances σ_H^2, σ_M^2 and σ_L^2 could be different from each other. It can also be evaluated by a double convolution integral. However, unfortunately, an analytical formula does not exist for this distribution either. In this paper, the Hermite numerical integration method [25] is applied and a semi-analytical closed-form solution can be obtained for the distribution of $R_Q(t)$ as follows,

$$f_{RH}(x_1) = f_H(x_1) = x_1/\sigma_H^2 \exp(-x_1^2/2/\sigma_H^2) \tag{6}$$

$$f_{RP}(x_2) = f_{HM}(x_2) = 2\sum_{i=1}^{n} a_i z_i f_H(x_2 - \sqrt{2}\sigma_M z_i) \tag{7}$$

$$f_{RQ}(x_3) = f_{HML}(x_3) = 2\sum_{j=1}^{n} a_j z_j f_{HM}(x_3 - \sqrt{2}\sigma_L z_j) \tag{8}$$

where $f_{HM}(x_2)$ is the sum distribution of the HF and MF components and $f_{HML}(x_3)$ is the sum distribution of the HF, MF and LF components. z_i and z_j are the identical abscissas (zeros of the *n*th-order Hermite polynomial) and a_i and a_j are the identical weight factors. It should be noted that only the positive abscissas are applied ($z_i > 0$ and $z_j > 0$) and only the positive values are allowed for x_1 ($x_3 - \sqrt{2}\sigma_L z_j - \sqrt{2}\sigma_M z_i > 0$) because the Rayleigh distribution $f_{RH}(x_1)$ is defined over the positive half axis. In fact, the amplitude distribution of $Q(t)$, i.e. the distribution of $R_Q(t)$, is now expressed as a double sum of the Rayleigh distributions with positive origins and the *m*th equivalent stress range can be semi-analytically obtained when *m* is an integer. As an example, it is shown in Eq. (9) with *m*=3.

$$\overline{S_Q^m} = \sum_{j=1}^{n} 2a_j z_j \sum_{i=1}^{n} 2a_i z_i (8b_{ij}^3 + 12\sqrt{2\pi}\sigma_H b_{ij}^2 + 48\sigma_H^2 b_{ij} + 12\sqrt{2\pi}\sigma_H^3) \tag{9}$$

where $b_{ij} = \sqrt{2}\sigma_L z_j + \sqrt{2}\sigma_M z_i$.

Similarly, the *m*th equivalent stress range due to $P(t)$ is

$$\overline{S_P^m} = \sum_{i=1}^{n} 2a_i z_i (8b_i^3 + 12\sqrt{2\pi}\sigma_H b_i^2 + 48\sigma_H^2 b_i + 12\sqrt{2\pi}\sigma_H^3) \tag{10}$$

where $b_i = \sqrt{2}\sigma_M z_i$.

As long as the mean zero up-crossing rate ν_0 and the equivalent stress range $\overline{S^m}$ are obtained, Eq. (2) can be individually applied for the fatigue damage estimation of the processes $P(t)$ and $Q(t)$ under the narrow-band assumption.

Finally, the total trimodal fatigue damage can be estimated by Eq. (3).

The above procedure for fatigue damage estimation is also applicable to bimodal processes, for which Jiao and Moan obtained the analytical formula [15], while the numerical method is adopted in this paper. Moreover, the proposed method can be readily extended from trimodal to multi-modal Gaussian processes.

3. Generalization of the proposed method to general wide-band processes

A general wide-band process could have a continuous spectral density function with any possible shape. Based on a given spectrum, we try to define three equivalent component processes according to a certain rule by which the proposed method for an ideal trimodal process could be applied to estimate the general wide-band fatigue damage. Various principles for discretizing the wide-band process into trimodal approximation might be applied. We used the probably simplest way to do this, i.e. the equal-variance rule, as shown in Fig. 1. In this way, a wide-band spectrum is divided into three segments with the same variances, i.e. the same areas under the spectral density function, e.g. $var_1 = var_2 = var_3$ in Fig. 1. This implies that three processes with the same energy could be extracted from a general wide-band process for fatigue damage estimation.

A numerical discretization of the spectrum has to be applied probably based on an iterative procedure. The equal-variance rule has a big advantage in terms of numerical computation effort since it only uses the *0*th-order moment of the spectrum. Other rules might be also applicable, e.g. the rules based on equal bandwidth parameter or equal fatigue damage for each component. However, higher-order spectral moments must be calculated and it could be very time-consuming especially based on an iterative numerical procedure.

When the three segments are determined, the corresponding mean zero up-crossing rate of each process could be calculated based on the discretized spectrum, e.g. $\omega_1, \omega_2, \omega_3$ in Fig. 1.

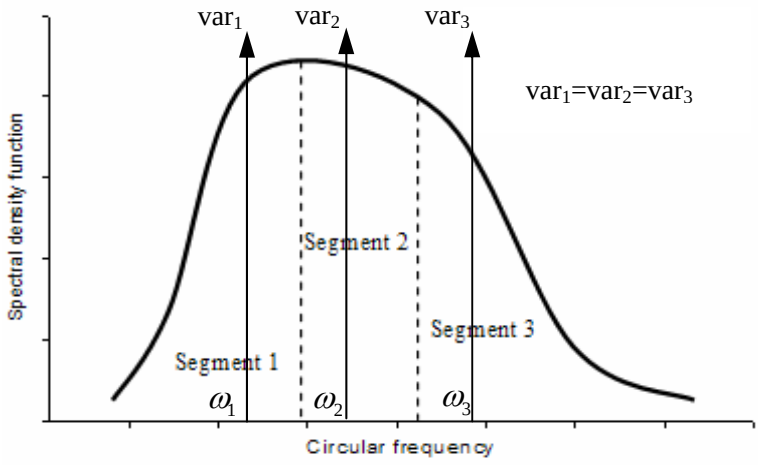

Fig. 1 Discretization of the spectrum into three segments based on the equal-variance rule (where, var_i and ω_i represent the variances and central frequencies of the three components, respectively)

In order to apply the proposed method, the narrow-band assumption is made for each segment. This might not be strictly true and could introduce certain overestimation in the

fatigue damage estimates.

In addition, the distribution of $R_Q(t)$ is now simplified to an independent and identically distributed (IID) Rayleigh sum distribution, because the variances are equal for the three components. Under this condition, accurate closed-form approximations are available. For instance, the small argument approximation (SAA) was proposed by Schwartz et al. [26]. Hu and Beaulieu [27] discussed the accuracy of the SAA and proposed an empirical modified approximation based on the SAA.

The *m*th equivalent stress range obtained based on the amplitude distribution is necessary for fatigue damage estimation. A closed-form solution of the *m*th equivalent stress range can only be obtained for the SAA and numerical integration must be involved in Hu and Beaulieu's approximation. As an example, the accuracy of the *m*th (*m*=3) equivalent stress range is shown in Table 2. Results are shown as the ratios to the Monte Carlo simulations, which have been carried out for Rayleigh sum random variables with 3-5 components and are believed to give the most accurate estimates since there is no theoretical solution. Unfortunately, the SAA always underestimates the equivalent stress range, while Hu and Beauliu's approximation overestimates it for a small number of components. The Hermite numerical integration method has also been checked. It provides quite acceptable estimates and therefore in the following case studies, this method is still applied.

Table 2 Comparison of the *m*th (*m*=3) equivalent stress range of an IID Rayleigh sum distribution obtained by different methods

Number of components	Monte Carlo simulation	Hermite integration	SAA	Hu and Beauliu's approximation
3	1.000	1.014	0.935	1.433
4	1.000	1.027	0.926	1.632
5	1.000	1.045	0.922	1.087

4. Verification of the proposed method for ideal trimodal processes

In order to check the accuracy of the proposed method, extensive time series of ideal trimodal Gaussian processes have been simulated with different combinations of the central frequencies (ν_{0H}, ν_{0M} and ν_{0L}) and variances (σ_H^2, σ_M^2 and σ_L^2) of the HF, MF and LF components. Values of the frequency ratios (ν_{0H}/ν_{0M} and ν_{0M}/ν_{0L}) have been selected as 2, 4, 6, 8, 10 and 20, while values of the variance ratios (σ_H^2/σ_M^2 and σ_M^2/σ_L^2) have been selected as 1/9, 3/7, 1, 7/3 and 9. In total, there are 6*6*5*5=900 cases with 20 simulations for each.

Frequency-domain methods, including the proposed method, Dirlik's formula (DK), Benasciutti and Tovo's formula (BT), the simple sum of the components (SS) and the narrow-band assumption (NB), are compared with the rainflow counting results (RFC) obtained using the WAFO Matlab toolbox [28]. The obtained fatigue damage ratio to RFC is shown as a function of Vanmarcke's bandwidth parameter in the following figures.

In order to validate the numerical procedure, ideal bimodal processes have first been

simulated with the same frequency and variance ratios as for the trimodal processes. The results are shown in Fig. 1. For bimodal processes, the proposed method is basically the same as Jiao and Moan's explicit formula and quite close estimates of fatigue damage are obtained by these two methods, therefore only the results obtained by the current numerical procedure are provided. It is seen in the figure that the proposed method and the DK and BT formulae quite accurately estimate the bimodal fatigue damage, except that the proposed method overestimates the fatigue damage in some cases with a Vanmarcke's bandwidth parameter which is less than 0.35 where the narrow-band assumption can be very well made. As expected, the SS method always underestimates the fatigue damage and the NB method significantly overestimates the fatigue damage for higher bandwidth parameters.

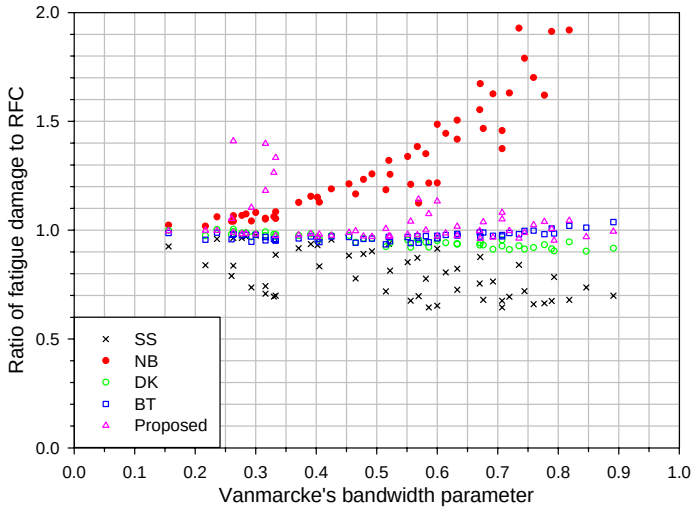

Fig. 2 Ratio of fatigue damage of ideal bimodal spectra to RFC as a function of bandwidth parameter

Figs. 3-4 show only the comparisons between the trimodal fatigue damage obtained by the proposed method and the RFC results as functions of frequency and variance ratios, respectively. Each data point in the figures corresponds to one case and a total of 900 cases are provided. It is shown that the fatigue damage ratio to RFC in most of the cases is close to 1 (from 0.9 to 1.2) and, in general, the accuracy of the proposed method is quite acceptable. However, when the LF component dominates and the central frequencies of the three components are close, the fatigue damage ratio is large and could reach 1.5 in the extreme cases. In such cases, the conservative approximation of both the mean zero up-crossing rate and the amplitude distribution of $Q(t)$ explains the overestimation of the proposed method.

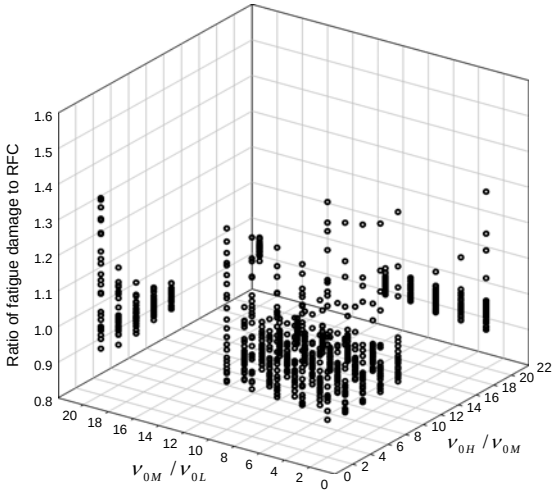

Fig. 3 Ratio of fatigue damage of ideal trimodal spectra to RFC obtained by the proposed method as a function of frequency ratio

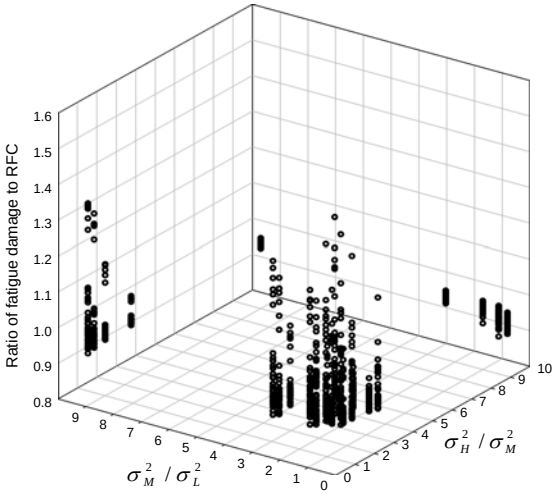

Fig. 4 Ratio of fatigue damage of ideal trimodal spectra to RFC obtained by the proposed method as a function of variance ratio

Both the DK and BT methods are also applied by considering the trimodal processes as general wide-band processes, see Fig. 5. The SS and NB results are provided as well, but the NB estimates with a fatigue damage ratio greater than 2 are not shown in the figure. In general, the DK and BT empirical formulae give quite good fatigue damage estimates for all of the bandwidths considered herein, although they slightly underestimate the fatigue damage in most of the cases and slightly overestimate it for bandwidth parameters quite close to 1. When the bandwidth parameter is less than 0.5, the narrow-band approximation is reasonably good with a maximum overestimation of 30%. In some of such cases, when the central frequencies of the HF, MF and LF components are not well separated, i.e. the whole process is not wide-banded, this could lead to even more conservative results than the NB estimates by applying the proposed method, as explained in the above paragraph. For bandwidths greater than 0.5, the proposed method predicts the fatigue damage quite close to the rainflow method on average, especially when the bandwidth parameter is close to 1. The traditional

method to calculate the fatigue damage due to the combined VIV and wave and low frequency loads is also applied where the HF fatigue damage is simply added to the combined MF and LF fatigue damage. As shown in the figure, this method underestimates the total fatigue damage for almost all of the cases by 20% on average and by 40% in the worst cases and is just slightly better than the SS estimates. The SS method is believed to be the most underestimating method where no interaction between the frequency components is considered.

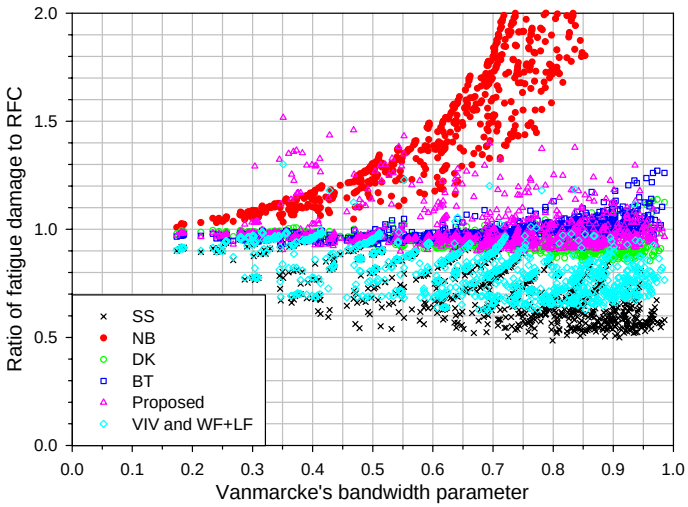

Fig. 5 Ratio of fatigue damage of ideal trimodal spectra to RFC as a function of bandwidth parameter

5. Case studies of general wide-band processes

Wide-band stationary Gaussian processes with a variety of spectral shapes have been simulated. They include spectra of wave- and wind-induced marine structural responses, spectra used in Dirlik's thesis [8], spectra defined by Benasciutti and Tovo [14] and other generally defined spectra by the authors. The comparisons between the frequency-domain methods and the rainflow cycle counting results are shown in Figs. 6-11.

Wave-induced responses are of main concern for fixed and floating marine structures. Four typical linear structural responses are applied in this paper, including the mudline shear force of a gravity platform [29], the vertical motion of a TLP [30], the vertical mid-ship bending moment of a FPSO [31] and stresses in a brace-column joint of a semi-submersible [31]. Response spectra are obtained by using a doubly peaked wave spectrum [32] with two parameters H_S and T_P which are varied from 1m in 1m increments to 15m and from 2s in 2s increments to 20s, respectively. A total of 15*10=150 spectra have been considered for each response type. Multiple peaks in the response spectra are expected with a doubly peaked wave input spectrum. The obtained fatigue damage is shown in Fig. 6 as a function of bandwidth parameter. Most values of the obtained bandwidth are less than 0.5 where the narrow-band approximation shows only a slight overestimation by a maximum of 20%. In such cases, the proposed method seems to significantly overestimate the fatigue damage,

while it works very well for bandwidths of 0.5-0.6 with an accuracy of 90-110%. The DK and BT methods yield fatigue damage slightly less than 1 and the underestimation increases with the bandwidth parameter.

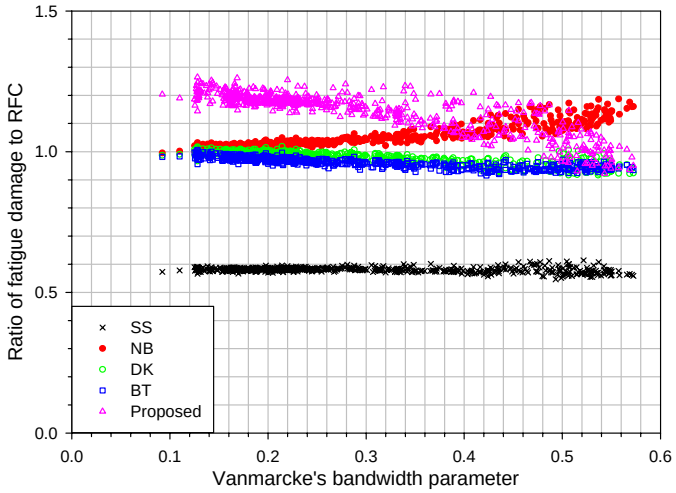

Fig. 6 Ratio of fatigue damage of wave-induced response spectra to RFC as a function of bandwidth parameter

The mudline bending stress of a wind turbine tower [33] has been considered as an example of wind-induced structural responses and an NPD wind spectrum [34] with a parameter U_M from 2m/s in 2m/s increments to 60m/s has been applied. Only a few cases are analysed and results are shown in Fig. 7. According to the calculated bandwidth parameter, the wind-induced response is more wide-band than the wave-induced response because the wind input spectrum normally has a higher contribution from the low frequency part than the wave spectrum, which leads to a higher bandwidth parameter. The BT formula gives very accurate estimates, while the DK formula and the proposed method slightly underestimate the fatigue damage by 5% and 10%, respectively. Nevertheless, it should be noted that only one type of wind-induced responses is considered herein. It might be necessary to carry out more case studies before any conclusion can be made for general wind-induced responses.

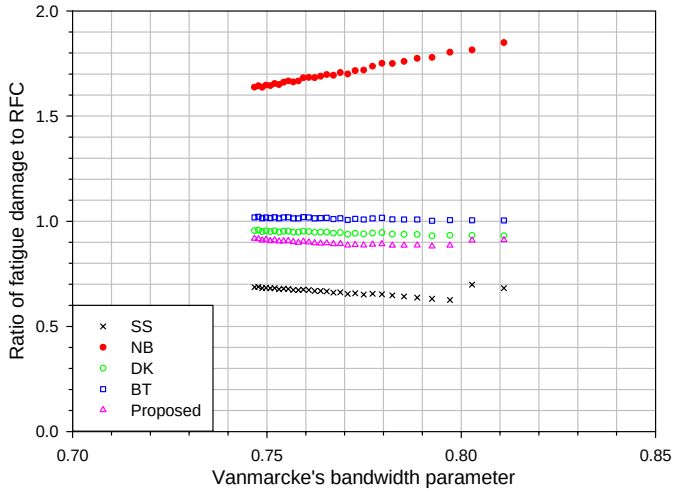

Fig. 7 Ratio of fatigue damage of wind-induced response spectra to RFC as a function of bandwidth parameter

Benasciutti and Tovo [14] defined a series of spectral densities with simple geometry (e.g. uniform, linear and parabolic shapes) to obtain their empirical formula. These spectra are also used in this paper to check the accuracy of the proposed method for generally defined spectra. The fatigue damage obtained for 1800 cases is shown in Fig. 8. For these cases, the Vanmarcke's bandwidth parameter almost covers the whole range from 0 to 1. The very conservative NB results for a high bandwidth parameter are not shown. Both the DK and BT methods estimate the fatigue damage accurately but underestimate it by 5% on average as in the previous examples. The BT method gives better results than the DK method. The narrow-band approximation is again quite good for bandwidths less than 0.5 and a maximum 20% overestimation is obtained. The proposed method predicts the fatigue damage quite accurately in most of the cases for bandwidths of 0.5-0.85 where the overestimation of the narrow-band approximation increases significantly. For bandwidths greater than 0.85, the proposed method probably significantly overestimates the fatigue damage because it might not be adequate to divide the spectrum into only three segments. In such cases, even the SS method gives conservative results. In particular, it may be conservative to assume each of the three modes to be narrow-banded, especially for the HF component. In addition, spectra with the bandwidth parameter quite close to 1 might be unrealistic and at least the wave- or wind-induced response spectra used in this paper have a maximum bandwidth parameter of only 0.81. In this sense, the accuracy of the proposed method with the trimodal spectral formulation is practically acceptable for bandwidth parameters not greater than 0.85. Anyway, if desired, the accuracy of the proposed method may be improved by discretizing the spectra with more segments (e.g. 4 or 5 segments) of equal variances. The corresponding fatigue damage is obtained by the four-modal and five-modal formulations as shown in Fig. 9. It is clearly shown that the overestimation of the proposed method could be alleviated for large values of the bandwidth by increasing the number of segments.

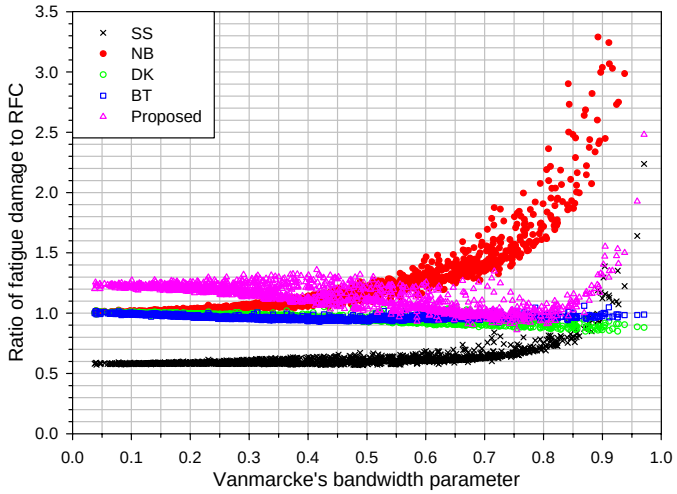

Fig. 8 Ratio of fatigue damage of Benasciutti and Tovo's spectra to RFC as a function of bandwidth parameter

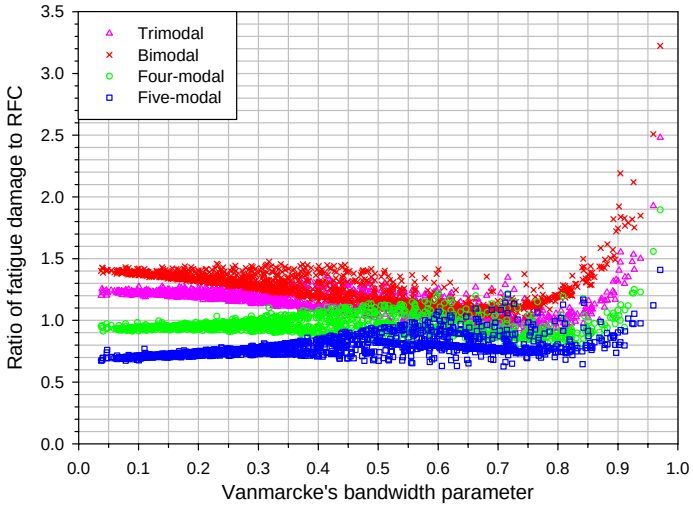

Fig. 9 Ratio of fatigue damage of Benasciutti and Tovo's spectra to RFC obtained by the multi-modal formulations as a function of bandwidth parameter

Dirlik [8] applied two kinds of spectral types to obtain the empirical formula. One is a combination of two uniform spectra and the other is a mathematically defined continuous spectrum with two peaks. A total of 70 different spectra were used by Dirlik and they are also adopted in this paper. Fatigue damage results are shown in Fig. 10 and the obtained bandwidth parameter is from 0.1 to 0.85. The accuracy of the frequency-domain methods is similar to that for Benasciutti and Tovo's spectra.

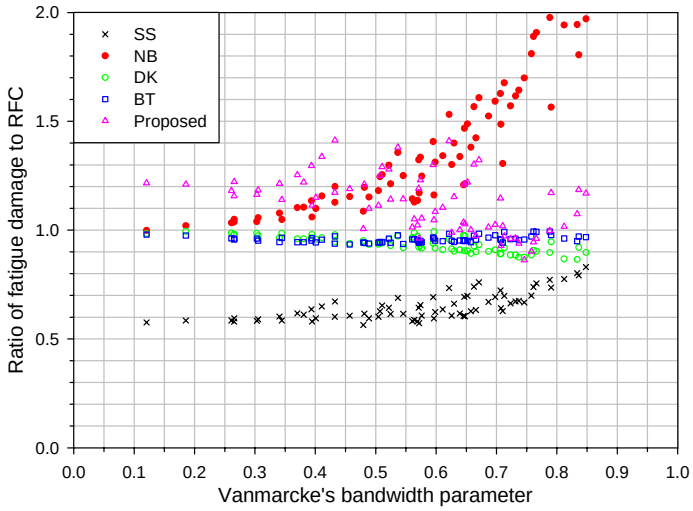

Fig. 10 Ratio of fatigue damage of Dirlik's spectra to RFC as a function of bandwidth parameter

Some other general wide-band spectra are also defined in this paper, where combinations of one, two or three sub-spectra with a uniform, linear or parabolic shape are used. Results are shown in Fig. 11. The obtained bandwidth parameters are all less than 0.65 due to a certain restriction on the definition of these spectra. Anyway, similar conclusions can be made for these spectra as for the previous cases.

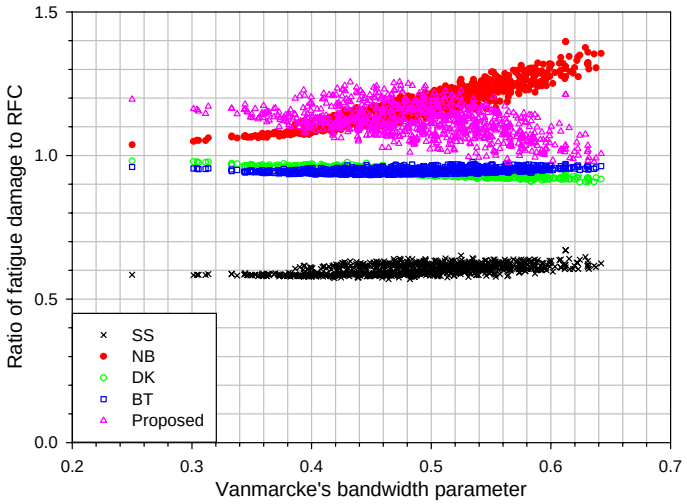

Fig. 11 Ratio of fatigue damage of generally defined wide-band spectra to RFC as a function of bandwidth parameter

6. Conclusions

A method for trimodal Gaussian fatigue damage estimation has been proposed based on the theory of Jiao and Moan for bimodal processes using the envelopes of narrow-band components. The accuracy of the proposed method and other general frequency-domain methods has been checked with the rainflow cycle counting results obtained based on extensive time-domain simulations of ideal trimodal processes. As long as the trimodal process has well separated frequency components and is not dominated by the LF component, the proposed method predicts the fatigue damage quite close to the rainflow results. Both the empirical formulae proposed by Dirlik and by Benasciutti and Tovo are also found to give quite accurate estimates of the trimodal fatigue damage.

Fatigue damage with a more general wide-band spectrum has also been obtained by generalizing the proposed method with a trimodal (or even a multi-modal) spectral formulation where the spectrum is equally divided into three (or multiple) segments with the same variances. Other rules for the spectrum discretization might be applied as well, e.g. the equal-bandwidth parameter rule or the equal-fatigue damage rule. However, further work need to be carried out to check the efficiency and accuracy.

Case studies have also been carried out considering various spectra relevant for typical offshore structural responses induced by waves and wind and generally defined spectra. In most of the cases with a Vanmarcke's bandwidth parameter which is less than 0.5, it is found that the narrow-band assumption can very well be used to estimate the fatigue damage, since a maximum 30% overestimation is expected. Therefore, it is very important and necessary as a first step to calculate the bandwidth parameter for wide-band fatigue analysis. When the bandwidth parameter is in the range of 0.5-0.85, the proposed method predicts the fatigue damage close to that obtained by the rainflow counting method on average, while it might significantly overestimate the fatigue damage for bandwidth parameters greater than 0.85.

Such cases are however not practical for the type of responses investigated herein. If frequency-domain analyses are still applied in such cases, it is shown that more accurate estimates can be obtained by refining the proposed method by dividing the general wide-band spectrum equally into more segments. In this connection, further development of this method might be necessary.

Although Dirlik's and Benasciutti and Tovo's formulae were empirically obtained based on simulations with assumed spectral shapes and the fatigue damages predicted by both formulae might be slightly underestimated in most of the cases, it is demonstrated that these two formulae give quite accurate fatigue damage estimates for all of the spectral shapes and bandwidth parameters considered herein.

Acknowledgements

The authors wish to acknowledge the support from the Research Council of Norway through the Centre for Ships and Ocean Structures at the Norwegian University of Science and Technology in Trondheim, Norway.

References

[1] Miner MA. Cumulative damage in fatigue. Journal of Applied Mechanics 1945; Vol. 12, pp. 159-164.

[2] Matsuishi M, Endo T. Fatigue of metals subjected to varying stress. Japan Society of Mechanical Engineers, Fukuoka, Japan; 1968.

[3] Rychlik I. A new definition of the rainflow cycle counting method. International Journal of Fatigue 1987; Vol. 9, No. 2, pp. 119-121.

[4] Dowling NE. Fatigue-failure predictions for complicated stress-strain histories. Journal of Materials, ASTM 1972; Vol. 7, No. 1, pp. 71-87.

[5] Watson P, Dabell BJ. Cycle counting and fatigue damage. Symposium on statistical aspects of fatigue testing, Warwick University; 1975.

[6] Krenk S. A double envelope for stochastic processes. Report No. 134, Danish Centre for Applied Mathematics and Mechanics; 1978.

[7] Wirsching PH, Light MC. Fatigue under wide band random stresses. Proceedings of the ASCE, Journal of the Structural Division 1980; Vol. 106, No. ST7, pp. 1593-1607.

[8] Dirlik T. Application of computers in fatigue. Ph.D. Thesis, University of Warwick; 1985.

[9] Gall DS, Hancock JW. Fatigue crack growth under narrow and broad band stationary loading. Glasgow University, Marine Technology Centre; 1985.

[10] Zhao W, Baker MJ. A new stress-range distribution model for fatigue analysis under wave loading. Environmental Forces of Offshore Structures and their Prediction, Kluwer Academic Publishers 1990; pp. 271-291.

[11] Larsen CE, Lutes LD. Predicting the fatigue life of offshore structures by the single-moment spectral method. Probabilistic Engineering Mechanics 1991; Vol. 6, No. 2, pp.

96-108.

[12] Naboishikov S. On the distribution of local extremes, ranges and means of Gaussian processes. Proceedings of the 4th IFIP WG 7.5 Conference, Munich 1991; pp. 305-312.

[13] Bouyssy V, Naboishikov SM, Rackwitz R. Comparison of analytical counting methods for Gaussian processes. Structural Safety 1993; Vol. 12, pp. 35-57.

[14] Benasciutti D, Tovo R. Spectral methods for lifetime prediction under wide-band stationary random processes. International Journal of Fatigue 2005; Vol. 27, pp. 867-877.

[15] Jiao G, Moan T. Probabilistic analysis of fatigue due to Gaussian load processes. Probabilistic Engineering Mechanics 1990; Vol. 5, No. 2, pp. 76-83.

[16] Sakai S, Okamura H. On the distribution of rainflow range for Gaussian random processes with bimodal PSD. JSME International Journal Series A 1995; Vol. 38, No. 4, pp. 440-445.

[17] Fu TT, Cebon D. Predicting fatigue lives for bi-modal stress spectral densities. International Journal of Fatigue 2000; Vol. 22, pp. 11-21.

[18] Benasciutti D, Tovo R. On fatigue damage assessment in bimodal random processes. International Journal of Fatigue 2007; Vol. 29, pp. 232-244.

[19] Lotsberg I. Background for revision of DNV-RP-C203 fatigue analysis of offshore steel structure. Proceedings of the 24th OMAE Conference, Halkidiki, Greece; 2005; Paper No. OMAE2005-67549.

[20] Huang W, Moan T. Fatigue under combined high and low frequency loads. Proceedings of the 25th OMAE Conference, Hamburg, Germany; 2006; Paper No. OMAE2006-92247.

[21] DNV. Offshore standard - Position mooring. DNV-OS-E301; 2004.

[22] API. Recommended practice for design and analysis of stationkeeping systems for floating structures. API RP 2SK; 2005.

[23] ISO. Petroleum and natural gas industries - Specific requirements for offshore structures - Part 7: Stationkeeping systems for floating offshore structures and mobile offshore units. ISO 19901-7; 2005.

[24] Cartwright DE, Longuet-Higgins MS. The statistical distribution of the maxima of a random function. Proceedings of the Royal Society of London, Series A, Mathematical and Physical Sciences 1956; Vol.237, Issue 1209, pp.212-232.

[25] Karagiannidis GK, Kotsopoulos SA. On the distribution of the weighted sum of *L* independent Rician and Nakagami envelopes in the presence of AWGN. KICS Journal of Communications and Networks 2001; Vol. 3, No. 2, pp. 26-30.

[26] Schwartz M, Bennet WR, Stein S. Communication Systems and Techniques. McGraw-Hill, New York; 1966.

[27] Hu J, Beaulieu NC. Accurate simple closed-form approximations to Rayleigh sum distributions and densities. IEEE Communications Letters 2005; Vol. 9, No. 2.

[28] The WAFO Group. WAFO - A Matlab toolbox for analysis of random waves and loads.

August 2000, Version 2.0.02.

[29] Holand I, Kavlie D, Moe G, Sigbjornsson R. Safety of structures under dynamic loading. TAPIR Publishers 1978; Vol. 1, p. 525.

[30] Faltinsen OM. Sea loads on ships and offshore structures. Cambridge Ocean Technology Series. Cambridge University Press 1990; p. 74.

[31] Moan T, Gao Z, Ayala-Uraga E. Uncertainty of wave-induced response of marine structures due to long-term variation of extratropical wave conditions. Marine Structures 2005; Vol. 18, No. 4, pp. 359-382.

[32] Torsethaugen K. Model for a doubly peaked wave spectrum. Technical Report STF22 A96204, SINTEF; 1996.

[33] Tempel J van der. Design of support structures for offshore wind turbines. Ph.D. Thesis, Delft University of Technology; 2006.

[34] Norwegian Petroleum Directorate. Guidelines concerning loads and load effects to regulations concerning loadbearing structures in the petroleum activities. 1992.

Paper 3

Uncertainty of wave-induced response of marine structures due to long-term variation of extratropical wave conditions

Published in
Marine Structures 2005; Vol. 18, No. 4, pp. 359-382

Available online at www.sciencedirect.com
SCIENCE DIRECT®
Marine Structures 18 (2005) 359–382
MARINE STRUCTURES
www.elsevier.com/locate/marstruc

Uncertainty of wave-induced response of marine structures due to long-term variation of extratropical wave conditions

Torgeir Moan[a,*], Zhen Gao[a], Efren Ayala-Uraga[b]

[a]*Centre for Ships and Ocean Structures, Norwegian University of Science and Technology, Otto Nielsens v 10, N-7491 Trondheim, Norway*
[b]*Department of Marine Technology, Norwegian University of Science and Technology, Otto Nielsens v 10, N-7491 Trondheim, Norway*

Received 18 October 2005; received in revised form 31 October 2005; accepted 1 November 2005

Abstract

Wave conditions in extratropical regions have seasonal variations. The wave condition in a period of one or more years exhibits variation, as displayed by samples of data for such a period. It is important to have a measure of the variability in the wave-induced extreme response and fatigue damage for marine structures due to this statistical uncertainty for sea states in various service periods. For instance, this variability needs to be considered when assessing the safety of a structure until next inspection or repair after damage. Moreover, this variability illustrates the uncertainty due to limited data, say in connection with measuring service behaviour in periods of limited duration. Scatter diagrams for the northern North Sea for 1-, 2- and 4-year periods as well as a 29-year period are applied in this study to determine the typical wave-induced response of an FPSO and a semi-submersible. The wave conditions are considered representative for extratropical climate. The marginal distribution of the significant wave height is modelled with a hybrid lognormal-Weibull model and the conditional distribution of peak period is fitted by a lognormal distribution. The long-term response of fatigue stress ranges is fitted by a generalized gamma distribution, which includes the frequently used two-parameter Weibull distribution as a special case. The extreme values are described by a two-parameter Weibull tail model. Compared with the 29-year distribution, the variation in the annual distributions is quite considerable as measured either by the distribution parameters, or the predicted extreme value of significant wave height, or the long-term response for extreme and fatigue loading. The correlation between the extreme and fatigue response and various measures of the significant wave height, H_S, is also studied. High correlation is for instance found

*Corresponding author. Tel.: +47 73595541; fax: +47 73595528.
E-mail address: torgeir.moan@marin.ntnu.no (T. Moan).

0951-8339/$ - see front matter
doi:10.1016/j.marstruc.2005.11.001

between the extreme H_S and extreme response, as well as between the H_S which is exceeded by a probability of 10% and fatigue damage.

Keywords: Significant wave height; Peak period; Statistical variability; Extreme response; Fatigue damage; Generalized gamma distribution

1. Introduction

Offshore structures and ships are commonly designed to withstand extreme climate conditions during their service life corresponding to a certain return period, e.g. 100- and 20-year periods, respectively. Moreover, they are designed for a certain fatigue life which is usually a multiple of the service life time.

Normally, a large amount of data is required in order to achieve an accurate prediction of extreme conditions. Wave design parameters may be determined by extrapolation of either actual measurements or hindcast values. The long-term variation of ocean waves is often expressed in terms of significant wave height (H_S) and peak period (T_P), assuming stationary conditions of sea states with a duration of, e.g. 3 h based on a 20-min time-history record. The number of occurrences of each sea state is described by a frequency table or scatter diagram that represents a discrete (long-term) joint distribution H_S-T_P of the sea conditions in a certain location. Since the observations of the most extreme wave events are subjected to particular uncertainty, it is important that the observed data are smoothed by fitting a joint probability density function (pdf). Different pdf models have been used to fit the data with a smoothed joint distribution. The lognormal and Weibull models are often used to fit H_S, e.g. Battjes [1], Nordenstrøm [2], Moan et al. [3]. Other possibilities are the beta and gamma distributions, e.g. Ferreira et al. [4]. Herein the marginal distribution of the significant wave height is modelled with a hybrid lognormal-Weibull model, while the conditional distribution of the peak period is fitted by a lognormal distribution (Haver [5]). This model gives a better fit of H_S than a pure lognormal or two-parameter Weibull model. To predict the extreme values with a return period of 20, 100 years and more, other models than those above based on the whole data set, can be adopted. This includes methods based on the annual extreme data as well as fitting the tail by a Type II asymptotic extreme distribution, or the peak over threshold (POT) method.

For the decision-making process in safety management of existing marine structures it is important to have a proper description of the uncertainty level in the sea conditions and responses during a limited period of time, e.g. 1 year or few years. For instance, assessing the safety level of a vessel for a certain period, e.g. until a repair is carried out, depends very much on a proper characterization of the sea conditions and responses for the period of interest. Variability in fatigue loading during the period between consecutive inspections, say 4–5 years, is of special interest. Another situation arises when in-service behaviour is monitored to validate the safety of existing structures. For instance, if the fatigue damage during a single year of operation is determined by monitoring, the monitored variability of fatigue damage from year to year should be observed before conclusions about the implied safety level are made. Obviously, even more caution needs to be exercised when inferring information about extreme responses based on limited wave

data. For instance, Nolte [6] shows that the significant wave height varies significantly from year to year. In addition, there are seasonal variations as exemplified by Guedes Soares et al. [7]. However, studies so far have only focused on the variation in wave data and not responses. Moreover, previous studies have been based on limited data.

Hence, the aim of this paper is to estimate the variability in the distribution of the wave-induced response resulting from the variability of wave conditions, by using the joint pdf of significant wave height and peak period based on annual environmental data. Twenty-nine annual scatter diagrams corresponding to a location in the northern North Sea are used and are also organized into groups of every 2 and every 4 independent years. To illustrate the effect of the statistical variability of wave conditions, the extreme response estimated by a linear theory and fatigue damage due to vertical bending moment of an FPSO in the head-on sea and stress on a brace-column joint of a semi-submersible in the beam sea are analysed and the corresponding uncertainties are estimated. It is noted that the transfer functions for these two response variables have peaks at wave periods of 14 and 7.5 s, respectively. Hence, the emphasis will be on different parts of the scatter diagram in these cases.

2. Wave data analysis

2.1. Wave data

The wave data used in this paper are provided by Statoil ASA (Haver [8]). These data are recorded in 29 years (from 1974 to 2002) by wave buoys in the northern North Sea. The scatter diagrams are the frequency tables of pairs of significant wave height (H_S) and peak period (T_P). The range of H_S is from 0.25 to 12.75 m with an interval of 0.5 m and the range of T_P is from 0.5 to 29.5 s with an interval of 1 s. The 29-year scatter diagram is shown in Table 1.

2.2. Joint probability density function for waves

The long-term variation in wave climate consists of a joint density function of the significant wave height (H_S) and the peak period (T_P), which is fitted to the observed sea-states in a scatter diagram.

Alternative joint probability distributions for H_S and T_P are envisaged. The probability model used here is developed by Haver [5] and his program PHT is also adopted. This model is suitable for the northern North Sea and involves a combined lognormal and two-parameter Weibull marginal distribution (the Lonowe model) for H_S and a conditional lognormal distribution for T_P. In the fitting procedure, the significant wave height is chosen to be the basic variable because of the importance of H_S in characterizing the sea-state. The marginal distribution of H_S is described by the following pdf:

$$f_{H_S}(h_S) = \begin{cases} \frac{1}{\sqrt{2\pi}\sigma_{\ln H} h_S} \exp\left(-\frac{(\ln(h_S)-\mu_{\ln H})^2}{2\sigma_{\ln H}^2}\right) & h_S \leqslant h_S^* \\ \beta_H \frac{h_S^{\beta_H-1}}{\alpha_H^{\beta_H}} \exp\left(-\left(\frac{h_S}{\alpha_H}\right)^{\beta_H}\right) & h_S \geqslant h_S^* \end{cases}, \quad (1)$$

where h_S^* is the shifting point from the lognormal distribution to the Weibull distribution, $\mu_{\ln H}$ and $\sigma_{\ln H}$ are the mean value and the standard deviation of $\ln(H_S)$ in the lognormal

Table 1
Twenty-nine-year scatter diagram for the northern North Sea

H_s/T_p	0–1	1–2	2–3	3–4	4–5	5–6	6–7	7–8	8–9	9–10	10–11	11–12	12–13	13–14	14–15	15–16	16–17	17–18	18–19	19–20	20–21	21–22	22–23	23–24	24–25	25–26	26–27	27–28	28–29	29–30	Sum
0.25	1	0	38	35	53	69	101	116	74	43	29	25	17	8	7	8	2	5	6	0	0	0	1	0	0	0	0	0	0	0	638
0.75	0	0	9	50	331	822	1186	1187	1175	919	461	297	110	35	35	17	12	5	7	4	0	3	1	0	0	0	1	0	1	0	6668
1.25	0	0	4	27	458	1219	2059	1986	2148	1782	1060	804	407	193	126	49	29	14	8	4	1	2	0	3	0	1	4	0	0	0	12,388
1.75	0	0	0	1	112	894	1820	2344	2166	1911	1250	892	552	309	190	73	35	12	8	4	3	0	0	2	0	1	3	0	0	0	12,582
2.25	0	0	0	0	11	296	1253	1781	1964	1663	1282	924	614	309	247	83	27	22	7	2	2	0	1	0	0	2	3	0	0	0	10,493
2.75	0	0	0	0	0	71	604	1333	1857	1665	1067	955	668	310	285	116	41	18	5	3	2	2	0	0	1	4	1	1	0	0	9009
3.25	0	0	0	0	1	6	219	835	1375	1431	911	785	554	368	246	122	54	25	8	1	1	1	0	1	0	0	0	0	0	0	6944
3.75	0	0	0	0	0	0	48	427	983	1176	832	655	453	282	239	119	50	23	9	2	0	0	0	0	0	1	0	0	0	0	5299
4.25	0	0	0	0	0	0	5	165	642	997	672	549	426	194	199	97	41	30	9	3	0	1	0	0	0	0	0	0	0	0	4030
4.75	0	0	0	0	0	0	2	39	344	715	588	514	339	195	140	61	44	27	6	5	1	0	0	0	0	0	0	0	0	0	3020
5.25	0	0	0	0	0	0	0	4	109	468	555	457	289	162	120	41	31	16	6	4	0	0	0	0	0	0	0	0	0	0	2262
5.75	0	0	0	0	0	0	0	1	34	211	382	308	249	100	97	41	16	17	6	0	0	0	0	0	0	0	0	0	0	0	1462
6.25	0	0	0	0	0	0	0	0	9	92	221	232	190	106	62	18	16	3	4	2	2	0	0	0	0	0	0	0	0	0	957
6.75	0	0	0	0	0	0	0	0	0	30	143	209	151	73	59	24	8	4	2	0	0	0	0	0	0	0	0	0	0	0	703
7.25	0	0	0	0	0	0	0	0	0	7	44	126	103	61	47	21	6	8	1	1	0	0	0	0	0	0	0	0	0	0	425
7.75	0	0	0	0	0	0	0	0	0	0	20	69	79	43	32	11	5	3	1	0	0	0	0	0	0	0	0	0	0	0	263
8.25	0	0	0	0	0	0	0	0	0	0	9	32	50	34	30	11	5	1	0	0	0	0	0	0	0	0	0	0	0	0	172
8.75	0	0	0	0	0	0	0	0	0	0	3	18	31	25	16	12	0	0	0	0	0	0	0	0	0	0	0	0	0	0	105
9.25	0	0	0	0	0	0	0	0	0	0	1	5	26	20	20	4	1	1	0	1	0	0	0	0	0	0	0	0	0	0	79
9.75	0	0	0	0	0	0	0	0	0	0	0	3	6	10	8	3	2	0	0	0	0	0	0	0	0	0	0	0	0	0	32
10.25	0	0	0	0	0	0	0	0	0	0	0	3	4	13	6	5	1	0	1	0	0	0	0	0	0	0	0	0	0	0	33
10.75	0	0	0	0	0	0	0	0	0	0	0	0	6	2	3	1	2	0	0	0	0	0	0	0	0	0	0	0	0	0	14
11.25	0	0	0	0	0	0	0	0	0	0	0	0	2	2	5	0	2	0	0	0	0	0	0	0	0	0	0	0	0	0	11
11.75	0	0	0	0	0	0	0	0	0	0	0	0	0	1	1	0	0	0	0	0	0	0	0	0	0	0	0	0	0	0	2
12.25	0	0	0	0	0	0	0	0	0	0	0	0	0	0	0	1	0	0	0	0	0	0	0	0	0	0	0	0	0	0	1
12.75	0	0	0	0	0	0	0	0	0	0	0	0	0	0	0	0	0	1	0	0	0	0	0	0	0	0	0	0	0	0	1
Sum	1	0	51	113	966	3377	7297	10218	12880	13110	9530	7862	5326	2855	2220	938	430	235	94	36	12	9	3	6	1	9	12	1	1	0	77,593

model, α_H and β_H are the scale parameter and shape parameter in the Weibull tail. Parameters $\mu_{\ln H}$ and $\sigma_{\ln H}$ are estimated directly from the raw data using moment estimation, in the same way as the parameters obtained by applying a lognormal distribution only. Parameters α_H and β_H are obtained by imposing the continuity conditions on two pdfs and two cumulative distribution functions (cdfs) at h_S^*. The procedure for choosing of h_S^* is made to determine a proper location of the Weibull tail, which is quite important to get a good fit of the marginal distribution for H_S and will significantly affect the extreme value prediction. A simple iterative procedure based on chi-square (χ^2) testing is therefore applied in this study to obtain a reasonable estimate of the shifting point. This is done by estimating the χ^2 factor by

$$\chi^2 = n \sum_i \frac{(f_{H_S 0}(h_{Si}) - f_{H_S}(h_{Si}))^2}{f_{H_S}(h_{Si})}, \tag{2}$$

where n is the effective number of observations, $f_{H_S 0}(h_{Si})$ and $f_{H_S}(h_{Si})$ are the empirical and the estimated probability density for interval No. i in the scatter diagram, respectively.

The mean value (μ_H) and the standard deviation (σ_H) of H_S are transformed from the lognormal parameters $\mu_{\ln H}$ and $\sigma_{\ln H}$ according to the formula

$$\mu_H = \exp\left(\frac{\sigma_{\ln H}^2}{2} + \mu_{\ln H}\right),$$
$$\sigma_H = \exp\left(\frac{\sigma_{\ln H}^2}{2} + \mu_{\ln H}\right)\sqrt{\exp(\sigma_{\ln H}^2) - 1}. \tag{3}$$

Conditional distribution of the peak period is assumed to follow a pure lognormal distribution:

$$f_{T_P|H_S}(t_P|h_S) = \frac{1}{\sqrt{2\pi}\sigma_{\ln T} t_P} \exp\left(-\frac{(\ln(t_P) - \mu_{\ln T})^2}{2\sigma_{\ln T}^2}\right), \tag{4}$$

where the lower bound for T_P is assumed to be zero. Physically, the wave breaks when the steepness of wave ($S_P = (2\pi/g)(H_S/T_P^2)$) is larger than 0.1. However, it has a small effect on the overall fitting of T_P for practical purpose. The conditionality of T_P on H_S is described in such a way that the mean value ($\mu_{\ln T}$) of $\ln(T_P)$ and the variance ($\sigma_{\ln T}^2$) of $\ln(T_P)$ are smooth functions of H_S, applying the following forms:

$$\mu_{\ln T} = a_1 + a_2 h_S^{a_3}, \tag{5}$$

$$\sigma_{\ln T}^2 = b_1 + b_2 \exp(b_3 h_S), \tag{6}$$

where a_1, a_2, a_3 and b_1, b_2, b_3 are coefficients estimated from the raw data by nonlinear least-square method, and moreover in order to avoid the unphysical meaning when b_1 is smaller than 0, b_1 is chosen to be a small constant 0.001.

The long-term joint pdf for H_S and T_P is just the product of the marginal pdf for H_S and the conditional pdf for T_P:

$$f_{H_S,T_P}(h_S, t_P) = f_{H_S}(h_S) * f_{T_P|H_S}(t_P|h_S). \tag{7}$$

The prediction of extreme value, e.g. annual extreme H_S and extreme H_S with a return period of 100 years, can be determined directly from the Weibull tail. Extreme value

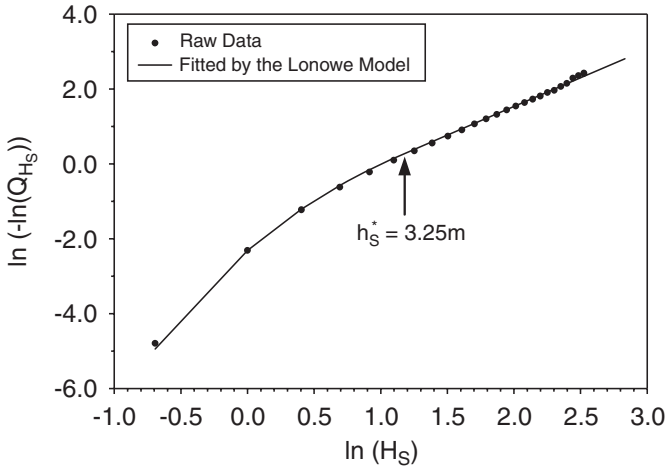

Fig. 1. Fitted significant wave height by the Lonowe model based on the 29-year scatter diagram, as plotted on Weibull paper.

with an exceedance probability P_E is calculated by

$$H_{SE} = \alpha_H(-\ln(P_E))^{1/\beta_H}. \tag{8}$$

A contour line could be defined as an iso-probability density curve. The contour line corresponding to a given return period can then be constructed by first identifying the iso-pdf curve that corresponds to H_S with a given return period based on the marginal distribution of H_S, see e.g. NORSOK N-003 [9]. The concept of contour line is later defined in a more refined manner [9] to provide a basis for determining the long-term response with a certain return period based on a few sea states with H_S and T_P on the relevant contour line [9]. Hence, it is useful to compare various scatter diagrams by comparing contour lines for, say, 1, 20 or 100 years mean return periods.

Fig. 1 shows the fitted marginal distribution of significant wave height on a Weibull paper by the Lonowe model using the 29-year scatter diagram. In this case, the fit is quite good and from the figure it is observed that the lower part of H_S distribution follows a lognormal model while the tail of the distribution is close to a straight line on the Weibull paper which indicates that it follows a Weibull model. Fig. 2 shows the mean value of $\ln(T_P)$ increases with the increasing H_S while Fig. 3 shows that a decreasing trend for the variance. The curves fitted by the models represented by Eqs. (5) and (6) are also shown and a quite good fit is obtained both for the mean value and the variance. Based on these functions and the marginal distribution of H_S, the joint density of H_S and T_P can be obtained by Eq. (7). For example, Fig. 4 shows the contour plot of pdf using the 29-year data.

2.3. Variations in the wave data

In order to study the variation in the environmental pdf models in different years, the joint model and fitting procedure described above, are applied for all of the 29 individual scatter diagrams and groups of every 2 and every 4 independent years together with the 29-year scatter diagram as a whole. This includes 14 2-year scatter diagrams and 7 4-year scatter diagrams with the scatter diagram in 1974 excluded. Based on the raw data, the

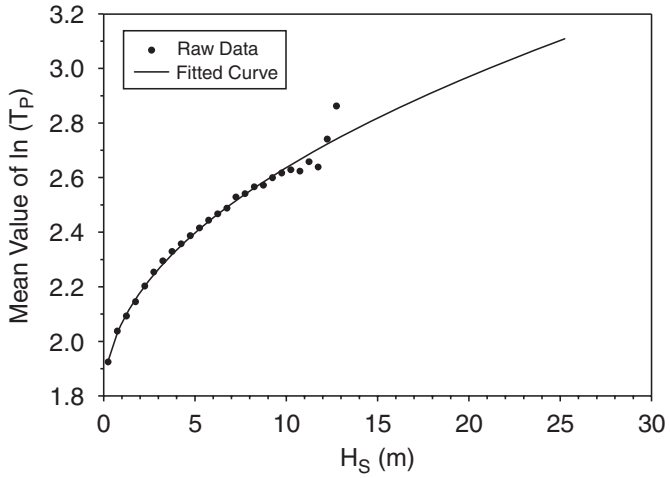

Fig. 2. Fitted mean value of $\ln(T_P)$ as a function of H_S based on the 29-year scatter diagram.

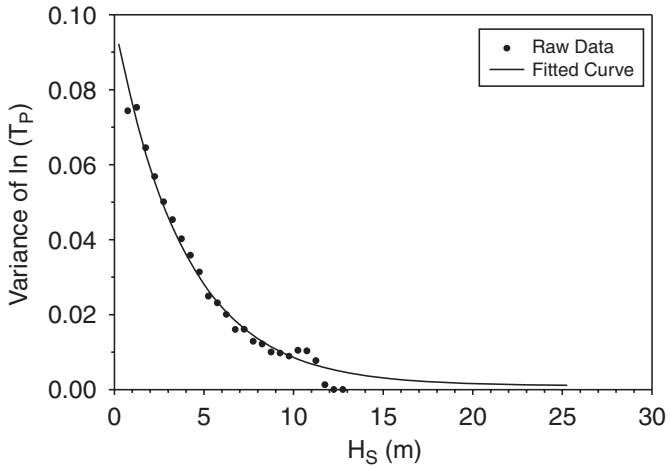

Fig. 3. Fitted variance of $\ln(T_P)$ as a function of H_S based on the 29-year scatter diagram.

empirical pdf of H_S is first calculated and the upper tail of 29-year data is shown in Fig. 5 together with the lower and upper bounds of annual, 2- and 4-year data. Significant difference of tail distribution indicates a significant difference in the extreme value prediction of H_S. Observed maximum of H_S in each scatter diagram for a 1-, 2- and 4-year period is collected into the histogram shown in Fig. 6. The histogram based on the annual data shows larger scatter than that of 2- and 4-year data. As shown later, the expected annual maximum H_S obtained by the 29 years of data and by proper smoothing of the data, are both about 10.5 m.

The estimated parameters in the distributions are compared, such as the mean value and standard deviation of H_S, the scale and shape parameters in the Weibull tail, the parameters in Eqs. (5) and (6). Due to lack of space, only the mean value of H_S is shown in Fig. 7. The mean value of H_S based on the 29-year scatter diagram is about 2.7 m, while the mean values are from 2.3 to 3.2 m using the annual scatter diagrams, from 2.5 to 2.9 m using the 2-year scatter diagrams, from 2.6 to 2.8 m using the 4-year scatter diagrams. A

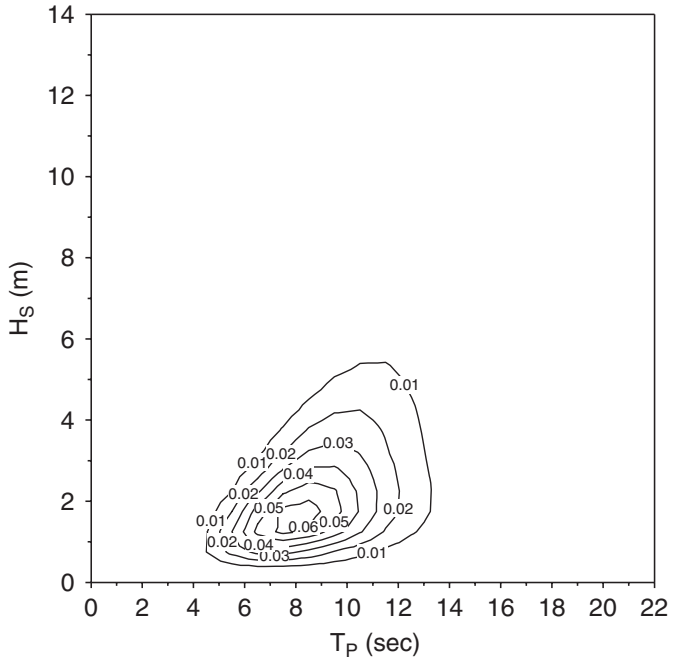

Fig. 4. Contour plot of the joint pdf of H_S and T_P using the 29-year data.

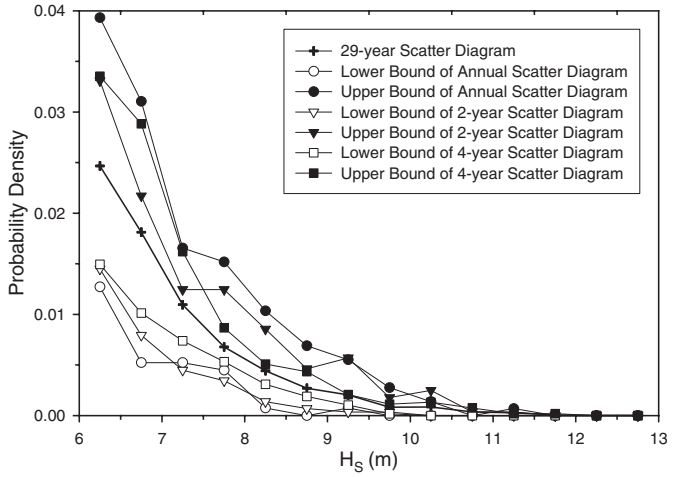

Fig. 5. Tail of probability density function of H_S based on raw data.

large annual variation of the mean value of H_S is obtained with a coefficient of variance (COV) of 0.26. When more data are used, the variation is reduced. COV is equal to 0.096 between every 2 years and 0.077 between every 4 years. Similar phenomena are observed for other parameters.

Figs. 8 and 9 show the predicted annual and 100-year extreme values of H_S by using the Lonowe model. These two figures show also the large variations in the predicted extreme values based on the data in different years. The annual extreme values vary between a maximum of 12.9 m in Case No. 13 (corresponding to 1986) and a minimum of 8.1 m in

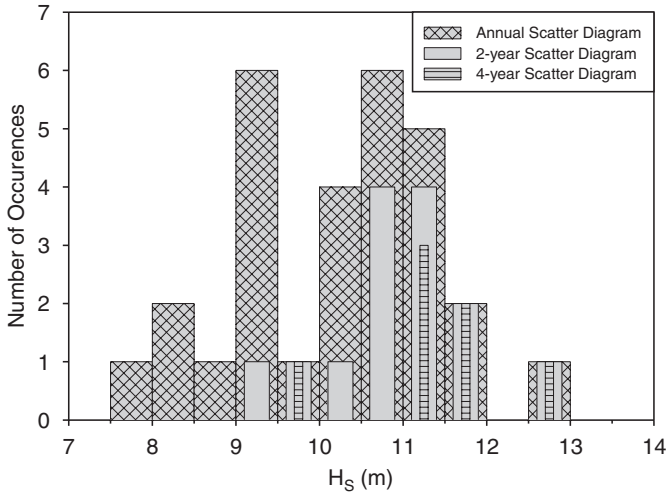

Fig. 6. Histogram of observed maxima of H_S in each scatter diagram.

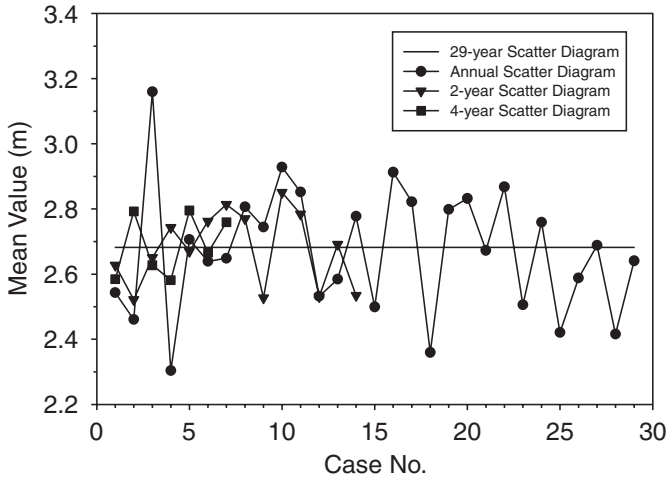

Fig. 7. Variations in the mean value of H_S.

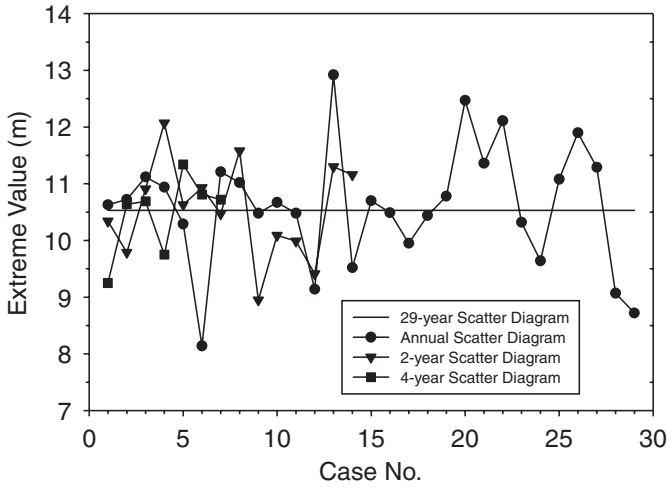

Fig. 8. Variations in the predicted annual extreme value of H_S.

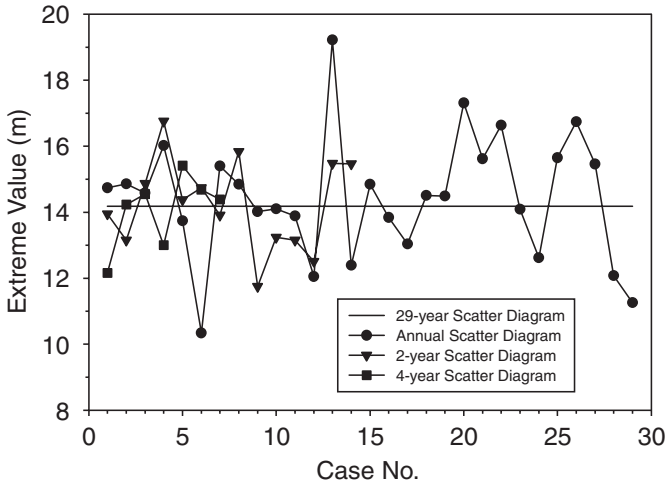

Fig. 9. Variations in the predicted 100-year extreme value of H_S.

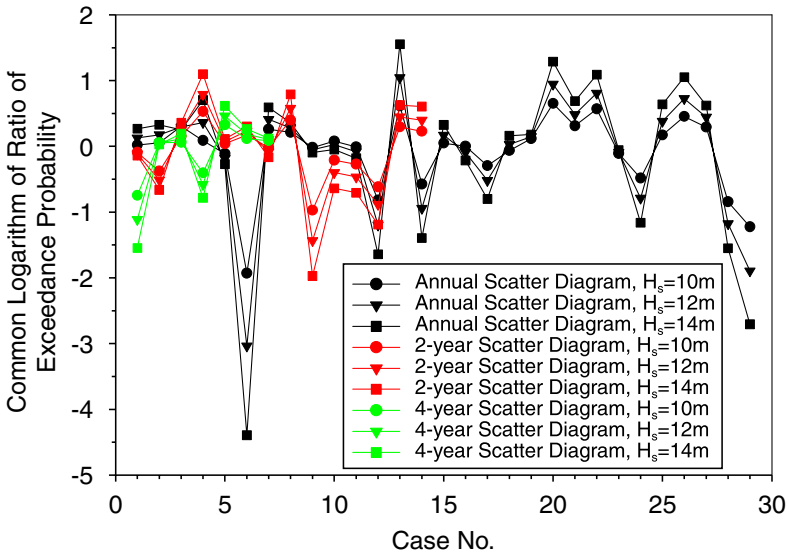

Fig. 10. Common logarithm of the ratio of the probability of exceeding $H_S = 10$, 12, 14 m, using annual, 2- and 4-year data, respectively, to the probability of exceeding the same H_S using 29-year data.

Case No. 6 (corresponding to 1979), while it is 10.5 m for the 29-year data. The predicted annual extreme values obtained by the 2-year scatter diagrams are from 9.0 to 12.1 m and from 9.3 to 11.3 m by the 4-year scatter diagrams. The 100-year extreme value varies almost by a factor of 2. The largest value is 19.2 m (in Case No. 13) and the smallest one is 10.3 m (in Case No. 6), while the extreme value based on the 29-year scatter diagram is 14.2 m. The predicted 100-year extreme values based on the 2-year scatter diagrams vary between 11.8 and 16.8 m, while the range of variation of the 100-year values based on the 4-year scatter diagrams is from 12.2 to 15.4 m. It is also indicated in the figures that using the whole database will underestimate the extreme value for some specific years while overestimate it for other years.

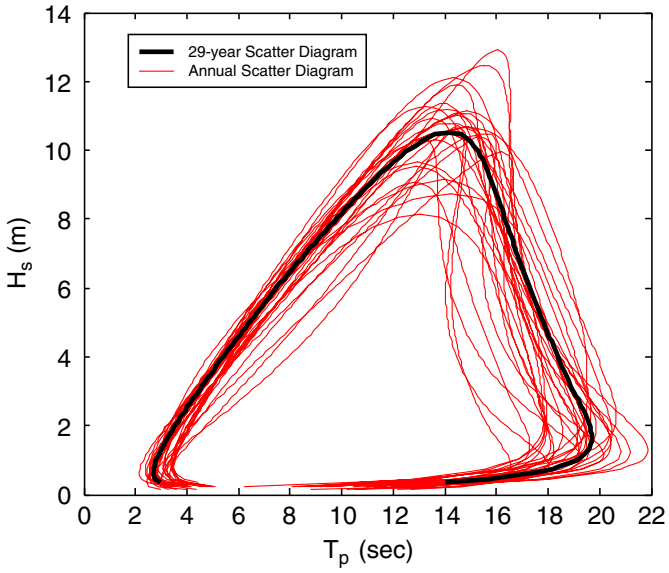

Fig. 11. One-year return period contour lines of significant wave height and peak period, using data with 29- and 1-year periods.

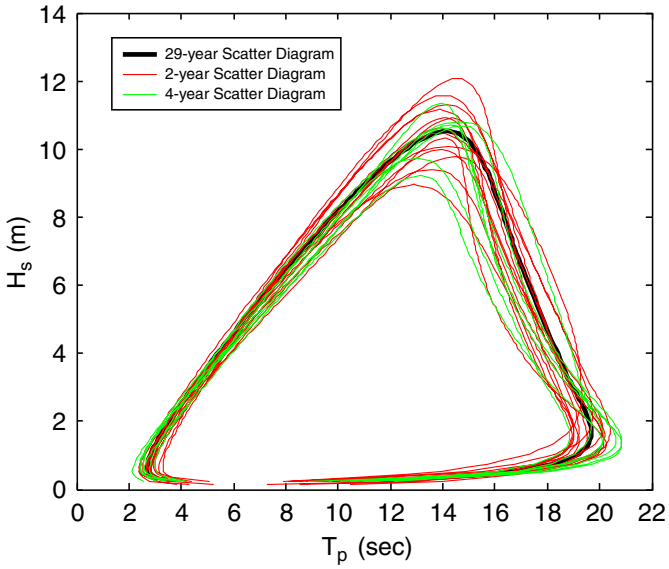

Fig. 12. One-year return period contour lines of significant wave height and peak period, using data with 29-, 2- and 4-year periods.

Fig. 10 illustrates the large scatter in the tail distribution of H_S by the ratio of the probability of exceeding larger H_S, e.g. 10, 12 or 14 m, using annual, 2- and 4-year data to the probability of exceeding the same H_S using 29-year data. The difference in exceedance probability between the annual data and the 29-year data is quite significant for some cases. In order to reduce the scatter, at least a data set with 2 years duration is needed.

The 1- and the 100-year return period contour lines of significant wave height and peak period are shown in Figs. 11–14, respectively. It is seen that the contour lines for H_S and T_P vary significantly due to the variation in wave data. It indicates that the structural responses in these design sea states will be quite different.

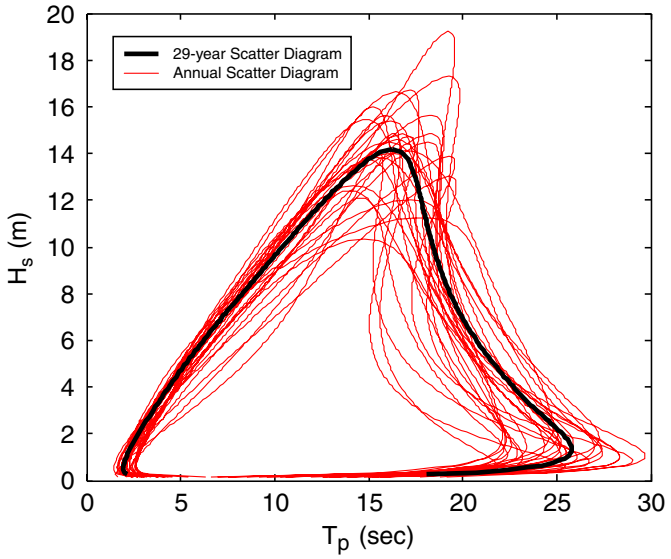

Fig. 13. One hundred-year return period contour lines of significant wave height and peak period, using data with 29- and 1-year periods.

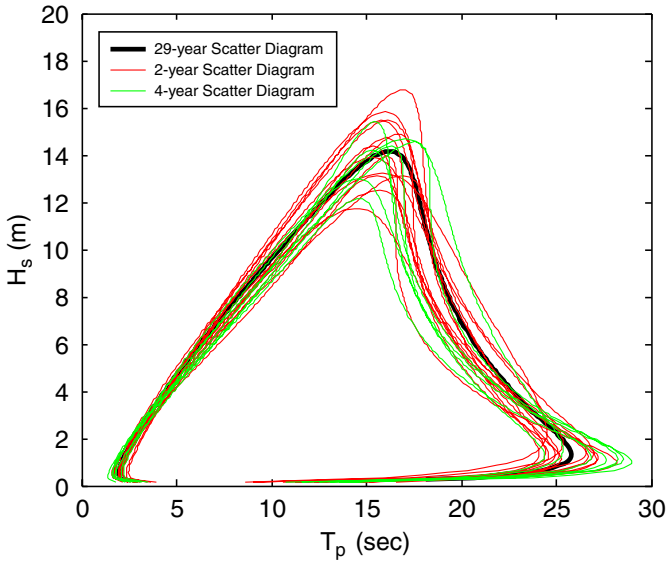

Fig. 14. One hundred-year return period contour lines of significant wave height and peak period, using data with 29-, 2- and 4-year periods.

3. Load effect statistics of an FPSO and a semi-submersible

3.1. General

In order to estimate the effect of statistical uncertainties in wave conditions on the linear load effect, long-term response analyses are carried out for the whole 29-year data as well as for groups of 1-, 2- and 4-year period, using the smoothed scatter diagrams generated by the above model. Both extreme load effects for ultimate strength and fatigue design checks are considered.

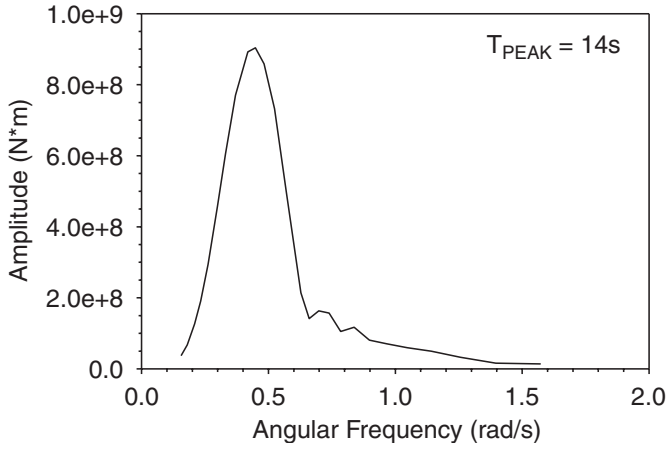

Fig. 15. Transfer function of vertical bending moment of the FPSO in head sea.

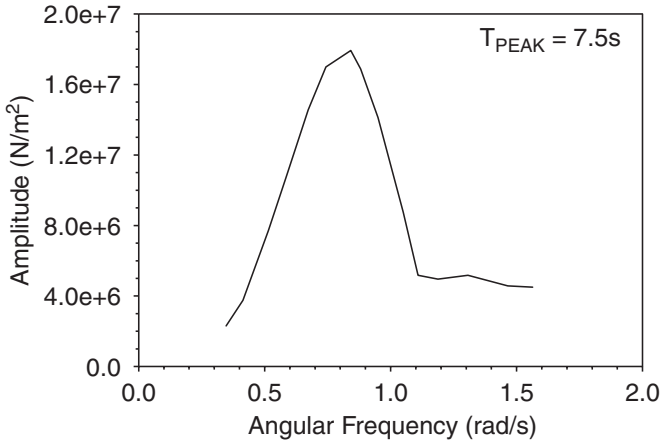

Fig. 16. Transfer function of stress on a brace-column joint of the semi-submersible in beam sea.

The response statistics are carried out on an FPSO as well as on a semi-submersible by using program SESAM Profast [10]. The main particulars of the FPSO are $L_{PP} = 320$ m, C_b of 0.77, total displacement of 186,942 tons, breadth of 58 m, height of 20 m, and draught in laden condition is 13 m. Only unidirectional, head-on waves are considered in the long-term statistics. The relevant transfer function for the vertical bending moment is shown in Fig. 15.

The semi-submersible is a twin hull configuration with a total of eight stability columns, sixteen braces and a main deck supported by these columns and braces. The overall dimensions are $L_{OA} = 90.5$ m, total weight of 22,100 tons, breath moulded of 67.4 m, upper deck height of 39.6 m, draft in operation is 21.3 m, and pontoon height of 6.7 m and width of 11 m. Beam sea is assumed for the response analysis of the semi-submersible. The transfer function of waved-induced stress on a brace-column joint is shown in Fig. 16.

In principle the long-term response of ship structures may be obtained as the summation of short-term probabilities of exceedance in all possible combinations of significant wave heights, peak periods, wave headings and spectral shapes. Herein, the Pierson–Moskowitz (P–M) spectrum is utilized.

3.2. Extreme load effects

A two-parameter Weibull (e.g. Nordenstrøm [2]) distribution is frequently used to fit the long-term response amplitude in marine structures. This distribution reads

$$F_X(x) = 1 - \exp(-(x/a)^{\beta}), \tag{9}$$

where the scale and shape parameters α and β are determined by means of the least-square method (e.g. Guedes Soares and Moan [11]).

In this paper, a two-paramenter Weibull distribution is only fitted to a probability of exceedance level corresponding to the upper tail namely from 10^{-5} to 10^{-10}. It is found this distribution gives an adequate accuracy in defining the extreme values based on the smoothed scatter diagram wave data.

Fig. 17 shows the calculated raw data of the vertical bending moment of the FPSO and the fitted data by the Weibull model on a Weibull paper when the smoothed 29-year scatter diagram is used. The accuracy of the fit is high.

Figs. 18 and 19 are the scatter plots of the distribution parameters for the FPSO and for the semi-submersible, respectively. From these figures it is observed that the shape parameter for the FPSO is 0.86 whereas for the semi-submersible it is equal to 1.16 when the smoothed 29-year scatter diagram is used with a focus on the upper tail response. The correlation coefficient between the logarithm of scale parameter and the reciprocal of shape parameter is also calculated. It is found to be -0.81 for the FPSO and -0.80 for the semi-submersible using the annual data sets.

Figs. 20 and 21 show the variability in extreme values with 10^{-8} probability of exceedance (corresponding to 10^8 response cycles, approximately a period of 20 years) using different data sets. In these two figures it is also shown that the largest variability in the estimates is obtained from the individual annual scatter diagrams. In the figures, the largest extreme value of vertical bending moment of the FPSO is (1.1×10^{10} Nm) almost as twice as the smallest one (6.6×10^9 Nm). However for the semi-submersible, the largest predicted extreme value is (1.5×10^8 N/m^2) 1.5 times the smallest one (1.1×10^8 N/m^2). It is reasonable that the scatter in the results for the semi-submersible is less than that for the

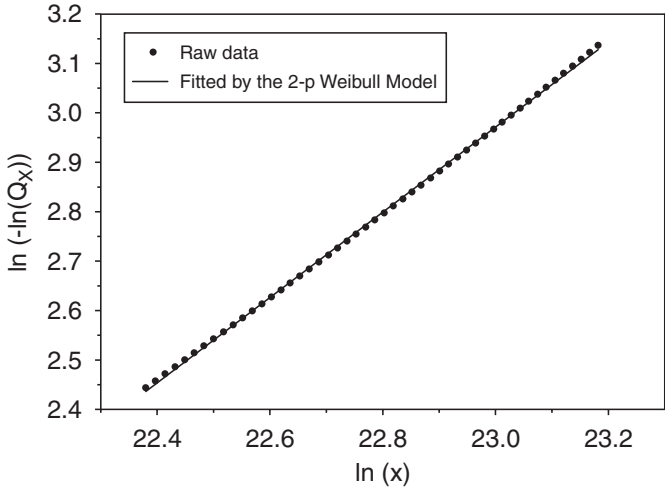

Fig. 17. Fit of the maxima of long-term vertical bending moment of the FPSO on Weibull paper.

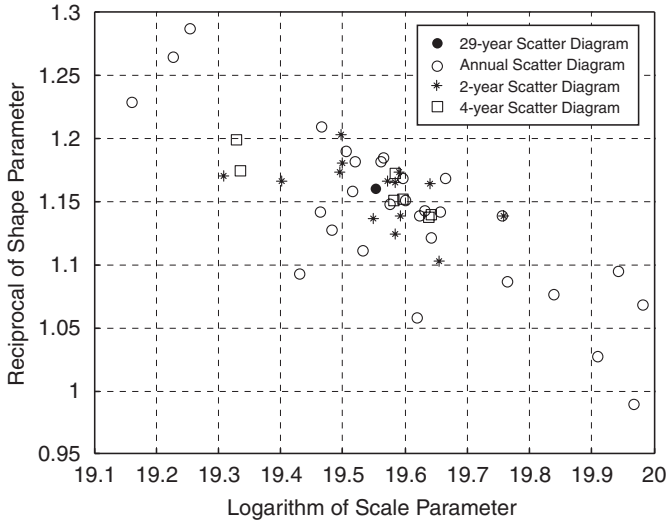

Fig. 18. Scatter plot of the parameters in the Weibull tail distribution for the FPSO.

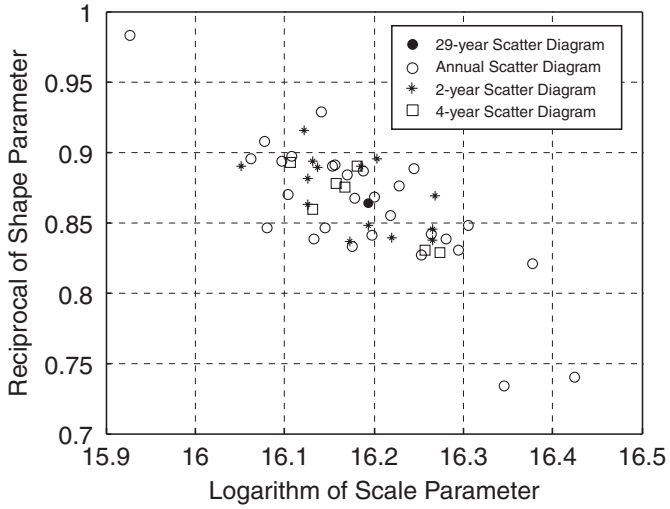

Fig. 19. Scatter plot of the parameters in the Weibull tail distribution for the semi-submersible.

FPSO. This may be explained with reference to the difference in the transfer functions. It is seen that the peak in the transfer functions are at 7.5 and 14 s for the semi-submersible and FPSO, respectively. Since the scatter in moderate waves (with a period of 7.5 s) is less than in more extreme waves (with a period of 14 s), see Table 1, the corresponding scatter in load effects is less.

3.3. Fatigue load effects

Nolte et al. [12] derived a closed-form expression for the fatigue damage under the assumption of two-parameter Weibull distributed long-term stress ranges and SN-data given by $N = KS^{-m}$:

$$D = \sum \frac{n_i}{N_i} = \frac{N}{K} E[S^m] = \frac{N}{K} \int_0^\infty s^m f_S(s)\,\mathrm{d}s = \frac{N}{K} \alpha^m \Gamma(m/\beta + 1) = \frac{N}{K} S_{\mathrm{equ}}^m, \tag{10}$$

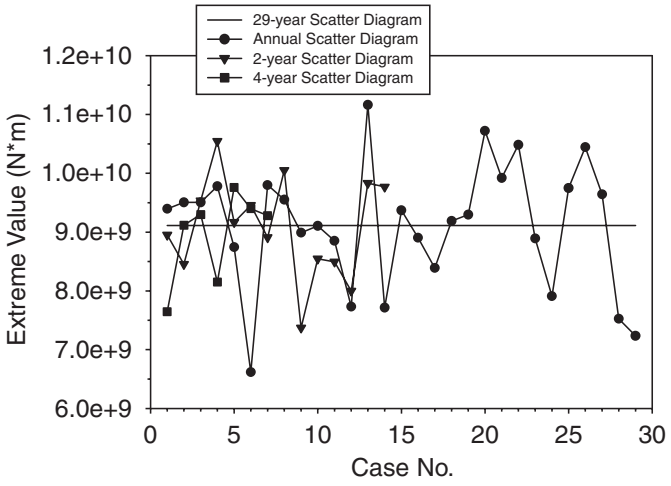

Fig. 20. Predicted most probable maximum value of vertical bending moment of the FPSO in 10^8 cycles (approximately a period of 20 years) by the Weibull model.

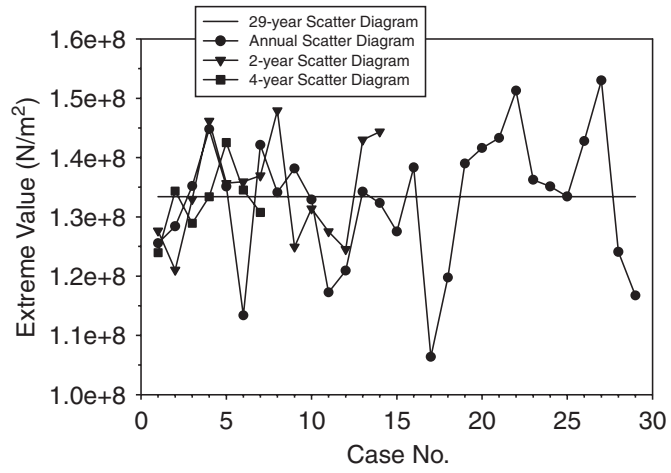

Fig. 21. Predicted most probable maximum value of stress on a brace-column joint of the semi-submersible in 10^8 cycles (approximately a period of 20 years) by the Weibull model.

where N is the number of cycles, K and $m = 3$ are the material parameters, S represents the long-term stress range with pdf $f_S(s)$, $\Gamma(\,)$ is the gamma function, and S_{equ} is the equivalent stress range. Expression (10) may be generalized for two segment SN-curves.

It is convenient to define the fatigue loading intensity as a function of stress range s by

$$FLI(s) = s^m f_S(s), \tag{11}$$

where $FLI(s)$ appears as the integrand in Eq. (10). However, this issue is not physical herein.

Instead of using a Weibull distribution it is interesting to apply a generalized gamma distribution, which also makes it possible to express the fatigue damage in a closed-form solution, as discussed below.

The pdf and cdf of the generalized gamma distribution with a zero lower bound read, respectively:

$$f_S(s) = \frac{b}{a\Gamma(c)}(s/a)^{cb-1}\exp\left(-(s/a)^b\right) \tag{12}$$

and

$$F_S(s) = \frac{\gamma(c;(s/a)^b)}{\Gamma(c)}, \tag{13}$$

where $\Gamma(\,)$ and $\gamma(;\,)$ are the gamma and incomplete gamma functions, respectively. a,b,c are the parameters of the distribution. The generalized gamma distribution is equivalent to the two-parameter Weibull distribution if $c = 1$.

Substituting Eq. (12) into Eq. (10), the equivalent m-th moment of stress range is

$$E[S^m] = \frac{b}{a\Gamma(c)}\int_0^\infty s^m(s/a)^{cb-1}\exp\left(-(s/a)^b\right)\mathrm{d}s = \frac{a^m}{\Gamma(c)}\Gamma(m/b+c). \tag{14}$$

It is seen that this equation specializes into Eq. (10) when $c = 1$ (two-parameter Weibull distribution).

Fig. 22 shows the distribution of fatigue loading intensity ($FLI(s)$) for the FPSO using a two-parameter Weibull distribution, a three-parameter Weibull distribution and a generalized gamma distribution. These distributions are compared to the numerically calculated raw data obtained by using the smoothed scatter diagram. In this case it was found that in order to include most of the contributions (about 99%) to fatigue damage an exceedance probability of $0.3–10^{-6}$ needs to be included. From the figure, it is observed that both the generalized gamma distribution and the three-parameter Weibull distribution

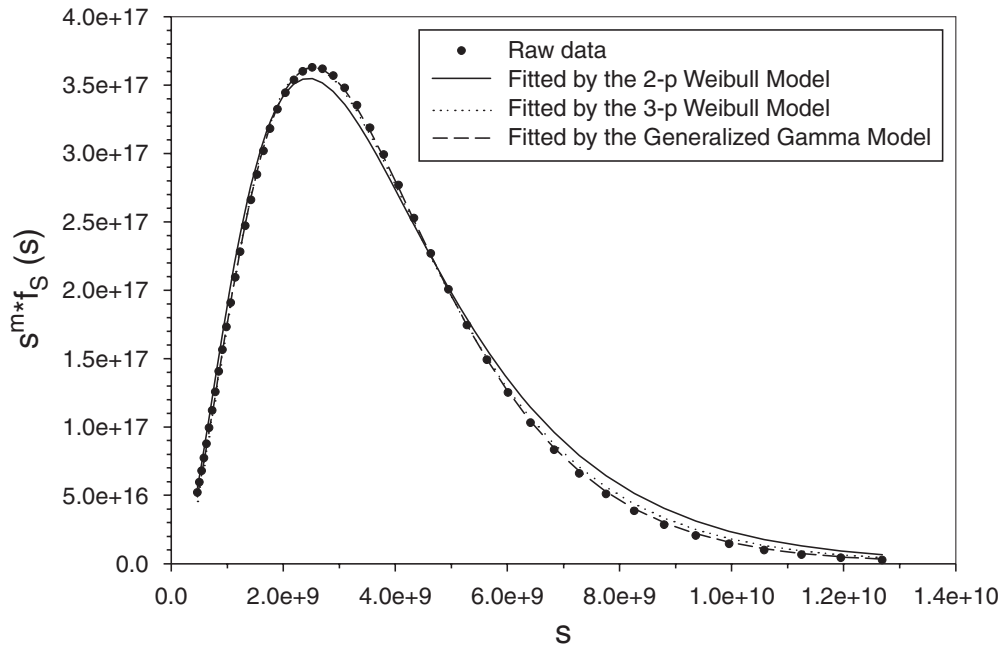

Fig. 22. Fatigue loading intensity due to the vertical bending moment of the FPSO.

fit the raw data better than the two-parameter Weibull model. In the following, only the results from the generalized gamma distribution will be given.

The scatter plots of three parameters in the generalized gamma distribution for the FPSO and the semi-submersible relating to fatigue analysis are shown in Figs. 23–26, respectively. The correlation coefficients between every two of the logarithm of parameter a, the reciprocal of parameter b and the parameter c are calculated to be -0.96, -0.92, 0.89 for the FPSO and -0.98, -0.98, 0.95 for the semi-submersible based on the 29 annual data sets.

Figs. 27 and 28 show the predicted fatigue damage for the FPSO and the semi-submersible, respectively. The fatigue damage based on 29-year data is calibrated to be 1.

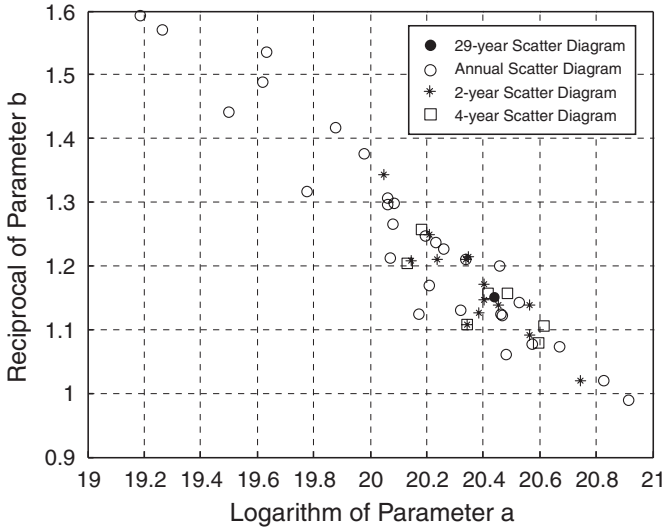

Fig. 23. Scatter plot of the parameters a and b in the generalized gamma distribution for the FPSO, relating to fatigue analysis.

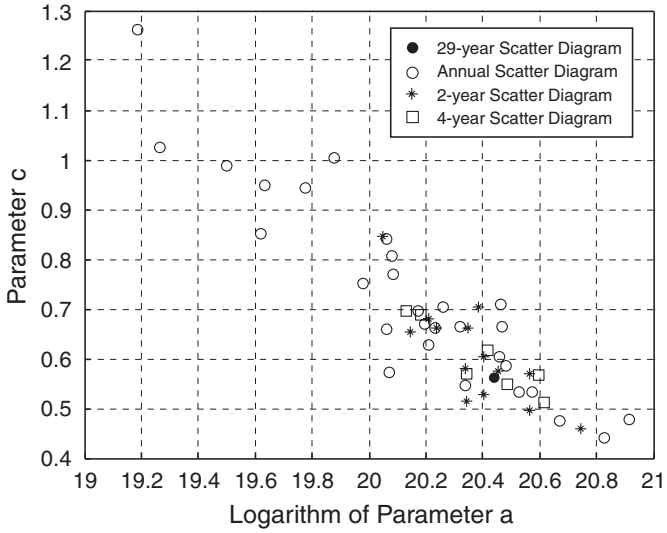

Fig. 24. Scatter plot of the parameters a and c in the generalized gamma distribution for the FPSO, relating to fatigue analysis.

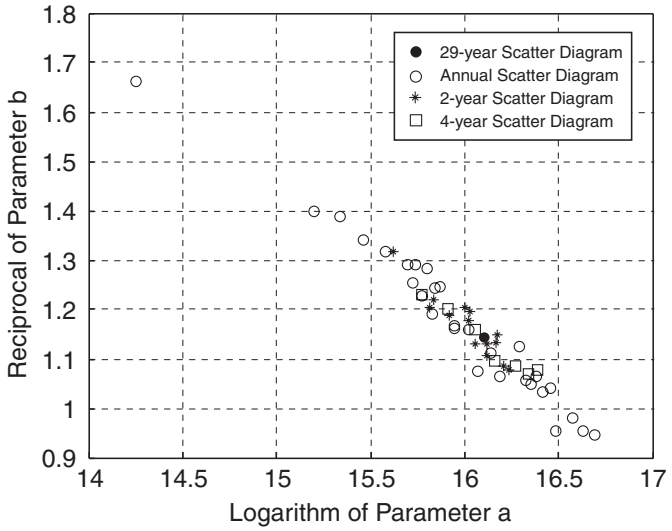

Fig. 25. Scatter plot of the parameters a and b in the generalized gamma distribution for the semi-submersible, relating to fatigue analysis.

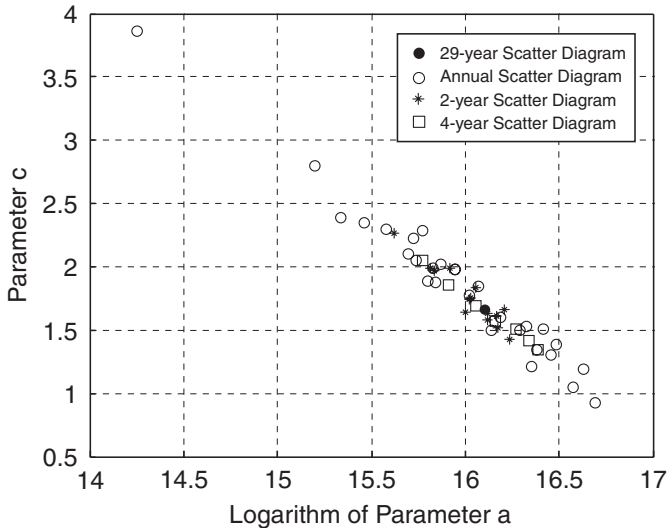

Fig. 26. Scatter plot of the parameters a and c in the generalized gamma distribution for the semi-submersible, relating to fatigue analysis.

The ratio of the largest and smallest value for the FPSO is 4.3 when the smoothed annual scatter diagram is used, while for the semi-submersible this ratio is 1.9.

When setting the derivative of $FLI(s)$ equal to zero, the stress range corresponding to the maximum contribution to fatigue damage can be determined. The solution is

$$s_{\max} = a(m/b + c - 1/b)^{1/b}. \tag{15}$$

The corresponding probability of exceedance is

$$1 - F_S(s_{\max}) = 1 - \frac{\gamma(c; m/b + c - 1/b)}{\Gamma(c)}. \tag{16}$$

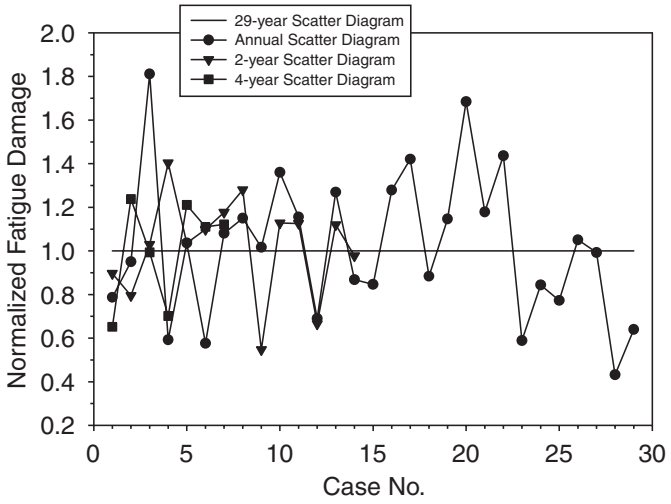

Fig. 27. Predicted fatigue damage of the FPSO by the generalized gamma model.

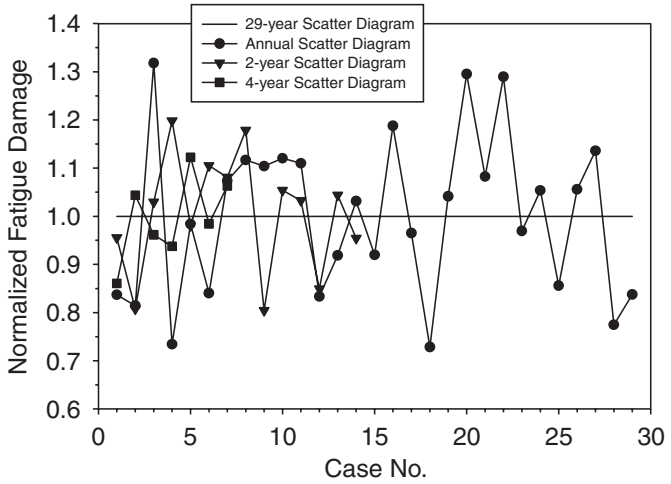

Fig. 28. Predicted fatigue damage of the semi-submersible by the generalized gamma model.

The probability of exceedance does not depend upon the distribution parameter a. For example, when the 29-year scatter diagram is used, the estimated generalized gamma distribution parameters for the FPSO are $b = 0.87$, $c = 0.56$ with a fatigue resistance parameter m equal to 3, and the probability of exceedance of the peak stress range is 0.02. This indicates that a major contribution to fatigue damage also comes from the tail of the stress range distribution. Moreover, the ratio of $s_{\max}$ to the mean value of stress range is about 5.8.

3.4. Correlation between wave condition and extreme and fatigue responses

It is also interesting to explore the correlation between various measures of the intensity of the sea state and response, say, annual or 100-year maximum value and the fatigue damage (or S_{equ}) as obtained by using data for periods of 1, 2 or 4 years. This information

Table 2
Correlation coefficients between the characteristic H_S and response

	Twenty-year extreme response of the FPSO	Fatigue damage of the FPSO	Twenty-year extreme response of the semi-submersible	Fatigue damage of the semi-submersible
Mean value of H_S	0.027	0.784	0.134	0.867
H_S with an exceedance probability of 10%	0.310	0.874	0.346	0.953
Annual extreme H_S	0.987	0.617	0.662	0.470
One hundred-year extreme H_S	0.985	0.474	0.628	0.296

is useful in generalizing e.g. full-scale observation of fatigue for a single year only based upon knowledge about the extreme wave height (H_S) for that period. Using the annual data sets, the correlation coefficients between the mean value of H_S, H_S with an exceedance probability of 10%, the annual extreme H_S or the 100-year extreme H_S and the 20-year extreme response or the fatigue damage are calculated and shown in Table 2 both for the FPSO and the semi-submersible. The extreme response is more correlated with the extreme H_S, while the fatigue damage is more correlated with the characteristic H_S with larger probability of exceedance, e.g. the mean value of H_S or H_S with an exceedance probability of 10%.

The contributions to extreme response from different sea states can be numerically estimated. Instead of using the cumulative probabilities, the exceedance probabilities are used, see e.g. Videiro and Moan [13]. Figs. 29 and 30 show the contour plots of relative probabilities of exceeding 20-year extreme response of the FPSO and the semi-submersible from all sea states, which are normalized by the total exceedance probability of 10^{-8}. Main contributions to the extreme response are due to the extreme sea states.

Moreover, based on the short-term stress range distributions and Eq. (10), the fatigue damage can also be obtained directly from each sea state without fitting a distribution to the long-term stress range. The contour plots of fatigue damage of the FPSO and of the semi-submersible in all sea states are shown in Figs. 31 and 32, respectively, using only the 29-year scatter diagram. The sea state corresponding to the maximum contribution to fatigue damage is identified to have H_S equal to 6 m and T_P equal to 12.5 s for the FPSO and H_S of 4.5 m and T_P of 10 s for the semi-submersible. It is again indicated that the total fatigue damage comes more from relatively moderate sea states.

4. Conclusions

(1) Time variability of wave climate in the northern North Sea is examined by considering the long-term variation of the scatter diagrams with periods of 1, 2, 4 and 29 years. Significant variations in the estimated distribution parameters and the predicted extreme values of H_S are observed.
(2) Extreme values of typical linear response of an FPSO and a semi-submersible are

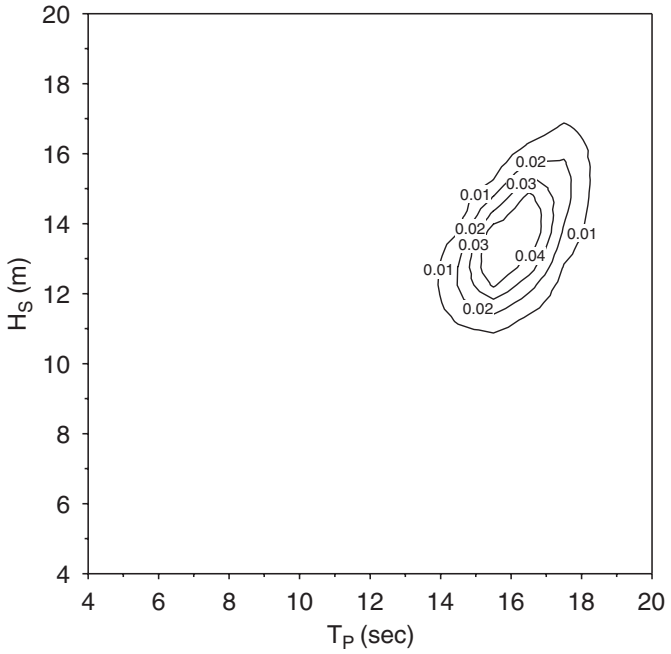

Fig. 29. Contour plot of probabilities of exceeding 20-year extreme response of the FPSO in all sea states using the 29-year data, normalized by the total exceedance probability of 10^{-8}.

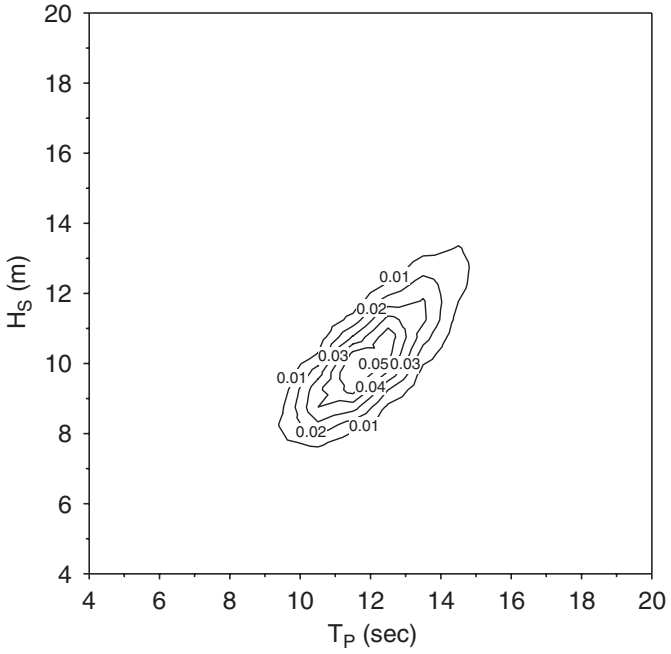

Fig. 30. Contour plot of probabilities of exceeding 20-year extreme response of the semi-submersible in all sea states using the 29-year data, normalized by the total exceedance probability of 10^{-8}.

estimated by a two-parameter Weibull model using the smoothed scatter diagrams. The statistical uncertainty in the predicted extreme values for the FPSO is larger than that for the semi-submersible, because the former response depends upon (more rare) waves

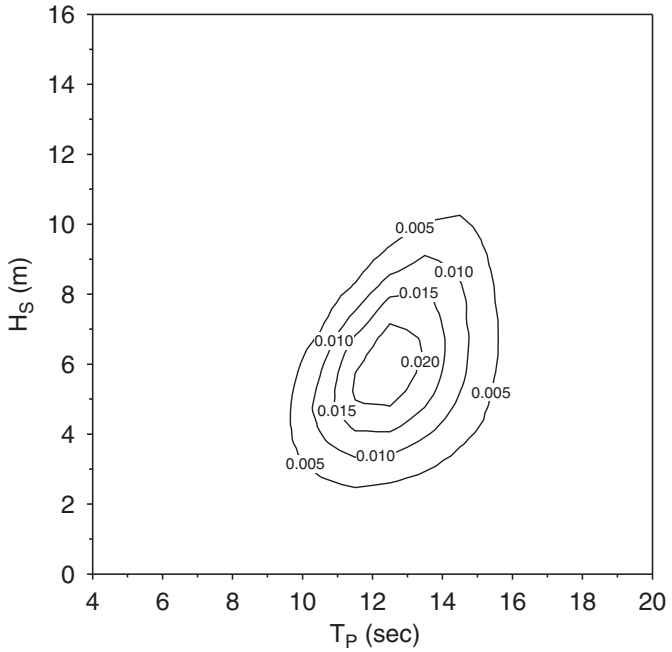

Fig. 31. Contour plot of fatigue damage of the FPSO in all sea states using the 29-year data.

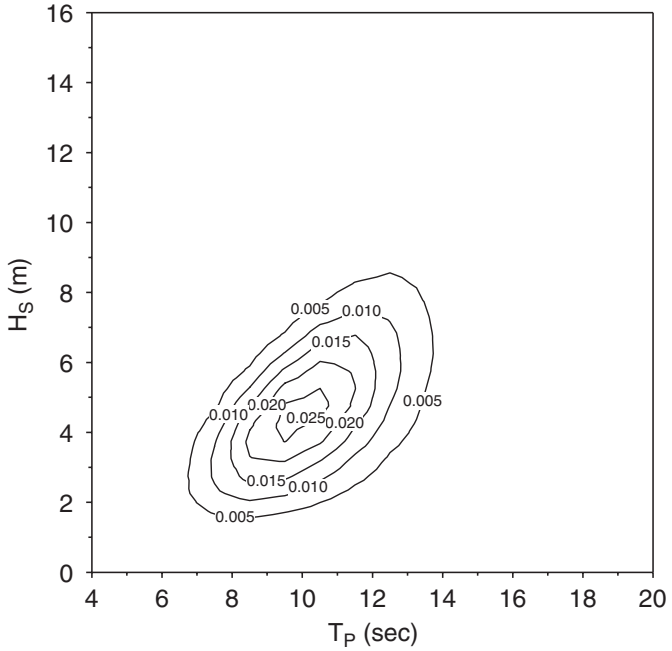

Fig. 32. Contour plot of fatigue damage of the semi-submersible in all sea states using the 29-year data.

with larger periods. The 20-year maximum varies by a factor 1.7 for the FPSO and 1.5 for the semi-submersible based on annual wave data.

(3) Typical fatigue damages are also calculated by a closed form with a generalized gamma distribution for the long-term stress range. The generalized gamma model gives more

accurate estimates than the two-parameter Weibull model. The calculated fatigue damage varies by a factor of 4.3 from year to year for the FPSO and 1.9 for the semi-submersible, based upon data for 29 years. The maximum contribution to the fatigue damage is due to stress range corresponding to a probability of exceedance of about 10^{-2}.

(4) Both for the FPSO and the semi-submersible, the extreme response is more correlated with the extreme sea states, while the fatigue damage depends more upon the moderate sea states.

The present study deals with the variability of extreme and fatigue responses due to the variability of H_S and T_P in consecutive 1, 2 and 4-year periods, using a semi-submersible platform in beam seas and a turret moored FPSO in head seas as examples. For structures which are sensitive to wave heading, the wave direction would also contribute to the variability of the response within the mentioned periods.

Acknowledgements

The authors are grateful to Statoil ASA for providing the wave climate data and to Sverre Haver for making the program PHT available and for rendering constructive comments.

References

[1] Battjes JA. Probabilistic aspects of ocean waves. In: Proceedings of safety of structures under dynamic loading. Trondheim: Tapir Publishers; 1977.
[2] Nordenstrøm N. Methods for predicting long term distributions of wave loads and probability of failure for ships, Part 1, Environmental conditions and short term response. DNV Report No. 71-2-S, 1973.
[3] Moan T, Syvertsen K, Haver S. Dynamic analysis of gravity platforms subjected to random wave excitation, Invited paper, Spring Meeting and Star Symposium-SNAME, San Francisco; 1977.
[4] Ferreira JA, Guedes Soares C. Modeling the long-term distribution of significant wave height with the beta and gamma models. Ocean Eng 1999;26:713–25.
[5] Haver S. Analysis of uncertainties related to the stochastic modeling of ocean waves. Ph.D. thesis, Norway: Norwegian Institute of Technology, Trondheim; 1980.
[6] Nolte KG. Statistical methods for determining extreme sea states. POAC Conference, Reykjavik, Iceland, 1973.
[7] Guedes Soares C, Ferreira AM. Analysis of the seasonality in non-stationary time series of significant wave height, Computational Stochastic Mechanics. Rotterdam: A.A. Balkema; 1995. p. 559–78.
[8] Haver S. Private communication, 2004.
[9] NORSOK. Actions and action effects, NORSOK Standard N-003. Oslo: Norwegian Technology Standards Institution; 1999.
[10] SESAM Profast Version 2.2-03. User's Manual, 2004.
[11] Guedes Soares C, Moan T. Model uncertainty in the long-term distribution of wave-induced bending moments for fatigue design of ship structures. Marine Struct 1991;4:295–315.
[12] Nolte KG, Hansford JE. Closed form expressions for determining the fatigue damage of structures due to ocean waves. In: Proceedings of the offshore technology conference, OTC Paper No. 2606, 1976.
[13] Videiro PM, Moan T. Efficient evaluation of long-term distributions. OMAE99/S&R-6014. St. Johns, Newfoundland, 1999.

Paper 4

Time variant reliability of mooring system considering corrosion deterioration

Published in
Proceedings of the 24th International Conference of Offshore Mechanics and Arctic Engineering (OMAE2005)
June 12-16, 2005, Halkidiki, Greece

Proceedings of OMAE2005
24th International Conference on Offshore Mechanics and Arctic Engineering
June 12-16, 2005, Halkidiki, Greece

OMAE2005-67429

TIME VARIANT RELIABILITY OF MOORING SYSTEM CONSIDERING CORROSION DETERIORATION

Zhen Gao
Centre for Ships and Ocean Structures,
Norwegian University of Science and Technology
Otto Nielsens v 10, N-7491 Trondheim, Norway
Email: zhen.gao@marin.ntnu.no

Torgeir Moan
Centre for Ships and Ocean Structures,
Norwegian University of Science and Technology
Otto Nielsens v 10, N-7491 Trondheim, Norway
Email: torgeir.moan@marin.ntnu.no

Svein E. Heggelund
MARINTEK
Otto Nielsens v 10, N-7450 Trondheim, Norway
Email: svein.e.heggelund@marintek.sintef.no

ABSTRACT

This paper deals with time variant overload reliability analysis of a mooring system due to corrosion deterioration. A probabilistic model for uniform corrosion is adopted to predict the strength degradation. A simplified method and nonlinear finite element analysis are used to calculate the breaking strength of the chain link and comparison is made. The strength of one mooring line is modeled by a weakest link system. The effect of correlation in corrosion models for different chain links in one mooring line and the effect of higher corrosion rate in the splash zone are discussed. The annual failure probability of the most loaded mooring line of a semi-submersible is calculated. The first and second order motions of the semi-submersible and the corresponding line tensions are found by a simplified analysis. The time variant reliability analysis is performed by approximating the degraded strength by a piece-wise constant model. The annual failure probability is obtained for different years. It is found that the annual failure probability increases significantly as the chain is corroded.

INTRODUCTION

In the traditional time invariant reliability analysis of mooring systems, the failure probability is obtained by considering the uncertainties in the mooring chain strength to be the same in the reference period, e.g. one year or the service life. In reality, mooring chains are subjected to various deteriorating conditions, such as seawater corrosion, crack growth and wear at the fairlead or at the sea bottom. As a result, the mooring line strength will degrade with a decreasing mean value and an increasing variance. Hence, a time invariant reliability model using the initial strength distribution for the whole reference period will underestimate the failure probability. Similarly, a time invariant model using the strength at the end of the service life will overestimate the failure probability. In this paper, the effect of corrosion on the reliability of a mooring system is studied using a time variant reliability model.

CORROSION MODEL

Seawater corrosion of steel structures is a quite complicated phenomenon. It is dependent on the material properties of the structure and on the properties of the marine environment into which it is placed. Important environmental properties are seawater composition, dissolved oxygen, temperature, velocity of water particles, salinity, etc. The effect of corrosion can be expressed in terms of material loss from the steel surface. Most corrosion models are simplified models based on a constant corrosion rate. In offshore standards for mooring chains, such as DNV-OS-E301 [1] and API RP 2SK [2], it is required that a corrosion allowance of 0.4 mm/year in chain diameter should be considered in design. However, due to the large number of factors influencing the corrosion rate, these models are uncertain. Many long term tests on seawater corrosion also show a significant variation of corrosion rate. A probabilistic model for corrosion of steel plates is proposed by Melchers [3]. In this model, the time dependency of both the

mean value and the standard deviation of the uniform corrosion depth are considered. A log-normal model was found to fit very well to the corrosion data.

However, there is no particular corrosion database for mooring chains in cold and harsh conditions. A linear probabilistic model is used for the Northern North Sea environmental conditions

$$\begin{cases} \mu_d = 0.4t(mm) \\ \sigma_d = 0.2t(mm) \end{cases} \quad (1)$$

where μ_d and σ_d denote the mean value and the standard deviation of the corrosion depth d in chain diameter and t is the time in years. Basically, the model in Eq. (1) means a mean corrosion rate of 0.4 mm/year with a COV equal to 0.5. According to the limited experiences of Statoil, the mean corrosion rate might be slightly smaller [4]. In this paper, the mean corrosion of 0.4 mm/year is used as required in [1]. Moreover, this value is applied for the submerged parts of the line while the mean corrosion rate in the splash zone is taken to be twice this value [1].

Fig. 1 shows the log-normal distributions of the corrosion depth at 5 different time instants by the model in Eq. (1).

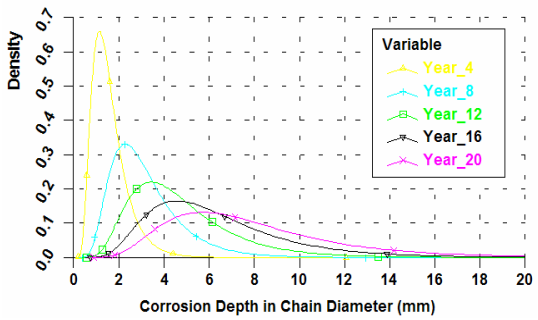

Fig. 1 Distributions of corrosion depth in chain diameter in 5 different years

STRENGTH DETERIORATION DUE TO CORROSION

The breaking strength of one single chain link

In order to get an accurate prediction of the breaking strength of a corroded chain, non-linear FE-analyses [5] for studless chain links are performed. It is assumed that the corrosion is uniform. Hence, the time dependency of the breaking strength can be found by studying chains with different diameters. The geometry of a studless chain with diameter, D, width, $A = 3.35\ D$, and length, $B = 6\ D$ is shown in Fig. 2.

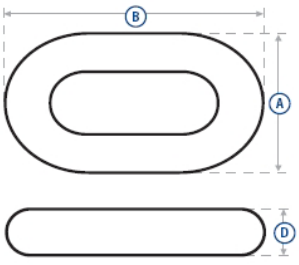

Fig. 2 Geometry of a studless chain link

The non-linear FE-analyses are performed using the computer program ABAQUS [6]. An FE-model of two chain links with $D = 125$ mm is made. The FE-model is shown in Fig. 3 together with boundary conditions at one end and the applied tension load at the other. In order to reduce the computation time, symmetry boundary conditions are applied.

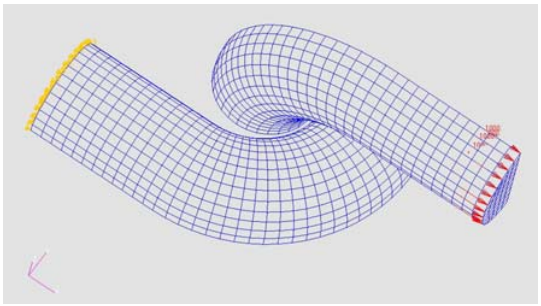

Fig. 3 FE-model of two 1/8 studless chain links

Grade NV R4 material specified in [1] is selected for the chain material model. The mechanical properties are shown in Table 1. These values represent the engineering properties and they are transformed into true stress and true strain in ABAQUS. Elongation with 6% other than 12% is assumed when the stress reaches the tensile strength. The elastic modulus and Poisson's coefficient are $E = 207$ GPa and $\nu = 0.29$.

Table 1 Mechanical properties for chain links

Grade	Minimum yield strength (MPa)	Minimum tensile strength (MPa)	Minimum elongation (%)
NV R4	580	860	12

The load level in the FE-calculation is based on the breaking test load for chain links defined in [1], which is considered to be the Minimum Breaking Strength (MBS). The formula for R4 material is

$$MBS = 0.0274D^2(44 - 0.08D)(kN) \quad (2)$$

where $D(mm)$ is the diameter of chain link.

The distribution of von Mises equivalent stress for a 125 mm chain link at a load level of 70% of MBS is shown in Fig. 4. The chain link that is subjected to the applied force is excluded from the figure. High stresses are observed at the bend and the crown of the chain link, while the stress level at the weld is relatively low. The equivalent plastic strain at the MBS load level is shown in Fig. 5.

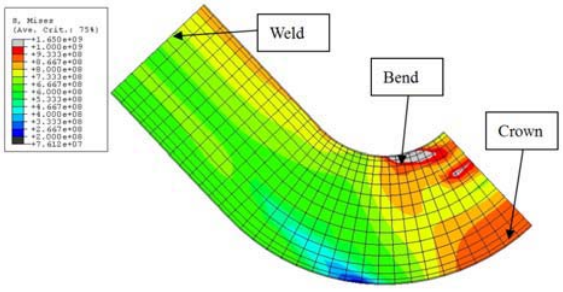

Fig. 4 Von Mises equivalent stress distribution

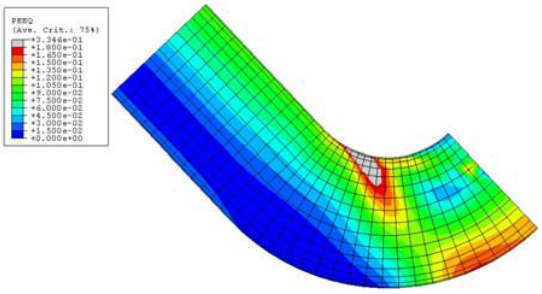

Fig.5 Equivalent plastic strain distribution

In order to determine the breaking strength of the chain link, a proper failure criterion is needed. In this paper, the breaking strength as predicted by several failure criteria are compared. The simplest way is to assume that the breaking strength is proportional to the square of the chain diameter without considering the geometry effect [7]. A more accurate criterion is based on the critical plastic strain. Failure is defined when the maximum plastic strain in the chain link reaches the critical plastic strain. Another way is to use the critical volume criterion, which is associated with a predefined plastic strain limit. Moreover, the stress state should also be considered in the failure criterion. However, FE-analyses for different chain diameters show that the stress and the strain distributions and histories are quite similar to each other when the corrosion depth is not very large. This indicates that the plastic strain criterion is sufficiently accurate to determine the chain breaking strength.

Table 2 and Fig. 6 show the MBS calculated by the above criteria in different years in a deterministic sense. A mean corrosion rate of 0.8 mm/year is selected here, which is applied for the links in the splash zone. Comparison is made at the MBS load level.

Table 2 Predicted MBS for chain links in 6 different years, with a mean corrosion rate of 0.8 mm/year (relevant for the splash zone)

Year	0	4	8	12	16	20
Mean corrosion depth in chain diameter (mm)	0	3.2	6.4	9.6	12.8	16
Chain diameter (mm)	125	121.8	118.6	115.4	112.2	109
DNV formula (Eq. (2)) (kN)	14556	13925	13301	12687	12081	11485
Simplified method (kN)	14556	13820	13104	12406	11728	11068
FEA_CV (kN)	14556	13551	12567	11583	10596	9697
FEA_MPS (kN)	14556	13692	12857	12000	11398	10629

(CV-the critical volume criterion; MPS-the critical plastic strain criterion)

The above analyses are performed in a relative sense with D = 125 mm as a basic case without corrosion deterioration. The simplified method and the FE-analyses are calibrated with the DNV formula (Eq. (2)) in the basic case and they all give the MBS of 14556 kN for the chain link. By this case, the critical volume criterion and the critical plastic strain criterion are obtained, i.e. the value of the critical volume is 14% with a plastic strain limit of 0.113 and the critical plastic strain is 0.3. Compared with the critical volume criterion (FEA_CV), the critical plastic strain criterion (FEA_MPS) seems to be more reasonable. Moreover, in order to verify the accuracy of the FEA_MPS, the FE-analysis with the critical plastic strain criterion is also performed for the green chain link in Fig. 7, which is a chain link of 109 mm diameter with the geometric form in Fig. 2. The result gives the MBS of 11059 kN, which is only a difference of 3.7% from the DNV formula.

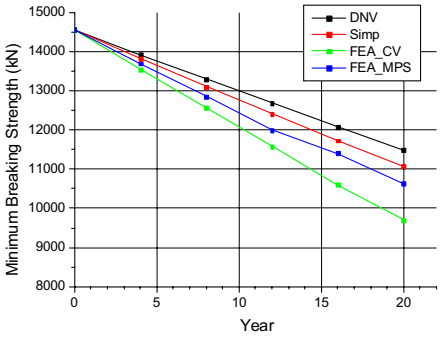

Fig. 6 Predicted MBS for chain links as a function of time, with a mean corrosion rate of 0.8 mm/year (relevant for the splash zone) (CV-the critical volume criterion; MPS-the critical plastic strain criterion)

In Table 2 and Fig. 6, the MBS of corroded chain links predicted by FE-analyses differ from that of the DNV formula. This is probably because the DNV formula is only associated with the chain diameter, see Eq. (2). It seems that the formula is based on the similar geometry of chains, see Fig. 2, and can not be directly applied for the corroded chain. In reality, when the corrosion occurs, the central line of the chain link is not changed as the red chain link in Fig. 7. The FE-calculations are performed for these exact corroded chains.

In the following, calculations and comparisons are made only for the simplified method and the FE-analysis with the critical plastic strain criterion (FEA_MPS).

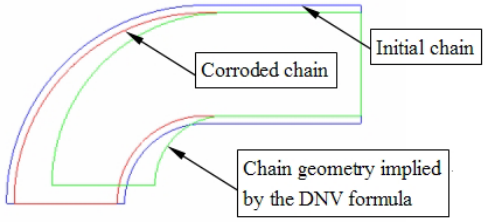

Fig. 7 Difference in the chain geometry (1/4 of chain link is shown)

The breaking strength of a single chain link is a little higher than MBS. DEEPMOOR [8] suggested a mean value of 1.2 times the MBS and a COV of 0.05 for the breaking strength of a single chain link based on the experience from the test data. A log-normal distribution with a lower threshold corresponding to the proof load level can be applied. When the uncertainties in both the initial chain link strength and the corrosion model are considered, the chain link breaking strength R at time t can be expressed as follows

$$R(t) = R_0 - f(d(t)) \tag{3}$$

where R_0 and $d(t)$ are the initial chain link strength and the corrosion depth in chain diameter respectively and they are both random variables as well as $R(t)$. $f(d(t))$ accounts for a reduction in strength as a function of corrosion depth, $d(t)$ and

it is a deterministic function fitted to the data in Table 2. It is found that even a linear model gives quite a good fitting. Therefore, Eq. (3) is simplified as

$$R(t) = R_0 - (a_1 * d(t) + a_2) \quad (4)$$

The fitted coefficients a_1 and a_2 are listed in Table 3.

Table 3 Fitted coefficients in Eq. (4)

Method	a_1	a_2
Simplified method	261.58	38.171
FEA_MPS	293.29	94.457

(MPS-the critical plastic strain criterion)

The mean value and the standard deviation of *R(t)* can be easily derived from Eq. (4). The distribution of *R(t)* is slightly different from a log-normal distribution as long as the corrosion depth is not too large and this distribution type is used in this paper. Fig. 8 shows the strength distributions at 6 different time instants using the corrosion model Eq. (1) with a mean corrosion rate of 0.4 mm/year. The following analyses are based on this model.

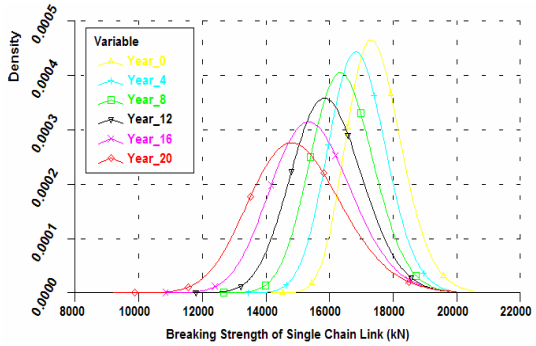

Fig. 8 Breaking strength distributions of one single chain link in 6 different years

The breaking strength of one mooring line

The breaking strength of one whole mooring line is derived from a weakest link system by assuming independence between the initial strength of each chain link. This gives a conservative result. In reality, the initial strength in different chain links are correlated, but it is very difficult to determine the correlation coefficient precisely due to the uncertainties in the fabrication. In this paper, only the effect of correlation between corrosion models in different chain links is examined.

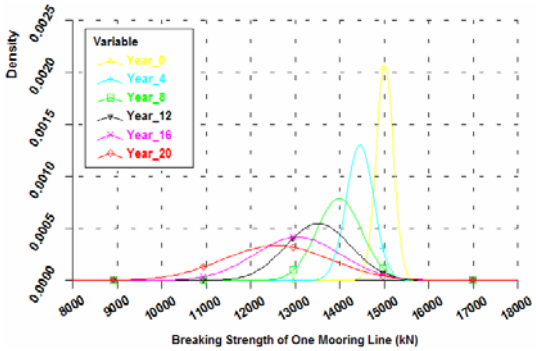

Fig. 9 Breaking strength distributions of one mooring line in 6 different years, under the full dependence assumption in corrosion models

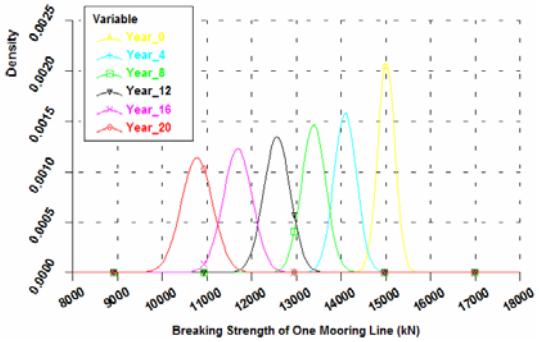

Fig. 10 Breaking strength distributions of one mooring line in 6 different years, under the independence assumption in corrosion models

Fig. 9 and Fig. 10 show the distributions of breaking strength of one mooring line under the full dependence assumption and the independence assumption, respectively. The normal distribution is applied. The results are given by FE-analyses. A chain-wire-chain mooring line is assumed and no corrosion effect is considered for steel wire part of the mooring line. The length of chain part is 824 m corresponding to 1648 links and the length of steel wire is 312 m.

The mean value and the COV of the breaking strength of a single chain link and one whole mooring line are compared in Fig. 11 and Fig. 12 for 20 years. Both results from the simplified method and from FEA are shown. Under the full dependence assumption, reduction in the mean value of the breaking strength for the whole mooring line is the same as that for the single chain link, while under the independence assumption, a lower strength is predicted. The increase of COV under the independence assumption is limited due to the weakest link system formulation, while under the full dependence assumption it is significant. Moreover, the simplified method gives a higher mean value and a lower COV than the FEA. In fact, the corrosion effect on chain links in the submerged parts of one mooring line or in the splash zone is very much correlated due to the similar environmental condition. Hence the full dependence assumption seems to be more reasonable.

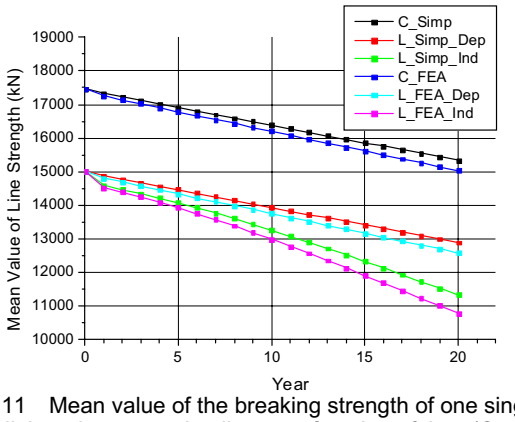

Fig. 11 Mean value of the breaking strength of one single chain link and one mooring line as a function of time (C-chain link; L-mooring line; Simp-simplified method; FEA-finite element analysis; Dep-full dependence assumption; Ind-independence assumption)

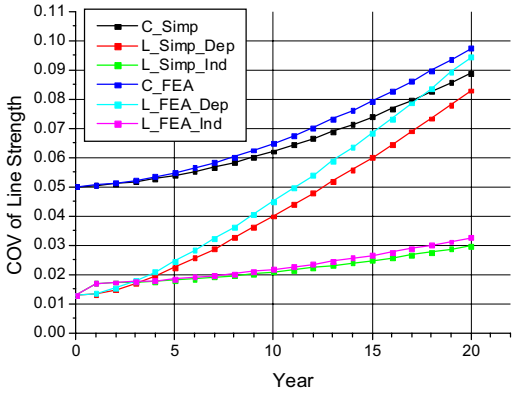

Fig. 12 COV of the breaking strength of one single chain link and one mooring line as a function of time

Splash zone effect on the mooring line breaking strength

The corrosion rate is higher in the splash zone than in the catenary part or at the bottom. In [1], a corrosion rate of 0.8 mm/year in the splash zone should be considered at design stage. For the catenary part and at bottom, only half the value is required. The reduction in the whole mooring line strength is significant when the splash zone is considered, see Fig. 13 and Fig. 14. This is mainly because the whole mooring line is modeled as a series system and the lowest strength in chain links gives a significant effect on the whole line strength. The total length of chain links in splash zone is selected as 9 m corresponding to 18 links.

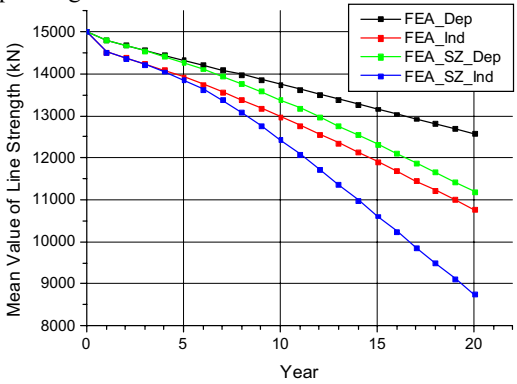

Fig. 13 Mean value of the breaking strength of one mooring line as a function of time, when the splash zone is considered (SZ-splash zone)

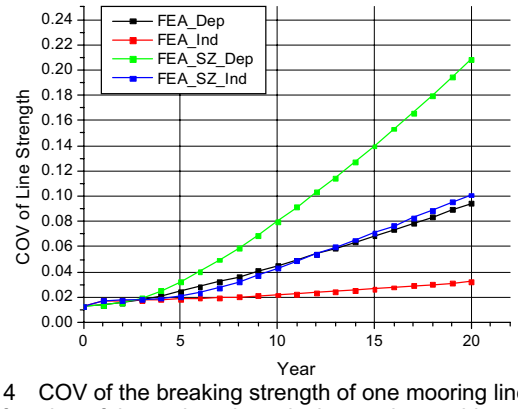

Fig. 14 COV of the breaking strength of one mooring line as a function of time, when the splash zone is considered

RESPONSE ANALYSIS

Mooring line tension depends on the wave, wind and current forces, including the steady force due to current, wind and wave, the first order wave force, and the slowly varying forces from wave and wind gust. In an ultimate limit state reliability problem, it is important that the extreme value of line tension is reasonably well modeled by combining wave frequency (WF) and low frequency (LF) response components.

In this paper, the formulation of overload reliability basically follows the method applied in [8]. Some simplifications have been made to reduce the computation effort. The analysis of mooring system response is carried out by the frequency domain program MIMOSA [9]. For extreme line tension due to WF motion, the model proposed by Lie [10] is selected even if this model probably overpredicts the extreme line tension. The line tension due to LF vessel motion is based on the model by Stansberg [11]. The WF and LF components of line tension are combined by the rule taking the maximum of two sums, i.e. the extreme WF (or LF) plus the significant LF (or WF) component. A model uncertainty of the predicted short term (3 hours) extreme line tension is included with the mean value 1.0 and the COV 0.1. A quadratic polynomial response surface is directly applied for the predicted extreme line tension within a short term with respect to the environmental variables, e.g. significant wave height, mean peak wave period, mean wind speed and environmental direction. The long term extreme response is determined by both the environmental model and the response surface. The safety of the mooring system is expressed by the annual failure probability and the nested FORM analysis [12] is adopted to calculate the failure probability by program SESAM Proban [13].

TIME VARIANT RELIABILITY

In the time variant reliability problem both the resistance and the load effect are considered to change with time. In general, this problem can be solved by applying the stochastic process theory and estimating the out-crossing rate, e.g. Hagen and Tvedt [14], Marley and Moan [15]. The stochastic process method can be applied easily when both the resistance process and the load process are well defined. For the purpose of efficient computation, simplifications might be made to formulate the problem in a time invariant sense [15].

The corrosion effect on the mooring line strength is usually a long term effect, which means the strength degradation within a short term, e.g. 3 hours, or even within a longer period, e.g. 1 month, can be neglected. It indicates that a piece-wise constant model and a series system formulation [16] can be adopted in a time variant reliability analysis of a mooring system. By this model, within each selected short time interval, the failure probability is calculated based on the extreme value prediction of the load and the constant assumption for the strength. The total failure probability in the whole period of interest is then calculated by a series system formulation assuming independence between all individual time intervals when considering the degradation of strength from one interval to the next. This model is applied in this paper to calculate the failure probability in the first year. The results are compared with the time invariant formulation. The failure probabilities in different years with strength degradation are computed in the time invariant sense.

CASE STUDY

The mooring system of a semi-submersible in the Northern North Sea is selected for the case study. The main particulars of the vessel are listed in Table 4.

Table 4 Main particulars of the semi-submersible

Displacement (ton)	52500
Length o.a. (m)	124
Breadth (m)	95.3
Draught (m)	21
Operational water depth (m)	340

The configuration of the mooring system is shown in Fig. 15. Mooring line No.10 is selected to be the target mooring line in the analysis.

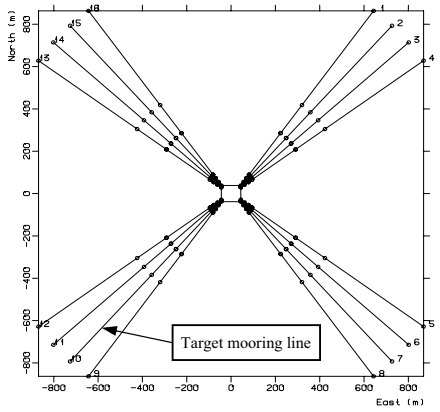

Fig. 15 Mooring system orientation

The joint environmental model proposed by Bitner-Gregersen and Haver [17] and the data from Haltenbanken (off central Norway) are adopted in this calculation. A 3-parameter Weibull distribution is applied for the significant wave height. For the mean peak period, a conditional log-normal is applied. The 1-hour mean wind speed is represented by a conditional 2-parameter Weibull distribution. The current velocity is assumed to be constant 1 m/sec. Collinear environmental direction for wave, wind and current is assumed and only the propagation direction section from 0^o to 90^o (relative to North, clockwise) is chosen for reliability analysis because most of the contributions on failure in line No.10 come from this direction section.

The annual failure probability is found by the reliability analysis. An acceptable level of 10^{-4} is selected for comparison.

Annual failure probability with the initial chain diameter and sensitivity study

A chain link with D = 125 mm in the initial stage is used giving a mean line strength of 15008 kN with a COV of 0.0128. The annual failure probability of mooring line No.10 is predicted to be $3.976 \cdot 10^{-6}$ ($-\log(P_f)$=5.401) without considering the effect of corrosion. The sensitivity of the annual failure probability P_f to the mean value and COV of line strength is shown in Fig. 16 and Fig. 17. The mean line strength corresponding to the acceptable level of 10^{-4} is 11500 kN and the COV is about 0.185. Fig. 17 also shows that the COV has little influence on the annual failure probability of the line strength when the COV is relatively small because the uncertainty in the load dominates.

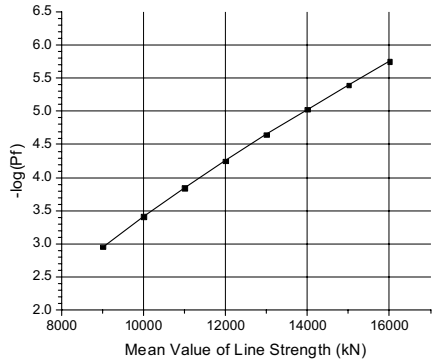

Fig. 16 Sensitivity of the annual failure probability P_f to the mean value of line strength, with the COV=0.0128

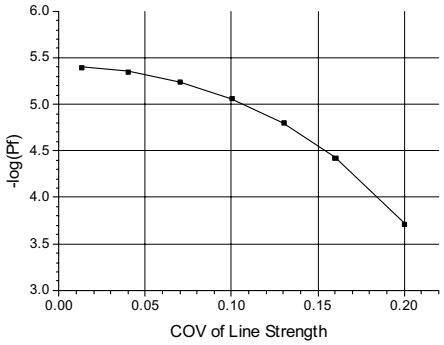

Fig. 17 Sensitivity of the annual failure probability P_f to the COV of line strength, with the mean value=15008kN

Failure probability in the first year

The piece-wise constant model is applied for calculating the annual failure probability in the first year considering the strength deterioration due to corrosion. 12 time intervals are selected for this year and the calculated failure probability is listed in Table 5 together with those computed by the initial line strength and the line strength after one-year corrosion.

Table 5 Failure probability of line No.10 in the first year

Line strength condition	P_f	$-\log(P_f)$
Initial condition	$3.976 \cdot 10^{-6}$	5.401
Time variant formulation by the piece-wise constant model	$4.334 \cdot 10^{-6}$	5.363
After one-year corrosion	$4.732 \cdot 10^{-6}$	5.325

Table 5 gives only the results from FEA_MPS under the full dependence assumption in the corrosion model and shows that the difference between these three conditions is quite limited. In reality, it means that the time invariant formulation for annual failure probability calculation can also give quite a good accuracy. Failure probability calculations for the following years and by other analyses give the same conclusion. Basically, the variation in the line strength over one year is quite limited.

Annual failure probability in different years

The annual failure probabilities in 20 years are calculated based on the time invariant formulation within one year but considering corrosion deterioration from one year to the following, see Fig.18. The increased annual failure probability due to corrosion is observed. The simplified method predicts a lower failure probability than the FE-analysis. Under the independence assumption in the corrosion model, the computed annual failure probability will reach the acceptable level of 10^{-4} within a period lower than 20 years. This is a quite conservative result as compared with the results under the full dependence assumption.

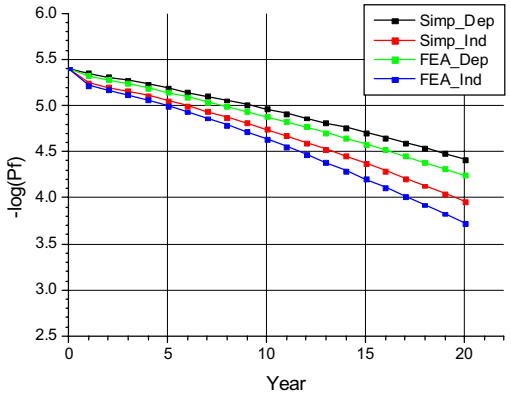

Fig. 18 Annual failure probability of line No.10 as a function of time, by simplified method and by FEA

Fig. 19 shows that a significant increase in the annual failure probability is predicted when the higher corrosion rate in the splash zone is also considered. The results are all obtained by FE-analysis. Under the full dependence assumption, the safe period corresponding to the annual acceptable P_f of 10^{-4} is about 14 years when the splash zone is considered.

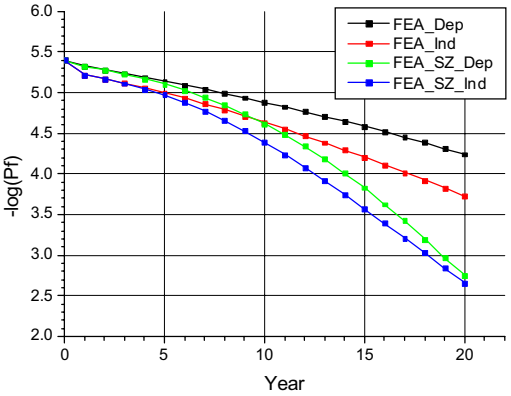

Fig. 19 Annual failure probability of line No.10 as a function of time, when the splash zone is considered and not considered

DISCUSSION AND CONCLUSION

The probabilistic corrosion model with constant corrosion rate and COV is adopted to predict the degradation of the ultimate chain strength. The line strength is significantly influenced by the corrosion rate and the correlation between the corrosion models in different chain links. The number of chain links in the splash zone is small, but these links are subjected to more severe corrosion deterioration and dominate the strength of the whole corroded mooring line. More long term corrosion data on marine chains are needed to validate the corrosion model.

The breaking strength of the chain links is calculated by a simplified method and by nonlinear FEA. The critical plastic strain criterion has been applied to define the failure and seems to be a simple and relatively reasonable failure criterion. A more accurate and complicated way to determine the chain link strength might be based on fracture mechanics assessment.

A time variant reliability analysis has been performed to assess the safety of a mooring system of a semi-submersible. It is found that the degradation can be well approximated by a time invariant model with constant strength over one year. The annual failure probability in different years is given considering corrosion deterioration. The annual failure probability could be significantly reduced due to corrosion over a period of 20 years. In the worst case, the safe service life predicted is about 12.5 years corresponding to an annual acceptable P_f of 10^{-4}. This indicates that an inspection of the mooring lines is needed and a reassessment of the safety of the mooring system should be carried out based on the measured corrosion data.

Future work is needed to study the combined effect of corrosion and fatigue degradation as well as the inspection to arrange the safety management of degrading mooring lines.

ACKNOWLEDGEMENTS

The first two authors would like to acknowledge the financial support from the Research Council of Norway to the Centre for Ships and Ocean Structures. Also, the authors would like to thank Advanced Production and Loading AS for the permission to use their chain link FE-models.

REFERENCES

[1] DNV, (2001), Offshore Standard-Position Mooring, DNV-OS-E301.
[2] API, (1995), Recommended practice for design and analysis of station keeping systems for floating structures, RP 2SK.
[3] Melchers, R.E., (1995), Probabilistic modeling of seawater corrosion of steel structures, ICASP 7; 1: 265-270.
[4] Larsen, K., (2004), Private communication on September 7, Statoil.
[5] Pedro, M.C.L.P., Paulo, P.K., Jorge, C.F.J., Marcelo, A.S., Hugo, G.S., (2004), Finite element residual stress analysis applied to offshore studless chain links, OMAE2004-51508.
[6] ABAQUS Version 6.4-1, (2003), Analysis User's Manual.
[7] Leira, B. J., Larsen, K., (1995), Service life reliability analysis for an anchor system subject to corrosion, OMAE 1995; II: 335-341.
[8] Mathisen, J., Hørte, T., Sogstad, B., (1998), DEEPMOOR-Design methods for deep water mooring system, Calibration of an ultimate limit state, DNV report no.96-3583, rev.03.
[9] MIMOSA Version 5.7, (2003), User's Documentation.
[10] Lie, H., Sødahl, N., (1993), Simplified dynamic model for estimation of extreme anchorline tension, Offshore Australia.

[11] Stansberg, C.T., (1991), A simple method for estimation of extreme values of non-Gaussian slow-drift responses, ISOPE-91; 3: 442-451.
[12] Wen, Y.K., Chen H.C., (1987), On fast integration for time variant structural reliability, Probabilistic Engineering Mechanics; 2(3): 156-162.
[13] SESAM Proban Version 4.4, (2003), User's Manual.
[14] Hagen, O., Tvedt, L., (1991), Vector process out-crossing as a parallel system sensitivity measure, Journal of Engineering Mechanics; 117(10): 2201-20.
[15] Marley, M.J., Moan, T., (1992), Time variant formulation for fatigue reliability, OMAE, paper No.92-1203.
[16] Ku, A., Serratella, C., Spong, R., Basu, R., Wang, G., Angevine, D., (2004), Structural reliability applications in developing risk-based inspection plans for a floating production installation, OMAE2004-51119.
[17] Bitner-Gregersen, E.M., Haver, S., (1991), Joint environmental model for reliability calculations, ISOPE-91; 1: 246-253.

Paper 5

Sensitivity study of extreme value and fatigue damage of line tension in mooring system with one line failure under varying annual environmental conditions

Published in
Proceedings of the 17th International Offshore and Polar Engineering Conference
(ISOPE2007)
July 1-6, 2007, Lisbon, Portugal

Proceedings of the Seventeenth (2007) International Offshore and Polar Engineering Conference
Lisbon, Portugal, July 1-6, 2007

ISBN 978-1-880653-68-5; ISBN 1-880653-68-0(Set); ISSN 1098-6189 (Set)

Sensitivity Study of Extreme Value and Fatigue Damage of Line Tension in Mooring System with One Line Failure under Varying Annual Environmental Conditions

Z. Gao and T. Moan
Centre for Ships and Ocean Structures, Norwegian University of Science and Technology
Trondheim, Norway

ABSTRACT

Mooring systems are usually designed against ultimate and fatigue failure of individual lines as well as to survive a certain environmental condition with one line failed. Depending on the system configuration, failure in one mooring line could obviously increase the loads in the remaining lines, especially in the adjacent lines. Increasing extreme line tension and induced fatigue damage will also depend on the environmental conditions that the mooring system could experience after damage. The annual variation of sea wave conditions also leads to a significant variation of the predicted line tension. In this paper, annual extreme values of mooring line tension have been estimated both by full long-term analyses and by the contour line method for an intact mooring system and for a damaged one, respectively. On the average, an increase of 20% and 30% in extreme tension are obtained in the adjacent line due to a single line failure in a 16-line system and in a 12-line system, respectively. Long-term fatigue damage induced by line tension has also been summed up from the short-term contributions which are estimated by a bi-model fatigue formulation and an average increase of the annual damage by 50% and 90% are obtained due to failure for the 16-line and 12-line systems.

KEYWORDS: mooring system; line failure; extreme tension; fatigue damage

INTRODUCTION

Mooring system of floating structures is usually designed against ULS (Ultimate Limit State), FLS (Fatigue Limit State) and ALS (Accidental Limit State) by using the LRFD (Load and Resistance Factor Design) method. Partial safety factors are calibrated by detailed structural reliability analyses and specified by many design codes, e.g. API RP 2SK (1997), DNV-OS-E301 (2004), ISO 19901-7 (2005), etc.

Design checks both for ULS and for ALS are made by comparing line capacity and extreme line tension under a design environmental condition for an intact system and for a damaged system with one line failure, respectively. Compared with an intact system, it is obvious that both static and dynamic tensions in the remaining lines of a damaged system, especially in the adjacent lines, increase under the same environmental condition. Moreover, the failure rate of one mooring line due to abnormal reasons (e.g. abnormal strength due to abnormal fabrication defects/lack of quality assurance or abnormal loads, e.g. by erroneous winching operation, etc.) is shown by experience high, around 1% annually (Haver et al., 1999). This problem can not be dealt with by structural reliability analysis. In a risk analysis perspective, it is useful to know the performance of a damaged mooring system and the corresponding safety level, i.e. conditional failure probability.

At the same time, the increased dynamic line tension in a damaged system will of course induce more fatigue damage. When the failed mooring line has not been identified or has been identified but not repaired or replaced for a long time, e.g. one winter season, the increased fatigue damage could be considerable. However, the design code gives no guidance on this consideration. Safety level implied by the ultimate strength check could be recovered from a damaged system to an initial intact system when the failed line is repaired or replaced, although it is also influenced by many degrading mechanisms in sea water, like corrosion, wear, cracking, etc. On the other hand, the accumulated fatigue damage under a damaged condition becomes permanently a part of the total damage the line could experience during a service life. The effect of increased fatigue damage does not disappear after line repair.

It is interesting to see how a mooring system behaves after one line failure and what effect is on the safety level in terms of extreme line tension and induced fatigue damage. It is believed that a steady state response of a damaged system over the next few hours, days or months gives the most critical situation for the remaining lines and a transient analysis of the first few minutes might not be necessary for ALS (DNV-OS-E301, 2004). Moreover, the safety level of a damaged mooring system is quite sensitive to the relevant environmental condition and the duration when the system is kept damaged. Environmental condition is varying even for a relative large time scale, e.g. one year, and variation in the averaged statistics can be significant. Response of a damaged mooring system under these varying conditions could also be of interest.

Therefore, in this paper, steady state analyses of a mooring system of a semi-submersible with one line failed have been performed in the

frequency domain and compared with the intact system using different annual environmental conditions. Annual extreme values of the mostly loaded line have been predicted by full long-term analyses and by the contour line method. In this way, some light is shed on the accuracy of the contour line method. Annual fatigue damages have also been estimated by a bi-modal fatigue formulation.

EXTREME MOORING LINE TENSION

Extreme value of marine structural response with a certain return period, e.g. 1 year or 100 years, is useful for design purpose and is typically determined by the long-term distribution of response maxima, which is obtained by a weighted sum of the short-term distributions (see e.g. Nordenstrom, 1971), as shown in Eq. (1) when a short-term sea state is characterized by significant wave height (H_S) and spectral peak period (T_P),

$$F_{LT}(x) = \frac{1}{\nu_{0LT}} \iint \nu_{0ST}(h_S, t_P) * f_{H_S T_P}(h_S, t_P) * F_{ST}(x|h_S, t_P) dh_S dt_P \tag{1}$$

where $f_{H_S T_P}(h_S, t_P)$ is the joint distribution of H_S and T_P, $F_{ST}(x|h_S, t_P)$ is the short-term distribution of response maxima with a given sea state of (h_S, t_P), $\nu_{0ST}(h_S, t_P)$ is the short-term mean zero up-crossing rate and ν_{0LT} is the long-term mean zero up-crossing rate

$$\nu_{0LT} = \iint \nu_{0ST}(h_S, t_P) * f_{H_S T_P}(h_S, t_P) dh_S dt_P \tag{2}$$

For a narrow-banded Gaussian response, $F_{ST}(x|h_S, t_P)$ becomes a Rayleigh distribution. However, mooring line tension comprises non-Gaussian wave and low frequency components and the corresponding short-term maximum distribution is hard to obtain analytically.

Alternatively, instead of using the distribution of each peak, an extreme value distribution of the short-term response can be applied to predict the long-term response distribution (Kleiven et al., 2003) and Eq. (1) can be modified as

$$F_{LTE}(x) = \iint f_{H_S T_P}(h_S, t_P) * F_{STE}(x|h_S, t_P) dh_S dt_P \tag{3}$$

where $F_{STE}(x|h_S, t_P)$ and $F_{LTE}(x)$ are defined as the short-term and long-term extreme response distributions corresponding to the duration of a sea state, e.g. 3 hours, respectively. In this paper, mooring line tension response is considered and $F_{STE}(x|h_S, t_P)$ can be very well modelled as a Gumbel distribution.

Long-term extreme value can be therefore determined by iteration based on Eq. (1) or Eq. (3) and it is called a full long-term response analysis. This method requires that the short-term response variability should be available for all relevant sea states and it will be quite time-consuming for complex responses, especially when time-domain simulations have to be performed to get correct response characteristics. In such cases, contour line method can be used to predict the extreme response based on limited short-term analyses along a well-defined environmental contour line (or surface) with a given return period.

Contour line method has been applied to marine structural responses by many researchers, e.g. Haver et al. (1998), Meling et al. (2000), Baarholm & Moan (2001), etc. When the short-term response variability is not considered, a reliability problem can be explicitly established based on the long-term variation of environmental conditions and the extreme response can be predicted iteratively by FORM (First Order Reliability Method) (Madsen et al., 1986) or directly by the IFORM (Inverse First Order Reliability Method) technique (Winterstein et al., 1993). However, it is non-conservative to neglect the short-term variability of response and corrections which are quite response-dependent must be given, such as artificial inflation of environmental contour lines, introduction of a correction factor on the predicted median value or use of a quantile higher than the median (Kleiven et al., 2003). According to Haver et al. (1998), a quantile of 85%~90% could be adopted in the contour line method when predicting extreme responses of both fixed and floating structures with a long return period of 100 years. Moreover, for mooring line tension, according to Meling et al. (2000), quantiles of 80% and 85% could be used to predict the 10-year and 100-year extreme values of quasi-static mooring line tension, respectively.

In this paper, dynamic mooring line tension has been analyzed by the frequency-domain code MIMOSA (2003) and full long-term analyses using a short-term extreme value distribution have been performed to predict annual extreme line tension under varying environmental conditions. Moreover, in order to find a suitable quantile when applying the contour line method, sensitivity study has been carried out and a quantile of 70% has been determined. The accuracy of the method has been verified by full long-term analyses.

FATIGUE DUE TO MOORING LINE TENSION

In a stationary sea state, both wave and low frequency mooring line tensions show slightly non-Gaussian properties and according to Gao & Moan (2006), it is quite acceptable to compute the resulting fatigue damage under a Gaussian assumption. Therefore, a formula for calculating bi-modal fatigue damage developed by Jiao & Moan (1990) has been applied in this paper to estimate short-term fatigue damage as shown in Eq. (4).

$$D_{JM} = \rho * D_{NB} \tag{4}$$

where D_{NB} is the fatigue damage under narrow-band assumption and $\rho = \frac{\nu_W}{\nu_Y}(\lambda_W)^{\frac{m}{2}} + \frac{\nu_P}{\nu_Y}[(\lambda_L)^{\frac{m}{2}+2}\left(1-\sqrt{\lambda_W/\lambda_L}\right) + \sqrt{\pi\lambda_L\lambda_W}\, m\Gamma\left((1+m)/2\right)/\Gamma\left((2+m)/2\right)]$ is a correction factor in which $\lambda_W = \sigma_W^2/(\sigma_W^2+\sigma_L^2)$ and $\lambda_L = \sigma_L^2/(\sigma_W^2+\sigma_L^2)$ are the normalized variances of the wave and low frequency parts, respectively, $\nu_Y = \sqrt{\lambda_L\nu_L^2 + \lambda_W\nu_W^2}$ and $\nu_P = \sqrt{\lambda_L^2\nu_L^2 + \lambda_L\lambda_W\nu_W^2\delta_W^2}$, ν_W and ν_L are the mean zero up-crossing rates of the wave and low frequency parts, respectively, δ_W =0.1 is the bandwidth parameter of the wave frequency part, Γ() represents the Gamma function and *m* is the material parameter.

This formula is quite accurate for responses with well-separated high and low central frequencies and is adopted in API RP 2SK (1997), DNV-OS-E301 (2004) and ISO 19901-7 (2005) for estimating fatigue damage induced by bi-modal mooring line tension.

Long-term fatigue damage of line tension is just a weighted sum of contributions from all sea states considering the occurrence probability of each one.

CASE STUDY

Description of Vessel and Mooring Lines

A semi-submersible, located in the Northern North Sea (NNS), has been used for case study. Main particulars of the vessel are listed in Table 1.

Table 1 Main particulars of the semi-submersible

Displacement	52500 (ton)
Length O.A.	124 (m)
Breadth	95.3 (m)
Draught	21 (m)
Operational water depth	340 (m)

Identical mooring lines have been considered and each one has a chain-wire-chain pattern with a length of the first segment 725m, the second 312m and the third 99m from bottom to top. Each mooring line has therefore a total length of 1136m with 550m lying on bottom in the initial stage and is under a pre-tension around 1200kN. Chain link with a diameter of 125mm and wire rope with a diameter of 136mm have been used.

Mooring System Configuration

Two configurations of mooring system of the semi-submersible have been applied to study the sensitivity of line tension due to failure, see Figs. 1~2. One system has 16 identical mooring lines with 4 at each corner and the other has 12 lines with 3 at each corner. Mooring analyses have also been performed for damaged conditions when Line No. 6 in the 16-line system and Line No. 5 in the 12-line system failed, respectively.

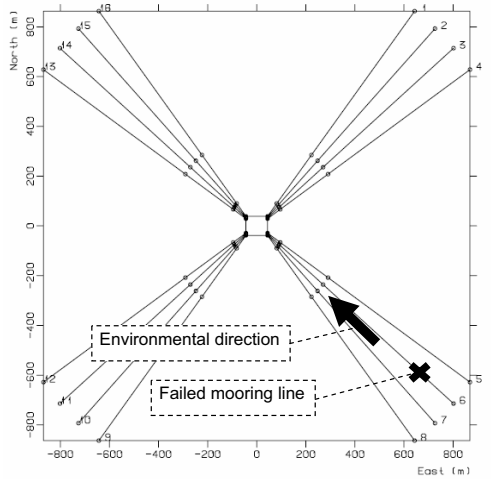

Fig. 1 Horizontal project of the 16-line mooring system

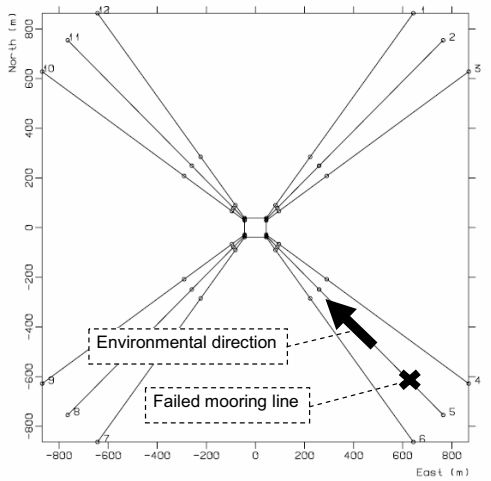

Fig. 2 Horizontal project of the 12-line mooring system

Environmental Data

Statoil ASA has measurements of short-term sea states of waves from buoys in the NNS for many years. In this paper, 30 annual scatter diagrams (from 1976 to 2005), provided by Dr. Sverre Haver, Statoil ASA, have been used to study the annual variation of mooring line tension. The dataset used herein is quite similar as those in the paper of Moan et al. (2005). Therefore, only the predicted annual extreme value of H_S has been plotted in Fig. 3 to show the long-term environmental variation.

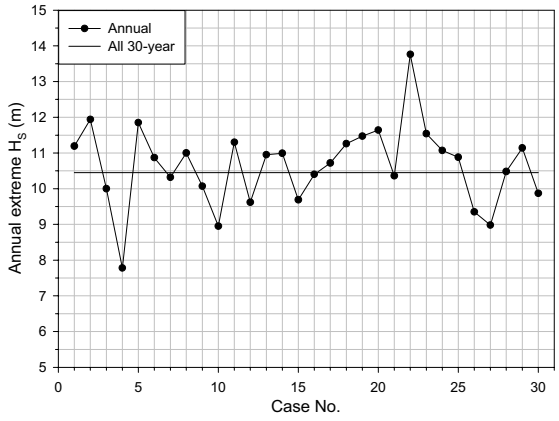

Fig. 3 Variation of annual extreme value of H_S

In mooring analyses, the 1-hour mean wind speed U_W is assumed to be a deterministic function of H_S as Eq. (5) (Bitner-Gregersen & Haver, 1991),

$$U_W = \alpha * \Gamma(1 + 1/\beta) \tag{5}$$

where $\alpha = 4.4 + 1.94 * H_S$, $\beta = 2.424 + 0.233 * H_S^{1.120}$ and $\Gamma()$ is the Gamma function. Current speed is selected to 0.9m/sec. Collinear environmental direction of wave, wind and current is assumed and is shown in Figs. 1~2.

Short-term Time-domain Simulations

Linear and nonlinear time-domain mooring analyses of the intact 16-line system have been carried out with a sea state of H_S =11.25m and T_P =14.5sec by use of program RIFLEX (2003). A Quantile-quantile plot of three 1-hour simulations of linear and nonlinear tensions in Line No. 7 is shown in Fig. 4. On the average, nonlinear effect on mooring line tension is not significant for this system. Therefore, linear analyses by frequency-domain program MIMOSA have been applied in the following calculations.

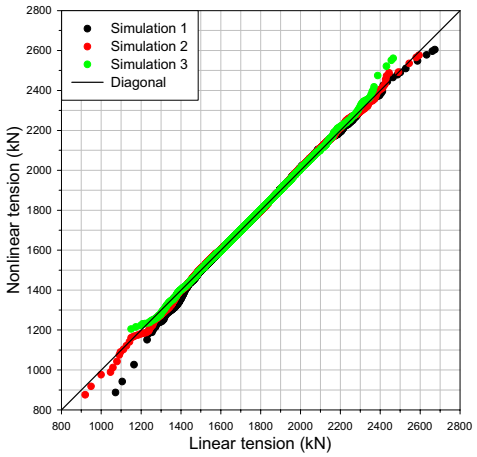

Fig. 4 Quantile-Quantile plot of linear and nonlinear line tensions with three 1-hour simulations

Moreover, in order to identify the distribution of short-term extreme line tension, 30 linear mooring simulations with the same short-term characteristics have been performed with RIFLEX. A Gumbel distribution is fitted to the obtained 1-hour extreme values as shown in Fig. 5, which gives a coefficient of variance (COV) about 0.05. Similarly, it is assumed in the following analyses that the short-term extreme line tension follows a Gumbel distribution with mean value given by MIMOSA and COV fixed as 0.05 in any sea state.

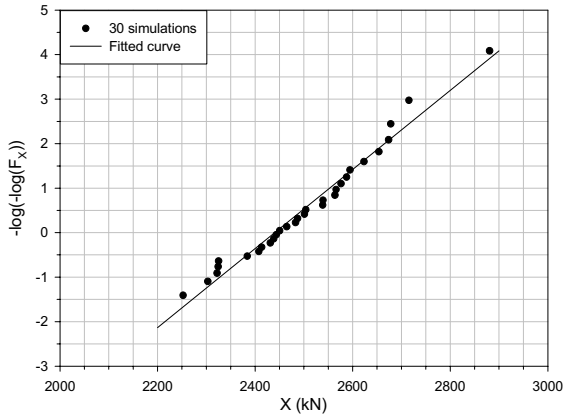

Fig. 5 Gumbel fitting of 1-hour extreme line tension of 30 simulations

Sensitivity Study of Annual Extreme Value

Thirty-year wave data in NNS have been applied for mooring analyses of each year by a full long-term analysis together with those when the 30-year data are used as a whole. Analyses are performed for the whole systems and results are shown only for the Line No. 7 and Line No. 6 in the 16-line and 12-line systems, respectively, which are the mostly loaded lines when a damage shown in Figs. 1~2 occurs.

Predicted annual extreme line tensions under intact and damaged conditions are shown in Figs. 6~7, which are normalized by the result of the intact condition with all environmental data. As shown, the predicted annual extreme values are quite sensitive to the environmental data used. Ratios between the largest one and the lowest one could reach 1.8 and 2.0 for the 16-line system under an intact condition and a damaged condition, respectively, and 2.0 and 2.3 for the 12-line system. On the average, increases of 20% and 30% of line tension have been observed due to failure for the 16-line and the 12-line systems, respectively. As expected, the 12-line system shows more increase in the predicted line tension when a failure occurs. Moreover, by comparing the results in Figs. 6~7 with Fig. 3, the annual extreme line tension is seen to be highly correlated with the annual extreme value of significant wave height.

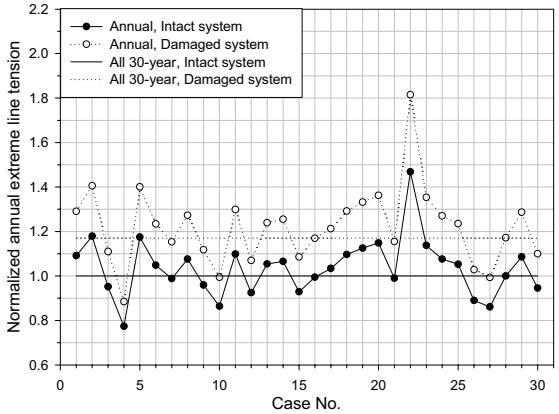

Fig. 6 Variation of annual extreme tension of Line No. 7 in the 16-line system

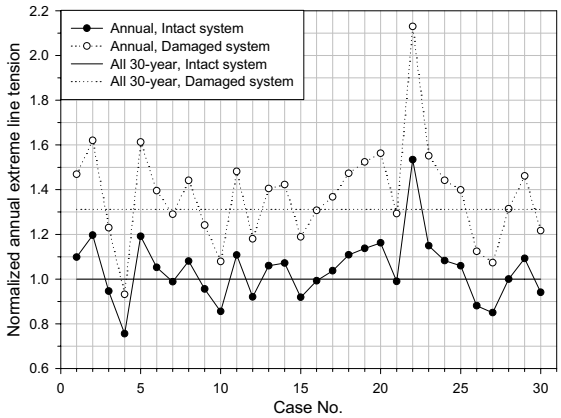

Fig. 7 Variation of annual extreme tension of Line No. 6 in the 12-line system

The contour line method for extreme value prediction has also been applied for all of the cases. Sensitivity study has been carried out with different quantiles and a quantile of 70% was found to yield accurate estimates of annual extreme line tension. Relative errors of the annual extreme tensions predicted by the full long-term analysis and the

contour line method have been plotted in Figs. 8~9 for the 16-line and 12-line systems, respectively. The absolute errors are within 4%, which indicates that the contour line method is quite accurate and a quantile of 70% could be consistently chosen as a reference for dynamic mooring analysis when applying the contour line method.

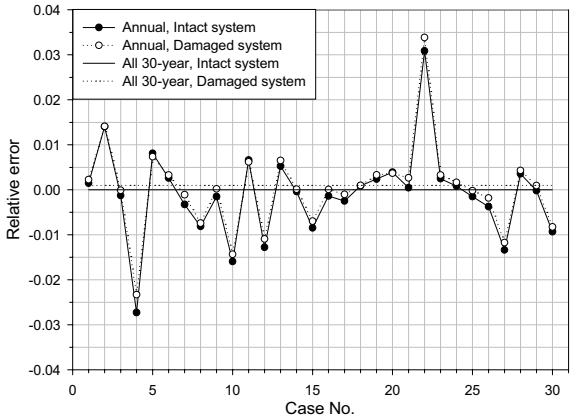

Fig. 8 Relative error of predicted annual extreme tension of Line No. 7 in the 16-line system by the contour line method

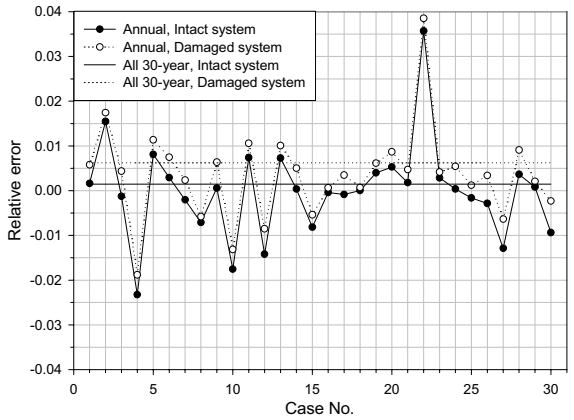

Fig. 9 Relative error of predicted annual extreme tension of Line No. 6 in the 12-line system by the contour line method

Sensitivity Study of Annual Fatigue Damage

Annual fatigue damage has also been predicted for each year by a bi-modal fatigue formulation, see Figs. 10~11. Compared with the extreme line tension, the predicted fatigue damage is more sensitive to the environmental data. Ratios of 4.4 and 4.6 between the maximum annual fatigue damage and the minimum one are obtained for the 16-line system under an intact condition and a damaged condition, respectively, and ratios of 4.5 and 6.0 for the 12-line system. Due to mooring line failure, increases of 50% and 90% in total fatigue damage have been obtained on average, which indicates that the fatigue damage is also more sensitive to failure when compared with the extreme line tension, especially for the 12-line system with less mooring lines at each corner.

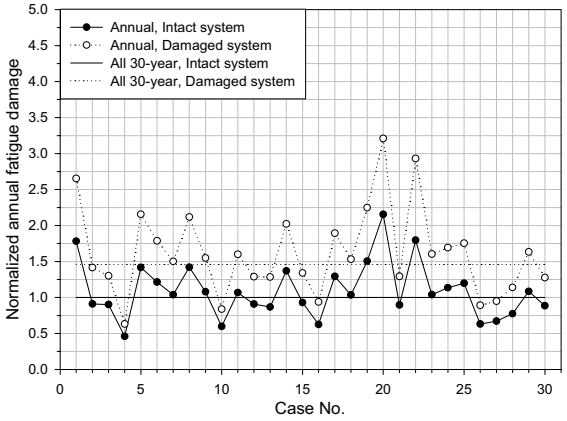

Fig. 10 Variation of annual fatigue damage of Line No. 7 in the 16-line system

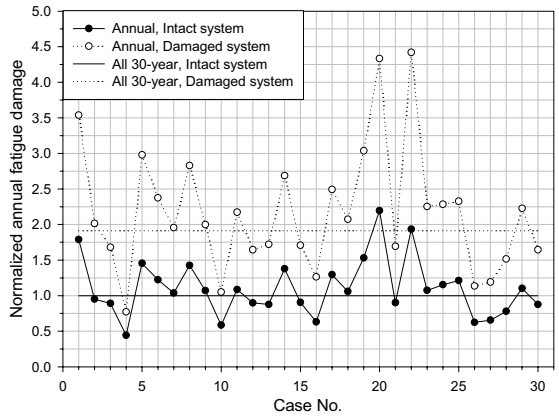

Fig. 11 Variation of annual fatigue damage of Line No. 6 in the 12-line system

It is noted that for extreme value prediction, only Case No. 22, which corresponds to the year 1997, shows a significant increase after line failure, while for fatigue damage estimation, both Case No. 20 (the year 1995) and 22 show significant increases and Case No. 20 has even large value than Case No. 22. This is because the extreme response is closely connected to the extreme sea state, while the long-term fatigue damage has contributions from a large number of sea states, as discussed below.

Short-term Contributions to Annual Extreme Value and Fatigue Damage

As indicated before, both the long-term extreme value and fatigue damage are predicted from short-term contributions. For each sea state, the relative contributions to these two variables are quite different.

For example, considering the 16-line system under the environment condition with all 30 years of wave data, relative short-term contributions of probability of exceeding the annual extreme value are plotted as contour lines in Figs. 12~13 for intact and damaged conditions, respectively. Fatigue damage contributions are plotted in Figs. 14~15.

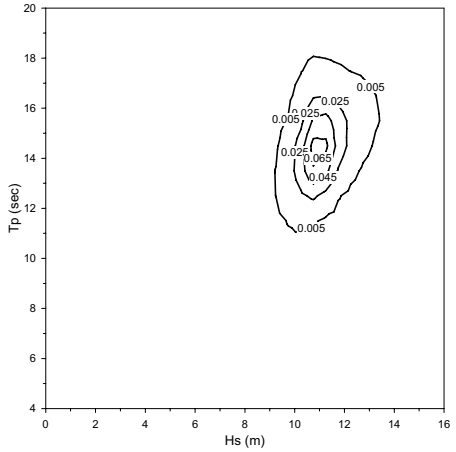

Fig. 12 Relative short-term contributions of probability of exceeding the annual extreme tension of Line No. 7 in the 16-line system under intact condition

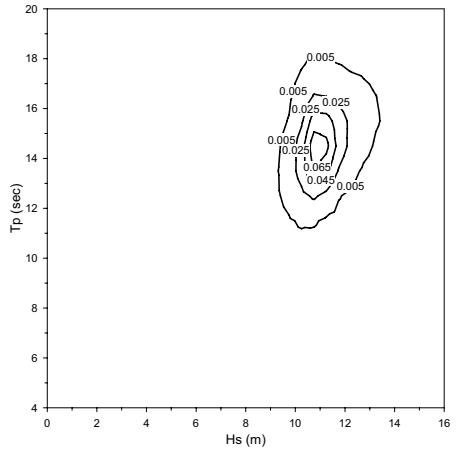

Fig. 13 Relative short-term contributions of probability of exceeding the annual extreme tension of Line No. 7 in the 16-line system under damaged condition

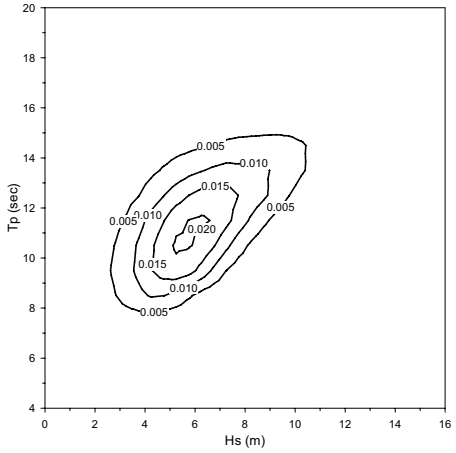

Fig. 14 Relative short-term contributions of annual fatigue damage of Line No. 7 in the 16-line system under intact condition

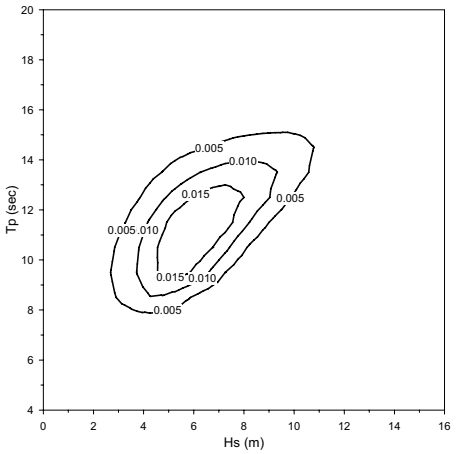

Fig. 15 Relative short-term contributions of annual fatigue damage of Line No. 7 in the 16-line system under damaged condition

For extreme line tension, centre of the main short-term contributions are similar for intact and damaged conditions, located in a sea state of H_S =11m and T_P =14sec, while for annual fatigue damage, the central sea state is identified as H_S =6m and T_P =11sec and the main contributions cover a larger part of the scatter diagram. In other words, extreme response depends strongly on the extreme sea state, while fatigue damage is mainly evaluated from the moderate sea states.

Moreover, there is quite little difference between the relative contributions for intact condition and for damaged condition. This means that the dynamic characteristics of the mooring system are not changed significantly after one line failure.

CONCLUSIONS

From a risk analysis perspective, it is interesting to know the performance of a mooring system under failure. Increases both in extreme line tension and in total fatigue damage suggest design checks under ALS both for ultimate and fatigue strength of mooring lines. In this paper, the sensitivity study of a mooring system has been carried out for steady-state responses after a failure of one line.

Time-domain simulations of mooring line tension have been performed to verify a linearized model of the mooring system considered and to identify the distribution for the short-term extreme value.

The annual environmental data used in this paper show a significant variation from year to year and as a result the predicted extreme line tension and the corresponding fatigue damage are also varying from year to year. Compared with the 30-year environmental data, the extreme line tension could increase by 80% and by 115% in the worst cases after damage for the 16-line and 12-line systems, respectively, when applying the annual environmental data, while the annual fatigue damage could increase by 225% and 350%. It indicates that the safety level of the mooring system is strongly dependent on the environmental condition that could be experienced after damage.

Full long-term analyses and simplified analyses based on the contour line method have been carried out to predict the annual extreme tension. When applying the contour line method, a quantile of 70% on the short-term extreme value of the dynamic mooring line tension was found to yield an accurate prediction.

On the average, increases of 25% and 70% in the annual extreme tension and in the total fatigue damage due to mooring line failure have been obtained and the fatigue damage is more sensitive to failure. In the paper, it is assumed that the mooring system is kept under the damaged condition for the following year. In reality, the failed mooring line could be identified and replaced within several months.

As expected, mooring configuration could also affect the load increase in the remaining lines after damage, especially when they are grouped at corners.

ACKNOWLEDGEMENTS

The authors wish to acknowledge the support from the Research Council of Norway through the Centre for Ships and Ocean Structures at Norwegian University of Science and Technology. The authors are also grateful to Dr. Sverre Haver, Statoil ASA for providing the environmental data.

REFERENCES

API (1997). "Recommended practice for design and analysis of stationkeeping systems for floating structures," API RP 2SK.

Baarholm, GS and Moan, T (2001). "Application of contour line method to estimate extreme ship hull loads considering operational restrictions," *Journal of Ship Research*, Vol. 45, No. 3, pp. 228-240.

Bitner-Gregersen, EM and Haver, S (1991). "Joint environmental model for reliability calculations," ISOPE-91, Vol. 1, pp. 246-253, Edinburgh.

DNV (2004). "Offshore standard - Position mooring," DNV-OS-E301.

Gao, Z and Moan, T (2006). "Wave-induced fatigue damage of mooring chain under combined non-Gaussian low and wave frequency loads," OMAE2006-92389, Hamburg.

Haver, S, Sagli, G and Gran, TM (1998). "Long term response analysis of fixed and floating structures," *Proceedings, Wave'98-Ocean Wave Kinematics, Dynamics and Loads on Structures*, International OTRC Symposium, Houston.

Haver, S, Meling, TS and Larsen, K (1999). "System failure analysis of Veslefrikk B mooring," Statoil Report NO. 99s97*5292.

ISO (2005). "Petroleum and natural gas industries - Specific requirements for offshore structures - Part 7: Stationkeeping systems for floating offshore structures and mobile offshore units," ISO 19901-7.

Jiao, G and Moan, T (1990). "Probabilistic analysis of fatigue due to Gaussian load processes," *Probabilistic Engineering Mechanics*, Vol. 5, No. 2, pp. 76-83.

Kleiven, G and Haver, S (2003). "Application of environmental contour lines for predicting design response," Statoil Report NO. PTT-KU-MA-2002/018.

Madsen, HO, Krenk, S and Lind, NC (1986). "Methods of structural reliability," Prentice-Hall, Englewood Cliffs, New Jersey.

MARINTEK (2003). "User's Documentation MIMOSA, Program Version 5.7," Report No. 516413.00.01.

MARINTEK (2003). "User's Manual RIFLEX, Version 3.2.3," Report No. 519619.

Meling, TS, Johannessen, K, Haver, S and Larsen, K (2000). "Mooring analysis of a semi-submersible by use of IFORM and contour surfaces," OMAE 2000/OSU OFT-4141, New Orleans.

Moan, T, Gao, Z and Ayala Uraga, E (2005). "Uncertainty of wave-induced response of marine structures due to long-term variation of extratropical wave conditions," *Marine Structures*, Vol. 18, No. 4, pp. 359-382.

Nordenstrom, N (1971). "Methods for predicting long term distributions of wave loads and probability of failure for ships," DNV Report 71-2-S.

Winterstein, SR, Ude, TC, Cornell, CA, Bjerager, P and Haver, S (1993). "Environmental parameters for extreme response: inverse FORM with omission factors," ICOSSAR-93, Innsbruk.

Paper 6

Fatigue damage under combined high and low frequency Gaussian load processes considering a two-slope SN curve

Published in
Proceedings of the 10th International Conference on Applications of Statistics and Probability in Civil Engineering (ICASP10)
July 31-August 3, 2007, Tokyo, Japan

Paper 6 Applications of Statistics and Probability in Civil Engineering – Kanda, Takada & Furuta (eds)
© 2007 Taylor & Francis Group, London, ISBN 978-0-415-45134-5

Fatigue damage under combined high and low frequency Gaussian load processes considering a two-slope SN curve

Z. Gao & T. Moan
Centre for Ships and Ocean Structures, Norwegian University of Science and Technology

ABSTRACT: Dynamic loads due to waves, wind and other sources of excitation often consist of combined high and low frequency components. This bimodal loading would then be a wide-band process and the fatigue cycles should be taken into account by rainflow counting. It is often computationally efficient to determine the fatigue damage under such a combined loading by separately considering high and low frequency load histories for a linear structural system. In the frequency domain different bimodal fatigue combination rules have been proposed and the accuracy of these methods has also been examined. Previous studies have, however, been limited to using a single-slope SN curve. In this paper, some of combination rules, e.g. those of Jiao and Moan, DNV and Huang and Moan, have been generalized to the case with a two-slope SN curve. New combination formulae have been derived for the two-slope case and the corresponding accuracy has been checked with the rainflow cycle counting algorithm.

1 INTRODUCTION

Structural components are often subjected to loads with combined high frequency (HF) and low frequency (LF) contributions. This combined effect would then be a wide-band process and the fatigue cycles should be taken into account by rainflow counting (Matsuishi & Endo 1968). The rainflow cycle counting is believed to be the best method to estimate the effective stress range for fatigue calculation (see e.g. Watson & Dabell 1975). But the exact frequency domain solution of rainflow stress range cycles for a general wide-band process can not be derived analytically. However, for a bimodal Gaussian process, the corresponding fatigue damage can be approximated theoretically as done by Jiao & Moan (1990). They expressed analytically the combined fatigue damage of two narrow-band Gaussian processes with well-separated spectra as a sum of the fatigue due to the HF process and the combined process of the envelope HF process plus the LF process. This method is found to quite accurate when compared with the time domain rainflow result. Gao & Moan (2006) extended Jiao and Moan's method to deal with fatigue damage due to combined non-Gaussian narrow-band wave frequency and low frequency mooring line dynamic tensions of a semi-submersible.

Moreover, it is often computationally efficient to determine the fatigue damage under such a combined load by separately considering high and low frequency load histories for a linear structural system. The combined fatigue damage is not just equal to the sum of individual damages because the fatigue damage is a nonlinear function of the stress range. The simple sum will generally be nonconservative and could be a lower bound. Moreover, the fatigue damage based on a narrow-band assumption of the total process will be too conservative, especially for a bimodal process with well separated high and low frequencies. But it could be considered as an upper bound. Therefore, an explicit and rational formula by which the combined damage can be expressed in terms of individual damages would be more practical and desirable.

Lotsberg (2005) derived a simple explicit formula for evaluating the bimodal fatigue damage, which is taken as DNV's rule formula. He obtained the combination by considering of the HF and LF damage-equivalent constant amplitude stress histories. However, the DNV formula may overestimate the total damage and in some cases it is even more conservative than the narrow-band approach as shown by Huang & Moan (2006). But its format is convenient for practical application because the combined fatigue damage is expressed explicitly by the individual damages. Huang & Moan (2006) developed a more accurate explicit formula by using the combined spectrum together with a bandwidth correction factor. They showed that in general their formula together with the correction factor proposed by Benasciutti & Tovo (2005) gives fatigue damage close to the rainflow prediction.

Alternatively, by considering the combined high and low frequency load as a general wide-band Gaussian process, the combined fatigue damage can be evaluated by following Wirsching & Light (1980), Dirlik (1985), Gall & Hancock (1985), Bouyssy et al. (1993) and Benasciutti & Tovo (2005). These methods are based on the empirical estimation of the bandwidth correction factor for the total process.

However, the accuracy of most of the above mentioned methods has only been checked for a single-slope SN curve. With the slope parameter of a SN curve m increasing, the sensitivity of these methods' accuracy will also increase because of the nonlinear relation between the fatigue damage and the response variance. This effect will also occur for the fatigue prediction with a two-slope SN curve. In this paper, the frequency domain methods of Jiao and Moan, the DNV formula and Huang and Moan's formula, are generalized to two-slope curves. New damage formulae have been derived which can easily be extended to a multi-slope SN curve and the corresponding accuracy has been illustrated.

2 FATIGUE DAMAGE FOR A NARROW-BAND GAUSSIAN PROCESS

Based on a narrow-band Gaussian stress process and a single-slope SN curve ($N = KS^{-m}$), the following general formula is usually applied to estimate the accumulated fatigue damage from individual stress cycles using the Miner-Palmgren rule (Miner 1945)

$$D = \sum \frac{n_i}{N_i} = \frac{N_0}{K} E[S^m] = \nu_0 T \frac{1}{K} (2\sqrt{2}\sigma)^m \Gamma(1 + m/2) \qquad (1)$$

where N_0 is the total number of cycles, $N_0 = \nu_0 T$. ν_0 and T are the mean zero up-crossing rate of the response and the total duration. $E[S^m]$ denotes the expectation of the response or stress range S powered by m, which leads to a complete gamma function $\Gamma(1 + m/2)$ multiplied with $(2^{3/2}\sigma)^m$ when the response range distribution is a Rayleigh distribution. σ is the standard deviation of the response process. m and K are the material parameters of the SN curve.

If a two-slope SN curve is applied, the narrow-band fatigue damage can still be explicitly computed by two incomplete gamma functions when the response range distribution is still assumed to be Rayleighian

$$D = \nu_0 T \left(\frac{1}{K_2} (2\sqrt{2}\sigma)^{m_2} \gamma(1 + m_2/2; (S_q/(2\sqrt{2}\sigma))^2) + \frac{1}{K_1} (2\sqrt{2}\sigma)^{m_1} \Gamma(1 + m_1/2; (S_q/(2\sqrt{2}\sigma))^2) \right) \qquad (2)$$

where S_q is the separation point along the stress range axis of the two-slope SN curve. An example of a two-slope SN curve is plotted in Figure 1 and the parameters are specified by the UK Department of Energy (1981). m_2, K_2 and m_1, K_1 are the material parameters corresponding to the lower segment ($S < S_q$) and the upper segment ($S \geq S_q$) of the SN curve, respectively. Clearly, the two segments coincide at $S = S_q$ with a relation of $K_1 S_q^{-m_1} = K_2 S_q^{-m_2}$. $\gamma(a; b)$ and $\Gamma(a; b)$ are the incomplete gamma functions with integration limit from zero to b and from b to infinity, respectively. Fatigue damage due to a multi-slope SN curve can easily be obtained by generalizing Equation 2 with multiple incomplete gamma functions. Herein, we focus on a two-slope SN curve.

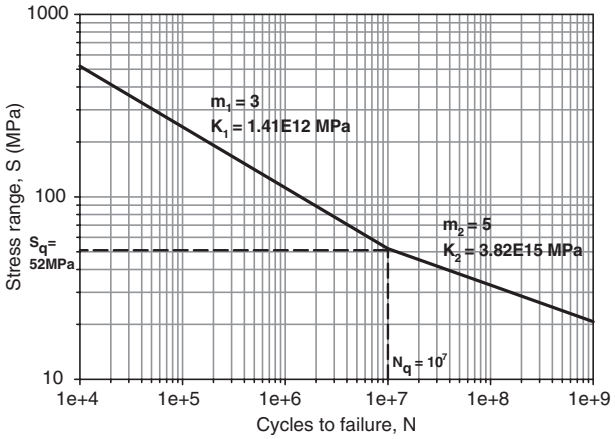

Figure 1. Example of two-slope SN curve specified by the UK Department of Energy.

In offshore engineering, $m = 3$ is the typical value for a single-slope SN curve, while $m_1 = 3$ and $m_2 = 5$ are normally applied to a two-slope SN curve. The separation stress range S_q is chosen at a high value of cycles to failure, e.g. $N_q = 10^7$. A two-slope SN curve with $m_2 = 5$ assumes that more cycles would be experienced until failure for stress ranges lower than S_q, which agrees much better with the experimental data. Hence, a lower fatigue damage is predicted by using a two-slope SN curve as compared with a single-slope one. Based on Equations 1 and 2, a reduction factor of fatigue damage due to a two-slope SN curve can be computed easily. According to Wirsching & Chen (1988), the reduction factor has been obtained with a Weibull distribution of the effective stress range depending on the relative comparison of the mean stress range and the separation stress range. The reduction factor obtained by Equations 1 and 2 with a Rayleighian assumption is a special case. However, for a general wide-band Gaussian process, the analytical stress range distribution is usually unknown. Effective stress cycles are typically counted by the rainflow algorithm in the time domain and the distribution are then numerically determined. Therefore, in the frequency domain fatigue combination methods

are usually applied to wide-band random processes, e.g. a bimodal Gaussian process.

3 FATIGUE DAMAGE COMBINATION FOR A BIMODAL GAUSSIAN PROCESS

For a general wide-band Gaussian process, when the time series of the response is available, rainflow cycle counting algorithm can be applied and gives a best estimation of the fatigue damage. However, the exact expression of fatigue damage based on the rainflow counting of effective stress range is very hard to obtain in the frequency domain. Herein, we consider a special wide-band Gaussian process, which is often applied in offshore engineering, i.e. a bimodal process. A bimodal process has well-separated high frequency and low frequency in spectral density and both the HF and LF processes are assumed to be narrow-banded and independent of the other. Fatigue damage due to a bimodal Gaussian process has been widely studied. Among them, the combination rule proposed by Jiao and Moan, the DNV combination formula and the formula proposed by Huang and Moan are briefly described in the following and are extended to a two-slope SN curve.

3.1 *Combination rule proposed by Jiao and Moan*

Jiao & Moan (1990) combined an envelope HF process and an LF process which have similar oscillation periods and expressed the bimodal fatigue as a sum of fatigue damages due to the HF process and the combined process. They assumed a bimodal process,

$$Y(t) = X_{HF}(t) + X_{LF}(t) \tag{3}$$

and the corresponding fatigue damage is estimated by

$$D_Y = D_{HF} + D_P \tag{4}$$

where $P(t) = R_{HF}(t) + X_{LF}(t)$ with $R_{HF}(t)$ as the envelope process of $X_{HF}(t)$.

HF fatigue damage D_{HF} can easily be computed with Equation 1 or Equation 2, while in order to calculate D_P, one need to know the amplitude distribution of $P(t)$. Based on an assumption of Gaussianity, the amplitude process of $P(t)$, denoted by $Q(t)$, has a distribution as follows when the LF process becomes relatively important as compared with the HF process,

$$\begin{aligned} f_Q(q) &= (\lambda_{LF} - \sqrt{\lambda_{HF}\lambda_{LF}})q\exp(-\frac{q^2}{2\lambda_{LF}}) \\ &+\sqrt{2\pi\lambda_{HF}\lambda_{LF}}(q^2-1)\exp(-\frac{q^2}{2}) \end{aligned} \tag{5}$$

where $\lambda_{HF} = \sigma_{HF}^2/(\sigma_{HF}^2 + \sigma_{LF}^2)$ and $\lambda_{LF} = \sigma_{LF}^2/(\sigma_{HF}^2 + \sigma_{LF}^2)$ are the relative variances of the HF and LF processes, respectively. Herein, the bimodal process is normalized with $\sigma_Y^2 = \sigma_{HF}^2 + \sigma_{LF}^2 = 1$.

By applying a single-slope SN curve, Jiao & Moan (1990) then derived a formula for the fatigue damage due to $P(t)$. In this paper, a two-slope SN curve is applied and the corresponding fatigue damage of $P(t)$ is

$$\begin{aligned} D_P &= \nu_{0P}T(\frac{1}{K_2}2^{\frac{3m_2}{2}}(\lambda_{LF}^{(2+\frac{m_2}{2})}(1-\sqrt{\frac{\lambda_{HF}}{\lambda_{LF}}})\gamma(1+\frac{m_2}{2};(\frac{S_q}{2\sqrt{2}\sigma_{LF}})^2) \\ &-\sqrt{\pi\lambda_{HF}\lambda_{LF}}(\gamma(\frac{1}{2}+\frac{m_2}{2};(\frac{S_q}{2\sqrt{2}\sigma_Y})^2 - \gamma(\frac{3}{2}+\frac{m_2}{2};(\frac{S_q}{2\sqrt{2}\sigma_Y})^2))) \\ &+\frac{1}{K_1}2^{\frac{3m_1}{2}}(\lambda_{LF}^{(2+\frac{m_1}{2})}(1-\sqrt{\frac{\lambda_{HF}}{\lambda_{LF}}})\Gamma(1+\frac{m_1}{2};(\frac{S_q}{2\sqrt{2}\sigma_{LF}})^2) \\ &-\sqrt{\pi\lambda_{HF}\lambda_{LF}}(\Gamma(\frac{1}{2}+\frac{m_1}{2};(\frac{S_q}{2\sqrt{2}\sigma_Y})^2 - \Gamma(\frac{3}{2}+\frac{m_1}{2};(\frac{S_q}{2\sqrt{2}\sigma_Y})^2)))) \end{aligned} \tag{6}$$

where ν_{0P} is the mean zero up-crossing rate of $P(t)$,

$$\nu_{0P} = \lambda_{LF}\nu_{0LF}\sqrt{1+\frac{\lambda_{HF}}{\lambda_{LF}}(\frac{\nu_{0HF}}{\nu_{0LF}}\delta_{HF})^2} \tag{7}$$

and is calculated from the mean zero up-crossing rates of the HF and LF processes, ν_{0HF} and ν_{0LF}, and the Vanmarcke's bandwidth parameter of the HF process, δ_{HF}.

The total bimodal fatigue damage is then easily estimated by adding the fatigue damages due to $X_{HF}(t)$ and $P(t)$.

3.2 *DNV combination formula*

Instead of computing the fatigue damage based on theoretical analysis of a bimodal process itself, some simple formulae have been proposed to estimate the total fatigue damage directly from the HF and LF components, e.g. the DNV formula and Huang and Moan's formula, etc.

By using a concept of damage-equivalent constant stress range defined as

$$\Delta\sigma = (\frac{K}{T}\frac{D}{\nu_0})^{\frac{1}{m}} \tag{8}$$

with a single-slope SN curve, Lotsberg (2005) approximated the combined fatigue damage as

$$\begin{aligned} D_Y &= D_{HF} + D_{LF}(\frac{\Delta\sigma_{HF}+\Delta\sigma_{LF}}{\Delta\sigma_{LF}})^m - D_{HF}\frac{n_{LF}}{n_{HF}} \\ &= D_{HF}(1-\frac{\nu_{0LF}}{\nu_{0HF}}) + \nu_{0LF}((\frac{D_{HF}}{\nu_{0HF}})^{\frac{1}{m}} + (\frac{D_{LF}}{\nu_{0LF}})^{\frac{1}{m}})^m \end{aligned} \tag{9}$$

where $n_{HF} = \nu_{0HF}T$ and $n_{LF} = \nu_{0LF}T$ are the number of cycles counted from the HF and LF processes, respectively.

When a two-slope SN curve (e.g. with $m_1 = 3$ and $m_2 = 5$) is applied to both the HF and LF processes,

Lotsberg (2005) suggested to compute the fatigue damage from Equation 9 with $m = 5$. This is a conservative procedure. In fact the value of m in Equation 9 depends on the comparison of the equivalent constant stress range and the separation stress range of the two-slope SN curve. We can rewrite Equation 9 as

$$D_Y = D_{HF} + D_{LF}' - D_{HF}\frac{n_{LF}}{n_{HF}} \tag{10}$$

where D'_{LF} is the fatigue damage due to the LF process with an equivalent constant stress range $\Delta\sigma'_{LF} = \Delta\sigma_{HF} + \Delta\sigma_{LF}$.

In order to calculate D'_{LF}, when the individual fatigue damages D_{HF} and D_{LF} are known, the equivalent number of cycles to failure are first obtained as $N_{HF} = v_{0HF}T/D_{HF}$ and $N_{LF} = v_{0LF}T/D_{LF}$.

Then the equivalent constant stress range of the HF and LF processes is computed as

$$\Delta\sigma_i = \begin{cases} (K_1/N_i)^{\frac{1}{m_1}}, & when\ N_i \le N_q \\ (K_2/N_i)^{\frac{1}{m_2}}, & when\ N_i > N_q \end{cases} \tag{11}$$

where $i = HF$ or LF, and N_q is the separation point of cycles to failure of the two-slope SN curve, e.g. $N_q = 10^7$.

Therefore, D'_{LF} is determined as

$$D'_{LF} = \begin{cases} \frac{v_{0LF}T}{K_1}(\Delta\sigma'_{LF})^{m_1}, & when\ \Delta\sigma'_{LF} \ge S_q \\ \frac{v_{0LF}T}{K_2}(\Delta\sigma'_{LF})^{m_2}, & when\ \Delta\sigma'_{LF} < S_q \end{cases} \tag{12}$$

where $\Delta\sigma'_{LF} = \Delta\sigma_{HF} + \Delta\sigma_{LF}$.

Finally Equation 10 is used to estimate the total fatigue damage.

3.3 *Combination formula proposed by Huang and Moan*

Huang & Moan (2006) proposed a formula suitable for a bimodal fatigue combination. The basis of Huang and Moan's formula is the summation of HF and LF spectra, i.e. $\sigma_Y^2 = \sigma_{HF}^2 + \sigma_{LF}^2$. For a Gaussian process and a single-slope SN curve, the combined fatigue damage is estimated by

$$D_Y = b_Y v_{0Y}\left(\left(\frac{D_{HF}}{b_{HF}v_{0HF}}\right)^{\frac{2}{m}} + \left(\frac{D_{LF}}{b_{LF}v_{0LF}}\right)^{\frac{2}{m}}\right)^{\frac{m}{2}} \tag{13}$$

where v_{0Y} is the mean zero up-crossing rate of the combined process,

$$v_{0Y} = \sqrt{\frac{v_{0HF}^2\sigma_{HF}^2 + v_{0LF}^2\sigma_{LF}^2}{\sigma_{HF}^2 + \sigma_{LF}^2}} \tag{14}$$

and $b_i (i = HF, LF \text{ or } Y)$ is the bandwidth correction factor. For a bimodal process, $b_{HF} = b_{LF} \approx 1$ because both the HF and LF processes are assumed to be narrow-banded. Huang & Moan (2006) suggested that b_Y can be taken as the regularity factor $\alpha_{2,Y}$, defined as

$$b_Y = \alpha_{2,Y} = \frac{m_{2,Y}}{\sqrt{m_{0,Y}m_{4,Y}}} = \frac{v_{0HF}^2\sigma_{HF}^2 + v_{0LF}^2\sigma_{LF}^2}{\sqrt{(\sigma_{HF}^2 + \sigma_{LF}^2)(v_{0HF}^4\sigma_{HF}^4 + v_{0LF}^4\sigma_{LF}^4)}} \tag{15}$$

where $m_{i,Y}$ $(i = 0, 2 \text{ or } 4)$ is the spectrum moment of the combined process. According to Benasciutti & Tovo (2005), based on extensive simulations, the bandwidth correction factor can also empirically be established as

$$b_Y = (\alpha_{1,Y} - \alpha_{2,Y})(1.112(1 + \alpha_{1,Y}\alpha_{2,Y} - (\alpha_{1,Y} + \alpha_{2,Y}))\exp(2.11\alpha_{2,Y}) + (\alpha_{1,Y} - \alpha_{2,Y}))/(\alpha_{2,Y} - 1)^2 \tag{16}$$

where $\alpha_{1,Y}$ is another frequently used bandwidth parameter,

$$\alpha_{1,Y} = \frac{m_{1,Y}}{\sqrt{m_{0,Y}m_{2,Y}}} = \frac{v_{0HF}\sigma_{HF}^2 + v_{0LF}\sigma_{LF}^2}{\sqrt{(\sigma_{HF}^2 + \sigma_{LF}^2)(v_{0HF}^2\sigma_{HF}^2 + v_{0LF}^2\sigma_{LF}^2)}} \tag{17}$$

When a single-slope SN curve is applied, according to Equation 1, the variance of a narrow-band process can explicitly be expressed in terms of the corresponding fatigue damage as

$$\sigma^2 = \frac{1}{8}\left(\frac{K}{T\Gamma(1 + m/2)}\right)^{\frac{2}{m}}\left(\frac{D}{v_0}\right)^{\frac{2}{m}} \tag{18}$$

Therefore, the total fatigue damage can be expressed by the individual damages through the variance of combined process. Obviously, the damage obtained in this way is the narrow-band fatigue damage if no bandwidth correction factor is considered. However a bimodal process is a wide-band process and a correction factor should be multiplied as shown in Equation 13. If a two-slope SN curve is applied, one can not obtain the explicit expression of the variance in terms of fatigue damage from Equation 2. However, we can write the relation between the variance and the corresponding narrow-band fatigue in a more general way as

$$D = v_0 f(\sigma^2) \tag{19}$$

where $f()$ is a monotonic function. Two examples of $f()$ can be seen from Equation 1 for a single-slope SN curve and Equation 2 for a two-slope SN curve, respectively.

Then the variance is implicitly expressed as

$$\sigma^2 = f^{-1}\left(\frac{D}{v_0}\right) \tag{20}$$

where $f^{-1}()$ is the inverse function of $f()$.

Therefore, as similar as Equation 13, the combined bimodal fatigue damage can in general be expressed as

$$D_Y = b_Y v_{0Y} f(f^{-1}(\frac{D_{HF}}{v_{0HF}}) + f^{-1}(\frac{D_{LF}}{v_{0LF}})) \quad (21)$$

In principle the bandwidth correction factor b_Y and the mean zero up-crossing rate $v_{0,Y}$ of the combined process, expressed by the individual HF and LF variances as shown in Equations 14 and 15 or 16, can be expressed purely by the individual damages through Equation 20. Therefore, the combination formula is still applicable when only the HF and LF fatigue damages, not the variances, are known.

4 CASE STUDY

In order to demonstrate the accuracy of these fatigue combination formulae, a series of bimodal Gaussian processes have been simulated in the time domain with different central frequencies and different variances of HF and LF processes. The simulated HF and LF processes are assumed to be independent to each other. A narrow-band and uniform spectrum has been assumed for each of the HF and LF components with a ratio of 5% between the range of effective frequencies and the central frequency, i.e. the Vanmarcke's bandwidth parameter for each of the HF and LF spectra is about 0.015. For each case, 50 time series with each of 6-hour duration have been simulated by using a simulation technique where both Gaussian random coefficients of sine and cosine components are used. It results in about 108000 HF cycles and 5400 LF cycles for each simulation case.

Based on these simulated time series of the bimodal Gaussian processes, the rainflow cycle counting algorithm is used together with a two-slope SN curve to compute the fatigue damage. The average fatigue damage over 50 time series is considered as a reference to check the accuracy of the frequency domain fatigue combination methods, i.e. Jiao and Moan's rule, the DNV formula and Huang and Moan's formula, which are described above. A two-slope SN curve specified by the UK Department of Energy is adopted in this paper, see Figure 1.

Fatigue damages obtained by the frequency domain combination methods are plotted in Figures 2–10 for different cases. Fatigue damage is shown as a ratio to the rainflow counting result. All symbols in these figures are defined in Table 1.

In the figures, the symbol R_{fre} is the ratio of central frequencies of the LF and HF processes, chosen as 0.05, 0.1, 0.125, 0.167, 0.25 and 0.5 with a high frequency of 0.1 Hz which is frequently used in offshore engineering. R_s, selected to 0.5, 1, and 1.5, is

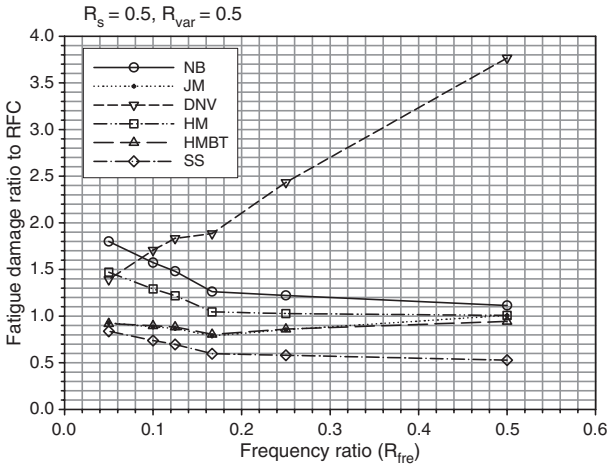

Figure 2. Ratio of the combined fatigue to the RFC result when $R_s = 0.5$, $R_{var} = 0.5$.

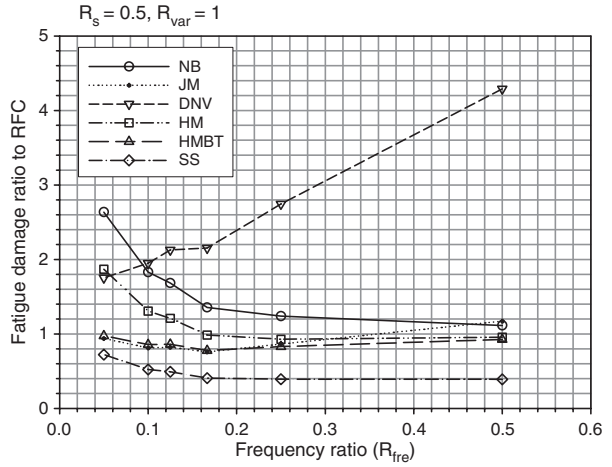

Figure 3. Ratio of the combined fatigue to the RFC result when $R_s = 0.5$, $R_{var} = 1$.

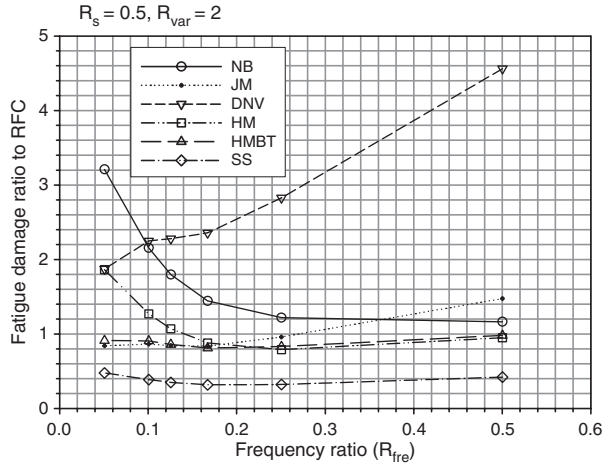

Figure 4. Ratio of the combined fatigue to the RFC result when $R_s = 0.5$, $R_{var} = 2$.

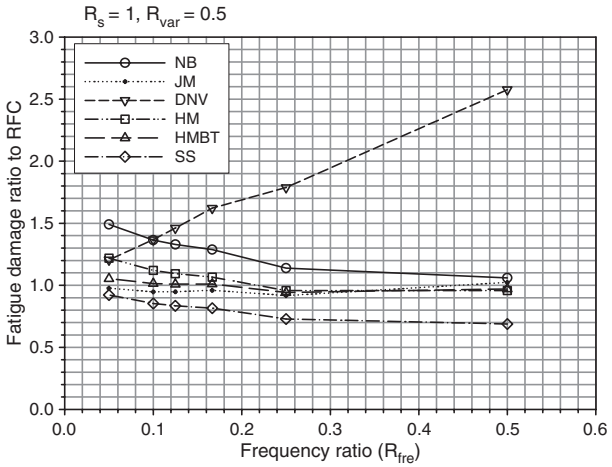

Figure 5. Ratio of the combined fatigue to the RFC result when $R_s = 1$, $R_{var} = 0.5$.

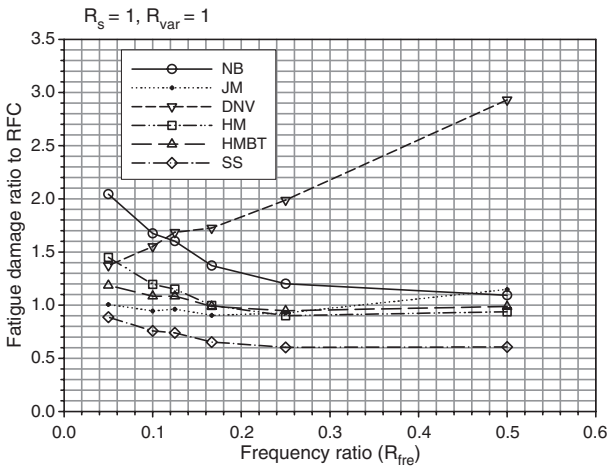

Figure 6. Ratio of the combined fatigue to the RFC result when $R_s = 1$, $R_{var} = 1$.

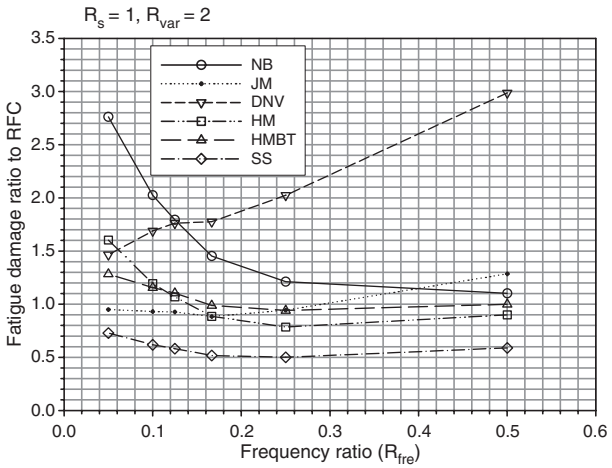

Figure 7. Ratio of the combined fatigue to the RFC result when $R_s = 1$, $R_{var} = 2$.

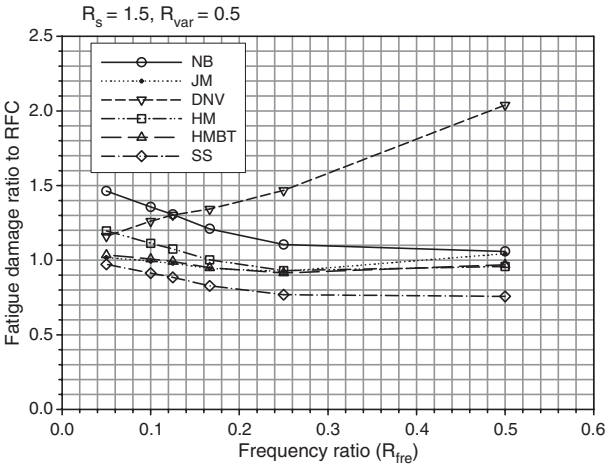

Figure 8. Ratio of the combined fatigue to the RFC result when $R_s = 1.5$, $R_{var} = 0.5$.

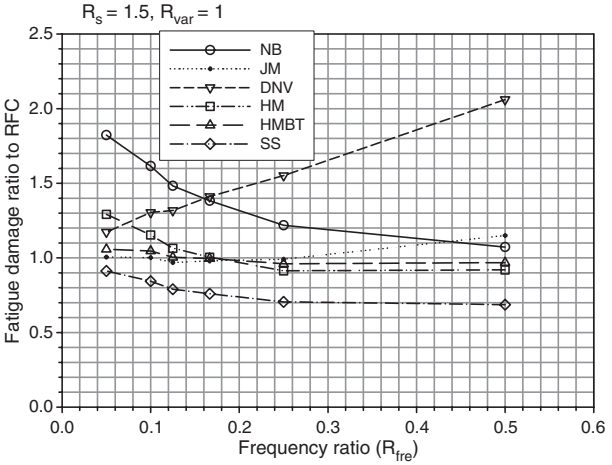

Figure 9. Ratio of the combined fatigue to the RFC result when $R_s = 1.5$, $R_{var} = 1$.

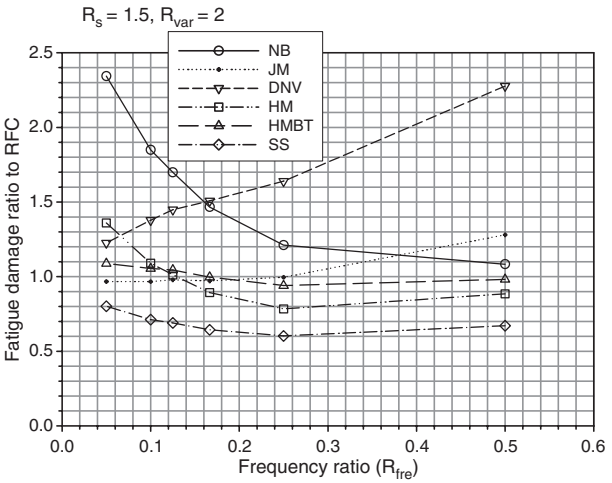

Figure 10. Ratio of the combined fatigue to the RFC result when $R_s = 1.5$, $R_{var} = 2$.

Table 1. Definition of symbols in Figures 2–10.

Symbols	Definition
NB	Narrow-band fatigue damage
JM	Fatigue damage obtained by Jiao and Moan's combination rule
DNV	Fatigue damage of the DNV formula
HM	Fatigue damage of Huang and Moan's formula with a bandwidth correction factor chosen as the regularity factor, i.e. Equation 15
HMBT	Fatigue damage of Huang and Moan's formula with a bandwidth correction factor chosen by Benasciutti and Tovo's suggestion, i.e. Equation 16
SS	Simple sum of the HF and LF fatigue damage components
R_{fre}	Ratio of central frequencies of the LF and HF components
R_s	Ratio of the equivalent stress range S_e to the separation stress range S_q
R_{var}	Ratio of variances of the LF and HF processes

the ratio of the equivalent stress range S_e to the separation stress range S_q when a two-slope SN curve is used, where the equivalent stress range is defined as $S_e = (E[S^m])^{1/m} = 2^{3/2}\sigma(\Gamma(1+m/2))^{1/m}$ with $m = 3$. This ratio is a measure of the relative fatigue contributions from large and small stress ranges. If the ratio is close to zero, it indicates that the small stress ranges are the main part of stress range distribution and the contribution from a SN curve segment with $m_2 = 5$ will dominate the total fatigue damage. Otherwise, if the ratio is much larger than zero, the two-slope fatigue will be close to the fatigue damage based on a single-slope SN curve with $m = 3$. R_{var} is the ratio of variances of the LF and HF components with values of 0.5, 1 and 2.

All these figures show that the frequency domain methods, based on a two-slope SN curve, in general have the same level of accuracy for different values of R_s. The accuracy is also as similar as those of Huang and Moan's results (see Huang & Moan 2006) of a single-slope SN curve with $m = 3$. It indicates that these methods can very well be extended to a two-slope SN curve, even to a multi-slope SN curve, and quite good fatigue damage approximations can be obtained especially by e.g. JM, HM and HMBT formulae, although the computation will become a little complicated.

In most of the cases, JM and HMBT formulae predict the bimodal fatigue damage quite close to the rainflow estimate. JM method is slightly conservative for the bimodal process with close high and low central frequencies. For example, with $R_{fre} = 0.5$, the ratio of the JM fatigue to the rainflow one is about 1.2 for most of the cases. Moreover, the parameter R_s has little effect on the relative accuracy of JM method, especially for the bimodal process with very well separated high and low frequencies, and in such case JM method always gives a very good approximation of the fatigue damage as compared with the time domain result. HMBT formula gives also a conservative fatigue estimate when R_{ss} is not close to zero and is not vary large. Compared with the rainflow result, the factor in such cases can reach 1.3. This is because the empirical coefficients in Benasciutti and Tovo's bandwidth correction factor as shown in Equation 16 are obtained based on a fatigue formulation with a single-slope SN curve. If R_s is close to one, both of the segments with $m_1 = 3$ and $m_2 = 5$ will contribute to the total fatigue damage, and this correction factor might not be very suitable for estimating the total fatigue. On the other hand, Benasciutti and Tovo's bandwidth correction factor is obtained from a series of time domain simulations with many spectrum types and therefore the fatigue by HMBT formula is not sensitive to R_{fre} and R_{var} and in general this formula gives quite good results.

As the same as the results for a single-slope SN curve (see Huang & Moan 2006), Huang and Moan's formula with a regularity correction factor results in a conservative estimate of fatigue damage for small values of R_{fre} and gives a relative good approximation for large values of R_{fre}. Moreover, as similar as JM method, this formula's precision is almost not affected by the parameter R_s.

The narrow-band fatigue and the simple sum of the HF and LF fatigues are still too conservative and nonconservative for all of the cases, respectively. Similarly, the DNV formula still predicts larger fatigue damage as compared with the time domain result, as already shown by Huang & Moan (2006) for a single-slope SN curve. It is noted that the DNV formula even gives more conservative fatigue damage than the narrow-band one when the central frequencies of the HF and LF processes are close. In other words, the DNV formula might be only suitable for the bimodal process with well separated high and low frequencies.

5 CONCLUSIONS

Some methods for determining the fatigue damage due to a bimodal Gaussian load process, e.g. Jiao and Moan's rule (Jiao & Moan 1990), the DNV formula (Lotsberg 2005) and Huang and Moan's formula (Huang & Moan 2006), have been generalized to damage calculation with a two-slope SN curve. The corresponding new fatigue damage formulae have been derived and the accuracy has been examined by the rainflow cycle counting.

Compared with the fatigue damages obtained by time domain simulations and rainflow cycle counting, the predicted fatigue damages are on the safe side in

most of the cases. The total fatigue damage obtained by Jiao and Moan's method agrees very well with the rainflow result when the bimodal process has the high central frequency far away from the low one, and the accuracy is quite consistent whenever the upper part of the two-slope SN curve contributes to the most fatigue or the lower part. When expressing the bimodal fatigue explicitly by the individual ones, Huang and Moan's formula with Benasciutti and Tovo's bandwidth correction factor gives a very good prediction for almost all of the cases, except the cases when both segments of the two-slope SN curve contribute equally to the total fatigue. This is because the correction factor is empirically determined with a single-slope SN curve. Huang and Moan's formula with a regularity correction factor predicts the fatigue conservatively for the ideal bimodal process. Moreover, the DNV formula always overestimates the fatigue damage and might only be suitable for the bimodal process with well separated high and low frequencies.

The approaches presented in this paper deal with fatigue damage due to combined HF and LF loading using a two-slope SN curve and can easily be extended to a multi-slope SN curve.

ACKNOWLEDGEMENTS

The authors wish to acknowledge the support from the Research Council of Norway through the Centre for Ships and Ocean Structures at Norwegian University of Science and Technology.

REFERENCES

Benasciutti, D. & Tovo, R. 2005. Spectral methods for lifetime prediction under wide-band stationary random processes. *International Journal of Fatigue*, Vol. 27, pp. 867–877.

Bouyssy, V., Naboishikov, S.M. & Rackwitz, R. 1993. Comparison of analytical counting methods for Gaussian processes. *Structural Safety*, Vol. 12, pp. 35–57.

Department of Energy 1981. *Offshore installations: guidance on design and construction; proposed new fatigue design rules for steel welded joints in offshore structures.* AERE Harwell, Oxfordshire, UK.

Dirlik, T. 1985. *Application of computers in fatigue*. Ph.D. Thesis, University of Warwick.

Gall, D.S. & Hancock, J.W. 1985. *Fatigue crack growth under narrow and broad band stationary loading*. Glasgow University, Marine Technology Centre.

Gao, Z. & Moan, T. 2006. Wave-induced fatigue damage of mooring chain under combined non-Gaussian low and wave frequency loads. *25th OMAE Conference*, Hamburg, Germany; Paper No. OMAE2006-92389.

Huang, W. & Moan, T. 2006. Fatigue under combined high and low frequency loads. *25th OMAE Conference*, Hamburg, Germany; Paper No. OMAE2006-92247.

Jiao, G. & Moan, T. 1990. Probabilistic analysis of fatigue due to Gaussian load processes. *Probabilistic Engineering Mechanics*, Vol. 5, No. 2, pp. 76–83.

Lotsberg, I. 2005. Background for revision of DNV-RP-C203 fatigue analysis of offshore steel structure. *24th OMAE Conference*, Halkidiki, Greece; Paper No. OMAE2005-67549.

Matsuishi, M. & Endo, T. 1968. Fatigue of metals subjected to varying stress. Paper presented at *Proc. of the Kyushu District Meeting of the Japan Society of Mechanical Engineers*, Fukuoka, Japan.

Miner, M.A. 1945. Cumulative damage in fatigue. *Journal of Applied Mechanics*, Vol. 12, pp. 159–164.

Watson, P. & Dabell, B.J. 1975. Cycle counting and fatigue damage. *Symposium on statistical aspects of fatigue testing*. Warwick University.

Wirsching, P.H. & Chen, Y.N. 1988. Considerations of probability-based fatigue design for marine structures. *Marine Structures*, Vol. 1, pp. 23–45.

Wirsching, P.H. & Light, M.C. 1980. Fatigue under wide band random stresses. *Proc. of the ASCE, Journal of the Structural Division*, Vol. 106, No. ST7, pp. 1593–1607.

Paper 7

Mooring line damping estimation by a simplified dynamic model

Published in
Proceedings of the 26th International Conference on Offshore Mechanics and Arctic Engineering (OMAE2007)
June 10-15, 2007, San Diego, California, USA

Proceedings of the 26th International Conference on Offshore Mechanics and Arctic Engineering
OMAE2007
June 10-15, 2007, San Diego, California, USA

OMAE2007-29155

MOORING LINE DAMPING ESTIMATION BY A SIMPLIFIED DYNAMIC MODEL

Halvor Lie
MARINTEK
halvor.lie@marintek.sintef.no

Zhen Gao
CeSOS, NTNU
zhen.gao@marin.ntnu.no

Torgeir Moan
CeSOS, NTNU
torgeir.moan@marin.ntnu.no

ABSTRACT

When predicting slowly varying resonant vessel motions, a realistic estimate of the motion damping is crucial. Mooring line damping, which is mainly induced by the drag force on line, can dominate the total damping of catenary moored systems and methods for predicting mooring line damping are therefore required. Based on a simplified dynamic model of mooring line tension, an approach to estimate the corresponding damping is presented in this paper. Short-term time domain simulations of dynamic line tension are carried out to verify the accuracy of the simplified frequency domain approach. Compared with the simulation results, the practical simplified method proposed herein gives a maximum 30% lower prediction of the damping coefficient of each mooring line and an about 20% smaller estimate of the total line damping and therefore yields conservative estimates of the low frequency vessel motions.

INTRODUCTION

For a moored offshore structure, damping is crucial to estimate the low frequency (LF) vessel motions. Main sources of the LF damping are wave drift, viscous hull and mooring line damping. Relative importance of these damping sources to the LF vessel motions have been discussed by Wichers and Huijsmans [1], Molin [2], Triantafyllou et al. [3], etc.

A catenary mooring system produces restoring force as well as damping due to the lateral motion of the line when it is tensioned. Mooring line damping might result from the drag force on line, the line friction on seabed and the internal deformation of the line. Influence of mooring line damping on the vessel motions have been shown by many researchers, e.g. Huse [4], Matsumoto [5], Le Boulluec et al. [6] and Brown et al. [7]. Mooring line damping can be a main damping source for the LF motions of moored systems. For instance, damping from the mooring system can contribute 80% of the total LF surge motion damping of a moored tanker in water depth of 200m, including other damping from e.g. viscous force on hull, wave drift damping, etc [8]. For a semi-submersible viscous force on the columns and pontoons is the main source of damping, however the mooring line damping can still contribute 30%-40% of the total damping. Therefore, accurately predicting the mooring line damping is necessary for obtaining a realistic level of the total motion damping and a realistic estimate of the LF vessel motions.

In order to estimate mooring line damping, model tests, fully dynamic finite element analyses and simple analytical models are usually applied.

Model tests of barge and TLP were carried out to validate analytical methods reported by Le Boulluec et al. [6]. Wichers and Huijsmans [1] also performed model tests to show the considerable increase of the overall mooring line damping due to the WF vessel motions. Raaijmakers and Battjes [9] presented an experimental verification of the simple quasi-static model of mooring line proposed by Huse [10] with harmonic surge excitations. Lin et al. [11] described model testing at approximately 1/3 scale on chain segments oscillated at drift frequencies with combined in-line and transverse wave motion.

By using rigorous nonlinear finite element approach in time domain, the dynamic effects in the mooring line can be accounted for when estimating the damping. Based on constant added mass coefficients, Nakamura et al. [12] proposed a numerical scheme for time domain simulations of moored floating structures when the dynamics of the lines are also considered and it is assumed that the slow drift motion occurs predominantly at the surge natural frequency. Coupled dynamics of a floating body and its mooring lines are numerically presented by Dercksen and Wichers [13], Ormberg et al. [14], Hwang [15], etc. Webster [16] used a time domain finite element approach to perform a parametric study of the influence on line damping of pre-tension, fairlead oscillation frequency and amplitude, line stiffness, line length/water depth, current and drag coefficients. More recently, Brown and Mavrakos [17] presented a comparative study on mooring line dynamics and damping based on both time domain and frequency domain methods.

However, model tests are expensive and time domain simulations are quite time consuming since the time step must be small enough to resolve the wave frequency (WF) dynamic effects, while at the same time the total duration of a simulation must include enough LF cycles. A number of contributions outline simple analytical models with a view to obtaining linear mooring line damping coefficients. Based on the linearization of the catenary line equation, Bompais et al. [18] proposed a simple method to calculate the slow-drift damping induced by mooring lines when considering both LF surge and WF heave motions of the fairlead. More recently, Liu and Bergdahl [19] and Bauduin and Naciri [20] proposed improvements on Huse's quasi-static model for mooring line-induced damping by approximating the deformation of the line shape and the transverse velocity of the line in more accurate ways, respectively.

Most of the above mentioned methods for mooring line damping estimation are derived from the harmonic excitation of the line fairlead. However, irregular sea states are practically applied in design of mooring system. A simplified frequency domain dynamic model of a single mooring line has been proposed by Larsen and Sandvik [21] and Lie and Sødahl [22] to compute the dynamic mooring line tension and to estimate the extreme value of the tension during a short-term sea state. The purpose of this paper is to extend the simplified model to predict the drag force induced mooring line damping and investigate the accuracy of the model by comparison with time domain simulations. Estimation of the damping coefficients from each mooring line and from the whole mooring system are performed and are available in the mooring analysis program Mimosa [23]. By using the time domain program Riflex [24], simulations of the WF and LF mooring line tensions in a stationary sea state are also carried out and the damping coefficients for the LF vessel motions are estimated based on the tension time series.

MOORING LINE DAMPING OBTAINED BY THE SIMPLIFIED DYNAMIC MODEL

According to References [21] and [22], the simplified model of mooring line can be idealized in terms of a spring/damper system, confer Fig. 1. The crucial point is that the hydrodynamic damping and the geometric stiffness are both related to change in the geometry and are represented by a viscous damper and a linear elastic spring coupled in parallel. This system is further coupled in series to a linear elastic spring representing the elastic stiffness of the mooring line. Therefore, the dynamic tension T can be found as

$$T = k_E(x(t) - u(t)) = c^* |\dot{u}(t)| \dot{u}(t) + k_G u(t) \quad (1)$$

where $x(t)$ is the forced upper end displacement in tangential line direction, $u(t)$ and $\dot{u}(t)$ are the unknown amplitude of the assumed shape function (i.e. the generalized displacement) and its time derivative (i.e. the generalized velocity), c^* is the generalized damping, k_E and k_G are the elastic stiffness and the geometric stiffness, respectively.

It is the first term in the right hand side of Eq. (1), which is the drag term, that contributes to the damping effect on the vessel motions, while the second term provides the varying restoring force. In general, T has both WF and LF components and therefore has damping effects on both of the WF and LF vessel motions. However, the WF mooring line damping is very small compared with the hydrodynamic damping of the vessel itself. Herein, we consider only the LF line tension and the induced LF motion damping, which are also coupled with and hence have the contribution from the WF vessel motion.

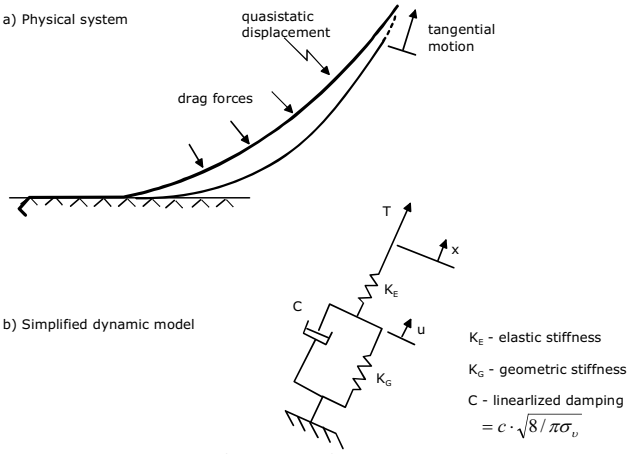

Fig.1. Idealized view of the simplified dynamic line model

Tangential fairlead motion x is the sum of WF motion x_{WF} and LF motion x_{LF}, i.e. $x=x_{WF}+x_{LF}$. The corresponding generalized displacement is also the sum of WF motion and LF motion $u=u_{WF}+u_{LF}$. The corresponding velocity component $\dot{u}_{LF}$ is assumed to vary slowly compared with the variation of the WF velocity $\dot{u}_{WF}$ and is therefore regarded as constant in the following expression. Provided that the WF motion u_{WF} is described by a Gaussian stochastic process, which is usually assumed when doing a short term sea state analysis, the WF velocity $\dot{u}_{WF}$ can also be described by a Gaussian process with zero mean value and variance $\sigma^2_{\dot{u}_{WF}}$. The probability distribution density of the normal total velocity component $\dot{u}$ for a given value of $\dot{u}_{LF}$ is described by

$$f_{\dot{U}}(\dot{u}) = \frac{1}{\sqrt{2\pi}\sigma_{\dot{u}_{WF}}} \exp\left(-\frac{1}{2}\left(\frac{\dot{u}_{WF}}{\sigma_{\dot{u}_{WF}}}\right)^2\right) \quad (2)$$

where $\dot{u} = \dot{u}_{WF} + \dot{u}_{LF}$.

Provided that the drag force can be expressed as

$$F_D = c^* \dot{u} |\dot{u}| = c^* z \quad (3)$$

the mean value of the drag force is

$$E[F_D] = c^* E[z] \quad (4)$$

This value is evaluated in [25] and can be expressed as

$$E[z] = \sigma^2_{\dot{u}_{WF}} \left(\frac{2}{\sqrt{2\pi}} \alpha \exp\left(-\frac{1}{2}\alpha^2\right) + (1+\alpha^2)\,\mathrm{erf}\left(\frac{\alpha}{\sqrt{2}}\right)\right) \quad (5)$$

where $\alpha = \dot{u}_{LF} / \sigma_{\dot{u}_{WF}}$ and erf() is the Error function. Fig. 2 shows a graph of the function $\beta = E[z] / (\alpha\sigma^2_{\dot{u}_{WF}})$. For small values of α Eq. (5) approaches $\sqrt{8/\pi}\sigma_{\dot{u}_{WF}}\dot{u}_{LF}$ and for large values of α it approaches $\dot{u}^2_{LF}$.

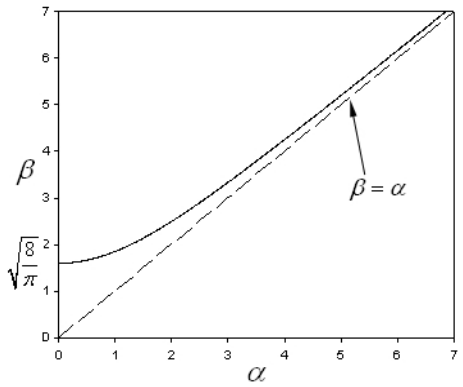

Fig.2. Mean value of drag force factor $\beta = E[F_d]/(\alpha\sigma^2_{u_{WF}})$

Moreover, compared with the WF motion, the LF motion is relatively slow due to the large oscillation period. Therefore we can approximate the slowly varying motion to be quasi-static and we obtain the following approximation of the generalized displacement $u_{LF} \approx 1/(1+k_G/k_E)\,x_{LF}$.

For small values of α the average drag force can now be expressed as

$$E[F_D] = c^* \sqrt{\frac{8}{\pi}}\sigma_{\dot{u}_{WF}} \frac{1}{1+k_G/k_E}\dot{x}_{LF} \tag{6}$$

This can also be regarded as a linear slowly varying damping force including the contribution from the wave frequency tension. Moreover, Eq. (6) expresses the drag force as a function of the line upper end tangential velocity, which gives a direct way to estimate the damping coefficient.

Neglecting the yaw motion, the total diagonal mooring line damping in surge and in sway can now be found as the sum from each mooring line,

$$C_{XXtot} = \sum_{il=1}^{NLIN} (c^* \sqrt{\frac{8}{\pi}}\sigma_{\dot{u}_{WF}} \frac{1}{1+k_G/k_E}\cos^2\beta\cos^2\theta)_{il} \tag{7}$$

$$C_{YYtot} = \sum_{il=1}^{NLIN} (c^* \sqrt{\frac{8}{\pi}}\sigma_{\dot{u}_{WF}} \frac{1}{1+k_G/k_E}\cos^2\beta\sin^2\theta)_{il} \tag{8}$$

where C_{XXtot} and C_{YYtot} represent the total damping coefficients in surge and sway directions due to the surge and sway motions, respectively, β is the mooring line angle from the horizontal plane, and θ is the line angle in the horizontal plane from the surge direction.

Moreover, the vessel surge (or sway) motion can also induce the mooring line dynamic force in the sway (or surge) direction when the mooring line is not coincident with the motion direction. Therefore, we have the identical cross damping coefficients as follows,

$$C_{XYtot} = C_{YXtot} = \sum_{il=1}^{NLIN} (c^* \sqrt{\frac{8}{\pi}}\sigma_{\dot{u}_{WF}} \frac{1}{1+k_G/k_E}\cos^2\beta\sin\theta\cos\theta)_{il} \tag{9}$$

where C_{XYtot} and C_{YXtot} represent the total damping coefficients in surge and sway directions due to the sway and surge motions, respectively.

It is possible to compute the LF mooring line damping coefficients in the mooring analysis program Mimosa [23]. The simplified dynamic mooring line model is applied with wave frequency vessel motions as input. The coefficients are to be calculated in static equilibrium position when the vessel is exposed to mean environmental forces. However, in the present version of the program, the estimated coefficients must be given manually to the vessel description file in order to include the estimated mooring line damping in the low frequency motion calculation (i.e. no automatic mooring line damping is calculated in the LF motion analysis).

TIME DOMAIN SIMULATIONS OF MOORING LINE DYNAMICS AND DAMPING ESTIMATION

In order to verify the mooring line damping coefficients obtained by the simplified dynamic model in frequency domain, the computer program Riflex [24] is selected and finite element method (FEM) is applied to simulate the mooring line dynamics for the whole mooring system. This program has been used in several studies of moored vessel where the riser and mooring system has been model by use of the FE memthod, confer e.g. [14]. Results as vessel motion and dynamic mooring line tension have been compared and found to agree well to results from model tests undertaken in the Ocean Basin at MARINTEK [27]. In the present study the WF and LF vessel motions are assumed to be uncoupled with the mooring analysis and are independently imposed on the centre of gravity of the vessel to accurately describe the fairlead motions. Linearized mooring system is assumed in the same way as in the frequency domain approach, while the nonlinearity due to the drag force on the line is completely included in the time domain simulations. The effect on line dynamics of the nonlinearity of the mooring line stiffness and the sea bottom contact and the wave and current forces on lines have been also checked.

A method based on the energy dissipation is used to estimate the line damping coefficient from the time series of the upper end line tension and the upper end tangential velocity as shown in Eq. (10),

$$C'_{il} = \int_0^{T_e} T_{il}(t) * \dot{x}_{LFil}(t)dt \Big/ \int_0^{T_e} \dot{x}_{LFil}(t) * \dot{x}_{LFil}(t)dt \tag{10}$$

where C_{il}' is the *il*th mooring line damping coefficient in tangential direction, $T_{il}(t)$ is the upper end dynamic line tension which includes both the WF and LF tension components and $\dot{x}_{LFil}(t)$ is the LF upper end tangential velocity, T_e is the duration of the simulation. In order to minimize the uncertainty induced by the simulation with a limited sample, the coefficients are obtained by averaging three one-hour simulations. The diagonal and cross damping coefficients in surge and sway directions from each mooring line can be easily obtained by decomposing the tangential damping coefficient and the total coefficients are described as follows,

$$C'_{XXtot} = \sum_{il=1}^{NLIN} C'_{il}(\cos^2\beta\cos^2\theta)_{il} \tag{11}$$

$$C'_{YYtot} = \sum_{il=1}^{NLIN} C'_{il}(\cos^2\beta\sin^2\theta)_{il} \tag{12}$$

$$C'_{XYtot} = C'_{YXtot} = \sum_{il=1}^{NLIN} C'_{il}(\cos^2\beta\sin\theta\cos\theta)_{il} \tag{13}$$

CASE STUDY

Vessel description

A semi-submersible and its catenary mooring system are used in case study. The semi-submersible is assumed to operate in the North Sea environment. The main particulars of the semi-submersible are listed in Table 1.

Table 1 Main particulars of the semi-submersible

Displacement (ton)	52500
Length O.A. (m)	124
Breadth (m)	95.3
Draft (m)	21

Mooring system

The mooring system consists of sixteen identical mooring lines distributed at four corners of the vessel with four lines each and each mooring line has an identical chain-wire-chain configuration. The horizontal projection of the mooring system with water depth of 340m is plotted in Fig. 3. In the figure, North denotes the surge direction and East denotes the sway direction.

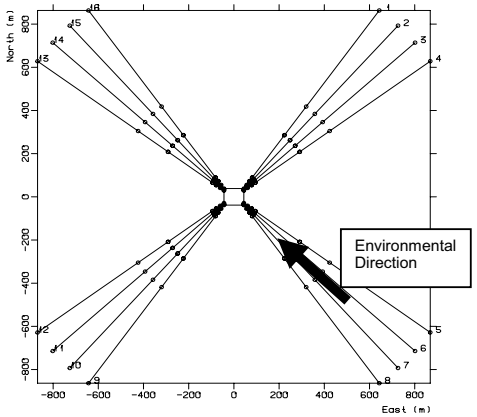

Fig.3. Horizontal projection of the mooring system with 340m water depth

The characteristics of the chain and wire components of each mooring line are listed in Table 2.

Table 2 Characteristics of chain and wire components

Characteristics	Chain	Wire
Nominal diameter (mm)	125	136
Weight in water (kN/m)	2.67	0.80
Axial stiffness, EA (kN)	1.03E6	1.64E6
Non-dimensional normal drag coefficient	2.73	2.33
Non-dimensional longitudinal drag coefficient	0.30	0.17
Breaking strength (kN)	14556	15000

Three different water depths, 70m, 340m and 1000m, were selected to check the accuracy of the frequency domain approach in relatively shallow, moderate and deep water. The corresponding mooring systems are adjusted and the lengths of the chain and wire parts are listed in Table 3.

Table 3 Mooring line components and lengths

Water depth (m)	Component length (m)			Total length (m)
	Chain (lower)	Wire (middle)	Chain (upper)	
70	310	100	20	430
340	725	312	99	1136
1000	1000	2400	150	3550

Mooring line characteristics

The environmental direction is assumed to be 45° west from the North direction defined in Fig. 3 and is also marked on the same figure. First, we quasi-statically move the vessel along the environmental direction and the obtained offset-tension curves of mooring line No. 4, 8, 12 and 16 from Mimosa and Riflex are plotted in Figs. 4-7 for the three mooring systems with water depth of 70m, 340m and 1000m, respectively.

In these four figures, we observed that there are some differences in pre-tensions and in the tensions obtained by Mimosa and Riflex when the vessel has the same offset. It is related to the different methods applied in these two programs. The method used in Mimosa is the catenary equation, while Riflex uses the FEM. However, the errors are within 5% for all of the three mooring systems and when the slopes of these curves are considered, which are believed to be more relevant to the dynamic analysis, the errors become even smaller. Therefore, the quasi-static analyses by Mimosa and Riflex are quite consistent.

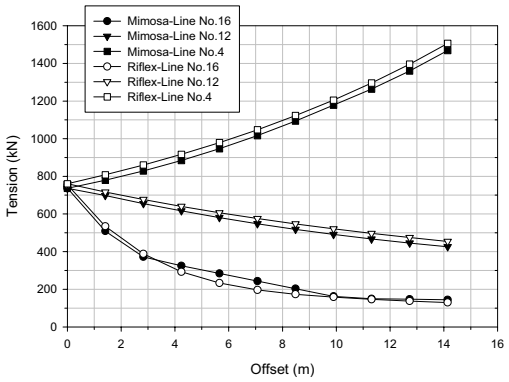

Fig.4. Offset-tension curves of line No. 4, 12 and16 with water depth of 70m

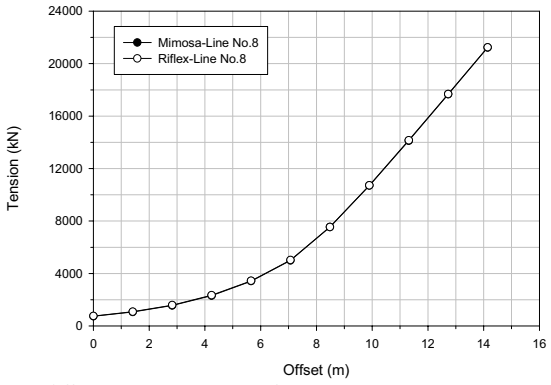

Fig.5. Offset-tension curves of line No. 8 with water depth of 70m

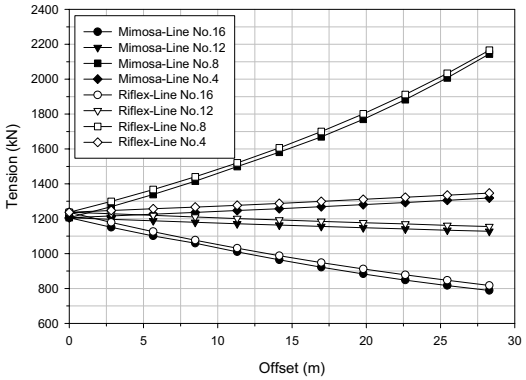

Fig.6. Offset-tension curves of line No. 4, 8, 12 and16 with water depth of 340m

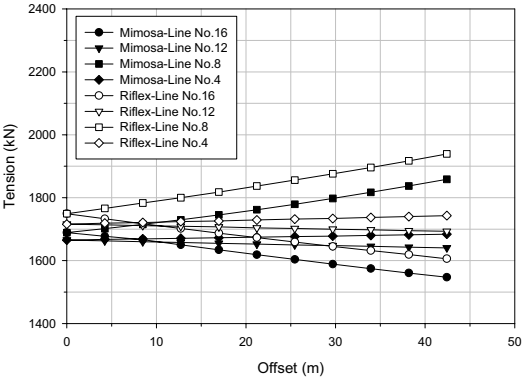

Fig.7. Offset-tension curves of line No. 4, 8, 12 and16 with water depth of 1000m

Mooring line damping coefficients

A moderate sea state of wave with significant wave height Hs=6.25m and mean wave period Tz=8.878s and a high sea state with Hs=14m and Tz=12.074s have been selected for dynamic analyses. Both sea states are applied for the 340m mooring system and only the high sea state is applied for the 70m and 1000m mooring systems. Pierson-Moskowitz spectrum has been applied. The environmental direction is defined in Fig. 3. According to the previous sections, the mooring line damping coefficients were obtained both from Mimosa and Riflex by linear analyses without considering the current force on line. The diagonal damping coefficients of each line (C_{XX} and C_{YY}) and the cross term (C_{XY} or C_{YX}) are plotted and compared in Figs. 8-15. In the figures, shaded area denotes the damping coefficients calculated by the simplified frequency domain approach and error bar corresponds to the coefficients obtained from the time domain simulations. The errors of the diagonal and cross damping coefficients of each mooring line between the Mimosa and the Riflex results are the same because they are all derived from the tangential line damping. The coefficient errors are also plotted in Fig. 16.

In these figures, there are some discrepancies between the frequency domain results and the simulation results, but the relative errors of the surge and sway damping coefficients are in general from 5% to 30%. The diagonal damping coefficients (see Figs. 8, 10, 12 and 14) are all positive and Mimosa always gives lower values than Riflex. This fact indicates that the larger LF motions will be predicted when the Mimosa damping coefficients are applied and it is conservative. The standard deviation of a slow-drift motion x for cases with small damping can be approximated [25] to

$$\sigma_x = \sqrt{S_F(\mu_n)\frac{\pi}{2KC}} \qquad (14)$$

Where S_F is slow drift excitation force at resonance, μ_n = natural frequency $= \sqrt{K/M}$, K is mooring stiffness, M is vessel mass and C is the damping. As seen from the equation the standard deviation of the slow drift motion is inverse proportional with the square root of the damping coefficient. This information is useful to estimate how the discrepancies of the damping estimates will influence the slow drift motion. E.g. if simplified method estimated damping coefficient that is say 15% too low, the corresponding standard deviation of the slow drift motion will be over predicted by 7%.

The cross damping coefficients of mooring line No. 5-8 and No. 13-16 (see Figs. 9, 11, 13 and 15) are positive, while those of No. 1-4 and No. 9-12 are negative. It leads to a total cross surge (or sway) damping coefficient to be slightly positive.

It is also important to note that for the 340m mooring system the relative errors of the coefficients in the high sea state, about 10%, are smaller than those in the moderate sea state, about 25%. This is because in the high sea state the WF vessel motions are dominant compared with the LF motions, which is consistent with the assumption made in the simplified dynamic model of the mooring line tension.

In Fig. 16, we can also see that the relative coefficient errors are quite close for different systems with different water depth of 340m, 70m and 1000m and it indicates that the simplified method is not sensitive to the mooring systems. In general, the accuracy of the simplified method is acceptable and conservative.

The total damping coefficients of the whole mooring system, both the diagonal and cross terms in surge and sway directions, are listed in Table 4. The simplified method shows an overall conservative result. The diagonal coefficients in surge and in sway are very close due to the symmetric configuration of the mooring system. However, the cross term is only about 10% of the diagonal term because of the cancellation of the cross terms from different mooring lines.

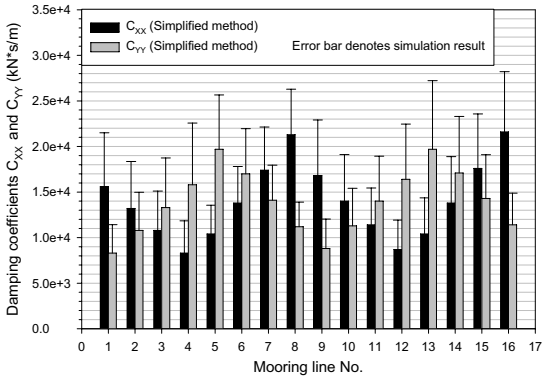

Fig.8. Diagonal mooring line damping coefficients of 340m mooring system with Hs=6.25m and Tz=8.878s

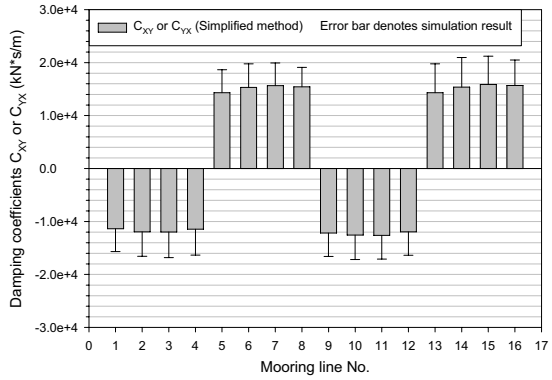

Fig.9. Cross mooring line damping coefficients of 340m mooring system with Hs=6.25m and Tz=8.878s

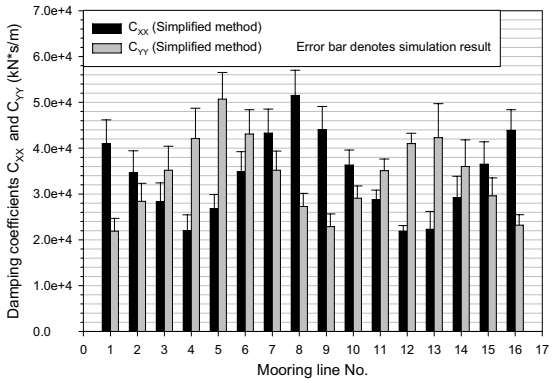

Fig.10. Diagonal mooring line damping coefficients of 340m mooring system with Hs=14m and Tz=12.074s

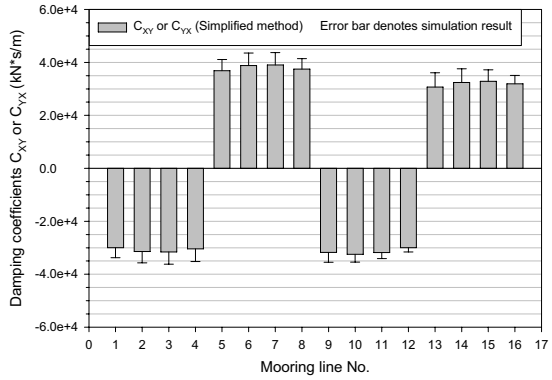

Fig.11. Cross mooring line damping coefficients of 340m mooring system with Hs=14m and Tz=12.074s

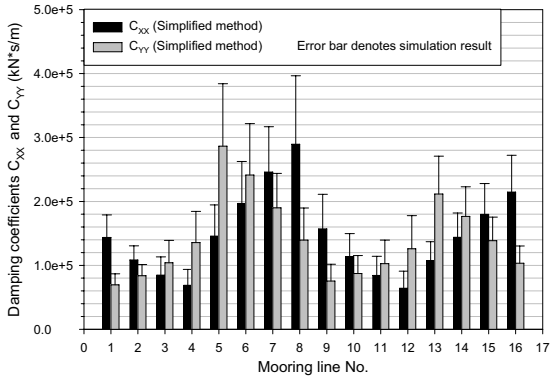

Fig.12. Diagonal mooring line damping coefficients of 70m mooring system with Hs=14m and Tz=12.074s

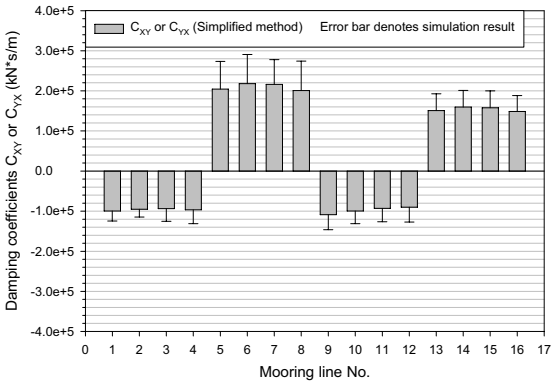

Fig.13. Cross mooring line damping coefficients of 70m mooring system with Hs=14m and Tz=12.074s

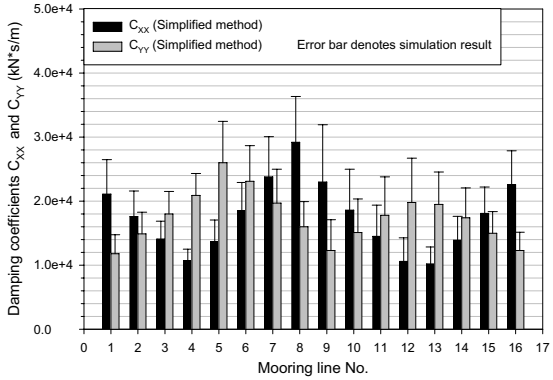

Fig.14. Diagonal mooring line damping coefficients of 1000m mooring system with Hs=14m and Tz=12.074s

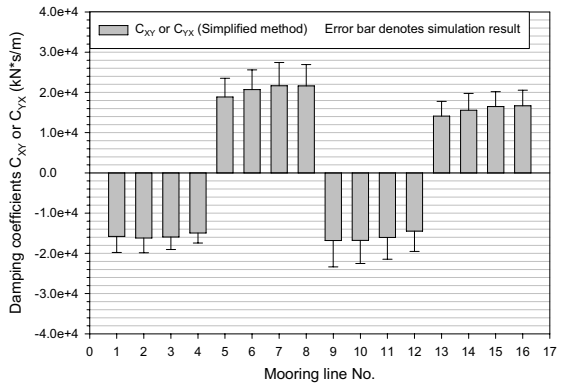

Fig.15. Cross mooring line damping coefficients of 1000m mooring system with Hs=14m and Tz=12.074s

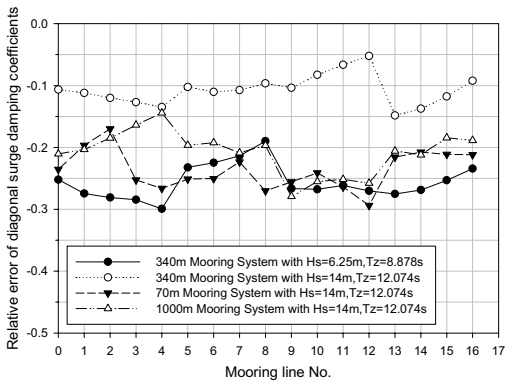

Fig.16. Errors of diagonal surge damping coefficients of each mooring line and the whole mooring system (Mooring line No. 0 corresponds to the whole mooring system)

Table 4 Total mooring line damping coefficients (kN*s/m)

Case	Component of the damping coefficient	Coefficients obtained by the simplified method	Coefficients calculated from the simulations	Error percentage
340m mooring system with Hs=6.25m and Tz=8.878s	Diagonal surge term	2.25E5	3.01E5	-25%
	Diagonal sway term	2.23E5	3.00E5	-26%
	Cross term	2.59E4	2.72E4	-5%
340m mooring system with Hs=14m and Tz=12.074s	Diagonal surge term	5.45E5	6.10E5	-11%
	Diagonal sway term	5.43E5	6.09E5	-11%
	Cross term	3.07E4	3.83E4	-20%
70m mooring system with Hs=14m and Tz=12.074s	Diagonal surge term	2.35E6	3.07E6	-23%
	Diagonal sway term	2.27E6	2.98E6	-24%
	Cross term	6.79E5	8.71E5	-22%
1000m mooring system with Hs=14m and Tz=12.074s	Diagonal surge term	2.80E5	3.55E5	-21%
	Diagonal sway term	2.80E5	3.53E5	-21%
	Cross term	1.86E4	1.87E4	-1%

Wave, current and nonlinear effect on the damping estimation

So far, a linearization of the mooring system has been assumed and current forces have not been considered. Moreover, the results by Mimosa do not include wave forces directly acting on the line, while they are considered in the analyses by Riflex. We also checked the effects of considering the nonlinear stiffness of mooring line, the sea bottom contact and the wave and current forces by a single Riflex time domain simulation of 340m mooring system with the high sea state. A uniform current profile with a speed of 0.5m/s is applied in the same direction as the wave. The obtained diagonal surge damping coefficients of line No. 8 are plotted in Fig. 17.

In Fig. 17, we can see that there is almost no effect of the direct wave force on mooring line. This is because it is the excitation of the fairlead motion that induces the most drag force on mooring line which results in the main contribution to the damping coefficient [26]. Moreover, there is also a quite limited effect of the nonlinear analysis. It is because the drag force on the part of mooring line near sea bottom is small compared with those on the whole line. When the current force is considered, the damping coefficient of this mooring line increases but within 15%.

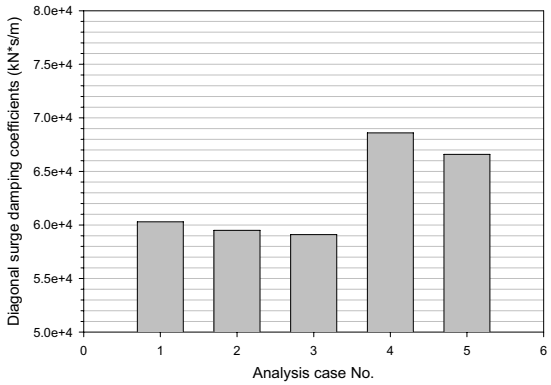

Fig.17. Diagonal surge damping coefficients of line No. 8 of 340m mooring system considering nonlinear effect and wave and current forces (Analysis case No. 1 represents the linear case, No. 2 represents the case when the wave force acting on line is not considered, No. 3 represents the nonlinear analysis, No. 4 represents the case when current force is also considered and No. 5 represents the nonlinear case with current force)

CONCLUSIONS

Drag force on mooring lines contributes to the LF vessel motion damping. An approach for predicting the mooring line damping coefficients by a simplified method has been proposed and verified by time domain simulations. For the cases considered the differences in the coefficients obtained by the frequency domain method and the time domain simulations are less than 30% for moderate sea states and less than 15% for high sea states. Moreover, the simplified method always gives smaller damping coefficients which leads to a conservative assessment of mooring system safety. Moreover, the simplified method is obviously much more computationally efficient.

Depending on the mooring system configuration, the damping coefficients in surge and in sway are in general coupled. The cross coefficients can also be easily obtained by the simplified method.

Wave force and nonlinear mooring line stiffness have little effects on the line damping coefficients. There is an effect due to the presence of current, but the difference is also limited.

REFERENCES

[1] Wichers, J.E.W., Huijsmans, R.H.M. (1990), The contribution of hydrodynamic damping induced by mooring chains on low frequency vessel motions, OTC paper No. 6218.

[2] Molin, B. (1993), Second-order hydrodynamics applied to moored structures, 19th WEGEMT School, Numerical simulation of hydrodynamics: ships and offshore structures.

[3] Triantafyllou, M.S., Yue, D.K.P., Tein, D.Y.S. (1994), Damping of moored floating structures, OTC paper No. 7489.

[4] Huse, E. (1991), New development in prediction of mooring system damping, OTC paper No. 6593.

[5] Matsumoto, K. (1991), The influence of mooring line damping on the prediction of low-frequency vessel motions at sea, OTC paper No. 6660.

[6] Le Boulluec, M. et al. (1994), Recent advances on the slow-drift damping of offshore structures, BOSS'94 Conference, Vol. 2, pp. 9-30.

[7] Brown, D.T., Lyons, G.J., Lin, H.M. (1995), Advances in mooring line damping, Underwater Technology, Vol. 21, pp. 5-12.

[8] Huse, E. (1992), Mooring line damping – summary & recommendations, MARINTEK Report No. 513003.00.05, Trondheim.

[9] Raaijmakers, R.M., Battjes, J.A. (1997), An experimental verification of Huse's model on the calculation of mooring line damping, BOSS'97 Conference.

[10] Huse, E. (1986), Influence of mooring line damping upon rig motions, OTC paper No. 5204.

[11] Lin, H.M., Brown, D.T., Lyons, G.J. (1996), Large scale testing for mooring line hydrodynamic damping, OMAE96, pp. 79-86.

[12] Nakamura, N., Koterayama, W., Kyozuka, Y. (1991), Slow drift damping due to drag forces acting on mooring lines, Ocean Engineering, Vol. 18, No. 4, pp. 283–296.

[13] Dercksen, A., Wichers, J.E.W. (1992), A discrete element method on a chain turret tanker exposed to survival conditions, BOSS'92 Conference.

[14] Ormberg, H., Sødahl, N., Steinkjer, O. (1998), Efficient analysis of mooring systems using de-coupled and coupled analysis, OMAE98-0351.

[15] Hwang, Y.-L. (1998), Numerical model tests for mooring damping, OMAE98-0444.

[16] Webster, W.C. (1995), Mooring-induced damping, Ocean Engineering, Vol. 22, No. 6, pp. 571–591.

[17] Brown, D.T., Mavrakos, S. (1999), Comparative study on mooring line dynamic loading, Marine Structures, Vol. 12, pp. 131-151.

[18] Bompais, X. et al. (1994), Slow drift motion: practical estimation of mooring line damping, OMAE94, Vol. 1, pp. 383-391.

[19] Liu, Y.-G., Bergdahl, L. (1998), Improvements on Huse's model for estimating mooring cable induced damping, OMAE98-0353.

[20] Bauduin, C., Naciri, M. (2000), A contribution on quasi-static mooring line damping, Journal of OMAE, Vol. 122, pp. 125-133.

[21] Larsen, K., Sandvik, P.C. (1990), Efficient methods for the calculation of dynamic mooring line tension, 1st European Offshore Mechanics Symposium, Trondheim.

[22] Lie, H., Sødahl, N. (1993), Simplified dynamic model for estimation of extreme anchorline tension, Offshore Australia.

[23] User's Documentation Mimosa, Version 5.7 (2003), MARINTEK Report No. 516413.00.01.

[24] User's Manual Riflex, Version 3.2.3 (2003), MARINTEK Report No. 519619.

[25] Faltinsen, O. M. (1990), Sea loads on ships and offshore structures, Cambridge university press, ISBN 0 521 37285 2

[26] Larsen, C.M., Fylling, I.J. (1982), Dynamic behaviour of anchor lines, Norwegian Maritime Research No. 3.

[27] Ormberg, H., Standsberg, C. T., Yttervik, R., (1999), Integrated Vessel Motion and Mooring Analysis Applied in Hybrid Model Testing, Proceedings of the Ninth International Offshore and Polar Engineering Conference, Brest, France.

Appendix B

Extension of the Papers

Extension 1

Variability of structural responses of marine structures due to seasonal and yearly wave data

Variability of structural responses of marine structures due to seasonal and yearly wave data

Zhen Gao, Torgeir Moan

Abstract

This work briefly describes typical structural responses of marine structures, i.e. midship vertical bending moment of an FPSO, stresses on a brace-column joint of a semi-submersible and mooring line tension response, in terms of annual extreme value and fatigue damage, by using seasonal wave data. Wave data of thirty years at a site of the Northern North Sea have been used and analyzed for each spring/autumn, summer, winter and year as well as for all seasons and years. It is shown that the winter data contribute significantly to extreme value prediction of the significant wave height and to both extreme value and fatigue damage of structural responses as well. In addition, the accuracy of the contour line method for prediction of the extreme mooring line tension has been verified and a quantile of about 70% of the short-term extreme value distribution is found to give a good estimate of the annual extreme value.

1. Seasonal wave data of the Northern North Sea

Thirty-year (from 1976 to 2005) wave data at a site in the Northern North Sea have been collected by Statoil ASA [1] and are presented as seasonal scatter diagrams of the significant wave height (H_S) and the spectral peak period (T_P). Data for three periods have been defined for each year, namely SprAut (from March to May and from September to October, 5 months), Summer (from June to August, 3 months) and Winter (from November to next February, 4 months). The data are also combined to give annual scatter diagrams and 30-year scatter diagram as a whole.

Wave data analysis, i.e. fitting of the scatter diagram, has been performed by using the program PHT, developed by Haver [2], where the joint probability density of H_S and T_P is obtained by the combined log-normal and Weibull distribution for H_S and the conditional log-normal distribution for T_P. Details of the distribution model was given in Haver [2] and Moan et al. [3], and is therefore not repeated herein.

The obtained mean value and standard deviation of H_S are plotted in Figs. 1 and 2, respectively. It is shown that the mean values of H_S in winter are quite large and vary significantly from year to year, while the values in summer are small and only show a slight variation. The yearly mean value of H_S is close to that of the SprAut data since it is basically the average value of all the SprAut, Summer and Winter data and the data of all seasons almost equally contribute to the yearly mean value. However, it varies more significantly from year to year than the SprAut result due to the contribution of the Winter data.

The standard deviations of H_S of the SprAut, Winter and Year data are close and it implies that the variation of wave conditions within one year is quite significant except during the summer time.

The predicted annual and 100-year extreme values of H_S have also been provided and are plotted in Figs. 3 and 4, respectively. In the extreme value prediction, when only the seasonal data are used, it is assumed that the contribution of other months is zero. In most cases, the predicted extreme value based on the Year data is close to but slightly larger than that based on the Winter data. It indicates that this extreme value is obtained by the main contribution from the Winter data. The SprAut data predict smaller extreme values compared with the Winter and Year data. The ratio of the predicted annual or 100-year extreme value based on the Year and Summer data is about 2, while the ratio of the mean value is about 1.7. It implies that the Summer data contribute less for the extreme values.

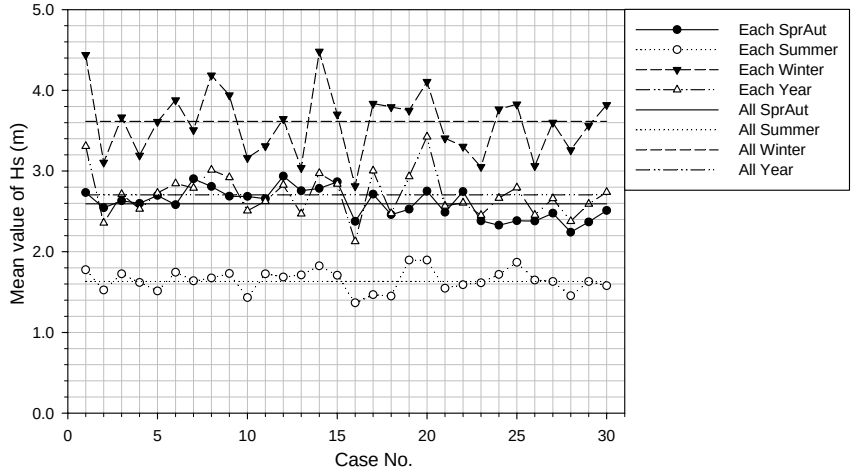

Fig. 1 Mean value of H_S

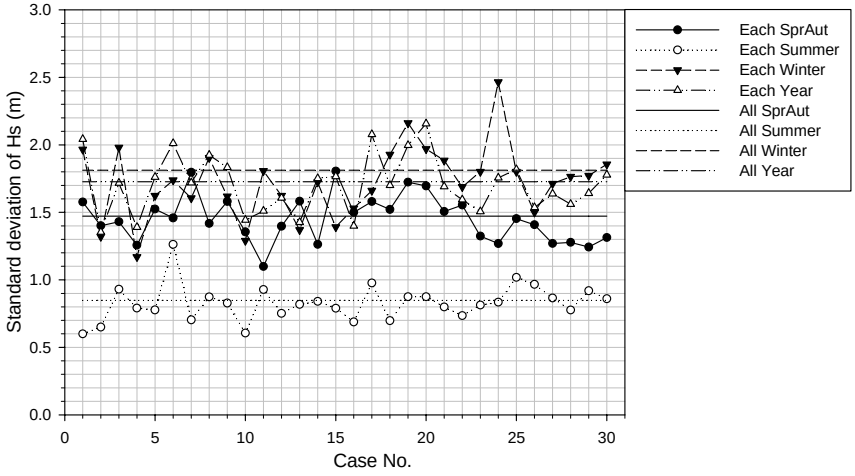

Fig. 2 Standard deviation of H_S

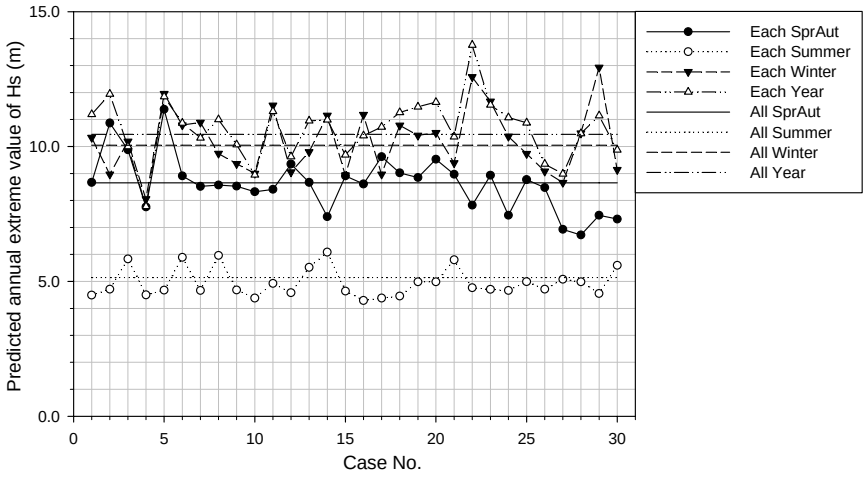

Fig. 3 Predicted annual extreme value of H_S

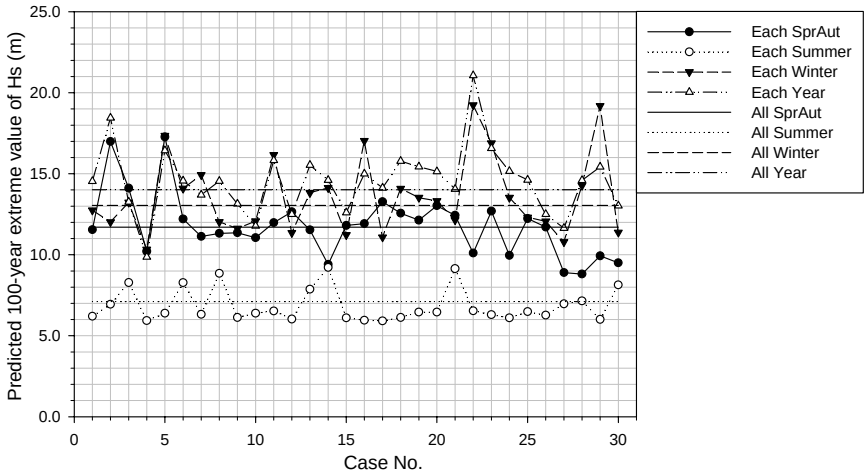

Fig. 4 Predicted 100-year extreme value of H_S

In general, no obvious increasing or decreasing trend in either seasonal or yearly data has been observed. Wave conditions vary quite randomly even at a scale of 30 years.

In order to study the contribution of the seasonal data to the annual prediction, the scatter plots of the SprAut, Summer and Winter data against the Year data are provided in Figs. 5 and 6 for the mean H_S and the annual extreme H_S, respectively. The obtained correlation coefficients of the mean H_S are similar for all three data groups, i.e. 0.55, 0.67 and 0.86, while a large correlation coefficient (i.e. 0.72) of the annual extreme H_S is obtained for the Winter data and very small correlation coefficients are calculated based on the SprAut and Summer data. It implies again that the Winter data contribute quite significantly to the extreme value prediction for the whole year.

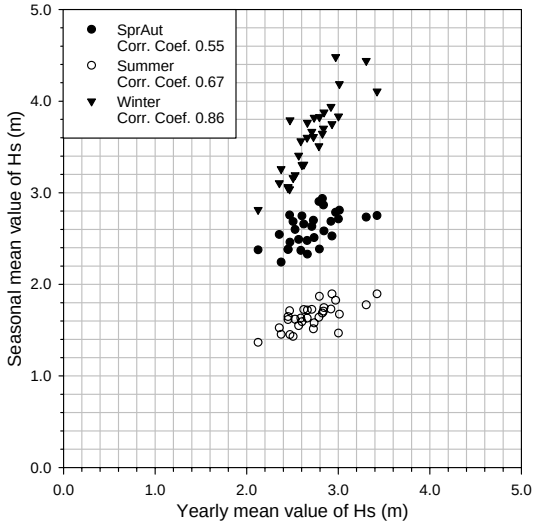

Fig. 5 Scatter plot of the seasonal and yearly mean values of H_S

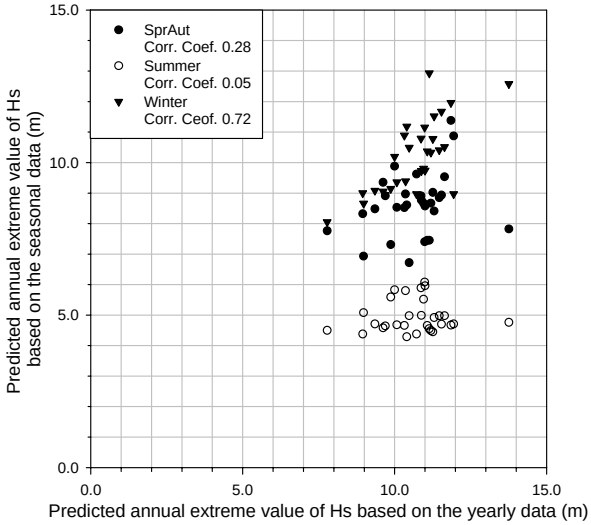

Fig. 6 Scatter plot of the predicted annual extreme values of H_S based on the seasonal and yearly data

2. Annual extreme values of structural responses

Typical structural responses of marine structures have been considered, i.e. midship vertical bending moment of an FPSO and stresses on a brace-column joint of a semi-submersible as shown in Moan et al. [3] and a 16-line mooring system of a semi-submersible as shown in Gao and Moan [4]. Both intact and damaged condition with one line failure have been assumed for mooring analysis, while responses of FPSO and semi-submersible are only analyzed for intact condition. Smoothed scatter diagrams of the seasonal and yearly wave data are used for prediction of extreme value and fatigue damage.

It is important to note that annual quantities, i.e. annual extreme value and annual fatigue damage, are used for comparison and when only the seasonal data are applied, it is assumed that the contribution of other months within one year is zero.

The predicted annual extreme responses are plotted in Figs. 7-10, which are normalized by the prediction when all 30-year data are used. The results are obtained by a full long-term analysis.

Similar as the extreme H_S, the extreme responses based on the Winter and Year data are close and the SprAut prediction is slightly smaller. Mooring response seems to vary more significantly from year to year than the other two responses, while the stress response of the semi-submersible has a smallest variation due to the varying environmental conditions.

Due to failure, mooring line tension increases 20% on average and presents more variations.

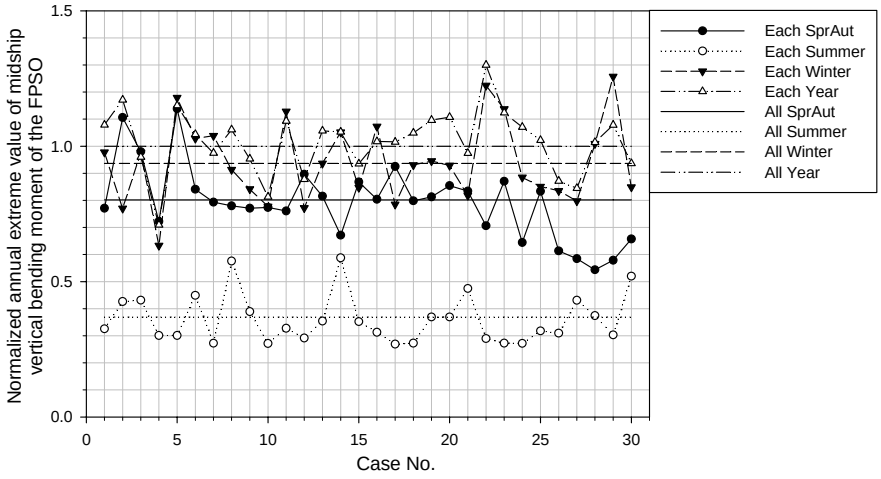

Fig. 7 Predicted annual extreme value of midship vertical bending moment of the FPSO, normalized by the result of all 30 years

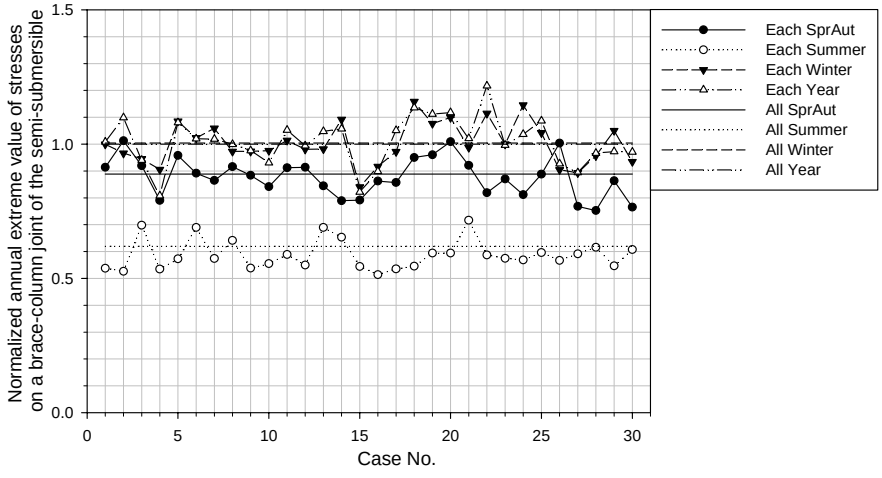

Fig. 8 Predicted annual extreme value of stresses on a brace-column joint of the semi-submersible, normalized by the result of all 30 years

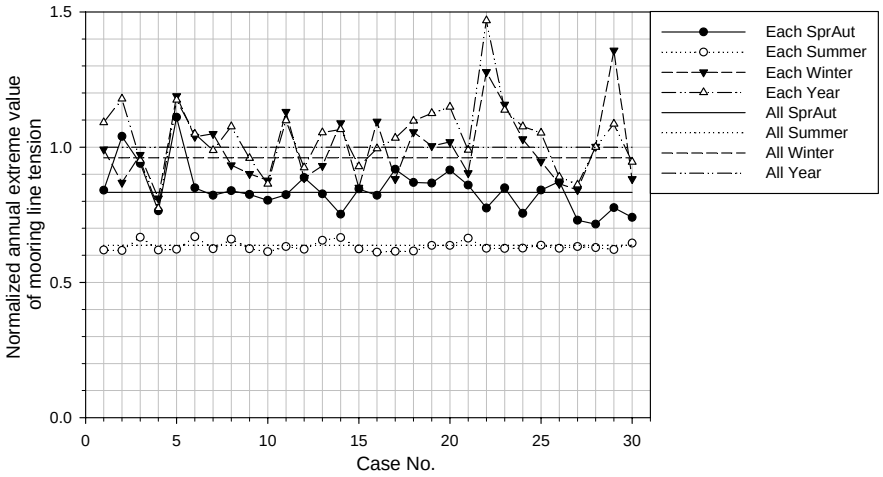

Fig. 9 Predicted annual extreme value of mooring line tension under the intact condition, normalized by the result of all 30 years

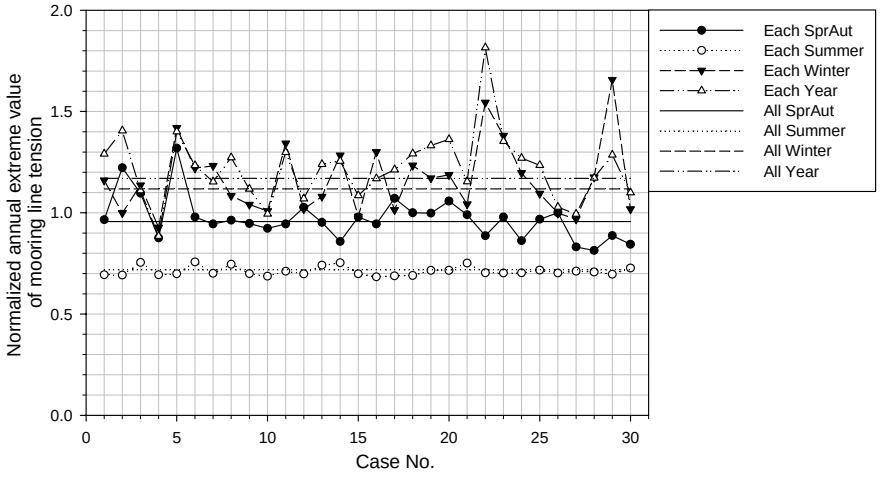

Fig. 10 Predicted annual extreme value of mooring line tension under the damaged condition, normalized by the result of all 30 years under the intact condition

3. Accuracy of the contour line method for predicting annual extreme mooring response

The contour line method has been applied to determine structural responses by many researchers, e.g. Haver et al. [5], Meling et al. [6] and Baarholm & Moan [7]. Herein, this method is applied to predict the annual extreme value of mooring line tension.

Since the contour line method actually uses an environmental contour line and does not depend on the response, it is crucial to establish the relevant quantile that corresponds to the particular response considered.

A sensitivity study has been carried out with quantiles of 0.6-0.8 of short-term extreme value distribution of mooring line tension. Mean values of absolute relative errors of predictions based on the seasonal and yearly wave data of 30 years as a function of quantile are plotted in Fig. 11. The relative error is defined as the difference between the predictions

by the contour line method and by the full long-term analysis divided by the full long-term estimate.

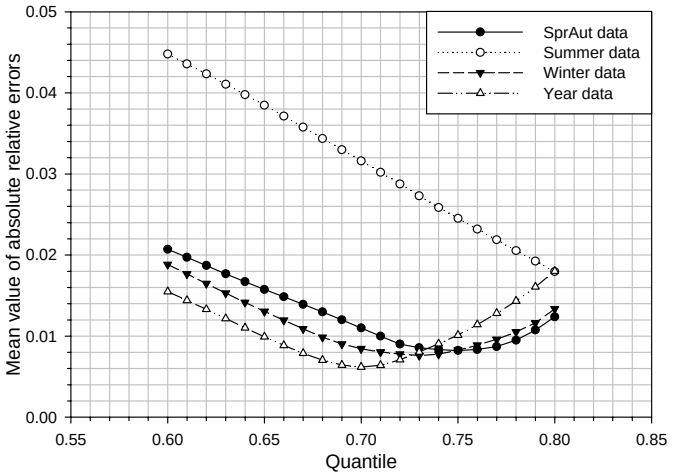

Fig. 11 Mean value of absolute relative errors of the contour line method for predicting the annual extreme mooring line tension using SprAut, Summer, Winter and Year data, compared with the full long-term analysis, as a function of quantile

As shown in the figure, the quantiles which give minimum errors of the contour line method when applying the SprAut, Winter and Year data are 0.75, 0.73 and 0.7, respectively. On average, the minimum error is quite small and is not sensitive to the value of the quantile. For instance, if the Year data are used, quantiles of 65-75% will give the relative errors less than 1%. In addition, if only the Summer data are applied, a higher value of quantile should be used for the contour line method. However, most of the sea states in summer are moderate sea states and do not contribute significantly to the annual extreme mooring line tension. It also implies that the mooring system behaves similarly under the annual extreme conditions of the SprAut, Winter and Year data, while different responses could be obtained by applying the Summer data.

4. Annual fatigue damage induced by structural responses

The annual fatigue damage associated with the structural responses mentioned above, is plotted in Figs. 12-15. The Winter data has the most important contribution to the fatigue damage of a whole year and accounts for about 70% of the total fatigue damage, while the SprAut fatigue damage contributes only 30%. Moreover, the fatigue damage in summer is negligible. More significant variation from year to year is observed for the fatigue damage.

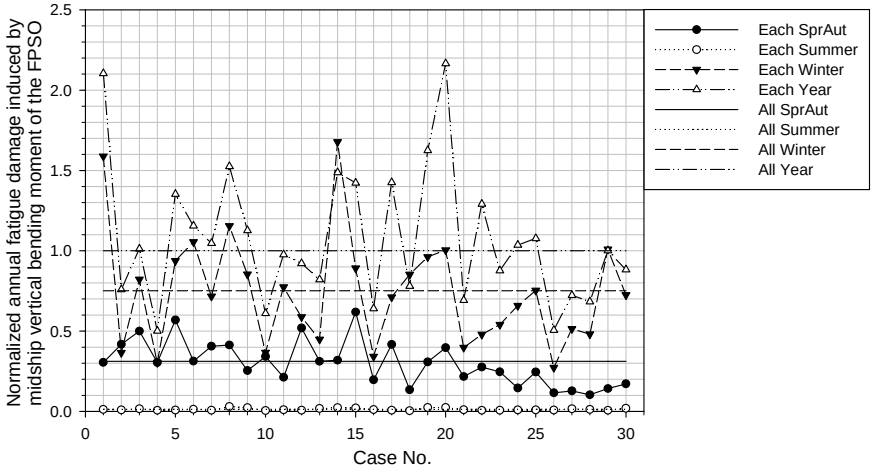

Fig. 12 Predicted annual fatigue damage induced by midship vertical bending moment of the FPSO, normalized by the result of all 30 years

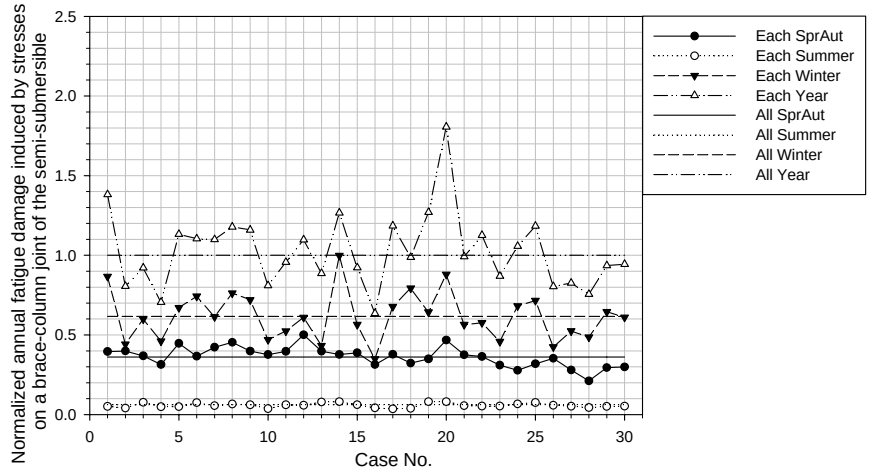

Fig. 13 Predicted annual fatigue damage induced by stresses on a brace-column joint of the semi-submersible, normalized by the result of all 30 years

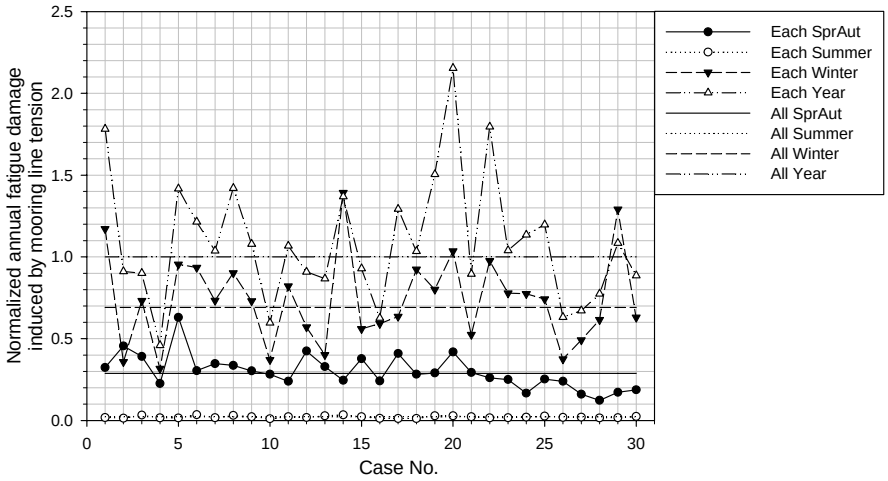

Fig. 14 Predicted annual fatigue damage induced by mooring line tension under the intact condition, normalized by the result of all 30 years

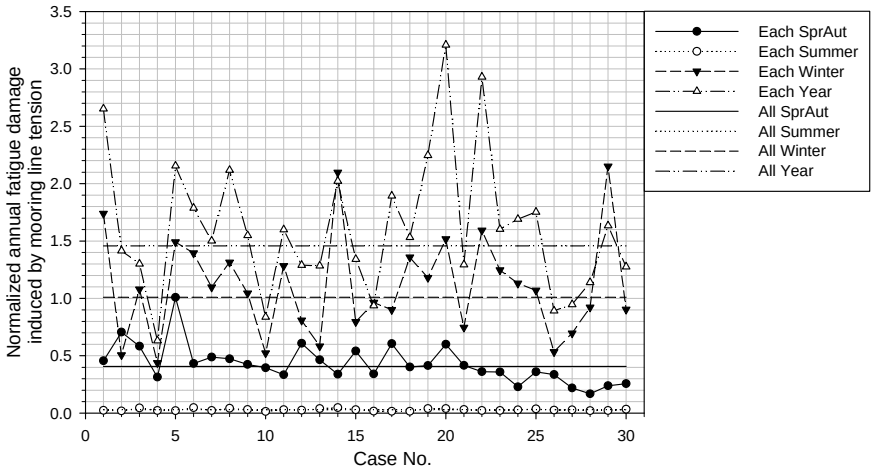

Fig. 15 Predicted annual fatigue damage induced by mooring line tension under the intact condition, normalized by the result of all 30 years under the intact condition

5. Conclusions

Thirty years of wave data typical for a Northern North Sea site have been analyzed seasonally and yearly. Similar to the yearly wave data, the seasonal data show variations from year to year. Wave data for the winter have a strong influence on the annual extreme value of the significant wave height.

The sensitivity of various structural responses to variations of the wave data has been studied. Both the extreme response and the induced fatigue damage of a whole year are governed by the winter data. Compared with the extreme values of the significant wave height and the structural responses, the predicted fatigue damage presents much more variations from year to year.

The contour line method for annual extreme line tension prediction has been applied. Based on a sensitivity study on the comparison with the results of the full long-term analysis, this method with a quantile of about 70% gives quite accurate estimates when applying the yearly wave data.

6. References

[1] Private communication with Dr. Haver, S., Statoil ASA; November, 2006.

[2] Haver, S. Analysis of uncertainties related to the stochastic modelling of ocean waves. Ph.D. thesis, Norwegian Institute of Technology, Trondheim, Norway; 1980.

[3] Moan, T., Gao, Z. and Ayala-Uraga, E. Uncertainty of wave-induced response of marine structures due to long-term variation of extratropical wave conditions. Marine Structures 2005; Vol. 18, No. 4, pp. 359-382.

[4] Gao, Z. and Moan, T. Sensitivity study of extreme value and fatigue damage of line tension in mooring system with one line failure under varying annual environmental conditions. Proceedings of the 17th International Offshore and Polar Engineering Conference, Lisbon, Portugal; 2007, paper No. JSC-361.

[5] Haver, S., Sagli, G. and Gran, T.M. Long term response analysis of fixed and floating structures. Proceedings of Wave'98-Ocean Wave Kinematics, Dynamics and Loads on Structures, International OTRC Symposium, Houston; 1998.

[6] Meling, T.S., Johannessen, K., Haver, S. and Larsen, K. Mooring analysis of a semi-submersible by use of IFORM and contour surfaces. OMAE 2000/OSU OFT-4141, New Orleans; 2000.

[7] Baarholm, G.S. and Moan, T. Application of contour line method to estimate extreme ship hull loads considering operational restrictions. Journal of Ship Research 2001; Vol. 45, No. 3, pp. 228-240.

R A P P O R T E R
UTGITT VED
INSTITUTT FOR MARIN TEKNIKK
(tidligere: FAKULTET FOR MARIN TEKNIKK)
NORGES TEKNISK-NATURVITENSKAPELIGE UNIVERSITET
PhD Theses (not all) from the Department of Marine Technology, NTNU

UR-79-01 Brigt Hatlestad, MK:	The finite element method used in a fatigue evaluation of fixed offshore platforms. (Dr.Ing. Thesis)
UR-79-02 Erik Pettersen, MK:	Analysis and design of cellular structures. (Dr.Ing. Thesis)
UR-79-03 Sverre Valsgård, MK:	Finite difference and finite element methods applied to nonlinear analysis of plated structures. (Dr.Ing. Thesis)
UR-79-04 Nils T. Nordsve, MK:	Finite element collapse analysis of structural members considering imperfections and stresses due to fabrication. (Dr.Ing. Thesis)
UR-79-05 Ivar J. Fylling, MK:	Analysis of towline forces in ocean towing systems. (Dr.Ing. Thesis)
UR-80-06 Nils Sandsmark, MM:	Analysis of Stationary and Transient Heat Conduction by the Use of the Finite Element Method. (Dr.Ing. Thesis)
UR-80-09 Sverre Haver, MK:	Analysis of uncertainties related to the stochastic modelling of ocean waves. (Dr.Ing. Thesis)
UR-85-46 Alf G. Engseth, MK:	Finite element collapse analysis of tubular steel offshore structures. (Dr.Ing. Thesis)
UR-86-47 Dengody Sheshappa, MP:	A Computer Design Model for Optimizing Fishing Vessel Designs Based on Techno-Economic Analysis. (Dr.Ing. Thesis)
UR-86-48 Vidar Aanesland, MH:	A Theoretical and Numerical Study of Ship Wave Resistance. (Dr.Ing. Thesis)
UR-86-49 Heinz-Joachim Wessel, MK:	Fracture Mechanics Analysis of Crack Growth in Plate Girders. (Dr.Ing. Thesis)
UR-86-50 Jon Taby, MK:	Ultimate and Post-ultimate Strength of Dented Tubular Members. (Dr.Ing. Thesis)
UR-86-51 Walter Lian, MH:	A Numerical Study of Two-Dimensional Separated Flow Past Bluff Bodies at Moderate KC-Numbers. (Dr.Ing. Thesis)
UR-86-52 Bjørn Sortland, MH:	Force Measurements in Oscillating Flow on Ship Sections and Circular Cylinders in a U-Tube Water Tank. (Dr.Ing. Thesis)
UR-86-53 Kurt Strand, MM:	A System Dynamic Approach to One-dimensional Fluid Flow. (Dr.Ing. Thesis)
UR-86-54 Arne Edvin Løken, MH:	Three Dimensional Second Order Hydrodynamic Effects on Ocean Structures in Waves. (Dr.Ing. Thesis)

UR-86-55 Sigurd Falch, MH:	A Numerical Study of Slamming of Two-Dimensional Bodies. (Dr.Ing. Thesis)
UR-87-56 Arne Braathen, MH:	Application of a Vortex Tracking Method to the Prediction of Roll Damping of a Two-Dimension Floating Body. (Dr.Ing. Thesis)
UR-87-57 Bernt Leira, MR:	Gaussian Vector Processes for Reliability Analysis involving Wave-Induced Load Effects. (Dr.Ing. Thesis)
UR-87-58 Magnus Småvik, MM:	Thermal Load and Process Characteristics in a Two-Stroke Diesel Engine with Thermal Barriers (in Norwegian). (Dr.Ing. Thesis)
MTA-88-59 Bernt Arild Bremdal, MP:	An Investigation of Marine Installation Processes - A Knowledge - Based Planning Approach. (Dr.Ing. Thesis)
MTA-88-60 Xu Jun, MK:	Non-linear Dynamic Analysis of Space-framed Offshore Structures. (Dr.Ing. Thesis)
MTA-89-61 Gang Miao, MH:	Hydrodynamic Forces and Dynamic Responses of Circular Cylinders in Wave Zones. (Dr.Ing. Thesis)
MTA-89-62 Martin Greenhow, MH:	Linear and Non-Linear Studies of Waves and Floating Bodies. Part I and Part II. (Dr.Techn. Thesis)
MTA-89-63 Chang Li, MH:	Force Coefficients of Spheres and Cubes in Oscillatory Flow with and without Current. (Dr.Ing. Thesis)
MTA-89-64 Hu Ying, MP:	A Study of Marketing and Design in Development of Marine Transport Systems. (Dr.Ing. Thesis)
MTA-89-65 Arild Jæger, MH:	Seakeeping, Dynamic Stability and Performance of a Wedge Shaped Planing Hull. (Dr.Ing. Thesis)
MTA-89-66 Chan Siu Hung, MM:	The dynamic characteristics of tilting-pad bearings.
MTA-89-67 Kim Wikstrøm, MP:	Analysis av projekteringen for ett offshore projekt. (Licenciat-avhandling)
MTA-89-68 Jiao Guoyang, MR:	Reliability Analysis of Crack Growth under Random Loading, considering Model Updating. (Dr.Ing. Thesis)
MTA-89-69 Arnt Olufsen, MK:	Uncertainty and Reliability Analysis of Fixed Offshore Structures. (Dr.Ing. Thesis)
MTA-89-70 Wu Yu-Lin, MR:	System Reliability Analyses of Offshore Structures using improved Truss and Beam Models. (Dr.Ing. Thesis)
MTA-90-71 Jan Roger Hoff, MH:	Three-dimensional Green function of a vessel with forward speed in waves. (Dr.Ing. Thesis)
MTA-90-72 Rong Zhao, MH:	Slow-Drift Motions of a Moored Two-Dimensional Body in Irregular Waves. (Dr.Ing. Thesis)
MTA-90-73 Atle Minsaas, MP:	Economical Risk Analysis. (Dr.Ing. Thesis)
MTA-90-74 Knut-Aril Farnes, MK:	Long-term Statistics of Response in Non-linear Marine Structures. (Dr.Ing. Thesis)

MTA-90-75 Torbjørn Sotberg, MK: Application of Reliability Methods for Safety Assessment of Submarine Pipelines. (Dr.Ing. Thesis)

MTA-90-76 Zeuthen, Steffen, MP: SEAMAID. A computational model of the design process in a constraint-based logic programming environment. An example from the offshore domain. (Dr.Ing. Thesis)

MTA-91-77 Haagensen, Sven, MM: Fuel Dependant Cyclic Variability in a Spark Ignition Engine - An Optical Approach. (Dr.Ing. Thesis)

MTA-91-78 Løland, Geir, MH: Current forces on and flow through fish farms. (Dr.Ing. Thesis)

MTA-91-79 Hoen, Christopher, MK: System Identification of Structures Excited by Stochastic Load Processes. (Dr.Ing. Thesis)

MTA-91-80 Haugen, Stein, MK: Probabilistic Evaluation of Frequency of Collision between Ships and Offshore Platforms. (Dr.Ing. Thesis)

MTA-91-81 Sødahl, Nils, MK: Methods for Design and Analysis of Flexible Risers. (Dr.Ing. Thesis)

MTA-91-82 Ormberg, Harald, MK: Non-linear Response Analysis of Floating Fish Farm Systems. (Dr.Ing. Thesis)

MTA-91-83 Marley, Mark J., MK: Time Variant Reliability under Fatigue Degradation. (Dr.Ing. Thesis)

MTA-91-84 Krokstad, Jørgen R., MH: Second-order Loads in Multidirectional Seas. (Dr.Ing. Thesis)

MTA-91-85 Molteberg, Gunnar A., MM: The Application of System Identification Techniques to Performance Monitoring of Four Stroke Turbocharged Diesel Engines. (Dr.Ing. Thesis)

MTA-92-86 Mørch, Hans Jørgen Bjelke, MH: Aspects of Hydrofoil Design: with Emphasis on Hydrofoil Interaction in Calm Water. (Dr.Ing. Thesis)

MTA-92-87 Chan Siu Hung, MM: Nonlinear Analysis of Rotordynamic Instabilities in High-speed Turbomachinery. (Dr.Ing. Thesis)

MTA-92-88 Bessason, Bjarni, MK: Assessment of Earthquake Loading and Response of Seismically Isolated Bridges. (Dr.Ing. Thesis)

MTA-92-89 Langli, Geir, MP: Improving Operational Safety through exploitation of Design Knowledge - an investigation of offshore platform safety. (Dr.Ing. Thesis)

MTA-92-90 Sævik, Svein, MK: On Stresses and Fatigue in Flexible Pipes. (Dr.Ing. Thesis)

MTA-92-91 Ask, Tor Ø., MM: Ignition and Flame Growth in Lean Gas-Air Mixtures. An Experimental Study with a Schlieren System. (Dr.Ing. Thesis)

MTA-86-92 Hessen, Gunnar, MK: Fracture Mechanics Analysis of Stiffened Tubular Members. (Dr.Ing. Thesis)

MTA-93-93 Steinebach, Christian, MM: Knowledge Based Systems for Diagnosis of Rotating Machinery. (Dr.Ing. Thesis)

MTA-93-94 Dalane, Jan Inge, MK:	System Reliability in Design and Maintenance of Fixed Offshore Structures. (Dr.Ing. Thesis)
MTA-93-95 Steen, Sverre, MH:	Cobblestone Effect on SES. (Dr.Ing. Thesis)
MTA-93-96 Karunakaran, Daniel, MK:	Nonlinear Dynamic Response and Reliability Analysis of Drag-dominated Offshore Platforms. (Dr.Ing. Thesis)
MTA-93-97 Hagen, Arnulf, MP:	The Framework of a Design Process Language. (Dr.Ing. Thesis)
MTA-93-98 Nordrik, Rune, MM:	Investigation of Spark Ignition and Autoignition in Methane and Air Using Computational Fluid Dynamics and Chemical Reaction Kinetics. A Numerical Study of Ignition Processes in Internal Combustion Engines. (Dr.Ing. Thesis)
MTA-94-99 Passano, Elizabeth, MK:	Efficient Analysis of Nonlinear Slender Marine Structures. (Dr.Ing. Thesis)
MTA-94-100 Kvålsvold, Jan, MH:	Hydroelastic Modelling of Wetdeck Slamming on Multihull Vessels. (Dr.Ing. Thesis)
MTA-94-102 Bech, Sidsel M., MK:	Experimental and Numerical Determination of Stiffness and Strength of GRP/PVC Sandwich Structures. (Dr.Ing. Thesis)
MTA-95-103 Paulsen, Hallvard, MM:	A Study of Transient Jet and Spray using a Schlieren Method and Digital Image Processing. (Dr.Ing. Thesis)
MTA-95-104 Hovde, Geir Olav, MK:	Fatigue and Overload Reliability of Offshore Structural Systems, Considering the Effect of Inspection and Repair. (Dr.Ing. Thesis)
MTA-95-105 Wang, Xiaozhi, MK:	Reliability Analysis of Production Ships with Emphasis on Load Combination and Ultimate Strength. (Dr.Ing. Thesis)
MTA-95-106 Ulstein, Tore, MH:	Nonlinear Effects of a Flexible Stern Seal Bag on Cobblestone Oscillations of an SES. (Dr.Ing. Thesis)
MTA-95-107 Solaas, Frøydis, MH:	Analytical and Numerical Studies of Sloshing in Tanks. (Dr.Ing. Thesis)
MTA-95-108 Hellan, øyvind, MK:	Nonlinear Pushover and Cyclic Analyses in Ultimate Limit State Design and Reassessment of Tubular Steel Offshore Structures. (Dr.Ing. Thesis)
MTA-95-109 Hermundstad, Ole A., MK:	Theoretical and Experimental Hydroelastic Analysis of High Speed Vessels. (Dr.Ing. Thesis)
MTA-96-110 Bratland, Anne K., MH:	Wave-Current Interaction Effects on Large-Volume Bodies in Water of Finite Depth. (Dr.Ing. Thesis)
MTA-96-111 Herfjord, Kjell, MH:	A Study of Two-dimensional Separated Flow by a Combination of the Finite Element Method and Navier-Stokes Equations. (Dr.Ing. Thesis)
MTA-96-112 Æsøy, Vilmar, MM:	Hot Surface Assisted Compression Ignition in a Direct Injection Natural Gas Engine. (Dr.Ing. Thesis)
MTA-96-113 Eknes, Monika L., MK:	Escalation Scenarios Initiated by Gas Explosions on Offshore Installations. (Dr.Ing. Thesis)

MTA-96-114 Erikstad, Stein O., MP: A Decision Support Model for Preliminary Ship Design. (Dr.Ing. Thesis)

MTA-96-115 Pedersen, Egil, MH: A Nautical Study of Towed Marine Seismic Streamer Cable Configurations. (Dr.Ing. Thesis)

MTA-97-116 Moksnes, Paul O., MM: Modelling Two-Phase Thermo-Fluid Systems Using Bond Graphs. (Dr.Ing. Thesis)

MTA-97-117 Halse, Karl H., MK: On Vortex Shedding and Prediction of Vortex-Induced Vibrations of Circular Cylinders. (Dr.Ing. Thesis)

MTA-97-118 Igland, Ragnar T., MK: Reliability Analysis of Pipelines during Laying, considering Ultimate Strength under Combined Loads. (Dr.Ing. Thesis)

MTA-97-119 Pedersen, Hans-P., MP: Levendefiskteknologi for fiskefartøy. (Dr.Ing. Thesis)

MTA-98-120 Vikestad, Kyrre, MK: Multi-Frequency Response of a Cylinder Subjected to Vortex Shedding and Support Motions. (Dr.Ing. Thesis)

MTA-98-121 Azadi, Mohammad R. E., MK: Analysis of Static and Dynamic Pile-Soil-Jacket Behaviour. (Dr.Ing. Thesis)

MTA-98-122 Ulltang, Terje, MP: A Communication Model for Product Information. (Dr.Ing. Thesis)

MTA-98-123 Torbergsen, Erik, MM: Impeller/Diffuser Interaction Forces in Centrifugal Pumps. (Dr.Ing. Thesis)

MTA-98-124 Hansen, Edmond, MH: A Discrete Element Model to Study Marginal Ice Zone Dynamics and the Behaviour of Vessels Moored in Broken Ice. (Dr.Ing. Thesis)

MTA-98-125 Videiro, Paulo M., MK: Reliability Based Design of Marine Structures. (Dr.Ing. Thesis)

MTA-99-126 Mainçon, Philippe, MK: Fatigue Reliability of Long Welds Application to Titanium Risers. (Dr.Ing. Thesis)

MTA-99-127 Haugen, Elin M., MH: Hydroelastic Analysis of Slamming on Stiffened Plates with Application to Catamaran Wetdecks. (Dr.Ing. Thesis)

MTA-99-128 Langhelle, Nina K., MK: Experimental Validation and Calibration of Nonlinear Finite Element Models for Use in Design of Aluminium Structures Exposed to Fire. (Dr.Ing. Thesis)

MTA-99-129 Berstad, Are J., MK: Calculation of Fatigue Damage in Ship Structures. (Dr.Ing. Thesis)

MTA-99-130 Andersen, Trond M., MM: Short Term Maintenance Planning. (Dr.Ing. Thesis)

MTA-99-131 Tveiten, Bård Wathne, MK: Fatigue Assessment of Welded Aluminium Ship Details. (Dr.Ing. Thesis)

MTA-99-132 Søreide, Fredrik, MP: Applications of underwater technology in deep water archaeology. Principles and practice. (Dr.Ing. Thesis)

MTA-99-133 Tønnessen, Rune, MH: A Finite Element Method Applied to Unsteady Viscous Flow Around 2D Blunt Bodies With Sharp Corners. (Dr.Ing. Thesis)

MTA-99-134 Elvekrok, Dag R., MP: Engineering Integration in Field Development Projects in the Norwegian Oil and Gas Industry. The Supplier Management of Norne. (Dr.Ing. Thesis)

MTA-99-135 Fagerholt, Kjetil, MP: Optimeringsbaserte Metoder for Ruteplanlegging innen skipsfart. (Dr.Ing. Thesis)

MTA-99-136 Bysveen, Marie, MM: Visualization in Two Directions on a Dynamic Combustion Rig for Studies of Fuel Quality. (Dr.Ing. Thesis)

MTA-2000-137 Storteig, Eskild, MM: Dynamic characteristics and leakage performance of liquid annular seals in centrifugal pumps. (Dr.Ing. Thesis)

MTA-2000-138 Sagli, Gro, MK: Model uncertainty and simplified estimates of long term extremes of hull girder loads in ships. (Dr.Ing. Thesis)

MTA-2000-139 Tronstad, Harald, MK: Nonlinear analysis and design of cable net structures like fishing gear based on the finite element method. (Dr.Ing. Thesis)

MTA-2000-140 Kroneberg, André, MP: Innovation in shipping by using scenarios. (Dr.Ing. Thesis)

MTA-2000-141 Haslum, Herbjørn Alf, MH: Simplified methods applied to nonlinear motion of spar platforms. (Dr.Ing. Thesis)

MTA-2001-142 Samdal, Ole Johan, MM: Modelling of Degradation Mechanisms and Stressor Interaction on Static Mechanical Equipment Residual Lifetime. (Dr.Ing. Thesis)

MTA-2001-143 Baarholm, Rolf Jarle, MH: Theoretical and experimental studies of wave impact underneath decks of offshore platforms. (Dr.Ing. Thesis)

MTA-2001-144 Wang, Lihua, MK: Probabilistic Analysis of Nonlinear Wave-induced Loads on Ships. (Dr.Ing. Thesis)

MTA-2001-145 Kristensen, Odd H. Holt, MK: Ultimate Capacity of Aluminium Plates under Multiple Loads, Considering HAZ Properties. (Dr.Ing. Thesis)

MTA-2001-146 Greco, Marilena, MH: A Two-Dimensional Study of Green-Water Loading. (Dr.Ing. Thesis)

MTA-2001-147 Heggelund, Svein E., MK: Calculation of Global Design Loads and Load Effects in Large High Speed Catamarans. (Dr.Ing. Thesis)

MTA-2001-148 Babalola, Olusegun T., MK: Fatigue Strength of Titanium Risers - Defect Sensitivity. (Dr.Ing. Thesis)

MTA-2001-149 Mohammed, Abuu K., MK: Nonlinear Shell Finite Elements for Ultimate Strength and Collapse Analysis of Ship Structures. (Dr.Ing. Thesis)

MTA-2002-150 Holmedal, Lars E., MH: Wave-current interactions in the vicinity of the sea bed. (Dr.Ing. Thesis)

MTA-2002-151 Rognebakke, Olav F., MH: Sloshing in rectangular tanks and interaction with ship motions. (Dr.Ing. Thesis)

MTA-2002-152 Lader, Pål Furset, MH:	Geometry and Kinematics of Breaking Waves. (Dr.Ing. Thesis)
MTA-2002-153 Yang, Qinzheng, MH:	Wash and wave resistance of ships in finite water depth. (Dr.Ing. Thesis)
MTA-2002-154 Melhus, Øyvin, MM:	Utilization of VOC in Diesel Engines. Ignition and combustion of VOC released by crude oil tankers. (Dr.Ing. Thesis)
MTA-2002-155 Ronæss, Marit, MH:	Wave Induced Motions of Two Ships Advancing on Parallel Course. (Dr.Ing. Thesis)
MTA-2002-156 Økland, Ole D., MK:	Numerical and experimental investigation of whipping in twin hull vessels exposed to severe wet deck slamming. (Dr.Ing. Thesis)
MTA-2002-157 Ge, Chunhua, MK:	Global Hydroelastic Response of Catamarans due to Wet Deck Slamming. (Dr.Ing. Thesis)
MTA-2002-158 Byklum, Eirik, MK:	Nonlinear Shell Finite Elements for Ultimate Strength and Collapse Analysis of Ship Structures. (Dr.Ing. Thesis)
IMT-2003-1 Chen, Haibo, MK:	Probabilistic Evaluation of FPSO-Tanker Collision in Tandem Offloading Operation. (Dr.Ing. Thesis)
IMT-2003-2 Skaugset, Kjetil Bjørn, MK:	On the Suppression of Vortex Induced Vibrations of Circular Cylinders by Radial Water Jets. (Dr.Ing. Thesis)
IMT-2003-3 Chezhian, Muthu	Three-Dimensional Analysis of Slamming. (Dr.Ing. Thesis)
IMT-2003-4 Buhaug, Øyvind	Deposit Formation on Cylinder Liner Surfaces in Medium Speed Engines. (Dr.Ing. Thesis)
IMT-2003-5 Tregde, Vidar	Aspects of Ship Design: Optimization of Aft Hull with Inverse Geometry Design. (Dr.Ing. Thesis)
IMT-2003-6 Wist, Hanne Therese	Statistical Properties of Successive Ocean Wave Parameters. (Dr.Ing. Thesis)
IMT-2004-7 Ransau, Samuel	Numerical Methods for Flows with Evolving Interfaces. (Dr.Ing. Thesis)
IMT-2004-8 Soma, Torkel	Blue-Chip or Sub-Standard. A data interrogation approach of identity safety characteristics of shipping organization. (Dr.Ing. Thesis)
IMT-2004-9 Ersdal, Svein	An experimental study of hydrodynamic forces on cylinders and cables in near axial flow. (Dr.Ing. Thesis)
IMT-2005-10 Brodtkorb, Per Andreas	The Probability of Occurrence of Dangerous Wave Situations at Sea. (Dr.Ing. Thesis)
IMT-2005-11 Yttervik, Rune	Ocean current variability in relation to offshore engineering. (Dr.Ing. Thesis)
IMT-2005-12 Fredheim, Arne	Current Forces on Net-Structures. (Dr.Ing. Thesis)
IMT-2005-13 Heggernes, Kjetil	Flow around marine structures. (Dr.Ing. Thesis)

IMT-2005-14 Fouques, Sebastien	Lagrangian Modelling of Ocean Surface Waves and Synthetic Aperture Radar Wave Measurements. (Dr.Ing. Thesis)
IMT-2006-15 Holm, Håvard	Numerical calculation of viscous free surface flow around marine structures. (Dr.Ing. Thesis)
IMT-2006-16 Bjørheim, Lars G.	Failure Assessment of Long Through Thickness Fatigue Cracks in Ship Hulls. (Dr.Ing. Thesis)
IMT-2006-17 Hansson, Lisbeth	Safety Management for Prevention of Occupational Accidents. (Dr.Ing. Thesis)
IMT-2006-18 Zhu, Xinying	Application of the CIP Method to Strongly Nonlinear Wave-Body Interaction Problems. (Dr.Ing. Thesis)
IMT-2006-19 Reite, Karl Johan	Modelling and Control of Trawl Systems. (Dr.Ing. Thesis)
IMT-2006-20 Smogeli, Øyvind Notland	Control of Marine Propellers. From Normal to Extreme Conditions. (Dr.Ing. Thesis)
IMT-2007-21 Storhaug, Gaute	Experimental Investigation of Wave Induced Vibrations and Their Effect on the Fatigue Loading of Ships. (Dr.Ing. Thesis)
IMT-2007-22 Sun, Hui	A Boundary Element Method Applied to Strongly Nonlinear Wave-Body Interaction Problems. (PhD Thesis, CeSOS)
IMT-2007-23 Rustad, Anne Marthine	Modelling and Control of Top Tensioned Risers. (PhD Thesis, CeSOS)
IMT-2007-24 Johansen, Vegar	Modelling flexible slender system for real-time simulations and control applications.
IMT-2007-25 Wroldsen, Anders Sunde	Modelling and control of tensegrity structures. (PhD Thesis, CeSOS)
IMT-2007-26 Aronsen, Kristoffer Høye	An experimental investigation of in-line and combined in-line and cross flow vortex induced vibrations. (Dr.avhandling, IMT)